Effects of Pressure on the Morphology of Semi-Crystalline Polymers

By Christopher Michael Baker

Sc.M., Brown University 2010

Thesis

Submitted in partial fulfillment of the requirements for

The Degree of Doctor of Philosophy

Biotechnology Program

Division of Biology and Medicine

Brown University

Providence, Rhode Island

May 30, 2017

This dissertation by Christopher Michael Baker is accepted in its present form by the Division of Biology and Medicine as satisfying the dissertation requirement for the degree of Doctor of Philosophy.

Date_____ _____

Edith Mathiowitz Ph.D., Advisor

Recommended to the Graduate Council

Date_____ _____

Edith Mathiowitz Ph.D.

Date_____ _____

Jeffrey R. Morgan Ph.D.

Date_____ _____

Anubav Tripathi Ph.D.

Date_____ _____

Eric Darling Ph.D.

Date_____ _____

Joshua Reineke Ph.D., External Reader

Approved by the Graduate Council

Date_____ _____

Andrew Campbell Ph.D., Dean of Graduate School

CURRICULUM VITAE

Name:	Christopher M. Baker
Address:	334 Jastram St. Providence, RI 02908
E-Mail:	Christopher.M.Baker81@Gmail.com
Phone:	1-401-633-4649
Place of birth:	Providence, RI. United States of America
LinkedIn:	www.linkedin.com/in/christophermbaker81
Orcid ID:	0000-0003-2616-2377
Research Gate:	www.researchgate.net/profile/Christopher_Baker20


LinkedIn


Orcid ID


Research Gate

Education

2017	Ph.D.	Brown University, Providence, RI
2010	Sc.M.	Brown University, Providence, RI
2009	Sc.B.	Brown University, Providence, RI
2007	A.S.	CCRI, Warwick, RI
2001	Reactor Operator License	Naval Nuclear Power Training Unit, Ballston Spa, NY
2000	Nuclear Electronics Technician	Naval Nuclear Power Training Command, Goose Creek, SC
1999	Diploma	Bishop Hendricken High School, Warwick, RI

Professional Experience

2013-2016 Molecular Pharmacology, Physiology, Biotechnology; Edith Mathiowitz, Ph.D.

Graduate Teaching Assistant: responsible for instructing 62 Drug and Gene Delivery students ranging from undergraduate seniors and graduate students to professional engineers, biologists, chemists and medical researchers. Implementing design based instruction utilizing current literature and concomitant lab experiments.

Techniques: Controlled Release, Non-erodible Reservoir & Matrix Devices, Bio-erodible Devices, Osmotic Pumps, Release Kinetics, Hydrogels, Live Cellular Encapsulation, Stabilization and Controlled Release of Proteins, Routes of Delivery, Fabrication of Controlled Delivery Devices: Microencapsulation, Liposome Preparation, Film Casting and Membrane Formation, Economics of Controlled Delivery Devices, Patents and Intellectual Property Rights in Drug Delivery, Polymer Synthesis & Characterization.

2011-2015 Community College of Rhode Island; Providence, RI

Adjunct Physiology Professor: Provided 36 students with a broad view of the current knowledge on how the human body works. Beginning with some historical background, study moved from the chemical level of atoms and molecules, to the cellular level, to the operation of individual organs and systems and finally to the interdependence required to maintain a functioning human body. Two concepts, homeostasis and the relationship of structure to function are themes of the course.

Techniques: Personnel Instruction, Lecturing, Public Speaking, Presentation, Performance Evaluation.

2011-2012 Perosphere Inc.; Providence, RI

Research Scientist: Developed and manufactured therapeutically novel drug delivery constructs specifically designed for the optimization of uptake and bioavailability of current oral and topical medications.

Techniques: Experimental Surgery, Cell Culture, Nano/Micro-Encapsulation, Drug Formulation, Pharmacokinetics, Charge Masking, IR/UV Spectroscopy, Confocal Microscopy, Scanning Electron Microscopy, Coulter Particle Sizing, Zeta Sizing and Potential, Differential Scanning Calorimetry, cGMP, High Throughput Assay Development, Statistical Analysis, Creating and Writing SOP's

2010-2011 Molecular Pharmacology, Physiology, Biotechnology; Jeffrey Morgan, Ph.D.

Research Assistant: Developed and implemented a high throughput bacterial growth and adherence assay for exploration of the efficacy related to drug eluting biomedical implant surface coatings used to inhibit or prevent biofilm formation.

Techniques: Bacterial Culture, Biofilm, IR Spectroscopy, High Throughput Assay Development, Statistical Analysis, Creating and Writing SOP's

2009-2016 Molecular Pharmacology, Physiology, Biotechnology; Edith Mathiowitz, Ph.D.

Graduate Teaching Assistant: responsible for instructing 30 undergraduate students in polymer science for biomaterials utilizing a hands on approach.

Techniques: Basic Polymerization Chemistry, Kinetics of Polymerization and De-Polymerization, Bioerodible Polymers, Characterization of Polymers by Physical Methods, Bulk and Surface Properties, Behavior of Polymers in Solutions, Crystallization, Gelation and Liquid Crystals.

2004-2005 United States Navy; USS Dwight D. Eisenhower CVN-69

Operational Readiness Safeguards Exam Drill Team: Developed standard operating procedures and training instruction programs specifically aimed towards assuring quality control and the safe instruction of all 500 reactor department personnel.

Techniques: Personnel Supervision, Industrial Safety, Radiological Control, Quality Assurance, Creating and Writing SOP's, Creating and Writing Training Instructions, Supervising Live Training Drills.

2002-2005 United States Navy; USS Dwight D. Eisenhower CVN-69 (IKE)

Reactor Operator: Qualified and licensed to operate the Westinghouse model A4 pressurized water nuclear reactor as well as to perform all preventative and corrective maintenance of its solid state and analog electronic instrumentation and controls systems.

Techniques: Nuclear Physics, Heat Transfer Fluid Flow, Reactor Theory, Industrial Safety, Radiological Control, Nuclear Chemistry, Materials Science, AC/DC Theory, AC/DC Circuit Troubleshooting and Repair, Solid State Circuit Troubleshooting and Repair, Personnel Supervision.

2002-2005 United States Navy; USS Dwight D. Eisenhower CVN-69 (IKE).

Reactor Controls Division Secondary Supervisor: Supervised and trained a work center consisting of 10 personnel thereby ensuring their timely qualification and safe operation in the department.

Techniques: Personnel Supervision, Industrial Safety, Radiological Control, AC/DC Theory, AC/DC Circuit Troubleshooting and Repair, Solid State Circuit Troubleshooting and Repair, Nuclear Physics, Heat Transfer Fluid Flow, Reactor Theory, Nuclear Chemistry, Materials Science

2001-2005 Stationed Onboard USS Dwight D. Eisenhower CVN-69 (IKE).

2001-2001 United States Navy; Naval Nuclear Power Training Unit Ballston Spa, New York

Nuclear Propulsion Plant Operator (Reactor Operator): Upon completion of the course, the student will be able to describe the fundamentals of nuclear propulsion
power and the interrelationship of its mechanical, electrical, and reactor subsystems; develop and exercise oral communication skills; understand the physical nature of nuclear radiation particles, their detection, interaction with matter, and human health consequences; gain knowledge of the safe operation of a complex nuclear power plant and its sophisticated subsystems with an emphasis on basic industrial safety principles;
identify, troubleshoot, and correct problems in nuclear mechanical, electrical, or reactor control systems at the component level with an emphasis on reactor systems; and apply earlier technical classroom knowledge to the practical, safe operation of Navy nuclear power plants.

Techniques: Oral Communication, Industrial Safety, Basic Health Physics, Introduction to power systems, Reactor Systems Practicum, Troubleshooting Reactor Power

2000-2000 United States Navy; Nuclear Power Training Command Charleston, South Carolina

Naval Nuclear Power School: Upon completion of the course, the student will have a comprehensive understanding of a pressurized-water nuclear power plant, including reactor core nuclear principles, heat transfer and fluid systems, plant chemistry
and materials, mechanical and electrical systems, and radiological control.

Techniques: General Physics, Heat Transfer and Fluid Flow, Nuclear Reactor Engineering, Atomic and Nuclear Physics, Radiation Protection Technology, General Chemistry and Principles of Materials, Technical Mathematics, Hydraulic Systems, DC Circuits, AC Circuits, Digital Principles, Electric Machines.

1999-2000 United States Navy; Nuclear Power Training Command Charleston, South Carolina

Nuclear Electronics Technician "A" School: Upon completion of the course, the student will have a basic knowledge of technical mathematics and a good working knowledge of DC and AC circuits, solid state devices, digital logic and systems, microprocessors, and instrumentation and control circuits.

Techniques: Technical Mathematics, DC circuits, AC circuits, Solid State Devices and Circuits, Electrical Troubleshooting and Repair, Digital Circuits and Microprocessors, Basic Instrumentation and Controls.

1999-2001 Commenced Naval Nuclear Power Program.

1999-1999 United States Navy; Recruit Training Command Great Lakes, Illinois

Recruit: Upon completion of the course, recruits are able to demonstrate knowledge of general military and Navy protocol.

Techniques: First Aid, Personal Health and Safety, Basic Swimming, Fire Fighting and Damage Control, Seamanship, Water Survival, Physical Fitness.

1998-1999 Enlisted in the United States Navy as a Nuclear Power Program Delayed Entry Candidate.

Research Experience

2012-2016 Molecular Pharmacology, Physiology, Biotechnology; Edith Mathiowitz, Ph.D.

Effect of Pressure on Semi-Crystalline Polymers: Characterized the physical morphology of the polymers poly-L-lactic acid, and Polycaprolactone upon processing them under specific time, temperature and pressure profiles.

Techniques: Fourier Transform Infrared Spectroscopy, Differential Scanning Calorimetry, Hydraulic Pressing, Polarized Light Microscopy, Scanning Electron Microscopy, Inductively Coupled Plasma, X-Ray Diffraction, Hot Stage Microscopy, Gel-Permeation Chromatography, Creating and Writing SOP's

2009-2010 Molecular Pharmacology, Physiology, Biotechnology; Edith Mathiowitz, Ph.D.

Development of a polymer based time temperature indicator for drug delivery applications: Manipulated and evaluated the physical structure of the polymer poly-L-lactic acid to produce a birefringence based time temperature indicator.

Techniques: Fourier Transform Infrared Spectroscopy, Differential Scanning Calorimetry, Hydraulic Pressing, Polarized Light Microscopy, Creating and Writing SOP's

2007-2009 Molecular Pharmacology, Physiology, Biotechnology; Jeffrey Morgan, Ph.D.

Development of an effective drug eluting antimicrobial surface coating and high throughput silver ion detection assay: Synthesized and evaluated a silver ion eluting metal-polymer hybrid surface coating to explore its antimicrobial properties utilizing wet chemistry techniques while simultaneously developing a high throughput spectrophotometric silver ion detection assay.

Techniques: Bacterial Culture, Infrared Spectroscopy, Wet Chemistry, High Throughput Assay Development, Statistical Analysis, Creating and Writing SOP's

Publications

C.M. Baker, A. Azagury, E. Mathiowitz, Effect of pressure on poly-l-Lactic Acid morphology, Polymer (Guildf). 99 (2016) 250–262. doi:10.1016/j.polymer.2016.07.028.

Abstracts

Baker, C. Jain, N. Munoz, K. Atherton, E. Mathiowitz, E. Controlled Release of Menthol from Polycaprolactone, in: 2015 CRS Annu. Meet., Controlled Release Society, Edinburgh, 2015: pp. 1–2.

J. Jarrell, N. Thomas, M. Young, C. Baker, J. Morgan, Bioactive Hybrid Material Surface Treatments for Infection Resistant Implants without Drugs, ASM Int. (2013) 143–148.

Baker, C. Suzin, D. Mathiowitz, E. Release of Small Molecules Utilizing Enhanced Polymer Films, in: 2013 CRS Annu. Meet., Contolled Release Society, Honolulu, 2013: pp. 1–2.

B. Laulicht, S. Bakhru, C. Lee, C. Baker, Small molecule antidote for anticoagulants, Circulation. (2012) 977.

Conference Presentations

C.M. Baker, Controlled Release of Menthol from Polycaprolactone, in: 2015 CRS Annu. Meet., Edinburgh, 2015.

Theses

C.M. Baker, Induced Birefringence of Poly-Lactic Acid for Implementation as Time Temperature Indicators, Brown University, 2010. doi:10.7301/Z07W6940.

C.M. Baker, Antimicrobial Properties of Bioactive Silver by Delivery via Novel Metal-Polymer Hybrid Surface Coatings, Brown University, 2009. doi:10.7301/Z0CN71V9.

Skills

Experimental and Micro-Surgery
JY Horiba 2000 ICP-OES V 5.4.2
Hitachi 2700 SEM with Quartz PCI Software
Bruker XRD with DaVinci & EVA Software
Zeiss Zen Software Package
Zeiss Axiovision Software Package
Malvern Zetasizer Software Package
Beckman Coulter LS 32 Software Package
SpectraMax Software Package
Perkin Elmer Spectrum Software Package
Pyris DSC Software Package
Radiological Control
3M Quality Assurance
Solid State and Analog Electronics Troubleshooting and Repair
Microsoft Office Suite

Professional and Academic Associations

2015	Controlled Release Society
2009	Sigma Xi Scientific Research Honor Society
2007	Phi Theta Kappa National Honor Society for Two Year Colleges

Awards and Honors

2014	Passed to Ph.D. Candidacy Status, Biotechnology, Brown University
2013	Awarded the Daniel Carter Beard Masonic Scouter Award
2009	Raised to the Degree of Master Mason, St. Johns Lodge No.1 P F&AM
2009	Passed to the Degree of Fellow Craft, St. Johns Lodge No.1 P F&AM
2009	Accepted to the Degree of Entered Apprentice, St. Johns Lodge No.1 P F&AM
2009	Honors, Biology, Brown University
2009	Karen T. Romer Undergraduate Teaching and Research Award (UTRA)
2009	National Science Foundation Research Experience for Undergraduates Award. (REU)
2007	Highest Honors, Science, Community College of Rhode Island
2007	National Deans List
2007	Tylenol Scholarship Award
2005	Honorably Discharged from United States Navy
2005	Navy Good Conduct Medal with Bronze Star in Lieu of 2nd Award.
2004	Designated Enlisted Surface Warfare Specialist (ESWS)
2001	Navy Good Conduct Medal
2001	Global War on Terrorism Service Medal
2001	National Defense Service Medal
2001	Promoted to Nuclear Electronics Technician Petty Officer Second Class
2000	Promoted to Nuclear Electronics Technician Petty Officer Third Class
1999	Awarded the rank of Eagle Scout by the Boy Scouts of America

Security Clearance

Secret-Inactive

Licenses

Reactor Operator-Inactive

Language Skills

Spanish-Basic Proficiency

Major Research Interests

Drug and Gene Delivery
Experimental Surgery
Bio-adhesion
Wound Healing
Percutaneous Implants
Biofilm Inhibition
Medical Devices
Pharmacokinetics
Polymer Based Drug Delivery Platforms
Polymer Chemistry
Physical and Chemical Manipulation of Polymer Based Constructs

Acknowledgements

I would first and foremost like to thank Professor Edith Mathiowitz Ph.D. for allowing me to become a member of the Mathiowitz lab. Prof. Mathiowitz has been more than just an adviser but a true friend and guide in my endeavor to pursue my education. To this, I will be forever indebted to her for her impact on my life. I could not have accomplished this without her.

I would like to thank Professor Jeffrey Morgan Ph.D. for agreeing to be the chairman of my committee. Professor Morgan's support of my studies throughout the many years has been a continuing factor in my drive to constantly improve myself. Additionally, I would like to thank Jeff for taking me into his lab as an undergraduate researcher. This experience was one of the most impactful times of my life and helped lay the foundation of my scientific career.

I would also like to thank the remaining members of my committee including, Anubav Tripathi Ph.D., Eric Daring Ph.D., and Joshua Reineke Ph.D.. Thank you for agreeing to read my thesis and sit on my committee. I hope to one day contribute to a young scientist's career as you have with mine.

I would like to thank Jessica Bello and Kris McKutcheon for their support and friendship.

I would like to extend a very special thanks to all of my students over the years who without their help, this work would not have been possible.

I would like to give a very sincere thanks to my friends Jeremy Messier, Katherine Messier MBA., Alexander Li, Aharon Azagury Ph.D., Hank & Arlene Latek, and Pat DePasquale.

I would like to also give a very sincere thanks to all the RUE's and fellow Student Veterans at Brown for their continued support as I progressed academically at Brown over the last 10 years.

Finally, I would like to give my deepest thanks to my parents Debra and Richard Baker along with my sister Ashley Baker, for without their endless and undying support throughout my academic experience, this would not have been possible.

Table of Contents

List of Figures

Chapter 1

Chapter 2

Chapter 3

Chapter 4

Chapter 5

Chapter 6

No Figures

Chapter 1

Introduction

Christopher M. Baker Sc.M., Edith Mathiowitz Ph.D.

Abstract:

When exposed to pressures below and above their glass transition temperature (T_g) and melting temperatures (T_m) over time, both the amorphous and crystalline regions of Poly-L-Lactic Acid (PLA) and Polycaprolactone (PCL) can be oriented. This effect was observed with the existence of an intense birefringence which lacked any sign of traditional crystalline structure as observed by polarized light microscopy. Differential Scanning Calorimetry (DSC) analysis of the materials revealed the existence of increased orientation of the materials in addition to increased crystallinity. Consequently, X-Ray Diffraction (XRD) revealed a morphological change which appeared to be more crystalline in structure. Additionally, PCL was explored for use in hot melt encapsulation of three different types of molecules. Specifically, volatile oil and menthol in addition to a therapeutic lithium carbonate salt. Results indicated that PCL was quite capable of releasing volatile oil and menthol in a controlled and time dependent manner with no observable burst release effects noted. However, initial loading and storage temperature was observed to have a direct impact on total release as increased loading and temperatures were observed to increase total release. Finally, PCL was proven quit effective in controlled release of therapeutic lithium in a simulated gastric environment. Lithium much like the volatiles was observed to release in a very controlled and time dependent manner. With total release being observed to rely on initial loading once again.

1. Introduction

Currently, an estimated 260 metric tons of petroleum based polymers are synthesized annually throughout the globe. [1] Unfortunately, only 50% of these polymers are produced for use as durable goods in long term applications leaving the remaining 50% designated and sold into the disposable single use consumer market. Furthermore, of this 130 metric tons slated for disposable use, only 30% or 39 metric tons are eventually recovered for recycling purposes leaving an estimated 91 metric tons of petroleum based polymers destined for the landfill.[2] While traditional polymers such as polypropylene and polyethylene cost about $0.40 to manufacture, their true costs are hidden as they do not degrade easily, often taking decades to centuries. Additionally, once landfilled or incinerated they release harmful degradation products into the watersheds and toxic byproducts into the air. [3] These environmental issues in turn destroy the natural habitat of our wildlife and cost us millions of dollars in cleanup as observed previously in the Hudson River PCB cleanup in New York. [2–4]

Consequently, these has been a large scale effort in the United States to produce second generation or bio-based polymers to alleviate the problems inherent with non-degradable petroleum based polymer use. These bio-based polymers are beneficial as they offer substantial sustainability in comparison to petroleum based polymers given they are produced from renewable bio-wastes (corn) with the additional benefit of being naturally biodegradable and PCB/BPA free. [3,4] To date, ≈ $750 million dollars has been invested in the United States

to commence producing a biodegradable polymer known as Poly-L-Lactide on a large scale. [5] PLA as it is currently synthesized costs ≈ $0.25/lb to manufacture. [6] This cost, when taken into account with the United States polymer consumer market, is projected to lead to sales of 3.4 million tons a year which translates to an approximate market value of 4.5 billion dollars/year. [7] Thus with global petroleum prices constantly fluctuating with reserves dwindling, growing a self-sustainable polymer source will be vital to economic health and growth.

2. Motivation

Given the finite nature of the global petroleum supply, the production of biodegradable polymers such as Poly-L-Lactic Acid and Polycaprolactone has greatly increased in order to replace or further limit the use of non-degradable polymers. However, these biodegradable based materials given their relatively new appearance in the consumer market have been characterized in a limited fashion, especially in regard to how their morphology is affected upon being exposed to pressure and temperature stresses over time. This represents a problem as this gap in their morphological characterization represents a lost opportunity for expanding their use in lieu of well characterized non-degradable polymers. Additionally, given these materials wide use in the fields of drug delivery, it is hypothesized that the polymer Polycaprolactone could prove useful in constructing a series of devices which are capable of releasing small molecules such as volatile oils and menthol along with small molecule

therapeutic agents. These gaps shall be explored within the following listed specific aims.

3. Specific Aims

Aim 1

Characterize the effect of pressure, temperature, and time on the morphology of Poly-L-(Lactic Acid) (PLA).

Aim 2

Characterize the effect of pressure, temperature, and time on the morphology of Polycaprolactone (PCL).

Aim 3

Develop and characterize a volatile molecule (Oil & Menthol) controlled delivery system using the polymer PCL.

Aim 4

Develop and characterize an anti-psychotic, small molecule controlled drug delivery system using the polymer PCL.

4. Background

4.1 Poly-L-Lactic Acid

Poly-L-Lactic Acid or PLA is a bio-based semi-crystalline thermoplastic polymer consisting of multiple lactide monomers chained together. Belonging to the family of aliphatic polyesters, PLA's synthesis process begins with the harvesting of food crops such as corn or soybeans. These crop products are then processed to remove and separate their sugars such as glucose, sucrose and dextrose which are then fed to bacterium strain Lactobacilli.[8] Upon gaining access to this sugary food source, the bacteria begin to feed on and ferment the mixture which produces large quantities of lactic acid in the process. This lactic acid in then in turn harvested and used as the stock monomer material from which the PLA will be synthesized from.

Currently, PLA is most commonly synthesized using ring opening polymerization which is capable of producing a high molecular product. [9] Initially, polymerization commences reacting the lactide monomers through a condensation reaction by which water is removed from the mixture. This is the preferred route of synthesis given the fact that the presence of water in the production process can and often does hydrolyze the PLA which can thus degrade or limit its molecular weight. [8] Next, the pre-polymers resulting from the condensation reaction are joined into ring structures, shielding the production process from infiltration by impurities and water. Finally, the ring is opened using

a tin (II) oxide catalyst, producing a polymer chain of high molecular weight and purity. This process as currently used by Cargill-Dow is depicted in Figure. 1..

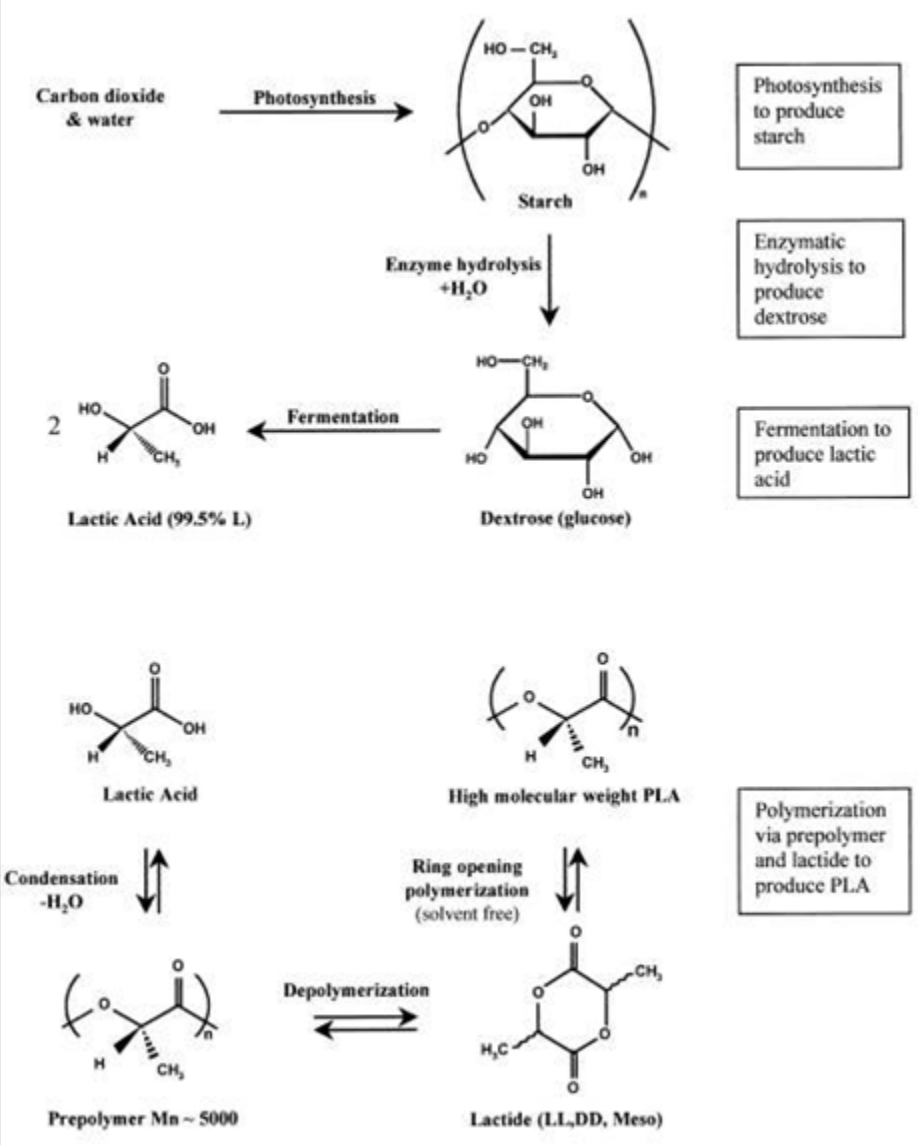

Figure. 1. Ring opening polymerization of PLA as currently produced by Cargill-Dow. [10]

PLA's physical properties are closely tied to the ratio of D-lactide and L-lactide used in its synthesis, as this ratio is capable of directly regulating PLA's inherent degree of amorphousness and crystallinity.[8] Specifically, when the D-lactide is present in greater numbers, PLA becomes more amorphous in nature and thus less ordered in structure. Conversely, as the content of L-lactide is increased, PLA becomes more crystalline and thus more ordered in structure.

The degree of order inherent in a sample of PLA has many impacts on the material's density, degradation rate, strength, flexibility, glass transition temperature and melting temperature. Amorphous PLA has been found to hold a density value of 1.248 g/ml while crystalline PLA due to its increased physical order, holds a density value of 1.290 g/ml. [8] Consequently, as PLA becomes more crystalline or ordered, it also becomes better able to resist permeation by water and is thus better able to retard hydrolytic degradation of its polymer backbone. This allows the material's life to be extended from weeks when amorphous in nature to months or even years as crystallinity increases. [8] Crystalline PLA is also stronger yet less flexible than amorphous PLA. Finally, PLA is typically observed to possess a glass transition temperature (T_g) range of 55-65 °C and melting point (T_m) range of 165-185 °C, both of which can be manipulated by adjusting the degree of amorphous orientation and crystallinity present in the material. [9]

4.2 Polycaprolactone

Polycaprolactone or PCL, similarly to PLA is a semi-crystalline linear aliphatic polyester characterized by long chains of connected repeating monomers. PCL was originally invented in the 1930's by scientists seeking to produce a biodegradable synthetically derived polymer. [11] Like its younger cousin PLA, PCL is also typically synthesized using ring opening polymerization with the exception that ε-caprolactone is used as the repeating monomer unit. [11] This process is depicted below in Fig. 2..

Figure. 2. Ring opening polymerization of Polycaprolactone. [12]

PCL's is a flexible, non-toxic, and hydrophobic polymer which quite easily renders itself to processing given its physical properties. PCL's T_g is typically observed to fall within the range of -65 °C to -60 °C in addition to its relatively low T_m of 60 °C. [12] Due to its low T_g and T_m, PCL is quite rubbery at room temperature, becoming extremely malleable upon approaching melt. However, just as with PLA, PCL's physical properties can be manipulated by altering its amorphous orientation and degree of crystallinity. By altering the structure of the material, PCL can be made to be more crystalline which as previously mentioned

can alter a polymers mechanical properties as well as its resistance to hydrolytic degradation. This flexibility along with its ability to reach high molecular weights in addition to how easy PCL can be blended with other polymers and materials thus make it an ideal candidate for the encapsulation and release of volatile and small molecules.

4.3 Birefringence and Polarized Microscopy

Birefringence or double refraction as depicted in Fig. 3. is defined as the decomposition of a ray of light into two rays, being an ordinary ray and an extraordinary ray, upon passing through a material with dependence on the polarization of the light. [13,14] This phenomenon may be further explained within the relational domain of isotropic and anisotropic physical orientations inherent in certain optically active materials. Previously, it has been observed that when light passes through a material of question and that material is of a single directionality in physical composition, that the passing light will thus also be aligned in this manner. This effect known as single refraction is thus termed isotropy and can be observed at any angle with the same result.[13,14] Consequently, as light passes through a material possessing multiple indices of refraction, it is broken down into a variety of different directionalities and can be observed as a colorful or birefringent effect. This phenomenon is thus termed anisotropy, as no two angles of incidence will produce the same effect.[14]

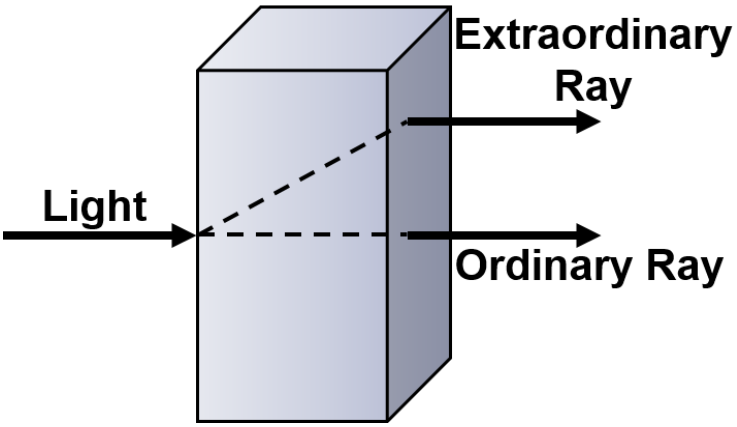

Figure. 3. Graphical representation of the birefringent effect.

Typically, the detection of this birefringent effect in a material is quite a simple process and can be accomplished using a microscope equipped with polarized filters. Polarized light, simply defined, is a beam of light which possesses a single vibrational directionality. Normally, natural or white light is found to consist of all possible directionalities but when passed through a single polarized filter for example, the beam of light becomes ideally restricted to one specific vibrational plane. Upon adding a second filter crossed at 90° to the first, we ideally observe the complete extinction of transmitted light. This optical property is depicted in Fig. 4.

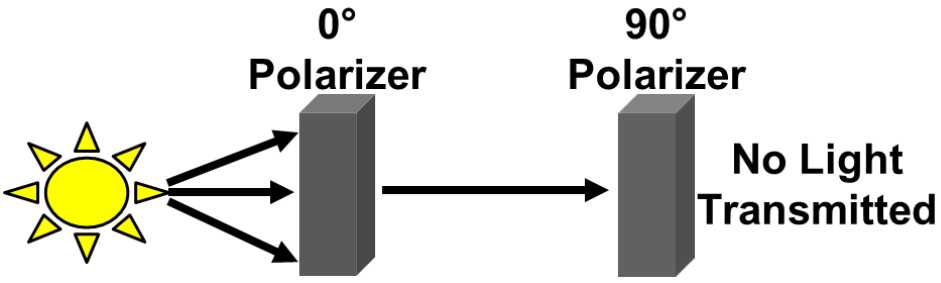

Figure. 4. Graphical representation of a polarized light microscope.

Thus when an optically transparent, and structurally oriented material is placed between the crossed polarizer's and exposed to a white light source, we observe a vibrant colorful effect known as birefringence. This is due to the double refractive or anisotropic alignment of the material in question. Upon passing through the first polarizer, the light source becomes restricted to the previously mentioned singular directionality, for example the horizontal direction. Ideally, the vertical directionality of the light passing through the first polarizer would be inhibited by the second polarizer crossed at 90°, but with a birefringent material sandwiched between the perpendicularly crossed polarizers, this does not occur. Instead, the beam of light is split into two different directionalities upon interaction with the material in question, one of which is able to pass through the second polarizer producing the colorful visual effect as previously described and depicted in Fig. 5..[14]

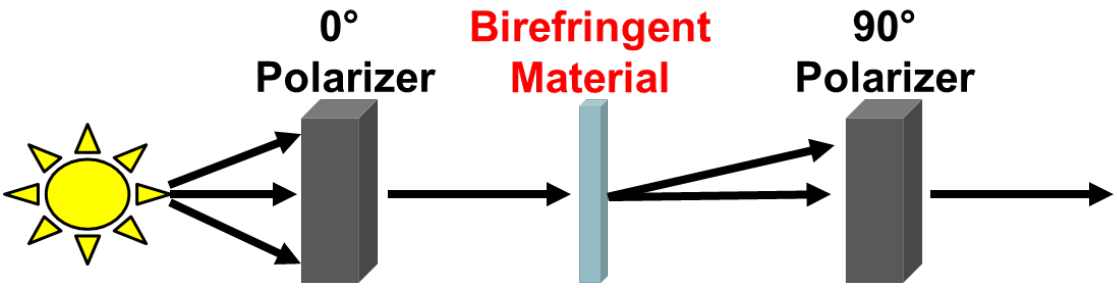

Figure. 5. Graphical representation of the birefringent effect under polarized light.

4.4 Differential Scanning Calorimetry

Differential scanning calorimetry or DSC is an analytical method which utilizes the measurement of heat flow into or out of a sample as a function of temperature or time. [15] To accomplish this measurement, a sample is placed in an aluminum sample pan which is then placed in the DSC's sample compartment. Conversely, an empty reference pan is placed in the reference compartment for comparison upon heating and cooling. Fig. 6. depicts this typical arrangement. By heating or cooling both compartments simultaneously while monitoring by thermocouple, the differential heat flows of each sample can be calculated. Using this data, the DSC software can calculate the materials glass transition temperature, melting temperature as well as additional thermal properties such as specific heat capacity and heat of fusion. [15]

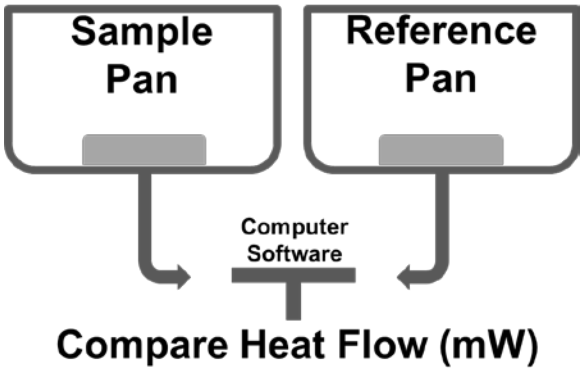

Figure. 6. Schematic of a typical DSC.

4.5 X-Ray Diffraction

X-Ray Powder Diffraction or XRD uses the concept of X-Ray diffraction or scattering upon encountering an obstacle to elucidate or provide its user with details as to the materials molecular structure. [16] These details while not limited to, include a materials crystal structure and size. XRD is capable of doing this as X-rays are a type of electromagnetic radiation possessing high energies with short wavelengths on the order of the inter-atomic spacing within solids. Thus when two x-ray beams diffract off of a material, the scattered waves either reinforce (constructively interfere) or destructively interfere with one another, as depicted in Fig. 7..[16] When the scattered waves remain in phase, the resulting wave from adding the two together is twice the amplitude of the original. If the scattered waves are out of phase, the resulting wave has an amplitude of zero. The resulting phase relationship can also be an intermediate between these two extremes. [16]

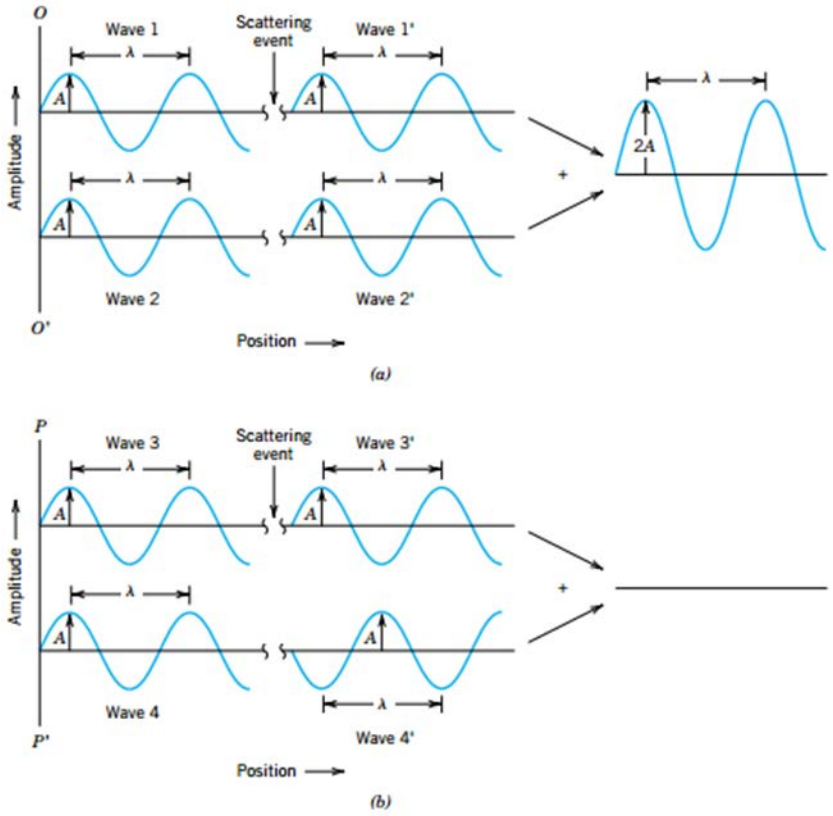

Figure. 7. X-Ray Phase Diagram. [16]

Depicted in Fig. 8., are a set of parallel x-rays of wavelength λ and two planes of atoms separated by distance d_{hkl}. Assuming the two x-rays are incident on the planes at an angle of θ, diffracting off of atoms P and Q at an angle of θ and mutually reinforcing each other. Assuming that only mutual reinforcement occurs and the difference between the two paths are a multiple of the wavelength, meaning nλ = $\overline{SQ}$ + $\overline{QT}$, we are lead to Bragg's Law.[16]

$$n\lambda = 2d_{hkl}sin\theta$$

where n is an integer called the order of reflection. This equation relates the X-Rays wavelength to the materials interatomic distance and incident angle. If this equation is not satisfied, the destructive interference will cause the intensity of the diffracted beam to be low.

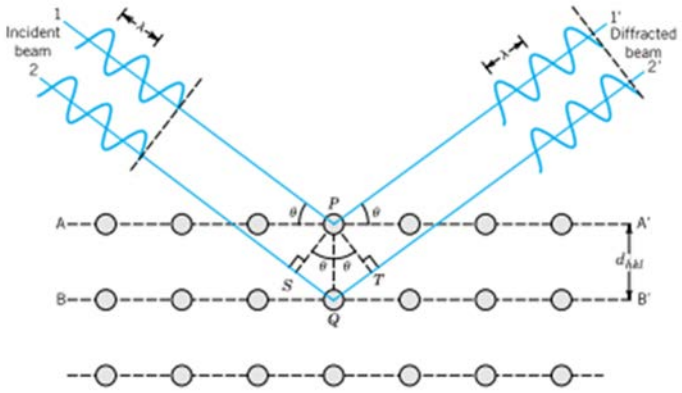

Figure. 8. Depiction of Bragg's Law. [16]

Depicted in Fig. 9. Is a graphical repsresentation of how an XRD fuctions. Components include an x-ray source, rotatable stage, and counter. The sample is rotated around the origin so it is at an angle θ from the fixed x-ray source. The counter measures the intensity of the diffracted beam and rotates around the origin an angle 2θ from the x-ray source. The counter rotates 2θ for every θ the specimen moves to maintain equal incident and reflection angles. As the counter rotates, the recorder automatically records the intensity as a function of the diffraction angle (2θ). [16]

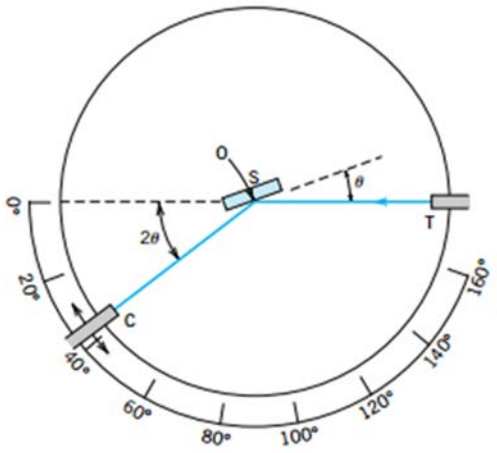

Figure. 9. Schematic of an XRD.

References:

[1] J. Hopewell, R. Dvorak, E. Kosior, Plastics recycling: challenges and opportunities., Philos. Trans. R. Soc. Lond. B. Biol. Sci. 364 (2009) 2115–26. doi:10.1098/rstb.2008.0311.

[2] B.P. Mooney, The second green revolution? Production of plant-based biodegradable plastics., Biochem. J. 418 (2009) 219–32. doi:10.1042/BJ20081769.

[3] R.C. Thompson, C.J. Moore, F.S. vom Saal, S.H. Swan, Plastics, the environment and human health: current consensus and future trends., Philos. Trans. R. Soc. Lond. B. Biol. Sci. 364 (2009) 2153–66. doi:10.1098/rstb.2009.0053.

[4] E.L. Teuten, J.M. Saquing, D.R.U. Knappe, M. a Barlaz, S. Jonsson, A. Björn, et al., Transport and release of chemicals from plastics to the environment and to wildlife., Philos. Trans. R. Soc. Lond. B. Biol. Sci. 364 (2009) 2027–45. doi:10.1098/rstb.2008.0284.

[5] E.T.H. Vink, K.R. Rábago, D. a Glassner, B. Springs, R.P. O'Connor, J. Kolstad, et al., The sustainability of NatureWorks polylactide polymers and Ingeo polylactide fibers: an update of the future., Macromol. Biosci. 4 (2004) 551–64. doi:10.1002/mabi.200400023.

[6] J. Dorgan, H. Lehermeier, M. Mang, Thermal and rheological properties of commercial-grade poly (lactic acid) s, J. Polym. Environ. 8 (2000) 1–9. http://link.springer.com/article/10.1023/A:1010185910301 (accessed July 3, 2013).

[7] K. Ho, A. Pometto, P. Hinz, Effects of temperature and relative humidity on polylactic acid plastic degradation, J. Environ. Polym. Degrad. 7 (1999) 83–92. http://link.springer.com/article/10.1023/A:1021808317416 (accessed July 3, 2013).

[8] D. Garlotta, A literature review of poly (lactic acid), J. Polym. Environ. 9 (2001) 63–84. http://link.springer.com/article/10.1023/A:1020200822435 (accessed July 3, 2013).

[9] R. a. Auras, B. Harte, S. Selke, R. Hernandez, Mechanical, Physical, and Barrier Properties of Poly(Lactide) Films, J. Plast. Film Sheeting. 19 (2003) 123–135. doi:10.1177/8756087903039702.

[10] E.T.H. Vink, K.R. Rábago, D. a. Glassner, P.R. Gruber, Applications of life cycle assessment to NatureWorks™ polylactide (PLA) production, Polym. Degrad. Stab. 80 (2003) 403–419. doi:10.1016/S0141-3910(02)00372-5.

[11] R. Langer, M. Chasin, Biodegradable polymers as drug delivery systems, 1990. http://ajprd.com/downloadebooks_pdf/38.pdf (accessed April 18, 2014).

[12] M. Labet, W. Thielemans, Synthesis of polycaprolactone: a review., Chem. Soc. Rev. 38 (2009) 3484–504. doi:10.1039/b820162p.

[13] M.F. Weber, Giant Birefringent Optics in Multilayer Polymer Mirrors, Science (80-.). 287 (2000) 2451–2456. doi:10.1126/science.287.5462.2451.

[14] E. Edwards, A Proposal for the Development of A Unifying Method of Designing a Wide Range of Time-Temperature Indicators Using Frozen-In Birefringence in Non-Mesogenic Polymers, Brown University, 2007.

[15] PerkinElmer, Differential Scanning Calorimetry (DSC) A Beginner ’ s Guide, (2014) 1–9.

[16] W.D. Callister, D.G. Rethwisch, Fundamentals of Materials Science and Engineering: An Integrated Approach, Wiley, 2012. https://books.google.com/books?id=-b2Tn74L6K0C.

Chapter 2:

Effect of pressure on poly-L-Lactic Acid morphology

Christopher M. Baker Sc.M., Aharon Azagury Ph.D.,

Edith Mathiowitz Ph.D.

The following chapter was accepted for publication in Polymer.

2016; DOI: 10.1016/j.polymer.2016.07.028

Abstract:

When exposed to pressures below and above its glass transition temperature (T_g) over time, both the amorphous and crystalline regions of Poly-L-Lactic Acid (PLA) can be oriented. The most pronounced effect was the existence of an intense birefringence which lacked any sign of crystalline structure as observed by polarized light microscopy as well as the existence of a non-birefringent area in some of the same samples. Differential Scanning Calorimetry (DSC) analysis of the birefringent areas revealed decreased enthalpy of relaxation (ΔH_{ER}) and specific heat capacity (ΔC_P) values as well as the existence of at least two T_g's when samples were treated at 63 °C and above, indicating increased orientation of the amorphous region. These same samples additionally displayed increased crystallinity which was depicted by an increased enthalpy of crystallization (ΔH). Additionally, X-Ray Diffraction (XRD) revealed a shift from an amorphous to a crystalline structure. Regions that did not display intense birefringence revealed minimal changes in T_g, ΔH_{ER}, and ΔC_P.

1. Introduction

Poly-L-Lactic Acid or PLA is a semi-crystalline thermoplastic polymer belonging to the family of aliphatic polyesters and possess' many beneficial properties such as high strength and modulus, similar transparency to Polyethylene Terephthalate (PET), good vapor blocking properties and biodegradability.[1–3] Aliphatic polyesters such as PLA are widely used in the medical field for the production of products such as bioresorbable sutures, drug eluting systems, and structural implants such as bone fixation devices. These materials are chosen as their bioresorbable nature is beneficial in many ways. One important benefit of which is that the patient would not require any additional intervention to remove the device. However, the polyesters used in these devices are often limited in their ultimate effective lifetime due to the materials structural orientation and order. It is well understood that polyester based materials possessing higher degrees of crystallinity or less accessible amorphous chains would hydrolytically degrade at slower rates. Additionally, materials possessing higher degrees of crystallinity are also observed to poses higher mechanical strength in comparison to their more amorphous counterparts.

PLA is predominately synthesized utilizing ring opening polymerization techniques which are capable of producing high molecular weight PLA's.[2,4–10] PLA's physical properties include a glass transition temperature that ranges from 55-65 °C and melting temperature of 155-165 °C with dependence on the morphological order inherent in the material.[1] Coincidently, the materials

characteristics are strongly associated with its glass transition and the degree of morphological order which impact the material's properties such as density, degradation rate, strength, flexibility, specific heat capacity, and approach towards thermal equilibrium or enthalpy.[1,8,11–13] Amorphous PLA has been found to hold density values of 1.248 g/mL while crystalline PLA due to its increased physical order, holds a density value of 1.290 g/mL.[1] Crystalline PLA is thus stronger yet less ductile than amorphous PLA. These properties are also strongly dependent on the polymers history and all the processing conditions that the polymer has been exposed to.

Additionally impactful on the polymers properties, is the process known as enthalpic relaxation or physical aging. Enthalpic relaxation is the process whereby a glass like material approaches a state of thermal equilibrium through the release of excess free energy (enthalpy) by means of structural/chain segment realignment and consequential loss of free volume with dependence on the materials proximity to its glass transition temperature and the time it remains there. [3,9,13–28] Celli Et al. showed that PLLA samples stored below their glass transition temperature at 30, 40, and 48 °C progressed respectively towards increasingly higher ΔH_{ER} values of 2.0, 2.9, and 3.8 J/g with relaxation time fixed at 22 h.[29] Additionally, Celli Et al. showed that when the annealing temperature was kept constant at 30°C, PLLA's ΔH_{ER} increased from 2.0 to ≈ 3.5 J/g when annealing time increased from 2.5 to 22 hours respectively.[29] Cai Et al. was also able to show that when PLA was aged at room temperature, that an increase in ΔH_{ER} from 3.79 to a high of 4.91 J/g could be observed when aged

for 144 h to one month respectively.[30] Cai Et al. also observed increases in the T_g when PLA was aged at 50 °C, which is thought to be due to a reduction in the materials free volume or subsequent reduction of molecular mobility.[30] Free volume or molecular mobility may be quantified by calculating the specific heat capacity of the T_g. Upon enthalpic relaxation of materials it is known that the polymer chains tighten up and lose their excess free volume and stored rotational energies as they relax. Tan Et al. were able to show this when aging poly (aryl ether ether ketone ketone) or PEEKK at two specific temperatures of 130 °C & 140 °C.[31] Tan showed that ΔC_P progressively decreases when PEEKK is aged at 130°C between 60-570 minutes such that the ΔC_P value dropped from 0.27 J/g °C to a low value of 0.24 J/g°C.[31] Additionally, Tan Et al. also showed that increasing the aging temperature to 140°C and aging time to 1140 minutes could cause further decreases in ΔC_P to a low of 0.21 J/g°C.[31] Thus a materials path to thermal equilibrium, while complex, is shown to be directly related to the temperature difference between the materials glass transition and the temperature which the material is stored (aging temperature) as well as the duration for which it is stored there.[22,28] Unfortunately, this structural realignment and loss of free volume often comes at a detrimental cost to the materials physical properties. This is most often observed as a loss of ductility and or fracture toughness which can limit the ultimate usability of the material, especially when strength or durability is of importance.[8,9,13,14,32] This process could be slow though, often taking months to years depending on the materials proximity to its glass transition temperature in storage.

The lifetime and usefulness of a material as mentioned previously is not only affected by aging but also by the processing conditions with which the material has been treated. Thus this paper shall discuss the effects of applying pressure on the morphological and thermal properties of polymeric materials. Like Celli Et al. & Cai, Wang was able to show that aging the amorphous polyester Poly (ethylene terephthalate (PET) with a T_g of 76 °C at 65 °C would increase ΔH_{ER} from 1.8 to 4.25 J/g when aging for 0 to 100 h respectively.[33] However, he included the effects of applying pressure stresses at specific temperatures over time. Wang showed us that by applying 500 MPa (≈72,000 psi) of pressure for a period of 10 min at room temperature, the effects of aging or rejuvenation of the amorphous polymer could be reversed by increasing the density and decreasing the ΔH_{ER} of the polyester.[33] To explain this phenomena he states that the concept cannot be explained simply by increases or decreases in the specific volume of the amorphous material but may be resultant of the disruption of the materials cohesional entanglement spacing.[33] This in turn leads to what he terms as a less ordered or higher in energy state than what is observed in aged glasses.[33] The effects of these aging and processing conditions can be assessed through the use of DSC and XRD analysis.

The aim of the current paper is to investigate the effect of applying high pressure stresses at different temperatures over specific periods of time on the morphology of both the amorphous and crystalline states of the commercially available Poly-L-Lactic Acid based film, in hopes of developing a systematic approach for evaluating homogeneity in film or melt cast polymers.

2. Materials and Methods

2.1 Preparation of Poly-L-Lactic Acid

The PLA was donated from Spartech® Packaging Technologies (Spartech, Kohler, Wisconsin) for scientific use. Upon receiving the PLA sheets, 1 inch x 1 inch x 0.32 inch squares were cut from the bulk material. The samples were then placed in individual containers and stored on the bench top at room temperature.

2.2 Processing of Poly-L-Lactic Acid

PLA samples were used as received from Spartech® as they were already in a sheet form. Samples were individually subjected to specific pressure (2,000 lbs, 5,000 lbs, 10,000 lbs, 15,000 lbs, 20,000 lbs) and temperature (52 °C, 63 °C, 74 °C, 85 °C) stress profiles over periods of time (5 min, 10 min, 15 min). Samples were placed between two 4 inch x 4 inch stainless steel plates. The samples were then subjected in a heating/cooling capable Carver Auto Series Hydraulic Press (Carver, Wabash, Indiana) to discrete stress profiles. These profiles began with an initial heat up cycle with a target end temperature both below and above PLA's glass transition temperature (T_g) of 64.37 °C. Upon reaching the temperature set point, pressure was increased to the desired condition. Once both the desired temperature and pressure conditions were met, the samples were maintained in a fixed temperature/pressure condition for a period of time (5, 10, or 15 min). Afterwards the samples were cooled to 22°C

over a 5 min period and released from the press. Additional samples were also produced for comparison purposes by both melt casting PLA on a glass slide as well as solvent casting using a 10% (w/v%) solution of polymer in methylene chloride. These dry samples were used to visualize the spherulitic structure of the material under polarized light.

2.3 Chemical Analysis

A Perkin Elmer Spectrum One Fourier Infrared Transform Spectroscopy (FTIR) unit (Perkin Elmer, Shelton, Connecticut) was used. Transparent PLA sheet samples were analyzed using a sample holder in the path of the transmission beam. In addition, the samples were soaked in two solvents, acetone and ethanol. The extracts derived from soaking the PLA were then solvent evaporated on a NaCl crystal (Sigma-Aldrich, St. Louis, MO) for analysis.

2.4 Size Exclusion Gel Permeation Chromatography

A Gel Permeation Chromatography (GPC) system configured for size exclusion (Perkin Elmer Flexar Ultra High Performance Liquid Chromatography system Totalchrom WS MI software V 6.2 Perkin Elmer, Shelton, Connecticut) was used to determine molecular weight. Transparent PLA sheet samples were dissolved in HPLC grade Tetrahydroflurane (THF) (Fisher Scientific, Pittsburgh, Pennsylvania), filtered with a .22µm filter and run through two serially connected Waters HR 4 & HR 5E Columns (Waters, Milford, Massachusetts) at a flowrate of 1 mL/min. The GPC was calibrated using a monodisperse polystyrene standard.

2.5 Thermal Analysis

A DSC (DSC 7 with Pyris software, Perkin Elmer, Shelton, CT) was used. The DSC was calibrated with a pure indium standard at a heat up rate of 10 °C/min. Samples (3-5 mg) weighed on a Perkin Elmer AD.4 Microbalance (Perkin Elmer, Shelton, CT) were analyzed under dry nitrogen purge conditions. Samples were cooled to -25 °C and held for a period of one minute prior to commencing the DSC cycle. Samples were cycled from -25 °C to 200 °C at a rate of 10 °C/min. Once at 200 °C, samples were held for a period of one minute and then cooled from 200 °C to -25 °C at a rate of 10 °C/min and then once gain held for one minute at -25 °C. Samples were then reheated from -25 °C to 200 °C at a rate of 10 °C/min. Glass transition temperature (T_g), Δ Specific Heat Capacity (ΔC_P), Enthalpic Recovery (ΔH_{ER}), and Enthalpy of Crystallization (ΔH) were then calculated using Pyris software (Perkin Elmer, Shelton, CT).

2.6 Structural Analysis

X-Ray Powder Diffraction (XRD) was performed using a Bruker D-8 Advance X-Ray Powder Diffraction system running DaVinci Software and a Cu X-Ray tube operating at 40 kV and 40 mA equipped with a Bruker Vantec-500 Xe-CO_2 gas filled detector with a 13.5 cm diameter window set at 20 cm from the goniometer center. The system optics consisted of a polycap with an output beam divergence of 0.25° for Cu and a spot diameter of less than 4.0 mm and a 79 mm long 0.3 mm collimator on the incident beam path (Bruker, Billerica, Massachusetts). Scans were run from 15°- 70° 2θ with a virtual step size of 0.02°

and a counting time of 30 s per step. Upon completion of the scan, data was analyzed using the Bruker Diffrac-Eva software package (Bruker, Billerica, Massachusetts).

2.7 Polarized Light Microscopy

Polarized light microscopy was performed using an Olympus Model BX-60 (Olympus, Center Valley, Pennsylvania) microscope equipped with polarized filters and 10X & 50X objectives. Images were captured utilizing a PixeLINK (PixeLINK, Ottawa, Canada) model PL-E421CU color enabled camera running PixeLINK Capture OEM Software Version 2.3.5.0 (PixeLINK, Ottawa, Canada).

3. Results and Discussion

3.1 Treatment of the PLA Samples

Figure. 1. is a diagram depicting the processing procedure used to pressure treat the PLA as described in section 2.2. The first temperature of 52 °C was chosen as it fell well below the glass transition of the untreated PLA (64 °C). The second temperature of 63 °C was chosen to obtain a better understanding of how the material would behave when pressed just below the glassy/rubbery transition point. Finally, to provide a view of how the material would react to processing in a rubbery state we chose two temperatures above glass transition at 74 °C and 85 °C yet well below the melting temperature of 150 °C. Upon lapse of time t, the samples were cooled to T_C with P maintained. Once cooled to T_C, the pressure P was terminated and the sample released for further

analysis. Table. 1SI. (Supporting Information) provides a full accounting of all parameters explored in this characterization study. In total, 60 different processing conditions were analyzed.

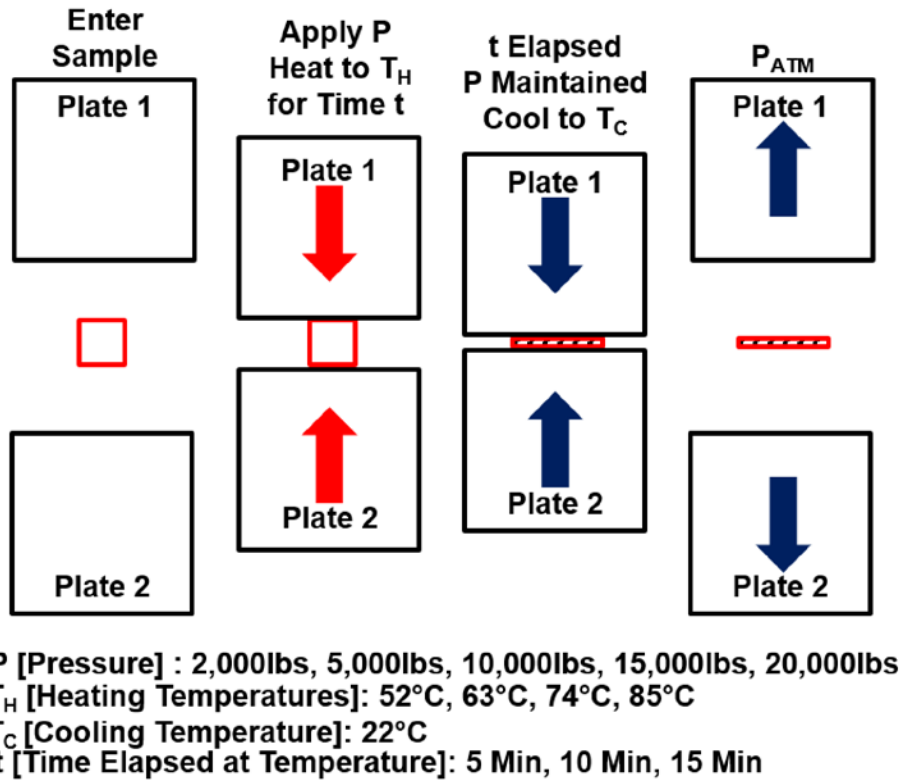

Figure. 1. Schematic representation of the process. Samples are placed into the Carver Auto Press and exposed to pressures (P) ranging from 2,000 lbs to 20,000 lbs at temperatures (T_H) ranging from 52 °C to 85 °C for a period of time (t). Once the prescribed time has elapsed, samples are cooled to the temperature (T_C) and released from the press.

Prior to treating the material, XRD and polarized light microscopy images taken revealed a rather amorphous structure in the material as received which is depicted in Figure. 2. Prior to treating the material, samples were found to possess a thickness of 0.032 in. This however quickly changed in response to both changes in pressure and temperature. Ultimately we achieved a maximum

reduction in thickness of 56.25% and a maximum increase in surface area of 55.0% as depicted in Table. 2. SI. This sample deformation resulted in quite an intense change in the materials birefringence as observed under polarized microscopy. Figure. 3. depicts full size images from left to right of 5 typical examples starting from the untreated material to samples treated at each of the temperatures. Upon treatment, each sample displayed a different level of birefringence intensity which was indicative of some degree of orientation. Most samples excluding the 52 °C cohort were quite homogeneously birefringent. While some had specific dark regions, especially in the middle of the sample without any visually apparent orientation, indicating an amorphous structure. What was very interesting is the lack of spherulites and lamellar structures in the PLA samples which are usually found for the same material upon being either melt or solvent casted (see Figure. 4.) These polarized light results were the motivation to start the process of systematically evaluating both the oriented as a well as the disordered regions through both thermal and XRD analysis.

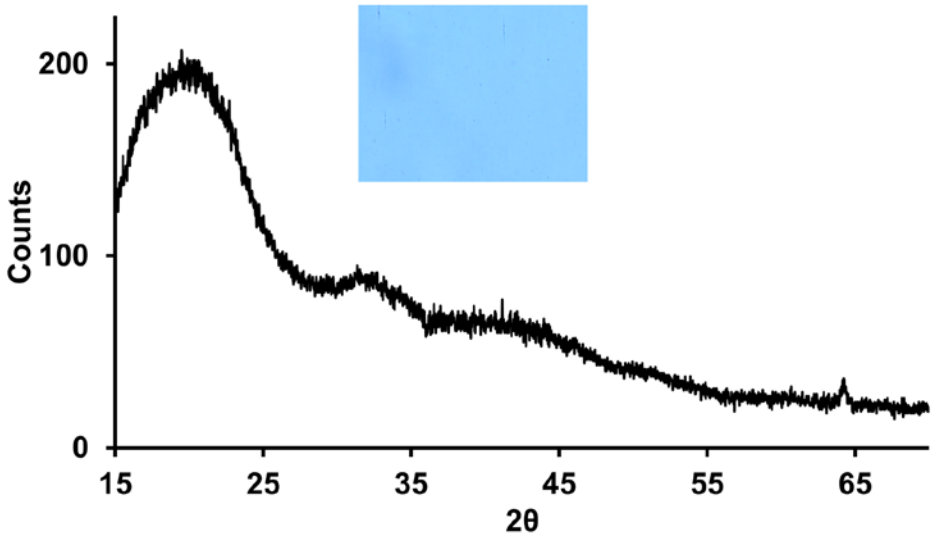

Figure. 2. XRD profile of the untreated PLA as received with polarized microscopy image.

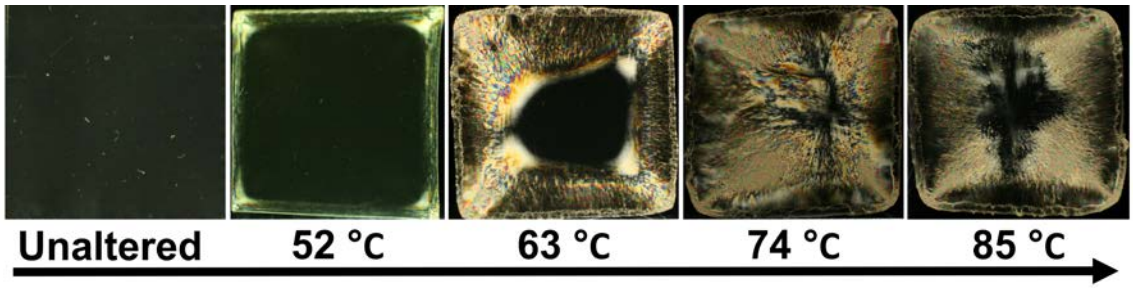

Figure. 3. Crossed polarized images of PLA both before and after treatment.

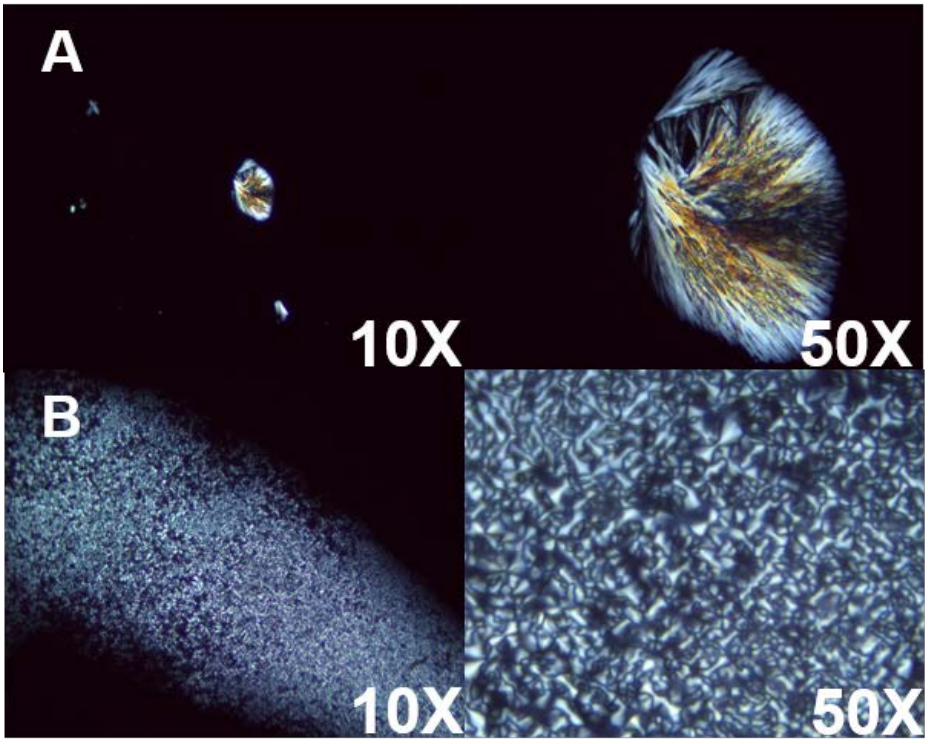

Figure. 4. Crossed polarized microscopy image of PLA after being solvent casted (A). Crossed polarized microscopy image of PLA after being melt casted (B).

3.2 Characterization of the Original PLA Film

The FTIR analysis of the PLA is represented in Figure. 5. The first interferogram plot (black line) labeled PLA depicts the material as received and displays the typical FTIR peaks associated with PLA which occur at approximately 1080-1180 cm^{-1} (RCOOR), 1750 cm^{-1} (C=O) and 2950-3000 cm^{-1} (CH_3). The next FTIR plot (red line) depicts the purified polymeric material after extraction in acetone. This extraction was performed to determine the presence of excipients in the films that were received. The material continues to display characteristic peaks associated with PLA. The next plot (green line) depicts PLA

sample after extraction in acetone, the same indicative peaks of PLA are present. Lastly, the (blue line) depicts an unknown excipient which was found in the ethanol extraction media, and may possibly be either a proprietary additive used by the manufacturer or it could also be a low molecular weight PLA component which was extracted and is soluble in acetone.

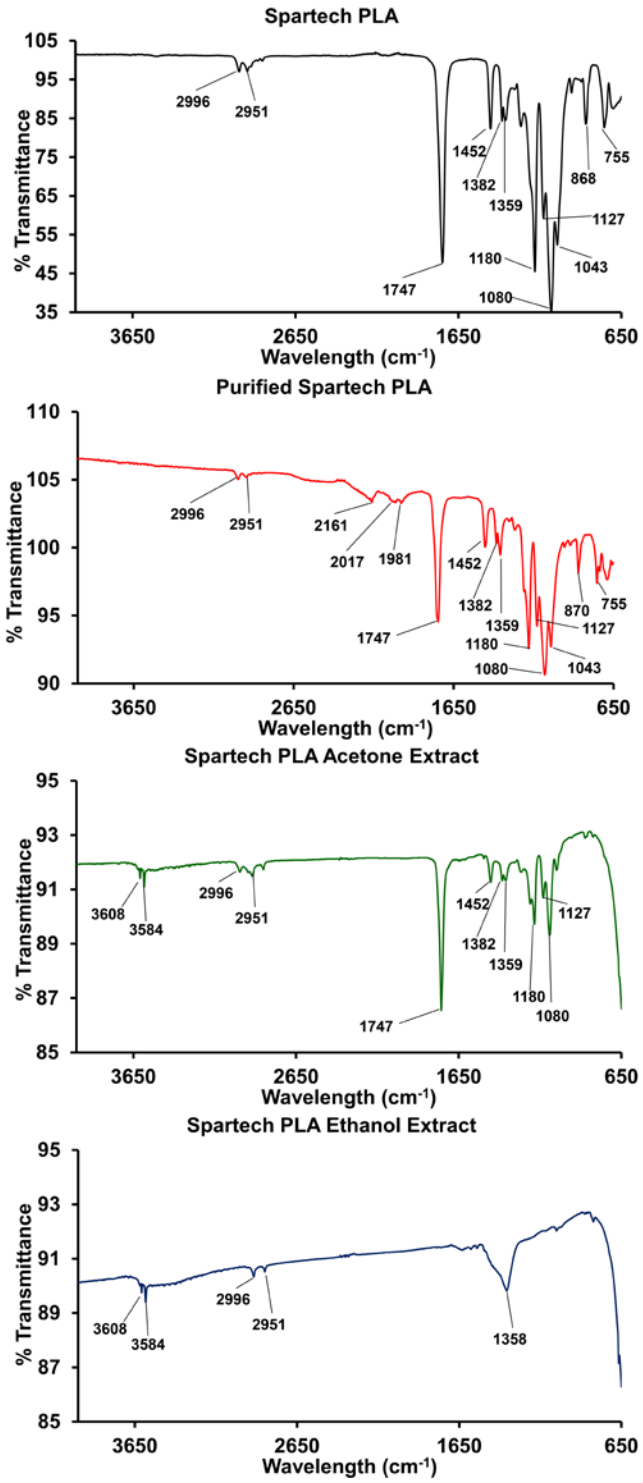

Figure. 5. FTIR analysis of the PLA. Typical peaks associated with PLA may be found at the following wavelengths (O-H [1330-1420] [3400-3700] CH_3 [2950-3000] C=O [1747] RCOOR [1080-1180])

3.3 GPC Characterization of the PLA

GPC analysis (Figure. 6.SI) revealed that the polymer had a weight average molecular weight (Mw), of 253 kDa and number average molecular weight (Mn) of 11.8 kDa. Poly Dispersity (Mw/Mn) of 21.318**.**

3.4 Thermal Characterization of the Amorphous Region

The objectives of this section were to determine the thermal changes which occurred in the amorphous state as a result of treating the material. Thermal analysis of the PLA as received is depicted in Figure. 7A.SI The PLA's first heat glass transition temperature was determined to be 64.37 °C and falls within the known literature values of 55-65 °C for PLA.[1] Initial first heat analysis reveals an ΔH_{ER} of 5.73 J/g and ΔC_P of 3.16 J/g°C upon heating and will along with this calculated T_g, serve as a point of reference for the discussion of the effects of the processing conditions on the PLA's properties. The materials second heat analysis for the untreated and treated samples as well as for all other samples was found to be close to 59.5 °C. Second heat analysis revealed a typical ΔH_{ER} of 2.00 J/g and ΔC_P of 0.60 J/g°C. Interestingly, when processing the polymer at 20,000 lbs and 85 °C for 15 min, both a reduction in ΔH_{ER}, ΔC_P and T_g location were observed. This change is depicted in Figure. 7B.SI. The samples T_g was 61.79 °C with a first heat analysis also showing a dramatic drop in ΔH_{ER} from the original value of 5.73 J/g to 1.30 J/g after treating. ΔC_P was observed to decrease to 0.822 J/g°C. Finding these decreases in T_g, ΔH_{ER}, and ΔC_P further motivated us to systematically study the amorphous region after

processing the samples under different treatment conditions which are listed in Table. 1.SI.

The T_g, ΔH_{ER}, and ΔC_P for each treatment were calculated from the data acquired by the DSC profiles depicted in Figure. 8.

Figure. 8. is arranged in the following manner. Each individual box contains 4 pairs of DSC graphs representing the first heat (solid line) and the second heat (dotted line) of each temperature condition used (52 °C, 63 °C, 74 °C, 85 °C). The boxes are organized by rows such that each row corresponds to the same specific pressure applied (for example the bottom row is 2000 lbs) and each box along the row represents an increasing period of time for the duration of that pressure (increases from left to right (5,10,15 min)), columns are ordered such that pressure increases as one progresses up each individual column. Figure. 8. will be discussed in detail in section 3.4.1 and 3.4.2 by addressing the effect of each treatment parameter.

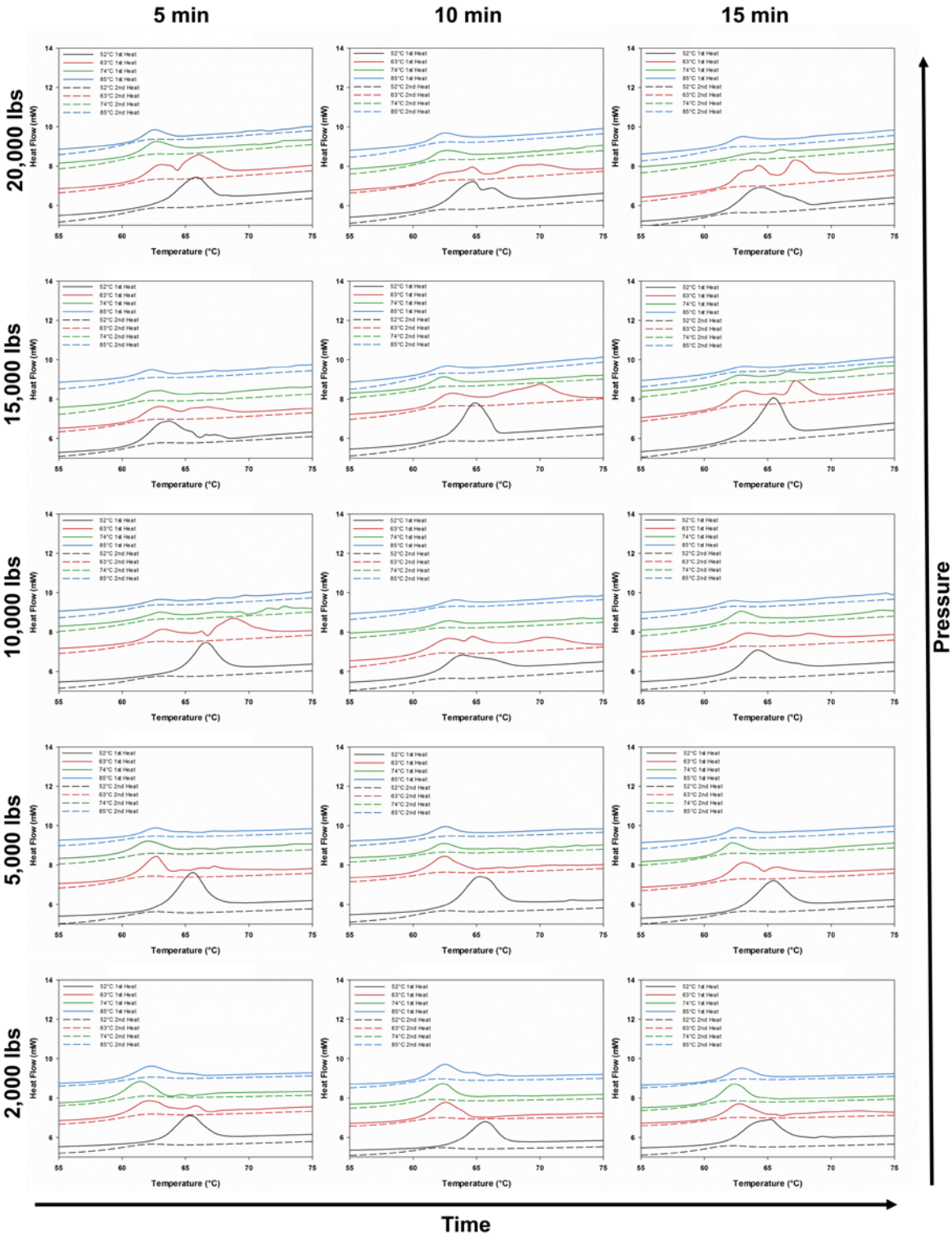

Figure. 8. Effects of applying different pressures at temperatures below and above the T_g of the PLA over specific periods of time. (Solid Line-1st Heat, Dotted Line-2nd Heat, Black-52 °C, Red-63 °C, Green-74 °C, Blue-85 °C)

In addition, to make the evaluation of the DSC data easier; the T_g, ΔH_{ER}, and ΔC_P values were graphed respectively in Figures. 9-11. (Numerical values may be found in the supporting materials, Table. 3.A-C.SI).

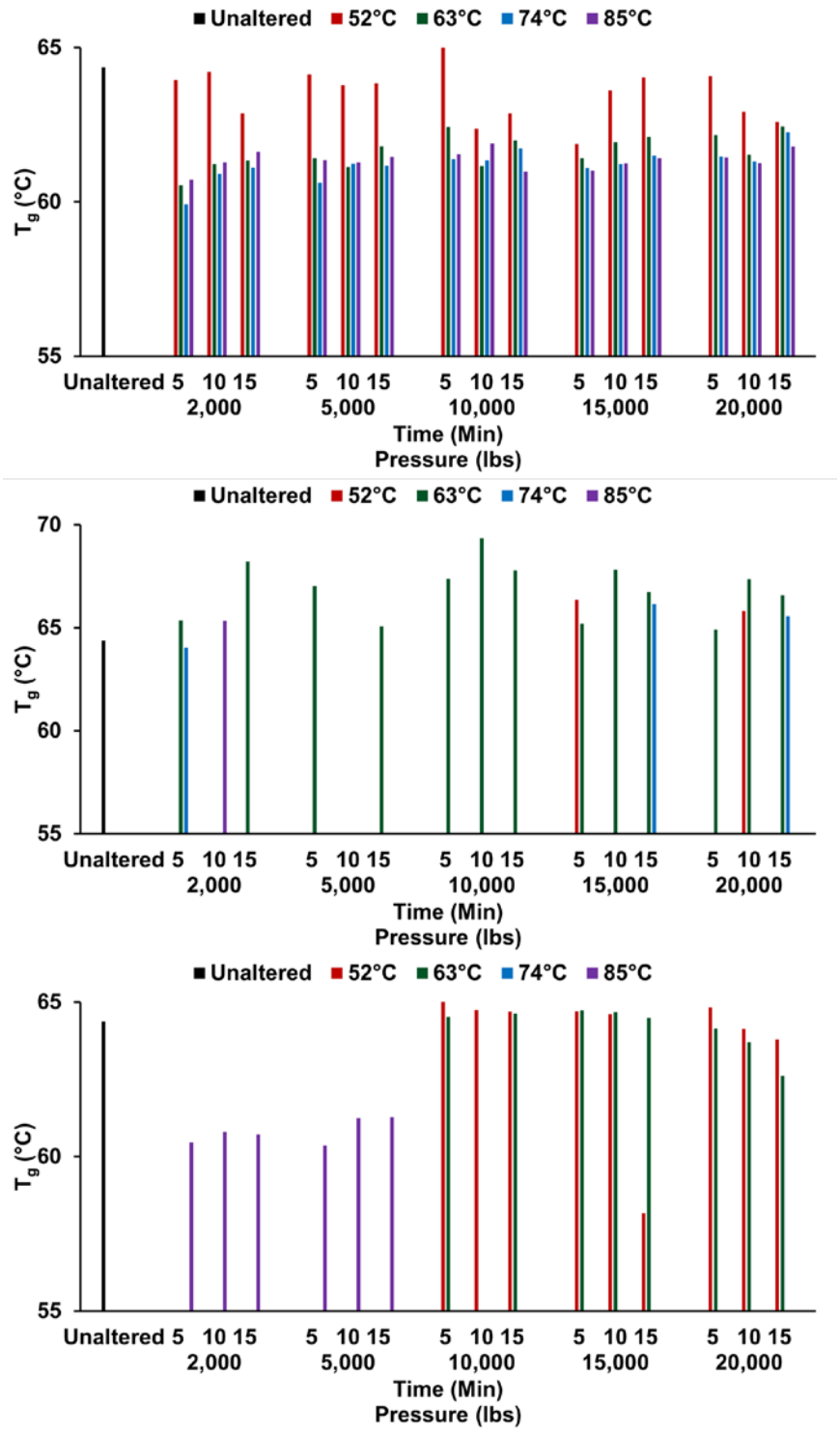

Figure. 9. Effect of processing conditions on T_g. (Top) 1st Heat T_g of samples displaying birefringent area. (Middle) Additional 1st Heat T_g of samples displaying birefringent area. (Bottom) 1st Heat T_g of samples displaying no birefringence area.

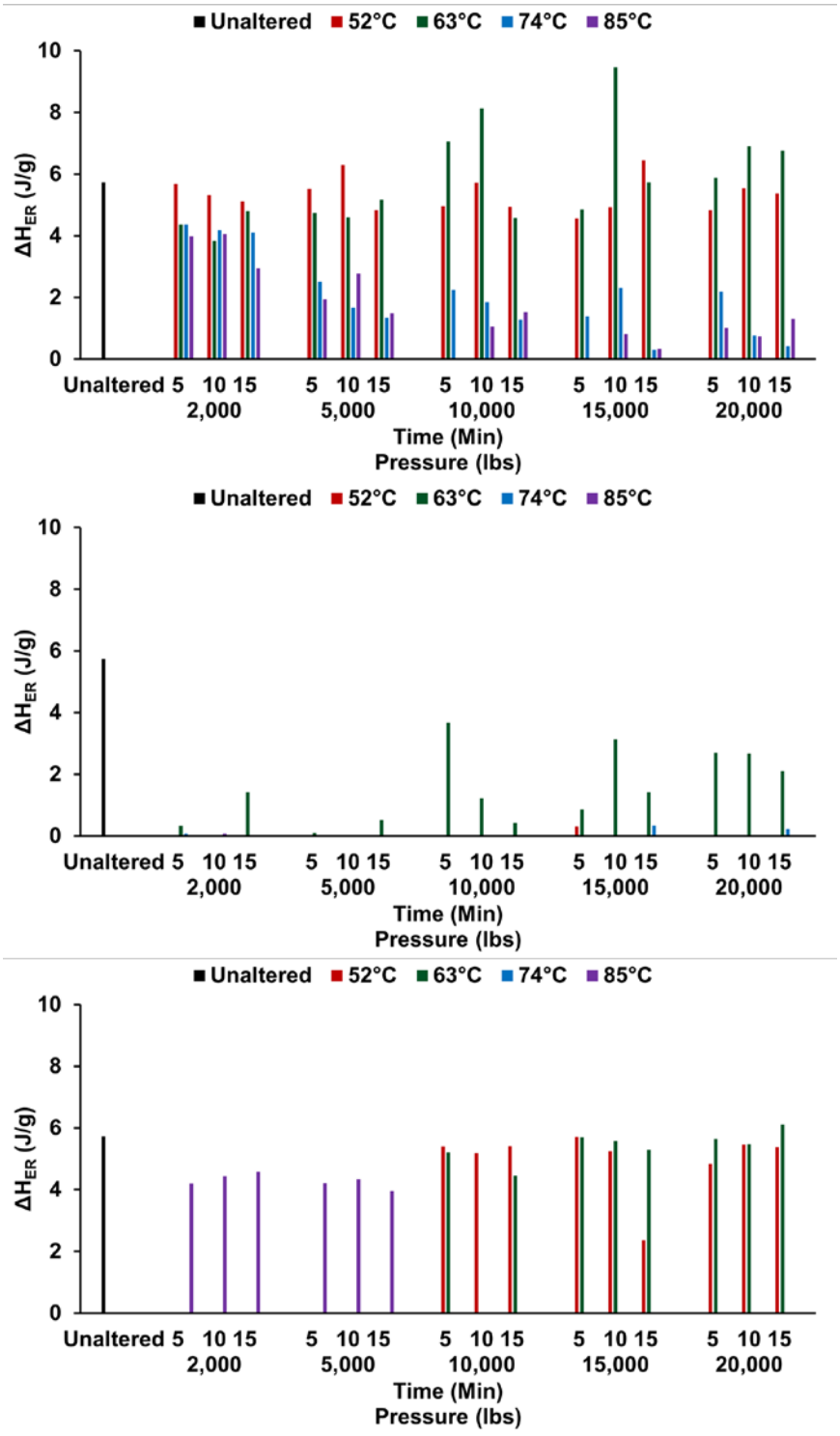

Figure. 10. Effect of processing conditions on ΔH_{ER}. (Top) 1st Heat ΔH_{ER} of samples displaying birefringent area. (Middle) Additional 1st Heat ΔH_{ER} of samples displaying birefringent area. (Bottom) 1st Heat ΔH_{ER} of samples displaying no birefringence area.

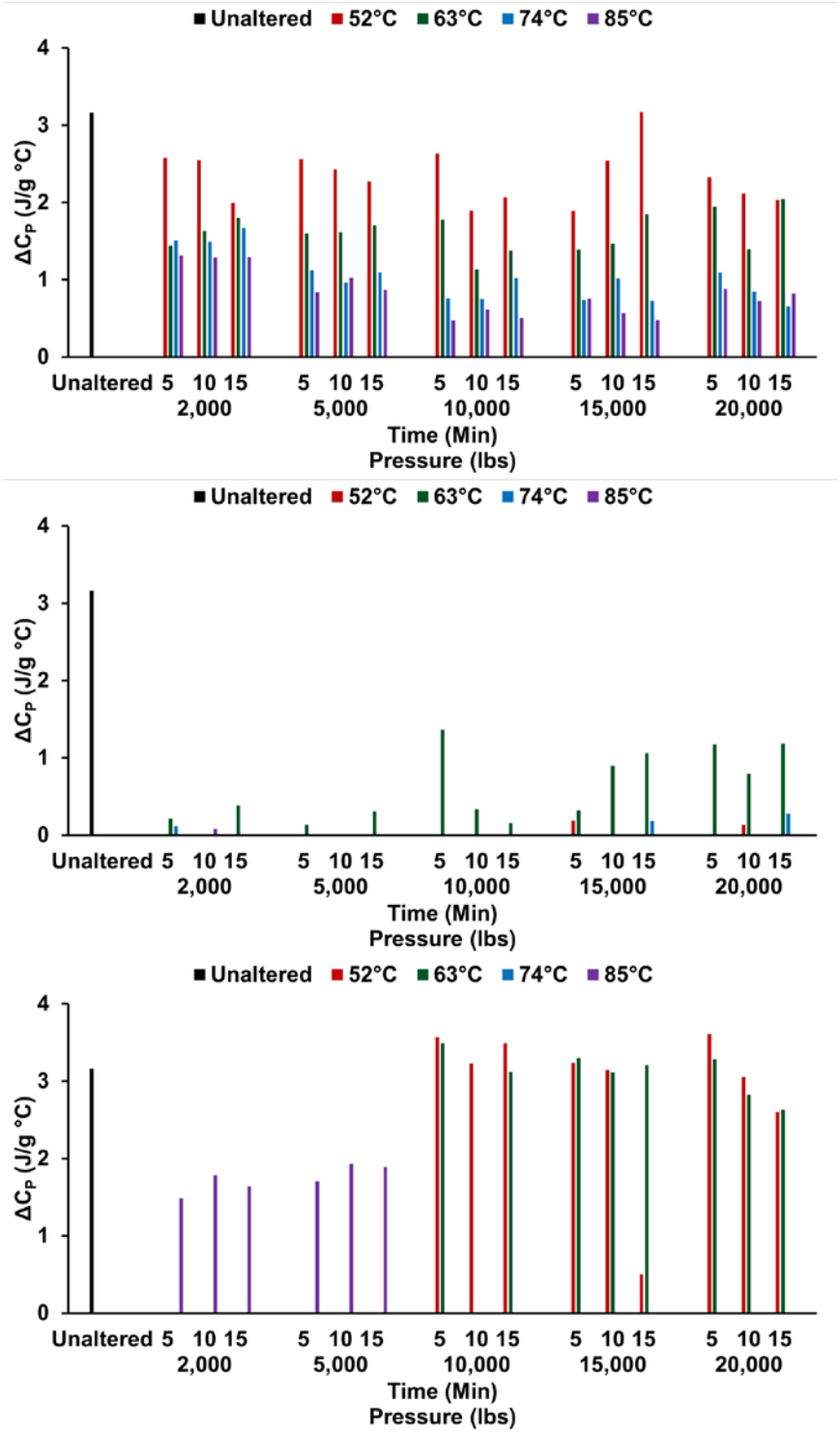

Figure. 11. Effect of processing conditions on ΔC_P. (A) 1st Heat ΔC_P of samples displaying birefringent area. (B) Additional 1st Heat ΔC_P of samples displaying birefringent area. (C) 1st Heat ΔC_P of samples displaying no birefringence area.

3.4.1 DSC Analysis of the Amorphous Region: Effect of Altering Processing Temperature on T_g, ΔH_{ER}, and ΔC_P when Pressure is Constant.

In order to analyze the large amount of DSC data present in Figure. 8. it was necessary to focus the discussion by fixing the pressure variable as the temperature variable changed. This section will discuss the trends observed as the treatment temperature is increased. Taking a broad look at Figure. 8., the first notable trend is that the treatment process has led to the creation of two or possibly more amorphous populations that possess their own respective T_g's both below and above the untreated materials T_g of 64 °C. These T_g's were also found to consistently remain higher than the T_g of the materials second heat value of 59 °C. Additionally, the materials respective values of ΔH_{ER} and ΔC_P were observed to consistently decrease below the untreated materials values in a temperature dependent fashion.

2,000 lbs:

Focusing on the bottom row of Figure. 8. which is representative of the samples treated under 2,000 lbs for three periods of time (5, 10 and 15 min). The first things that becomes clear is that treating the material at 52 °C produced minimal decreases in the T_g as depicted in Figure. 9.. Contingent with this minimal change in T_g, almost no change in the materials ΔH_{ER} was observed in Figure. 10. with a small decrease being noted in the materials ΔC_P values in Figure. 11.. This however changes drastically when treating the material at 63 °C

or higher as we not only observe an immediate decrease in the materials T_g, ΔH_{ER} and ΔC_P values but we also observe the beginnings of an additional T_g at lower temperature. The formation of which may be indicative of a new amorphous phase in the material and shall be explored as the discussion continues. Increasing the treatment temperature above 63 °C to 74 °C and 85 °C was found to progressively decrease the observed values for T_g, ΔH_{ER} and ΔC_P. Additionally, increasing the temperature lead to a broadening of the multiple higher temperature T_g's making them difficult to discern separately.

5,000 lbs:

Moving upward to the second row of Figure. 8. for materials treated at 5,000 lbs for 5, 10, and 15 min and whose T_g, ΔH_{ER} and ΔC_P values are graphed in Figures. 9-11. Interestingly, the formation of a T_g at lower temperature is once again observed, especially when the material is treated at 63 °C and above. In this series, the trend of decreasing T_g, and decrease in ΔH_{ER} and ΔC_P values continues with increasing temperature. However, the T_g at higher temperatures also had lower ΔH_{ER} and ΔC_P values and is only discernable for samples treated for 5 and 15 min.

10,000 lbs:

Moving up to the third row of Figure. 8. for materials treated at 10,000 lbs for 5, 10, and 15 min. In this series, we once again observe a trend where the values of T_g, ΔH_{ER} and ΔC_P in Figures. 9-11. decrease in response to increasing treatment temperature. However, it is this pressure condition we observe a

definitive formation of a second $T_{g,}$ especially when the material is treated at 63 °C and above. These additional $T_{g's}$ while also apparent in samples processed at 74 °C and 85 °C are quite subtle in appearance. In some cases, we may even observe three glass transitions as depicted in the sample treated for 10 min.

15,000 lbs:

Moving to the fourth row of Figure. 8. for materials treated at 15,000 lbs for 5, 10, and 15 min. It is once again apparent that increasing the treatment temperature leads to a decreasing trend in the values of the lower T_g and their respective ΔH_{ER} and ΔC_P values depicted in Figures. 9-11.. In this series, the 52 °C samples begin to display multiple T_g's in the 5 min cohort with decreased ΔH_{ER} and ΔC_P values. While the 63 °C samples consistently display two very distinct T_g's, falling both above and below the untreated samples original T_g. Increasing the treatment temperature above 63 °C at this pressure appears to diminish the appearance of the higher T_g, yet it still remains subtly visible in the samples processed at both 74 °C and 85 °C.

20,000 lbs:

Progressing to the fifth and final row of Figure. 8. for materials treated at 20,000 lbs for 5, 10, and 15 min, increasing the treatment temperature leads to decreases in the lower T_g, ΔH_{ER} and ΔC_P in Figures. 9-11.. In this series, samples processed at the 52 °C temperature and 10 min display the beginning of the formation of a second T_g, yet it remains indiscernible from the first T_g. Moving to samples treated at 63 °C, it is quite apparent that a second and higher in value

T_g has been formed. In this treatment condition, all discernible T_g's were found to possess decreased values of ΔH_{ER} and ΔC_P. Increasing the treatment temperature above 63 °C to both 74 °C and 85 °C was once again found to diminish the higher T_g.

Analyzing the effects of increasing treatment temperature at fixed pressures, it is quite obvious that as the treatment temperature is increased, a considerable amount of changes are specifically being observed in the amorphous region of the polymer. The treatment of the material has led to the creation of at least two amorphous populations, represented by two T_g's.

The first T_g we observed has a lower value of T_g, ΔH_{ER} and ΔC_P compared to those values of the original polymer. Interestingly, the additional or secondary T_g's were found to increase while their values of ΔH_{ER} and ΔC_P decreased. These findings are significant since that in the typical aging scenario without pressure we do not see decreases in the values of ΔH_{ER}. To explain, the typical aging scenario in a polymer is established when a material is brought below its T_g at a rate that prevents the material from reaching thermal equilibrium before entering the slow moving glassy state. Once the material reaches the glassy state, the polymers amorphous chains become effectively frozen thus trapping the excess enthalpy and free volume in its physical structure. The material will however relax or progress towards thermal equilibrium by releasing this excess enthalpy and free volume through small molecular and chain segmental shifts over time which can be quantified by DSC. Thus in a typical aging situation, DSC would reveal an increase in ΔH_{ER} decrease in ΔC_P and

increase in T_g as the material relaxes or loses this free energy on its way to equilibrium through physical relaxation.[13,24] Additionally, Hodge noted that when applying hydrostatic pressures to PVC during cooling that higher enthalpies were noted and associated with shorter enthalpic relaxation times.[21] However, it is observed in our process that this typical behavior does not occur. In our system we observe two T_g's and in both cases ΔH_{ER} decreases along with ΔC_P. This is unexpected and quite interesting as the typical polymer-aging scenario as mentioned previously results in one T_g with an increase in the ΔH_{ER}, as noted previously by Mathiowitz, Wang, and Celli Et al..[28,29,33] These results lead us to believe that the process may be creating a new amorphous phase possessing both a T_g below the original T_g of 64 °C and an amorphous phase whose T_g is observed to increase above 64 °C which may be connected to the crystallization process that is also taking place. This point however, shall be discussed later.

3.4.2 Thermal Analysis of the Amorphous Region: Effect of Altering Processing Pressure on T_g, ΔH_{ER}, and ΔC_P when Temperature is Constant.

While the analysis of the effect of altering the temperature while fixing the pressure variable was quite informative, it was necessary to in turn to briefly analyze the results while fixing the temperature and changing the pressure variable. Thus this section shall discuss the trends observed as the treatment pressure is increased. Once again while taking a broad look at Figure. 8. and its subsequent data plots in Figures. 9-11., the first notable trend is that the

pressure variable may not have had as large of an impact on altering the T_g of the material as did the temperature variable. However, the materials ΔH_{ER} and ΔC_P do display a pressure sensitive response as they decrease in response to increasing pressure.

52 °C:

Focusing on the black lines in Figure. 8. and subsequent data plots in Figures. 9-11. for samples treated at 52 °C for 5, 10 and 15 min. It becomes apparent that the materials T_g does not decrease in response to increasing pressures until pressure reaches 10,000 lbs and above. Additionally, when pressure is increased to 10,000 lbs and above we do observe the formation of a second T_g at low temperatures which may suggest that very high pressures may be needed when processing the material below its initial T_g.

63°C:

Changing our focus to the red lines of Figure. 8. (Data Graphed in Figures. 9-11.) for samples treated at 63 °C for 5, 10 and 15 min. It is this temperature where the formation of two T_g's becomes obvious. Starting at the bottom of Figure. 8. for samples treated at 2,000 lbs we observe a decrease in the first T_g in comparison to the untreated material yet the second T_g is found to increase. This trend continues as pressure increases. Taking the materials first ΔH_{ER} and ΔC_P values into consideration we see a downward trend in comparison to the untreated sample. The second T_g however does appear to be affected by pressure as once we treat the material at 10,000 lbs and above the temperature

of the second T_g increases to values that are even higher than the initial untreated materials T_g of 64 °C. Taking the materials second T_g's ΔH_{ER} and ΔC_P values into consideration, we observe decreasing ΔH_{ER} and ΔC_P values. These results are suggestive of the formation of two amorphous phases whose origin will be discussed in the final discussion section.

74°C:

Changing our focus to the green lines of Figure. 8. (Data Graphed In Figures 9-11.) for samples treated at 74 °C for 5, 10 and 15 min. In this temperature condition we once again observe a decrease in the materials first T_g in comparison to the untreated material. However, when we look at the materials ΔH_{ER} and ΔC_P values at this temperature, we observe a decreasing trend in response to increasing pressure. Additionally, a second T_g is observed to appear above 64 °C. While observed to be subtle due to its low ΔH_{ER} and ΔC_P values, it appears to diminish in intensity as pressure increases. These results further support the hypothesis that the material now possesses multiple amorphous phases with varying degrees of chain entanglement.

85°C:

Ending our discussion on the effects of pressure when the temperature variable is fixed, we bring our attention to the blue lines on Figure. 8. (Data Graphed In Figures. 9-11.) for samples treated at 85 °C for 5, 10 and 15 min. It is at this temperature that the low T_g emerges immediately under all pressure

conditions. ΔH_{ER} and ΔC_P are also observed to decrease in response to increasing pressures.

Enthalpic relaxation as previously defined, is a process whereby a polymers chains approach a state of thermal equilibrium while enthalpy recovery is defined as the returning of that released energy such that the polymer chains regain their lost free volume and rotational energies. Referring to the data from Figure. 8. which is graphed in Figures. 9-11. it may be concluded that applying pressures above the materials glass transition and then cooling that material while pressure is maintained may restrict that polymers chains from randomly orienting and by doing so may reduce the amount of energy that the material must release to relax which would in turn reduce the expected enthalpic recovery. This result could potentially mean that the materials approach to equilibrium could be perhaps pre-tailored to occur over a more determinable time which could lead to better shelf life and further possibilities for applications in material or medical science. It is also of note that materials possessing lower ΔC_P have been shown to resist temperature driven breakdown.[22] This leads us to believe that using the specific sequence of processing may strengthen the material and make it viable for implementation in temperature domains where it was previously unusable.

3.5 Polarized Light Microscopy Analysis of the Amorphous Region

One of the most interesting results in this study was the observation of the polymer under polarized light. Figure. 2. and Figure. 12. (A-C). are a combination of collages that depict all the morphological observations that resulted from the birefringent samples studies. Each sub figure (A-C) is indicative of the specific processing time to which the polymer was exposed, (A) 5 min, (B) 10 min, and (C) 15 min. In addition, each sub-figure contains 5 columns of combined DSC, XRD and polarized light microscopy data. Each column moving from left to right is representative of increasing processing pressure from 2,000 lbs to 20,000 lbs while descending down each row is representative of increasing processing temperature from 52 °C to 85 °C. It is this sections purpose to discuss the results obtained by using polarized light microscopy, which reflects the structural orientation of the amorphous state.[34–37] Materials possessing structural order or alignment will display birefringence when placed between polarizers crossed as 90°, while those materials lacking birefringence (black) are considered amorphous. Thus the presence of birefringence is directly related to the morphology of the polymer and a qualitative indication of changes in its structure. In this particular case, the untreated or unaltered polymer displays a light blue hue as depicted in Figure. 2. while Figure. 4. reveals the material after it was both solvent and melt casted, and depicts the typical spherulitic structure seen in high molecular weight semi-crystalline polymers. By comparing Figure. 2. and

Figure. 4. It is clear that the typical spherulitic structure was not observed in the unaltered PLA which may be a result of the presence of an unknown excipient.

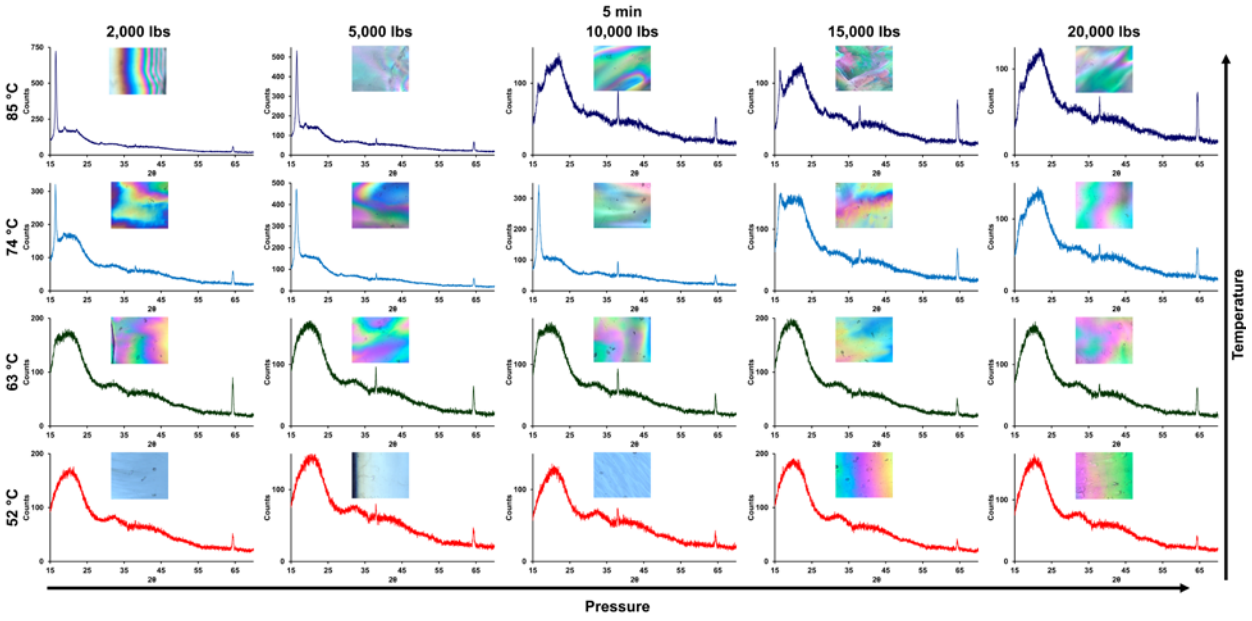

Figure. 12. (A) Effects of processing the PLA for 5 min under all temperature conditions (52 °C, 63 °C, 74 °C, 85 °C) and pressure conditions (2,000 lbs, 5,000 lbs, 10,000 lbs, 15,000 lbs, 20,000 lbs)

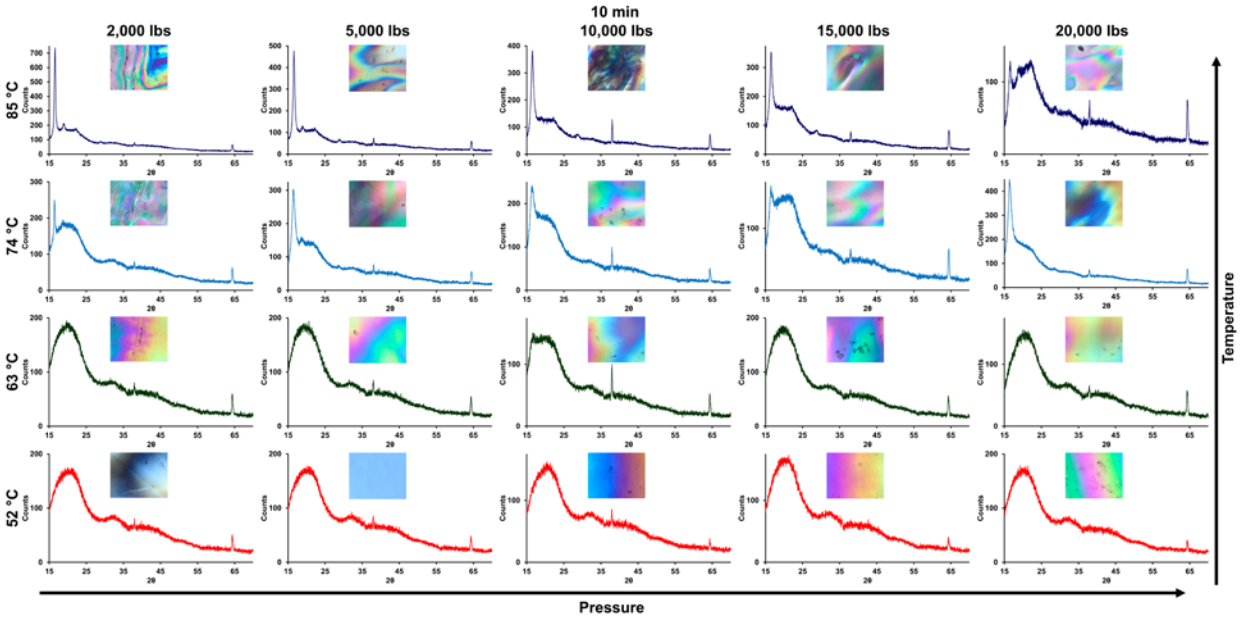

Figure. 12. (B) Effects of processing the PLA for 10 min under all temperature conditions (52 °C, 63 °C, 74 °C, 85 °C) and pressure conditions (2,000 lbs, 5,000 lbs, 10,000 lbs, 15,000 lbs, 20,000 lbs)

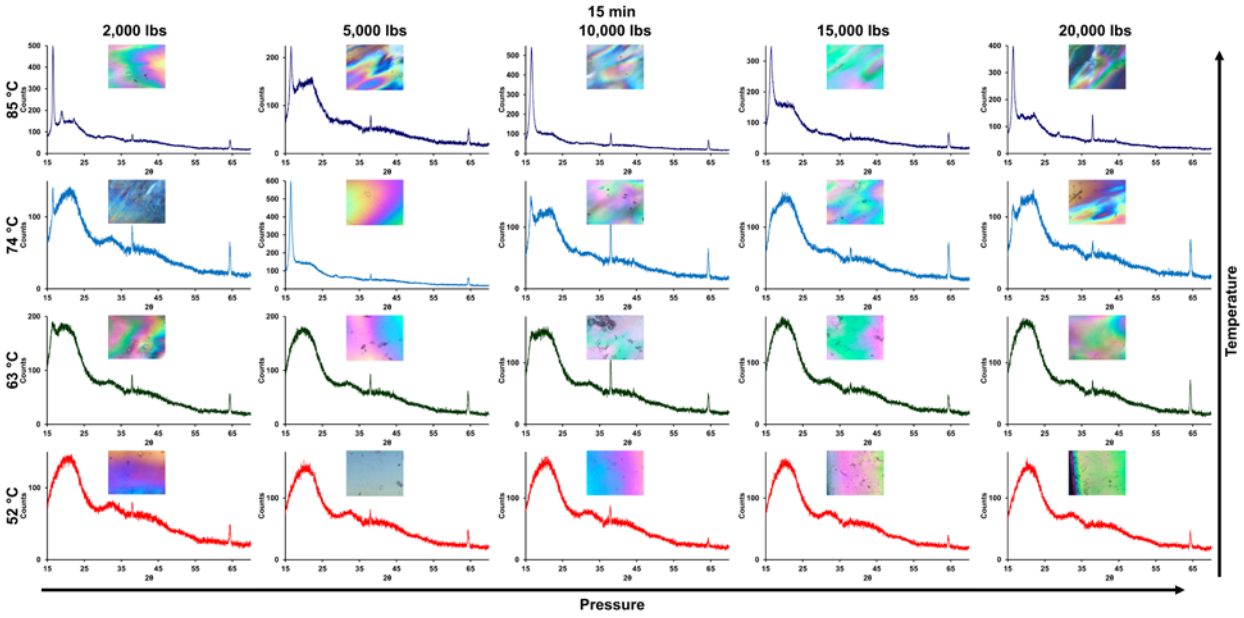

Figure. 12. (C) Effects of processing the PLA for 15 min under all temperature conditions (52 °C, 63 °C, 74 °C, 85 °C) and pressure conditions (2,000 lbs, 5,000 lbs, 10,000 lbs, 15,000 lbs, 20,000 lbs)

The polarized light microscopy images displayed in Figure. 12. (A-C) were taken at a higher magnification than those taken in Figure. 3. where the entire sample was imaged. Figure. 3. initially revealed that the morphology of the treated samples in comparison to the unaltered polymer was quite different. Additionally, to allow for comparison of our treated samples with the expected or typical morphology, Figure. 4. was created to depict the structure obtained when the PLA is either solvent or melt casted, after which it displayed the typically expected spherulitic structure.

Most samples depicted in Figure 12. (A-C) display a diverse birefringent palate as the material is processed under the various conditions. When processing the material at 2,000 lbs, the birefringence appears to be dependent on not only the temperature but also the duration of time that the material is pressed, especially when pressed below the polymers original T_g. In this series, pressing the material for 5 min induces no visible changes while pressing for 10 and 15 min has progressively more impactful alteration of the birefringence. It is noted that in the samples pressed at 63 °C and above, the change in birefringence was consistent and did not depend on processing time. Similar results were obtained for samples processed at 5,000 lbs and 10,000 lbs with the exception that those samples processed at 63 °C, 74 °C, and 85 °C displayed a very intense increase in birefringence without any observable dependence on time. Samples that were processed at 15,000 lbs and 20,000 lbs in the fourth and fifth columns of Figure. 12. (A-C) depict an intense birefringence in all temperature conditions with no apparent dependence on processing time. Additionally, all of the samples

depicted in Figure. 12. (A-C) displayed a birefringence which lacked any apparent lamellar structures, or spherulites like those that were found in Figure. 4., leading us to believe that the amorphous phase is indeed oriented and any crystal structures which are present may be smaller than is visible by optical microscopy.

The results from the polarized light microscopy section combined with the previous section depicting the reduction in ΔC_P and ΔH_{ER} and the formation of multiple T_g's indicates strongly that we are orienting the amorphous phase in most of the samples as pressure is applied. However, since PLA is a semi-crystalline material, it is important to evaluate the changes that occur in the materials crystalline region, as mentioned in section 3.4.1. This lack of any apparent crystalline evidence at the microscopic level may suggest that the crystallite population has become smaller in size but may constitute yet a higher percentage of the bulk material. Thus we decided to further characterize the system by studying the T_m (melting temperature) and ΔH (Enthalpy of Crystallization) combined with XRD for all the samples that were processed in Table. 1S.

3.6 Effect of Processing Conditions on the Crystalline Region of the PLA

Analyzing the results of both the DSC (ΔH), and XRD patterns, changes occurring in the polymers crystallinity can be systematically and independently compared in relation to the pressure and temperature processing conditions with

which the samples are subjected to. Figure. 12. (A-C) as previously described will be used with focus on the crystalline region as depicted by the XRD profiles. Additionally, all samples ΔH values are graphed in Figure. 13.(A) while their respective numerical values and calculated % crystallinity's being found in Table. 4.(A)SI.. % Crystallinity in Table. 4.(A)SI. was calculated by dividing the DSC acquired ΔH value by the literature ΔH value of 100% crystalline PLA (93.1 J/g).[1,38] It is of note that during our study we did not possess a zero diffraction plate and that the peaks associated with the aluminum sample stage can be seen in our XRD profiles at times. The peaks associated with the aluminum sample stage are depicted in our XRD profiles at the 2Θ angles of 38° and 64°.

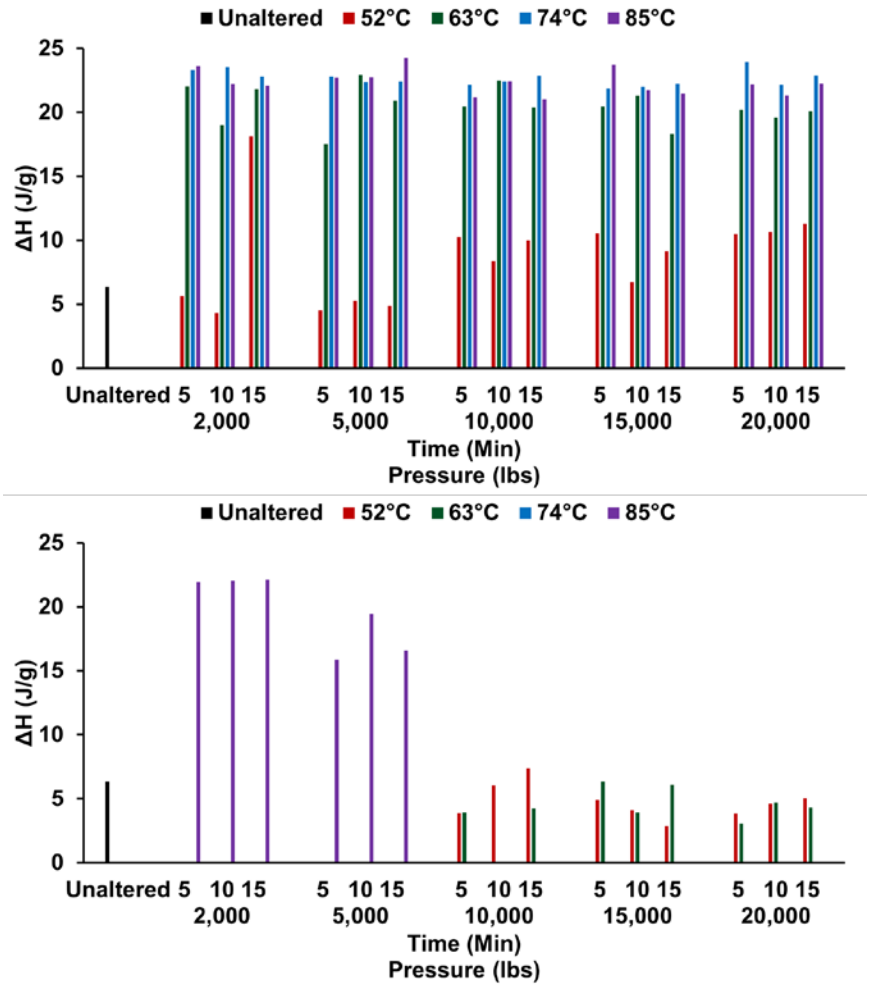

Figure. 13. Effect of treatment conditions on ΔH (heat of fusion). (Top) Samples displaying birefringent area. (Bottom) Samples displaying no birefringence area.

Much like our analysis of the amorphous region in section 3.4.1, we will narrow our focus in this section by fixing the pressure variable while describing the trends observed as treatment temperature is increased. To provide a general overview of the observed trends, it was found that crystallinity increased quite extensively as depicted by DSC in all treatment temperatures that were ≥ 63 °C. Likewise, this temperature dependent trend in increasing crystallinity was further

supported by XRD profile shifts towards crystallinity when treatment temperatures were ≥ 63 °C.

2,000 lbs:

Focusing on the first column of Figure. 12. (A-C) and Figure. 13. which are representative of the samples treated under 2,000 lbs for three periods of time (5, 10 and 15 min). The first things that becomes clear is that treating the material at 52 °C produces quite minimal change in ΔH as well as almost no noticeable change in the XRD profile in comparison to the untreated material. However, upon increasing the treatment temperature to 63 °C, a remarkable increase in ΔH as well as the beginning of an XRD crystalline shift begin to take shape. Increasing the treatment temperature to 74 °C drives the value of ΔH to increase to yet even higher values while also producing a very large shift in the XRD profile to a crystalline peak. Finally, treating the material at 85 °C produced a very large increase in the ΔH while XRD of this series displays a very crystalline structure.

5,000 lbs:

Moving to the second column of Figure. 12. (A-C) and Figure. 13. which are representative of the samples treated under 5,000 lbs for three periods of time (5, 10 and 15 min). It becomes immediately apparent that the treatment temperatures of 52 °C and 63 °C produce very similar increases in the values of ΔH and shifts in the XRD profile similar to those which were observed at 2,000 lbs. However, upon increasing the treatment temperature to 74 °C we observe a

much higher increase in ΔH value as well as a marketable XRD profile shift to a peak profile which is representative of a crystalline structure.

10,000 lbs:

Looking at the third column of Figure. 12. (A-C) and Figure. 13. which are representative of the samples treated under 10,000 lbs for three periods of time (5, 10 and 15 min). It is this pressure where we begin to see the samples treated at 52 °C temperature begin to show increases in the ΔH value in additional to the XRD profile beginning to take on a more ordered structure profile. Increasing the treatment temperature to 63 °C we observe a very sharp increase in the ΔH value in addition to a much more ordered XRD profile. Finally, both the 74 °C and 85 °C treatment temperatures display a similar increasing trend in ΔH value while the XRD profiles of both take on a much more crystalline peak structure.

15,000 lbs & 20,000 lbs:

Given that the results for both the 15,000 lbs and 20,000 lbs samples behaved quite similarly, we shall focus on both the fourth and fifth columns of Figure. 12. (A-C) and Figure. 13. for samples treated for three periods of time (5, 10 and 15 min). Initially looking at the samples treated at 52 °C we observe an increase in ΔH with minimal change in the XRD profile. Increasing the treatment temperature to 63 °C we observe a much higher increase in the ΔH with similar minimal changes noticed in the XRD profiles. However, upon increasing the treatment temperature to 74 °C 85 °C we observe the highest increase in ΔH for

this cohort along with XRD profiles which reflect a trend towards increasing crystallinity.

To summarize the results of the DSC and XRD analysis of the crystalline region, it was observed that crystallinity increased greatest when temperature was above the original untreated materials T_g of 64 °C. Interestingly, as the crystallinity of the material was observed to increase as depicted by both DSC and XRD, the aforementioned birefringence profiles while displaying increased orientation, did not display any of the spherulitic or lamellar structures typical of semi-crystalline polymers. This leads us to believe that in addition to generally increasing crystallinity under these treatment conditions, we are perhaps decreasing the crystal size.

3.7 Effect of Processing Conditions on the PLA Samples with no Birefringence

During the course of our study, several samples were observed to have a small centrally located zone which lacked any birefringence. These samples are interesting since they were exposed to the same processing conditions, which made us wonder whether they would display the same morphological characteristics which were observed in the birefringent area. This result may be beneficial in that it may also allow us to determine which experimental conditions are most effective for inducing homogeneous morphological changes.

Focusing first on the amorphous region of the non-birefringent zones depicted in the bottom of Figures. 9-11. It is immediately apparent that the non-birefringence zones did not see decreases in their T_g, ΔH_{ER} or ΔC_P values in the same manner that was previously observed in the birefringent areas, with the exception of the samples treated at 85 °C. Taking into account the materials values of T_g, ΔH_{ER} and ΔC_P depicted in the bottom of Figures. 9-11.. It can be observed that the material in these non-birefringent zones was found to maintain values that closely resembled that of the untreated material, again with the exception of the samples processed at 85 °C. These results are suggestive that both higher temperature and pressure treatment parameters are better able to homogenously effect the materials amorphous morphology.

Moving our focus to the crystalline region of the non-birefringent zones. It is once again apparent that very little change has occurred in the non-birefringent samples. Depicted in Figure. 13., the ΔH or crystallinity of the non-birefringent zones only increases for the samples which were processed at 85 °C while remaining in line with the values of the untreated material for all remaining conditions. Additionally, XRD analysis of the non-birefringent zones depicted an amorphous XRD structure as seen in the untreated material suggesting that very little morphological changes occurred in these zones. This once again provides support that higher temperatures and pressure are required in order to homogenously effect the materials structure.

In summary, Figure. 9-11. and 13. whose numerical values may be found in the supplemental materials Tables. 3.SI & Table. 4.SI, reveal a definitive

difference between the treated samples birefringent and non-birefringent zones. Interestingly we observed that when samples were treated at 85 °C and below 10,000 lbs, they were capable of undergoing limited amorphous reorientation (having non-birefringent zones) while displaying increased crystallinity as observed by DSC, yet they displayed an amorphous structure by XRD. Addtionaly, two T_g's were never observed in any of the non-birefringent zones with the XRD of those regions possessing the same morphology of the original material.

4. Discussion and Conclusions

Our work, in addition to others in the field, has shown that processing polymers with specific temperature, pressure and time treatment profiles could affect polymer morphologies, especially those that are classified as thermoplastics.[33,39–43].

In our current work, the combination of DSC, XRD, and polarized light microscopy allowed us to systematically characterize the treatment and concurrent morphological changes occurring in the PLA under specific temperature, pressure, and time conditions. Our DSC results revealed that these combined thermal and pressure stresses when delivered in specific sequence over time can have a significant impact on the materials T_g, ΔH_{ER}, and ΔC_P values. In fact, these results demonstrated this as we observed the formation of multiple morphologies, each possessing their own separate T_g's and congruent ΔH_{ER}, and ΔC_P values

To better explain what is possibly occurring with the materials structure we must look at the amorphous phases and also acknowledge that the materials increase in crystallinity is also playing a role in the structure changes.

To begin, the amorphous region and crystalline regions of semi-crystalline polymers are inherently linked together and are capable of influencing each other physically. When a material begins to crystalize, the crystals must be formed from the material present in the amorphous chains. Initially, this is easy as the necessary material is accessible and not restricted by neighboring crystallites. However, as the crystallinity increases as a percentage of the entire structure, the amorphous portion of the material required for crystallization becomes more difficult to access and results in regions of loosely entangled amorphous chains with excess free volume.[44,45] Congruently, the amorphous areas which are geographically located near the crystallites become much more entangled and more restricted. This difference in the entanglement has a direct impact on the materials T_g as more entangled amorphous regions require more energy to overcome their mobility restriction and enter a rubbery state.[44,45] In addition, due to the pressure that the we apply, the size of the crystals is decreased while their concentration is increased. These smaller and more concentrated crystals thus create a more restrictive environment which could form a glass transition with increased temperature. This is how we can explain the existence of the higher Tg in our system. However, at higher pressures this T_g almost disappears. This restrictive phenomenon on the amorphous regions mobility due to increased crystallinity has been observed in the polymer PEEK by Atkinson Et Al. They

have found that increases in both the T_g as well as its peak breadth occurred as a result of increasing crystallinity. [45] No pressure was used in their system, while additionally they only reported a single T_g. Thus overall, we can explain the formation of the higher T_g.

The formation of the lower T_g is a direct result of applying pressure close to or above the untreated materials T_g. These regions which are not in close proximity to the crystalline region are then oriented during the time the system is pressed under the desired temperature (for 5, 10, 15 min). For each condition the amorphous state increased in volume as the material was oriented. This orientation explains the increase in birefringence intensity as well as the formation of a less restricted structure with lower T_g. Additionally, based on the collective polarized light microscopy data depicted in Figures. 2. and 12. (A-C), and the fact that rotation of the samples under polarized light did not result in the extinction of the birefringent effect. This may strongly indicate that one of the morphologies we observe in the treated materials may be that of a semi liquid crystalline state or a state which closely resembles a liquid crystalline state.

Thus we suggest that the observed lower T_g is associated with a new amorphous orientation phase possessing more ordered yet loosely entangled amorphous chains which in addition are located geographically within a greater distance from the crystalline region. The formation of an amorphous region with higher and sometimes less defined T_g's are thus indicative of a more entangled and restricted amorphous region with a much closer geographical proximity to the crystalline domain. A crystalline domain which has additionally grown in

proportion by population to the bulk material while decreasing in individual crystal size under pressure.

Polarized microscopy demonstrated increased orientation of the amorphous state by exposing a distinct birefringence which lacked the typical spherulitic structure observed in the melt/solvent casted material. This birefringence, in samples that were processed near and below T_g, were found to have increased in intensity as pressure is increased. Additionally, a small population of samples were observed to possess discrete non-birefringent zones when processing below T_g and above 10,000 lbs or at 85 °C and below 10,000 lbs. This suggests that in the future attention should be paid to the morphologies which are created during film and melt casting as they may vary in properties.

XRD results support the DSC data in demonstrating that increased processing temperatures and pressures are capable of increasing both amorphous order and crystallinity. XRD results demonstrated that the most effective temperature and pressure condition for enhancing both the amorphous and crystalline regions is probably a temperature above T_g in unison with a pressure above 10,000 lbs.

The observed properties might be mainly attributed to the competition between the effects of free volume and the degree of entanglement varied with pressure and aging time under or close to the molten ($T_g<T<T_m$) or glassy ($T<T_g$) state. When the pressure is increased up to a certain level, this not only results in reduced amounts of free volume (Lower ΔC_P) but also gives rise to the

conformational transition from coil to stretched (or oriented) chain. This stretched or oriented chain is loosely entangled and thus has a low-order arrangement. As this contribution is larger than that of the free volume effect, the reduced endothermic peak (Lower ΔH_{ER}) and decrease in the values of T_g are observed. Moreover, owing to the crystallizable PLLA chain, under pressure the system is cooled allowing only small crystals to form with dense attached amorphous chains. This results in a higher T_g. As a result, the effects of the free volume, entanglement, and crystallinity on the thermal characterization of the semi-crystalline PLLA materials under various pressures and aging times are promising to be interpreted.

Supporting Information:

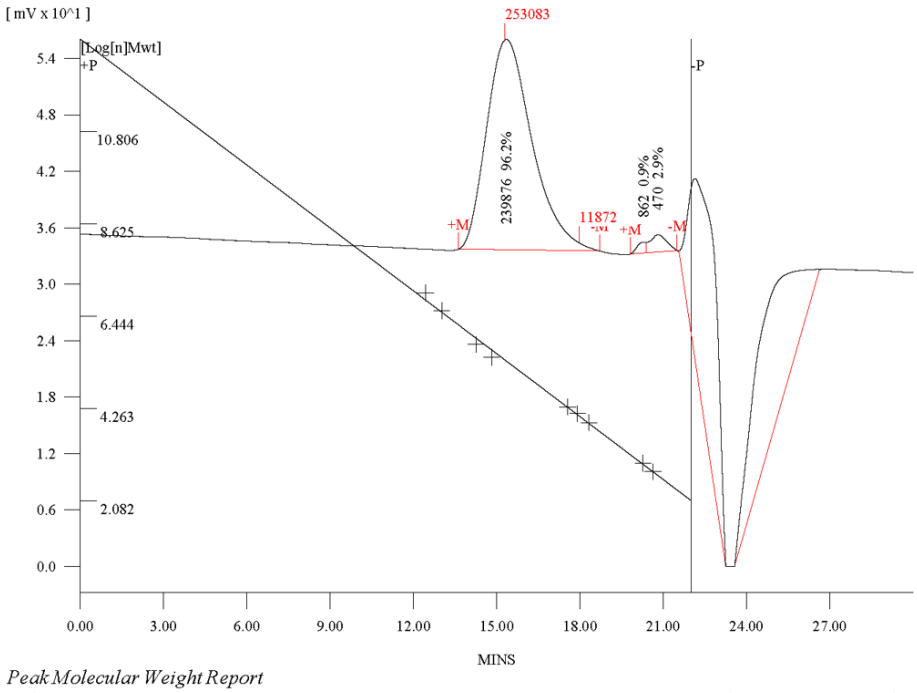

Peak Molecular Weight Report

Peak	Component	RT	Area	%Area	PMwt	Mw	Mn	Mw/Mn	StartMw	EndMw
1		15.346	2550673.2	96.177	239876.0	263118.2	112608.2	2.3366	1697117.8	5203.9
2		20.278	24658.7	0.930	862.4	966.1	946.8	1.0204	1450.2	766.4
3		20.808	76722.2	2.893	470.9	476.7	439.2	1.0854	766.4	213.3

(n - 1) Average : 484 Number Average (Mn) : 11872
Weight Average (Mw) : 253083 PolyDispersity (Mw/Mn) : 21.318
Total Area : 2.6520541e+006 (microvolt seconds)

Figure. 6SI. GPC analysis of the PLA.

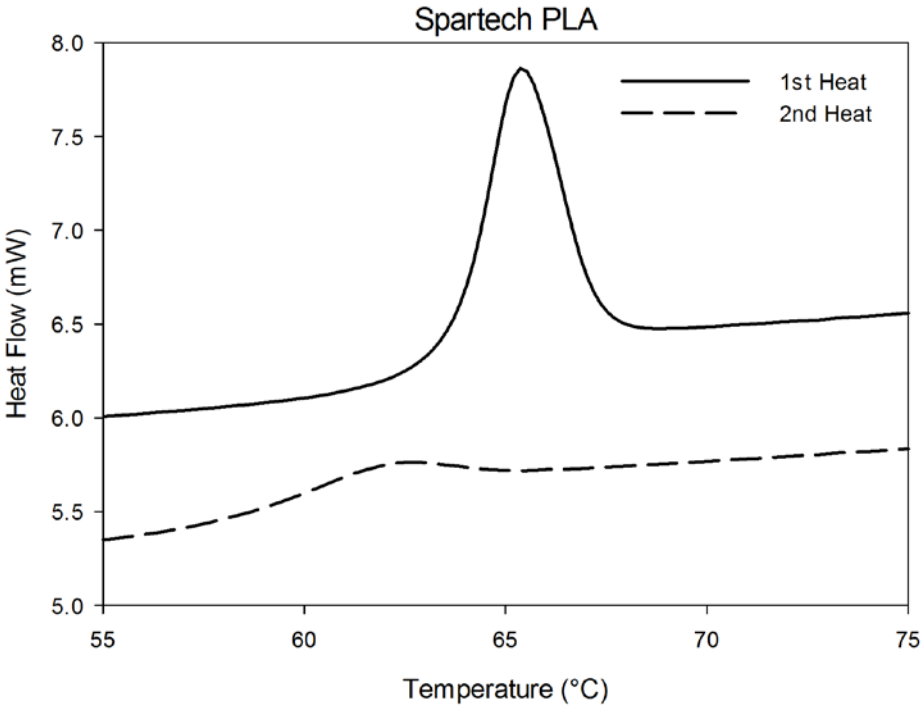

Figure. 7A.SI Initial DSC analysis of the PLA. T_g was calculated to be 64.37°C, T_m was found to be 149.53°C.

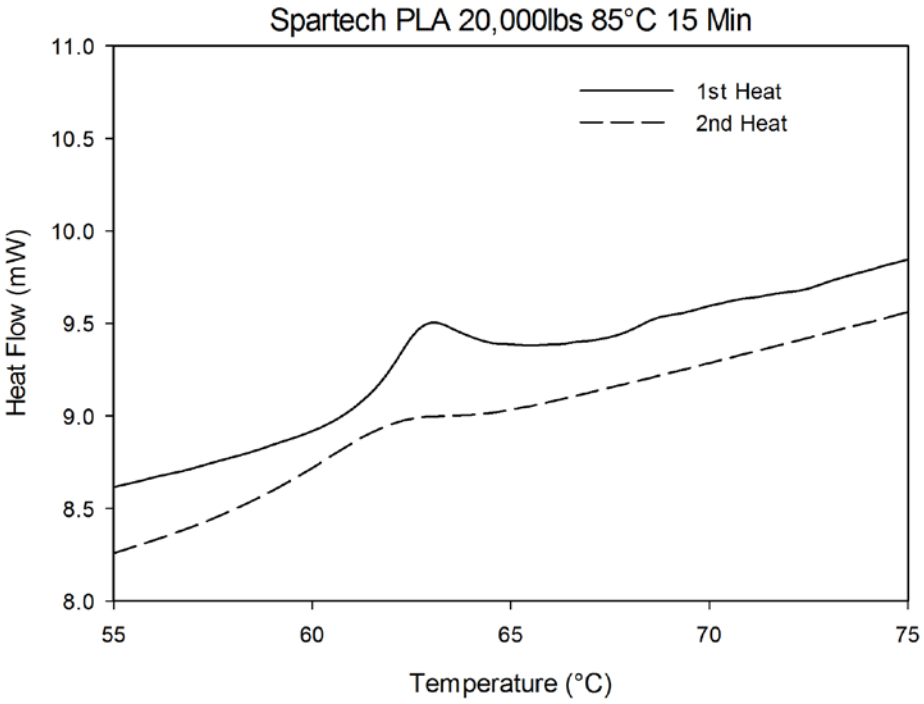

Figure. 7B.SI DSC analysis of the PLA sample that was processed at 20,000lbs at 85°C for 15 Min. T_g was calculated to be 61.79°C, T_m was found to be 149.67°C.

Processing Conditions						
Temperature						
Pressure	52°C	63°C	74°C	85°C		Time
	2,000lbs	2,000lbs	2,000lbs	2,000lbs	5 Min	
	5,000lbs	5,000lbs	5,000lbs	5,000lbs		
	10,000lbs	10,000lbs	10,000lbs	10,000lbs		
	15,000lbs	15,000lbs	15,000lbs	15,000lbs		
	20,000lbs	20,000lbs	20,000lbs	20,000lbs		
	2,000lbs	2,000lbs	2,000lbs	2,000lbs	10 Min	
	5,000lbs	5,000lbs	5,000lbs	5,000lbs		
	10,000lbs	10,000lbs	10,000lbs	10,000lbs		
	15,000lbs	15,000lbs	15,000lbs	15,000lbs		
	20,000lbs	20,000lbs	20,000lbs	20,000lbs		
	2,000lbs	2,000lbs	2,000lbs	2,000lbs	15 Min	
	5,000lbs	5,000lbs	5,000lbs	5,000lbs		
	10,000lbs	10,000lbs	10,000lbs	10,000lbs		
	15,000lbs	15,000lbs	15,000lbs	15,000lbs		
	20,000lbs	20,000lbs	20,000lbs	20,000lbs		

Table. 1SI. Processing profiles used in the Carver Auto Press.

Processing Conditions			Length	Width	Thickness	Surface Area	Δ Thickness	Δ Surface Area
Press (lbs)	Time (min)	Temp (°C)	(in)	(in)	(in)	(in^2)	(in)	(in^2)
Unaltered			1.002	0.994	0.032	2.120	N/A	N/A
2,000	5	52	0.976	0.990	0.032	2.058	0.000	-0.061
		63	1.059	1.215	0.029	2.705	-0.003	0.647
		74	1.238	1.088	0.028	2.824	-0.001	0.119
		85	1.233	1.138	0.026	2.930	-0.002	0.105
	10	52	1.051	1.039	0.032	2.318	0.006	-0.612
		63	1.034	1.058	0.027	2.301	-0.005	-0.017
		74	1.099	1.116	0.026	2.568	-0.001	0.267
		85	1.146	1.139	0.025	2.725	-0.001	0.157
	15	52	1.037	0.994	0.032	2.192	0.007	-0.533
		63	1.076	1.045	0.028	2.368	-0.004	0.176
		74	1.062	1.108	0.028	2.475	0.000	0.107
		85	1.163	1.120	0.024	2.715	-0.004	0.240
5,000	5	52	1.027	1.015	0.032	2.215	0.008	-0.499
		63	1.042	1.138	0.029	2.498	-0.003	0.283
		74	1.142	1.203	0.025	2.865	-0.004	0.367
		85	1.249	1.266	0.021	3.268	-0.004	0.403
	10	52	1.019	0.983	0.032	2.131	0.011	-1.137
		63	1.069	1.062	0.030	2.398	-0.002	0.267
		74	1.155	1.152	0.027	2.786	-0.003	0.387
		85	1.117	1.256	0.022	2.910	-0.005	0.125
	15	52	1.017	0.991	0.032	2.144	0.010	-0.766
		63	1.035	1.091	0.029	2.382	-0.003	0.237
		74	1.118	1.181	0.026	2.760	-0.003	0.379
		85	1.198	1.162	0.022	2.888	-0.004	0.128
10,000	5	52	1.049	1.041	0.032	2.318	0.010	-0.570
		63	1.077	0.971	0.029	2.210	-0.003	-0.107
		74	1.160	1.190	0.025	2.878	-0.004	0.668
		85	1.204	1.234	0.023	3.084	-0.002	0.205
	10	52	1.008	1.004	0.032	2.153	0.009	-0.931
		63	1.077	0.995	0.027	2.255	-0.005	0.102
		74	1.153	1.134	0.024	2.725	-0.003	0.470
		85	1.183	1.228	0.021	3.007	-0.003	0.282
	15	52	1.005	1.031	0.032	2.203	0.011	-0.804
		63	1.115	1.113	0.030	2.616	-0.002	0.413
		74	1.135	1.213	0.023	2.862	-0.007	0.246
		85	1.249	1.272	0.022	3.288	-0.001	0.427
15,000	5	52	0.953	1.053	0.032	2.135	0.010	-1.153
		63	1.116	1.073	0.028	2.517	-0.004	0.382
		74	1.183	1.275	0.024	3.135	-0.004	0.618
		85	1.243	1.198	0.019	3.071	-0.005	-0.064
	10	52	1.114	1.055	0.032	2.489	0.013	-0.582
		63	1.071	1.113	0.024	2.489	-0.008	0.000
		74	1.218	1.209	0.024	3.062	0.000	0.573
		85	1.187	1.228	0.020	3.012	-0.004	-0.050
	15	52	0.991	1.023	0.030	2.148	0.010	-0.863
		63	0.969	1.055	0.028	2.158	-0.002	0.010
		74	1.181	1.165	0.027	2.878	-0.001	0.720
		85	1.123	1.227	0.022	2.859	-0.005	-0.019
20,000	5	52	1.077	0.957	0.031	2.187	0.009	-0.672
		63	1.155	1.142	0.024	2.748	-0.007	0.561
		74	1.225	1.172	0.020	2.967	-0.004	0.219
		85	1.207	1.273	0.014	3.142	-0.006	0.175
	10	52	1.011	1.021	0.031	2.190	0.017	-0.952
		63	1.076	1.085	0.024	2.439	-0.007	0.248
		74	1.187	1.170	0.021	2.877	-0.003	0.438
		85	1.206	1.168	0.020	2.912	-0.001	0.036
	15	52	1.006	1.050	0.031	2.240	0.011	-0.672
		63	1.083	1.053	0.023	2.379	-0.008	0.139
		74	1.126	1.163	0.021	2.715	-0.002	0.336
		85	1.182	1.187	0.019	2.896	-0.002	0.181
(Surface Area=2TL + 2LH + 2HT)								

Table. 2. SI Table depicting the sample deformation of all processed samples.

Processing Conditions			T_g (°C)	ΔCp (J/g°C)	ΔH_{ER} (J/g)
Press (lbs)	Time (min)	Temp (°C)			
Unaltered			64.37	3.163	5.732
2,000	5	52	63.95	2.572	5.683
		63	60.54	1.440	4.356
		74	59.93	1.509	4.357
		85	60.72	1.312	3.980
	10	52	64.21	2.551	5.319
		63	61.22	1.627	3.829
		74	60.91	1.491	4.173
		85	61.28	1.289	4.059
	15	52	62.86	1.993	5.110
		63	61.34	1.801	4.794
		74	61.11	1.666	4.102
		85	61.63	1.291	2.946
5,000	5	52	64.13	2.560	5.519
		63	61.41	1.595	4.733
		74	60.62	1.119	2.512
		85	61.36	0.835	1.935
	10	52	63.78	2.427	6.302
		63	61.13	1.614	4.594
		74	61.23	0.962	1.671
		85	61.28	1.023	2.774
	15	52	63.84	2.272	4.831
		63	61.80	1.702	5.162
		74	61.18	1.093	1.345
		85	61.46	0.865	1.491
10,000	5	52	65.34	2.631	4.956
		63	62.43	1.777	7.056
		74	61.39	0.755	2.245
		85	61.55	0.471	-0.106
	10	52	62.37	1.892	5.710
		63	61.16	1.134	8.130
		74	61.35	0.750	1.853
		85	61.90	0.613	1.055
	15	52	62.86	2.066	4.941
		63	62.00	1.376	4.578
		74	61.74	1.016	1.277
		85	60.98	0.502	1.525
15,000	5	52	61.88	1.888	4.558
		63	61.41	1.391	4.858
		74	61.10	0.739	1.373
		85	61.02	0.752	0.038
	10	52	63.62	2.544	4.922
		63	61.94	1.467	9.465
		74	61.22	1.014	2.310
		85	61.24	0.568	0.809
	15	52	64.03	3.171	6.448
		63	62.11	1.845	5.735
		74	61.50	0.724	0.293
		85	61.41	0.474	0.336
20,000	5	52	64.08	2.327	4.827
		63	62.17	1.946	5.873
		74	61.47	1.088	2.183
		85	61.44	0.882	1.005
	10	52	62.92	2.117	5.538
		63	61.53	1.396	6.898
		74	61.31	0.846	0.768
		85	61.25	0.723	0.736
	15	52	62.59	2.031	5.372
		63	62.45	2.044	6.762
		74	62.26	0.652	0.421
		85	61.79	0.822	1.305

Table. 3ASI. Calculated T_g, ΔC_P and ΔH_{ER} values of the material before processing and after processing between 2,000lbs-20,000lbs while exposed to temperatures below and above the T_g over 5-15 min.

Processing Conditions			T_g (°C)	ΔCp (J/g°C)	ΔH_{ER} (J/g)
Press (lbs)	Time (min)	Temp (°C)			
Unaltered			64.37	3.163	5.732
2,000	5	52			
		63	65.36	0.212	0.331
		74	64.04	0.113	0.075
		85			
	10	52			
		63			
		74			
		85	65.35	0.080	0.075
	15	52			
		63	68.22	0.384	1.421
		74			
		85			
5,000	5	52			
		63	67.02	0.134	0.104
		74			
		85			
	10	52			
		63			
		74			
		85			
	15	52			
		63	65.08	0.308	0.521
		74			
		85			
10,000	5	52			
		63	67.39	1.365	3.664
		74			
		85			
	10	52			
		63	69.35	0.334	1.216
		74			
		85			
	15	52			
		63	67.79	0.158	0.418
		74			
		85			
15,000	5	52	66.36	0.185	0.309
		63	65.20	0.318	0.857
		74			
		85			
	10	52			
		63	67.82	0.897	3.129
		74			
		85			
	15	52			
		63	66.74	1.062	1.424
		74	66.16	0.182	0.344
		85			
20,000	5	52			
		63	64.90	1.176	2.701
		74			
		85			
	10	52	65.82	0.135	-0.067
		63	67.36	0.792	2.671
		74			
		85			
	15	52			
		63	66.59	1.184	2.099
		74	65.56	0.277	0.221
		85			

Table. 3BSI. Calculated 2nd T_g, ΔC_P and ΔH_{ER} values of the material before processing and after processing between 2,000lbs-20,000lbs while exposed to temperatures below and above the T_g over 5-15 min.

Processing Conditions			T_g (°C)	ΔCp (J/g°C)	ΔH_{ER} (J/g)
Press (lbs)	Time (min)	Temp (°C)			
Unaltered			64.37	3.163	5.732
2,000	5	52			
		63			
		74			
		85	60.46	1.484	4.202
	10	52			
		63			
		74			
		85	60.80	1.784	4.576
	15	52			
		63			
		74			
		85	60.71	1.641	4.576
5,000	5	52			
		63			
		74			
		85	60.35	1.704	4.211
	10	52			
		63			
		74			
		85	61.24	1.932	4.337
	15	52			
		63			
		74			
		85	61.28	1.890	3.956
10,000	5	52	65.04	3.568	5.391
		63	64.53	3.494	5.203
		74			
		85			
	10	52	64.74	3.228	5.187
		63			
		74			
		85			
	15	52	64.70	3.493	5.402
		63	64.63	3.121	4.462
		74			
		85			
15,000	5	52	64.71	3.239	5.710
		63	64.73	3.297	5.694
		74			
		85			
	10	52	64.61	3.143	5.250
		63	64.67	3.111	5.572
		74			
		85			
	15	52	58.16	0.501	2.365
		63	64.48	3.206	5.294
		74			
		85			
20,000	5	52	64.83	3.608	4.835
		63	64.15	3.282	5.647
		74			
		85			
	10	52	64.13	3.055	5.461
		63	63.70	2.823	5.475
		74			
		85			
	15	52	63.80	2.599	5.378
		63	62.62	2.632	6.110
		74			
		85			

Table. 3CSI. Calculated Non-Birefringent T_g, ΔC_P and ΔH_{ER} values of the material before processing and after processing between 2,000lbs-20,000lbs while exposed to temperatures below and above the T_g over 5-15 min.

Processing Conditions			T_m (°C)	ΔH (J/g)	% Crystallinity
Press (lbs)	Time (min)	Temp (°C)			ΔH/93.1 (J/g)
Unaltered			149.53	6.338	6.81%
2,000	5	52	151.87	5.642	6.06%
		63	150.00	22.043	23.68%
		74	150.53	23.318	25.05%
		85	150.53	23.638	25.39%
	10	52	150.83	4.300	4.62%
		63	151.17	18.994	20.40%
		74	149.67	23.518	25.26%
		85	149.33	22.207	23.85%
	15	52	150.53	18.107	19.45%
		63	149.17	21.837	23.46%
		74	148.70	22.795	24.48%
		85	151.70	22.077	23.71%
5,000	5	52	151.17	4.517	4.85%
		63	151.03	17.541	18.84%
		74	149.20	22.801	24.49%
		85	148.37	22.731	24.42%
	10	52	150.20	5.252	5.64%
		63	150.20	22.936	24.64%
		74	148.17	22.372	24.03%
		85	148.87	22.755	24.44%
	15	52	151.53	4.881	5.24%
		63	150.00	20.926	22.48%
		74	148.03	22.408	24.07%
		85	151.20	24.277	26.08%
10,000	5	52	151.37	10.260	11.02%
		63	150.53	20.481	22.00%
		74	150.03	22.158	23.80%
		85	149.03	21.174	22.74%
	10	52	149.87	8.355	8.97%
		63	148.87	22.489	24.16%
		74	149.20	22.418	24.08%
		85	149.53	22.438	24.10%
	15	52	150.83	9.973	10.71%
		63	150.37	20.374	21.88%
		74	148.37	22.853	24.55%
		85	148.20	21.002	22.56%
15,000	5	52	151.37	10.544	11.33%
		63	150.87	20.471	21.99%
		74	148.53	21.880	23.50%
		85	147.87	23.710	25.47%
	10	52	151.03	6.727	7.23%
		63	148.33	21.293	22.87%
		74	149.00	22.022	23.65%
		85	148.87	21.727	23.34%
	15	52	150.03	9.144	9.82%
		63	150.20	18.299	19.65%
		74	148.70	22.233	23.88%
		85	149.70	21.459	23.05%
20,000	5	52	150.53	10.474	11.25%
		63	149.53	20.213	21.71%
		74	149.03	23.927	25.70%
		85	148.67	22.162	23.80%
	10	52	149.87	10.651	11.44%
		63	149.53	19.588	21.04%
		74	147.70	22.160	23.80%
		85	148.70	21.321	22.90%
	15	52	150.83	11.293	12.13%
		63	149.37	20.090	21.58%
		74	148.37	22.884	24.58%
		85	149.67	22.264	23.91%

Table 4ASI. Calculated ΔH and % Crystallinity values of the material before processing and after processing between 2,000lbs-20,000lbs while exposed to temperatures below and above the T_g over 5-15 min.

Processing Conditions			T_m (°C)	ΔH (J/g)	% Crystallinity
Press (lbs)	Time (min)	Temp (°C)			ΔH/93.1 (J/g)
Unaltered			149.53	6.338	6.81%
2,000	5	52			
		63			
		74			
		85	149.70	21.942	23.57%
	10	52			
		63			
		74			
		85	149.70	22.026	23.66%
	15	52			
		63			
		74			
		85	149.03	22.130	23.77%
5,000	5	52			
		63			
		74			
		85	149.37	15.864	17.04%
	10	52			
		63			
		74			
		85	150.03	19.457	20.90%
	15	52			
		63			
		74			
		85	149.87	16.570	17.80%
10,000	5	52	151.70	3.889	4.18%
		63	149.87	3.924	4.21%
		74			
		85			
	10	52	151.17	6.045	6.49%
		63			
		74			
		85			
	15	52	150.20	7.373	7.92%
		63	150.03	4.242	4.56%
		74			
		85			
15,000	5	52	151.53	4.899	5.26%
		63	150.83	6.343	6.81%
		74			
		85			
	10	52	151.50	4.109	4.41%
		63	150.37	3.941	4.23%
		74			
		85			
	15	52	150.03	2.851	3.06%
		63	150.70	6.074	6.52%
		74			
		85			
20,000	5	52	150.70	3.850	4.13%
		63	149.87	3.043	3.27%
		74			
		85			
	10	52	152.87	4.627	4.97%
		63	150.00	4.685	5.03%
		74			
		85			
	15	52	151.70	5.052	5.43%
		63	149.37	4.328	4.65%
		74			
		85			

Table 4BSI. Calculated Non-Birefringent ΔH and % Crystallinity values of the material before processing and after processing between 2,000lbs-20,000lbs while exposed to temperatures below and above the T_g over 5-15 min for samples that lacked birefringence.

References

[1] D. Garlotta, A literature review of poly (lactic acid), J. Polym. Environ. 9 (2001) 63–84. http://link.springer.com/article/10.1023/A:1020200822435 (accessed July 3, 2013).

[2] R. a. Auras, B. Harte, S. Selke, R. Hernandez, Mechanical, Physical, and Barrier Properties of Poly(Lactide) Films, J. Plast. Film Sheeting. 19 (2003) 123–135. doi:10.1177/8756087903039702.

[3] M. Kwon, S.C. Lee, Y.G. Jeong, Influences of physical aging on enthalpy relaxation behavior, gas permeability, and dynamic mechanical property of polylactide films with various D-isomer contents, Macromol. Res. 18 (2010) 346–351. doi:10.1007/s13233-010-0410-7.

[4] E.T.H. Vink, K.R. Rábago, D. a Glassner, B. Springs, R.P. O'Connor, J. Kolstad, et al., The sustainability of NatureWorks polylactide polymers and Ingeo polylactide fibers: an update of the future., Macromol. Biosci. 4 (2004) 551–64. doi:10.1002/mabi.200400023.

[5] E.T.H. Vink, K.R. Rábago, D. a. Glassner, P.R. Gruber, Applications of life cycle assessment to NatureWorks™ polylactide (PLA) production, Polym. Degrad. Stab. 80 (2003) 403–419. doi:10.1016/S0141-3910(02)00372-5.

[6] G. Kale, R. Auras, S.P. Singh, R. Narayan, Biodegradability of polylactide bottles in real and simulated composting conditions, Polym. Test. 26 (2007) 1049–1061. doi:10.1016/j.polymertesting.2007.07.006.

[7] G. Kale, R. Auras, S.P. Singh, Degradation of Commercial Biodegradable Packages under Real Composting and Ambient Exposure Conditions, J. Polym. Environ. 14 (2006) 317–334. doi:10.1007/s10924-006-0015-6.

[8] K. Madhavan Nampoothiri, N.R. Nair, R.P. John, An overview of the recent developments in polylactide (PLA) research., Bioresour. Technol. 101 (2010) 8493–501. doi:10.1016/j.biortech.2010.05.092.

[9] C.C. Chen, J.Y. Chueh, H. Tseng, H.M. Huang, S.Y. Lee, Preparation and characterization of biodegradable PLA polymeric blends., Biomaterials. 24 (2003) 1167–73. http://www.ncbi.nlm.nih.gov/pubmed/12527257.

[10] D.W. Grijpma, J.P. Penning, A.J. Pennings, Chain entanglement, mechanical properties and drawability of poly(lactide), Colloid Polym. Sci. 272 (1994) 1068–1081. doi:10.1007/BF00652375.

[11] A.A. Shah, F. Hasan, A. Hameed, S. Ahmed, Biological degradation of plastics: a comprehensive review., Biotechnol. Adv. 26 (2008) 246–65. doi:10.1016/j.biotechadv.2007.12.005.

[12] R. a Gross, B. Kalra, Biodegradable polymers for the environment., Science. 297 (2002) 803–7. doi:10.1126/science.297.5582.803.

[13] P. Pan, B. Zhu, Y. Inoue, Enthalpy relaxation and embrittlement of poly (L-lactide) during physical aging, Macromolecules. 40 (2007) 9664–9671. doi:10.1021/ma071737c.

[14] R. Surana, A. Pyne, M. Rani, R. Suryanarayanan, Measurement of enthalpic relaxation by differential scanning calorimetry—effect of experimental conditions, Thermochim. Acta. 433 (2005) 173–182. doi:10.1016/j.tca.2005.02.014.

[15] I.M. Hodge, Effects of Annealing and Prior History on Enthalpy Relaxation in Glassy-Polymers .4. Comparison of Five Polymers, Macromolecules. 16 (1983) 898–902.

[16] A.R. Berens, I.M. Hodge, Effects of annealing and prior history on enthalpy relaxation in glassy polymers. 1. Experimental study on poly(vinyl chloride), Macromolecules. 15 (1982) 756–761. doi:10.1021/ma00231a015.

[17] I.M. Hodge, Effects of Annealing and Prior History on Enthalpy Relaxation in Glassy Polymers. 2. Mathematical Modeling, Macromolecules. 15 (1982) 762–770.

[18] I.M. Hodge, G.S. Huvard, Effects of annealing and prior history on enthalpy relaxation in glassy polymers. 3. Experimental and modeling studies of polystyrene, Macromolecules. 16 (1983) 371–375. doi:10.1021/ma00237a006.

[19] I.M. Hodge, The Effects of Physical Aging on Enthalpy Relaxation in Polymers. A Phenomenological Approach, Relaxations Complex Syst. (1984) 65–79. http://imhodge.startlogic.com/pdfs/vpi (1).pdf.

[20] I.M. Hodge, Effects of Annealing and Prior History on Enthalpy Relaxation in Glassy-Polymers .6. Adam-Gibbs Formulation of Nonlinearity, Macromolecules. 20 (1987) 2897–2908. doi:10.1021/ma00177a044.

[21] I.M. Hodge, a. R. Berens, Effects of annealing and prior history on enthalpy relaxation in glassy polymers. 5. Mathematical modeling of nonthermal preaging perturbations, Macromolecules. 18 (1985) 1980–1984. doi:10.1021/ma00152a030.

[22] I.M. Hodge, Enthalpy relaxation and recovery in amorphous materials, J. Non. Cryst. Solids. 169 (1994) 211–266. doi:10.1016/0022-3093(94)90321-2.

[23] E. Jones Parry, D. Tabor, Effect of hydrostatic pressure on the mechanical properties of polymers: a brief review of published data, J. Mater. Sci. 8 (1973) 1510–1516. doi:10.1007/BF00551675.

[24] J. iain M.G. Cowie, V. Arrighi, Physical Aging, in: Polym. Phys., John Wiley & Sons, Inc., Hoboken, NJ, USA, 2010: pp. 357–389. doi:10.1002/9780470600160.ch9.

[25] J.M.G. Cowie, S. Harris, I.J. McEwen, Physical Aging in Poly(vinyl acetate). 2. Relative Rates of Volume and Enthalpy Relaxation, Macromolecules. 31 (1998) 2611–2615. doi:10.1021/ma970287t.

[26] S.C. Lee, J. Il Han, Y.G. Jeong, M. Kwon, Strain-Induced Enthalpy Relaxation in Poly(lactic acid), Macromolecules. 43 (2010) 25–28. doi:10.1021/ma901880a.

[27] B.S.J. J. K. Lee, K. H. Lee, Structure development and biodegradability of uniaxially stretched poly (L -lactide), Eur. Polym. J. 37 (2001) 907–914. doi:10.1016/S0014-3057(00)00213-5.

[28] N.A. Bailey, M. Sandor, M. Kreitz, E. Mathiowitz, Comparison of the enthalpic relaxation of poly(lactide-co-glycolide) 50:50 nanospheres and raw polymer, J. Appl. Polym. Sci. 86 (2002) 1868–1872. doi:10.1002/app.11109.

[29] a. Celli, M. Scandola, Thermal properties and physical ageing of poly(L-lactic acid), Polymer (Guildf). 33 (1992) 2699–2703. doi:10.1016/0032-3861(92)90440-8.

[30] H. Cai, V. Dave, R. a Gross, S.P. McCarthy, Effects of physical aging, crystallinity, and orientation on the enzymatic degradation of poly (lactic acid), J. Polym. Sci. Part B Polym. Phys. 34 (1998) 2701–2708. doi:10.1002/(SICI)1099-0488(19961130)34:16<2701::AID-POLB2>3.0.CO;2-S.

[31] S. Tan, A. Su, J. Luo, E. Zhou, S.Z.D. Cheng, Effect of physical aging on the microstructure and the crystallization of amorphous poly(aryl ether ether ketone ketone) (PEEKK), Macromol. Chem. Phys. 200 (1999) 2487–2493. doi:10.1002/(SICI)1521-3935(19991101)200:11<2487::AID-MACP2487>3.0.CO;2-#.

[32] S. Rathi, X. Chen, E.B. Coughlin, S.L. Hsu, C.S. Golub, M.J. Tzivanis, Toughening semicrystalline poly(lactic acid) by morphology alteration, Polymer (Guildf). 52 (2011) 4184–4188. doi:10.1016/j.polymer.2011.07.032.

[33] Y. Wang, D. Shen, Effects of mechanical deformation on endothermic peaks in aged amorphous poly(ethylene terephthalate), Polym. J. 29 (1997) 860–863. doi:10.1295/polymj.29.860.

[34] T. Schreiber, H. Schultz, O. Schmidt, F. Röser, J. Limpert, a Tünnermann, Stress-induced birefringence in large-mode-area micro-structured optical fibers., Opt. Express. 13 (2005) 3637–46. http://www.ncbi.nlm.nih.gov/pubmed/19495270.

[35] A.N. Gent, Stress-induced birefringence of swollen polymer networks, Macromolecules. 2 (1969) 262–265. http://pubs.acs.org/doi/abs/10.1021/ma60009a010 (accessed July 24, 2014).

[36] T.J. Hammack, R.D. Andrews, Temperature Dependence of Orientation Birefringence of Polymers in the Glassy and Rubbery States. II, J. Appl. Phys. 36 (1965) 3574–3581. doi:10.1063/1.1703043.

[37] M.F. Weber, Giant Birefringent Optics in Multilayer Polymer Mirrors, Science (80-.). 287 (2000) 2451–2456. doi:10.1126/science.287.5462.2451.

[38] G. Kokturk, E. Piskin, T.F. Serhatkulu, M. Cakmak, Evolution of phase behavior and orientation in uniaxially deformed polylactic acid films, Polym. Eng. Sci. 42 (2002) 1619–1628. doi:10.1002/pen.11057.

[39] I.J. Rao, K.R. Rajagopal, A study of strain-induced crystallization of polymers, Int. J. Solids Struct. 38 (2001) 1149–1167. doi:10.1016/S0020-7683(00)00079-2.

[40] Y. Wang, M. a. Rodriguez-Perez, R.L. Reis, J.F. Mano, Thermal and Thermomechanical Behaviour of Polycaprolactone and Starch/Polycaprolactone Blends for Biomedical Applications, Macromol. Mater. Eng. 290 (2005) 792–801. doi:10.1002/mame.200500003.

[41] H. Kranz, N. Ubrich, P. Maincent, R. Bodmeier, Physicomechanical properties of biodegradable poly(D,L-lactide) and poly(D,L-lactide-co-glycolide) films in the dry and wet states., J. Pharm. Sci. 89 (2000) 1558–66. http://www.ncbi.nlm.nih.gov/pubmed/11042603.

[42] Y. Wang, J.F. Mano, Effect of structural relaxation at physiological temperature on the mechanical property of poly(L-lactic acid) studied by microhardness measurements, J. Appl. Polym. Sci. 100 (2006) 2628–2633. doi:10.1002/app.22643.

[43] A. Wang, D. Sun, S. Yau, B. Edwards, Orientation softening in the deformation and wear of ultra-high molecular weight polyethylene, Wear. 204 (1997) 230–241. http://www.sciencedirect.com/science/article/pii/S0043164896073620 (accessed July 3, 2013).

[44] Q. Ma, G. Georgiev, P. Cebe, Constraints in semicrystalline polymers: Using quasi-isothermal analysis to investigate the mechanisms of formation and loss of the rigid amorphous fraction, Polymer (Guildf). 52 (2011) 4562–4570. doi:10.1016/j.polymer.2011.08.006.

[45] J.R. Atkinson, J.N. Hay, M.J. Jenkins, Enthalpic relaxation in semi-crystalline PEEK, Polymer (Guildf). 43 (2001) 731–735. doi:10.1016/S0032-3861(01)00668-1.

Chapter 3:

Effect of pressure on polycaprolactone morphology

Christopher M. Baker Sc.M., Aharon Azagury Ph.D., Eileen Ly, Rachel Lee, Edith Mathiowitz Ph.D.

The following chapter is being submitted to Polymer.

2016; October

Abstract: The effects of applying coordinated pressures and temperatures over specific periods of time on the polymer Polycaprolactone were characterized using differential scanning calorimetry (DSC), X-Ray Diffraction (XRD), and polarized light microscopy (PLM) equipped with a hot stage. During the course of this study, interesting morphological changes were observed. PLM was found to reveal a remarkable change in the polymers birefringence. Most notably, when pressed at temperatures close to the melting temperature, a liquid crystalline like phase was observed. Upon observing these samples under polarized hot stage microscopy, samples which were induced with liquid crystalline phases were found to melt at temperatures as high as 11 °C above the original melt of the untreated sample at 58 °C. Additionally, DSC analysis of the crystalline region revealed an average increase in crystallinity increase for all samples from 12.8% to 23.0%. XRD revealed that a maximum crystallinity of 45% was achieved by processing above 60 °C.

1. Introduction

Recently, our group explored the effect of applying pressure/temperature/time on the morphology of poly-L-Lactic acids film's (PLA). [1] Interestingly, it was discovered that applying pressures and temperatures in specific sequences over time could produce multiple distinguishable phases in PLA films, including one of which quite closely resembled that of a liquid crystalline phase. Given these findings, it was deemed prudent to expand this study to include additional polymers. Given our previous choice of PLA and the increasing importance and use of biodegradable polymers, Polycaprolactone was chosen as the focus of this study.

Polycaprolactone (PCL) is a semi-crystalline thermoplastic belonging to the family of polyesters and possess many properties which make it viable for a multitude of applications. These properties include customizable degradation, good mechanical properties (young modulus, elasticity, tensile strength), ease of manufacturing and addition of functional groups for enhancement of hydrophobicity, adhesiveness and biocompatibility.[2,3] PCL is typically synthesized using ring opening polymerization or by the free radical ring opening polymerization technique, both of which can affect the materials potential molecular weight and structure.[4] PCL's physical properties usually consist of a glass transition temperature (T_g) of -65 °C to -60 °C and a melting temperature (T_M) of 56 °C to 65 °C with dependence on the materials morphology.[2,5–7] PCL's molecular weight typically varies between 3,000-80,000 g/mol with

increasing molecular weight leading to decreased crystallinity due to the propensity for longer polymer chains to restrict the ability of the polymer to crystallize.[2,8,9] PCL is capable of reaching a crystallinity content as high as 69%.[6,7] PCL's physical characteristics such as degradability are greatly affected by the materials molecular weight and crystallinity.[9–13] PCL's degradation profile is usually quite slow, taking 2-4 years to degrade through hydrolytic cleavage and enzymatic fragmentation with dependence on the materials crystallinity, making it an ideal applicant for long term biodegradable use in many fields.[11,12,14] Additionally, PCL's ease of miscibility with other polymers as well as various small molecules makes it a very popular choice for biomedical applications such as long-term implant and oral drug delivery devices.[3,12,15]

Polycaprolactone, like many polymers, is susceptible to physical aging or enthalpic relaxation. This process is the result of the polymer possessing excess enthalpy upon reaching the glassy state, which it in turn attempts to release in order to achieve thermal equilibrium. This excess enthalpy release is generally reliant on small segmental chain realignments along with a reduction in the materials free volume with a direct dependence on the materials storage time and proximity to its T_g. [16–21] Unfortunately, this process generally has negative implications in regards to a materials ductility and fracture toughness, most often leading to materials with reduced durability. [17–19,22,23]

The aim of this paper is to investigate if the application of pressure under specific temperatures and times will have a similar effect as which was observed

in PLA in Polycaprolactone (PCL), thus allowing us to further understand the properties of the degree of crystallinity and the ability to induce a liquid crystalline phase in the polymer domain.

2. Materials and Methods

2.1 Preparation of Polycaprolactone Pellets

Dow Tone P-787 Polycaprolactone was donated from Durect Lactel® (Lactel, Birmingham, Alabama) for scientific use with an expected molecular weight of 50,000 g/mol. Upon receiving the PCL granules, pellet samples were produced by hot melting 4 granules weighing ≈100 mg together on a hot plate. Samples produced in this manner were found to have a thickness of 0.071 in with a diameter of .409 in. The samples were then placed in individual containers and stored on the benchtop at room temperature.

2.2 Processing of Polycaprolactone

100 mg pellet samples were initially placed between two 4 in x 4 in stainless steel plates. The pellets were then subjected in a heating/cooling capable Carver Auto Series Hydraulic Press (Carver, Wabash, Indiana) to discrete stress profiles. Specifically, pressures of (2,000 lbs, 5,000 lbs, 10,000 lbs, 15,000 lbs, 20,000 lbs) and temperatures of (22 °C, 50 °C, 60 °C, 70 °C) ranging over three periods of time (5 min, 10 min, 15 min). These profiles targeted temperatures both below and above PCL's melting temperature (T_m) of 60 °C.[7] Upon elapse of the allotted amount of time under pressure and

temperature, samples were cooled with pressure maintained to 22 °C over a 5 min period and then released from the press.

2.3 Chemical Analysis

A Perkin Elmer Spectrum One Fourier Infrared Transform Spectroscopy (FTIR) unit (Perkin Elmer, Shelton, Connecticut) was used. PCL sheet samples were analyzed using an attenuated total reflectance module (ATR).

2.4 Size Exclusion Gel Permeation Chromatography

A Gel Permeation Chromatography (GPC) system configured for size exclusion (Perkin Elmer Flexar Ultra High Performance Liquid Chromatography system Totalchrom WS MI software V 6.2 Perkin Elmer, Shelton, Connecticut) was used to determine molecular weight. PCL granules were dissolved in HPLC grade Tetrahydroflurane (THF) (Fisher Scientific, Pittsburgh, Pennsylvania), filtered with a .22 µm filter and run through two serially connected Waters HR 4 & HR 5E Columns (Waters, Milford, Massachusetts) at a flowrate of 1 mL/min. The GPC was calibrated using a monodisperse polystyrene standard.

2.5 Thermal Analysis

A differential scanning calorimeter (DSC 8500 with Pyris software, Perkin Elmer, Shelton, CT) was used. The DSC was calibrated with a pure indium standard at a heat up rate of 10 °C/min. Samples (3-5 mg) weighed on a Perkin Elmer AD.4 Microbalance (Perkin Elmer, Shelton, CT) were analyzed under dry

nitrogen purge conditions. Samples were cooled to -60 °C and held for a period of one minute prior to commencing the DSC cycle. Samples were cycled from -60 °C to 100 °C at a rate of 10 °C/min. Melting temperature (T_m) and enthalpy of crystallization (ΔH) was then calculated using Pyris software (Perkin Elmer, Shelton, CT).

2.6 Structural Analysis

X-Ray Powder Diffraction (XRD) was performed using a Bruker D-8 Advance X-Ray Powder Diffraction system running DaVinci Software and a Cu X-Ray tube operating at 40 kV and 40 mA equipped with a Bruker Vantec-500 Xe-CO2 gas filled detector with a 13.5cm diameter window set at 20 cm from the goniometer center. System wavelength was 0.15418 nm. The system optics consisted of a polycap with an output beam divergence of 0.25° for Cu and a spot diameter of less than 4.0 mm and a 79 mm long 0.3 mm collimator on the incident beam path (Bruker, Billerica, Massachusetts). Scans were run from 15°-70° 2Θ with a virtual step size of .02° and a counting time of 30 s per step. Upon completion of the scan, data was analyzed using the Bruker Diffrac-Eva software package (Bruker, Billerica, Massachusetts). All samples were scanned using a zero diffraction plate between the aluminum stage and sample.

2.7 XRD Crystallinity Calculation

A MATLAB graphical user interface (GUI) was created (available in the supporting materials section) to extract the required data from the XRD plots for

the purpose of calculating the PCL's % Crystallinity. Profile-fitting models are then applied by the user to define the amorphous region and baseline. The amorphous area and total area (above the baseline) can be calculated using integration within MATLAB. The intensity area due to the crystalline region can then be calculated by subtracting the amorphous region from the total area, and the percent crystallinity can be calculated by dividing the intensity area due to the crystalline region by the total area.

2.8 Hot Stage Polarized Light Microscopy

Hot Stage Polarized light microscopy (PLM) was performed using an Olympus Model BX-60 (Olympus, Center Valley, Pennsylvania) microscope equipped with polarized filters, 10X, and 50X objectives. The microscope stage was replaced with a Linkam Scientific Model THMS600 Hot Stage (Linkam Scientific Instruments, Tadworth, United Kingdom) which was operated with a TMS 94 temperature controller running Linksys32 Ver.2.2 software (Linkam Scientific Instruments, Tadworth, United Kingdom). Small pieces cut from the bulk PCL samples were placed in an optically transparent quartz dish and heated for the purposes of optical analysis at a rate of 10 °C/min from ≈22 °C until full melt was observed by complete extinction of the noted birefringence. Images were captured at a rate of 1 frame per 10 seconds utilizing a PixeLINK (PixeLINK, Ottawa, Canada) model PL-E421CU color enabled camera running PixeLINK Capture OEM Software Version 2.3.5.0 (PixeLINK, Ottawa, Canada).

3. Results and Discussion

3.1 Fabrication of the PCL

Fig. 1. is a diagram depicting the processing procedure used to pressure treat the PCL. Samples were placed in an auto press with sufficient pressure to engage the press plates and make contact with the material. Once contact was established, the material was heated to the desired temperatures. All samples were in effect, processed above the T_g given PCL's low T_g of -60 °C. The temperatures were chosen to be below the T_m at 22 °C & 50 °C and near and above the T_m at 60 °C & 70 °C. Upon lapse of time t (5,10,15 min), the samples were cooled to T_C (room temperature) with the pressure P maintained. Thus by doing this, crystallization of the PCL occurred under the restricted pressure. Once cooled to T_C, the pressure P was terminated and the sample was released for further analysis. Table. 1.SI in the appendix provides a record of all the conditions we explored. In total, 60 different processing conditions were characterized.

Once samples were processed, their dimensions were recorded and are depicted in Fig. 2.. Fig. 2. is arranged such that moving from left to right, we first observe the unaltered sample (Black) after which pressure increases from 2,000 lbs to 20,000 lbs. Similarly, temperatures increase from left to right in the following progression; 22 °C (Red), 50 °C (Green), 60 °C (Blue) and 70 °C (Purple). Initial unaltered sample thickness as depicted by the black line was 0.07 inches with samples predominately observed to decrease in thickness as

temperature was increased. Samples processed at 70 °C displayed the lowest thickness values at 0.001 inches. This trend in decreasing thickness was also observed as pressure increased but appears to have a lower affect than increasing temperature. This was observed as the sample processed at 22 °C and 2,000 lbs had a thickness of 0.039 inches while the sample processed at the same temperature of 22 °C but at 20,000 lbs was found to possess a thickness of 0.018 inches. Processing time appeared to have no discernible trend in decreasing sample thickness. Additionally, a complete accounting for all dimensional changes including surface area and volume may be found in the supporting information section in Table. 3.SI. Initial surface area of the unaltered material was measured at 0.354 in^2 with surface area being found to increase in response to processing at 10,000 lbs and 70 °C to a high of 11.282 in^2.

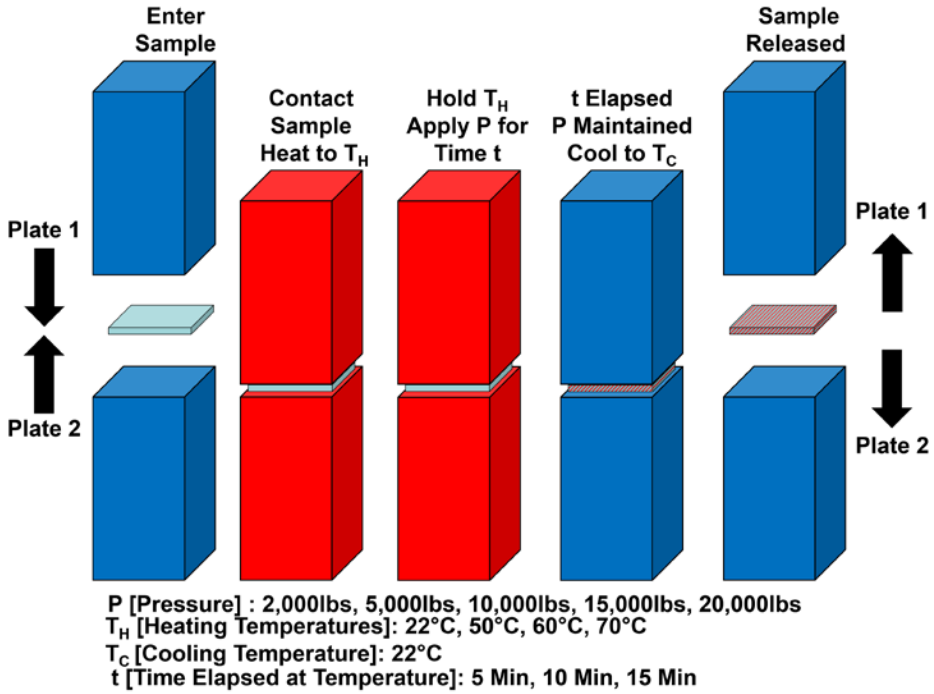

Figure. 1. Graphical representation of the processing procedure. Samples are placed into a Carver Auto Press and exposed to pressures (P) ranging from 2,000 lbs to 20,000 lbs at temperatures (T_H) ranging from 22 °C to 70 °C for a period of time (t). Once the prescribed time has elapsed, samples are cooled to the temperature (T_C) and released from the press.

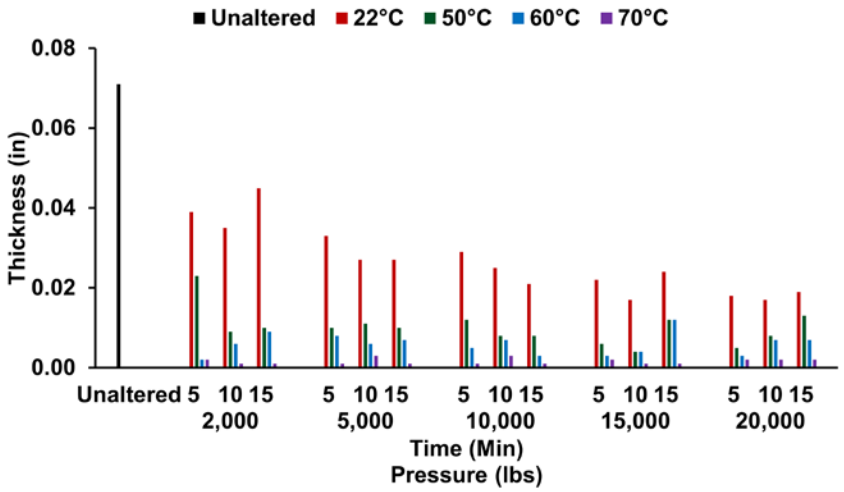

Figure. 2. PCL sample thickness measurements.

3.2 Characterization of the Unaltered PCL by FTIR, DSC, XRD, PLM and GPC

The objective of this section is to provide a characterization of the PCL material prior to it being processed. This allows for a better understanding of the polymers properties as well as provides a reference point for comparison post processing. To achieve this goal, the material was initially analyzed using FTIR, DSC, XRD, PLM and GPC. These techniques were chosen as they allow for the evaluation of the PCL's initial purity, morphological state, thermal properties, structural and molecular weight. Fig. 3. depicts the FTIR, DSC, XRD and PLM analysis of the polymer.

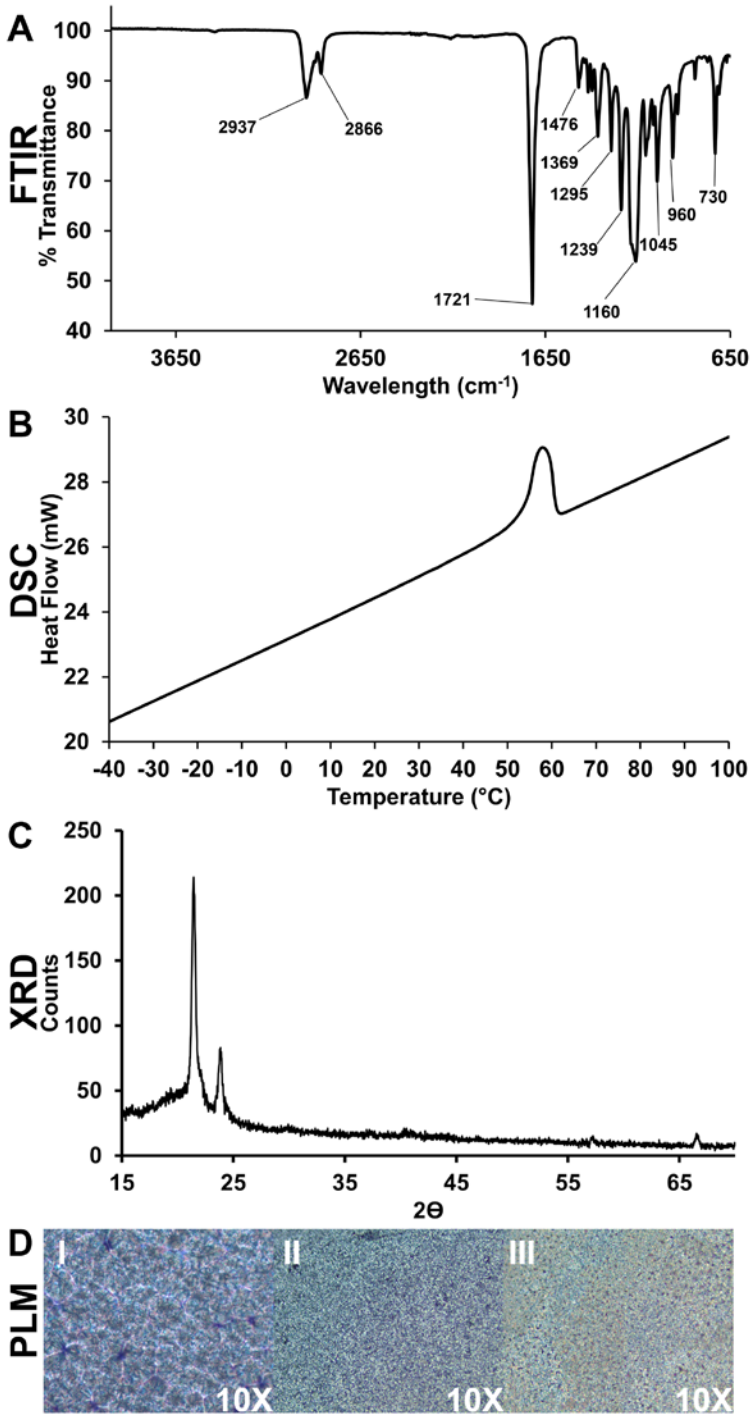

Figure. 3. FTIR interferogram of PCL using an ATR Module (A). DSC thermal profile of the Unaltered PCL. (B) XRD profile of the Unaltered PCL. (C) PLM images of PCL (D) Unaltered (D-I), Solvent casted (D-II), Melt casted (D-III).

Fig. 3.A. displays the typical FTIR peaks associated with PCL which occur at approximately 1160 cm^{-1} (C-O and C-C), 1721 cm^{-1} (C=O) and 2865-2949 cm^{-1} (CH_2).[24] FTIR results suggest the material is free of any detectable excipients and additives.

DSC analysis of the material as received and depicted in Fig. 3.B. revealed a melting temperature of 57.73 °C and enthalpy of crystallization (ΔH) of 17.8 J/g. % Crystallinity was observed to be 12.8% as calculated by dividing the PCL's heat of fusion (ΔH) by ΔH value of 100% crystalline PCL (139.5 J/g).[12,13,15]

XRD analysis of the depicted in Fig. 3.C. reveals a profile typical of the semi-crystalline structure found in PCL with peaks forming at 2Θ values of 21° and 24°.[14] % Crystallinity was observed to be 24.85% as calculated by integrating that area under the curve and as described in the experimental section.

Utilizing PLM, the PCL was analyzed for the presence of birefringence which indicates the existence of ordered phases in polymeric materials.[25–28] Conversely, materials which lack order, appear dark or black when imaged between crossed polarizers. Fig. 3.D. displays PLM of the polymer after it was allowed to crystalize under three different conditions. Fig. 3.D.(I) depicts the PCL as received and displays the typical spherulitic structure expected of semi-crystalline polymers. Fig. 3.D.(II) depicts the PCL after it was solvent casted and reveals very tiny crystals. While Fig. 3.D(III) depicts the PCL after it was melt

casted and similarly displays tiny crystals. Clearly the material displays a semi-crystalline morphology.

GPC analysis which is depicted in Fig. 1.SI revealed that the Lactel® PCL's Weight Average (Mw) was 37,600 g/mol and number average (Mn) was 18,200 g/mol. Poly Dispersity (Mw/Mn) was 2.067 respectively**.**

3.3 DSC Analysis of the processed PCL Samples

Systematic DSC analysis of the processed samples allowed for a clear understanding of how the effect of pressure, temperature and time affect both the PCL's melting point (Fig. 4.) and heat of fusion (Fig. 5.). The data is arranged such that all three processing conditions (pressure, temperature and time) increase as one progresses from left to right.

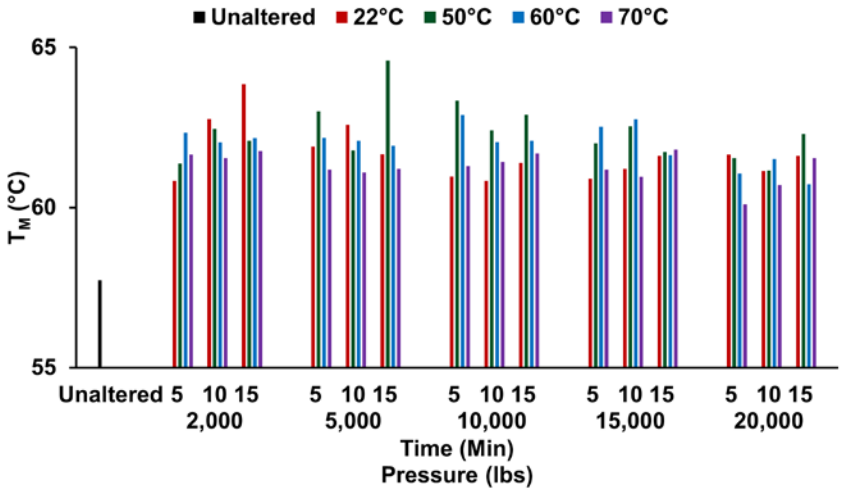

Figure. 4. Effect of processing conditions on PCL melting point as calculated by DSC.

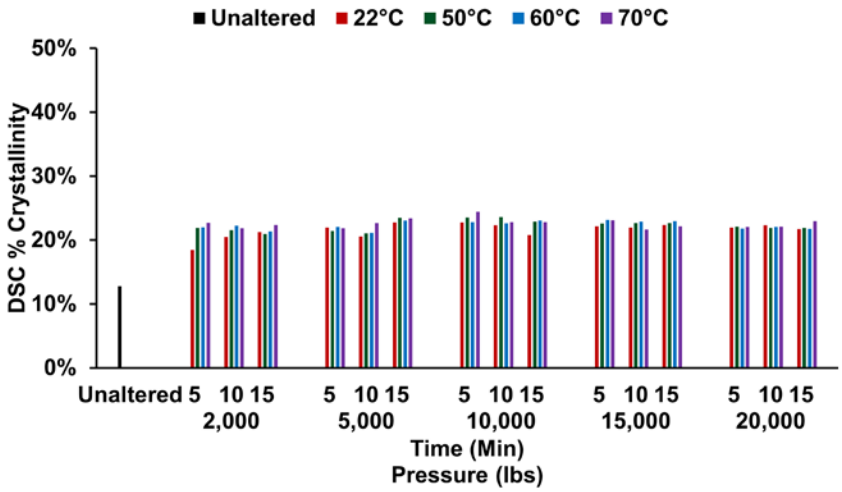

Figure. 5. Effect of processing conditions on PCL's crystallinity as calculated by DSC.

Looking to Fig. 4., the PCL's melting temperature as determined by DSC is observed to increase greatly from the unaltered samples peak value of 57.73 °C, to a maximum peak of 64.59 °C. Moving from left to right, the effect of pressure does not appear to produce any discernible trend in the PCL's increase in peak melting temperature. However, by focusing on the processing temperature, the peak melting temperature is observed to increase most for samples processed at both 50 °C and 60 °C.

Fig. 5. reveals the PCL's crystallinity as calculated by the polymers heat of fusion. Interestingly, the polymers crystallinity is clearly observed to increase from the unaltered polymers value of 12.79% to an average of 22-23%, yet when attempting to compare the results in relation to processing pressure, temperature and time, all the values display the same degree of crystallinity. This was intriguing as previous results observed in PLA displayed a definitive trend of

increasing crystallinity in response to increasing temperature and pressure processing conditions.[1] Given this apparent limit of 23% crystallinity as observed by DSC under the aforementioned processing conditions, it was determined that XRD should be performed to further characterize the material. Thus the changes in crystallinity as revealed by XRD will be the focus of the next section.

3.4 XRD analysis of the processed PCL

Using our previous experience studying PLA. [1] XRD analysis was performed on all processed PCL samples and is depicted in Fig. 6.. Fig. 6. (A-C) is a combination of three collages that display all the morphological changes in the PCL samples after processing. Each sub figure (A-C) is indicative of the specific time to which the polymer was exposed to under the recorded pressure, (A) 5 min, (B) 10 min, and (C) 15 min. Each column moving from left to right is representative of increasing processing pressure from 2,000 lbs to 20,000 lbs while ascending up each row is representative of increasing processing temperature from 22 °C to 70 °C. Additionally, Fig. 7. is a bar graph depicting the degree of crystallinity of all processed samples as calculated by integrating the crystalline portion of the XRD profiles depicted in Fig. 6. which was described in the experimental section.

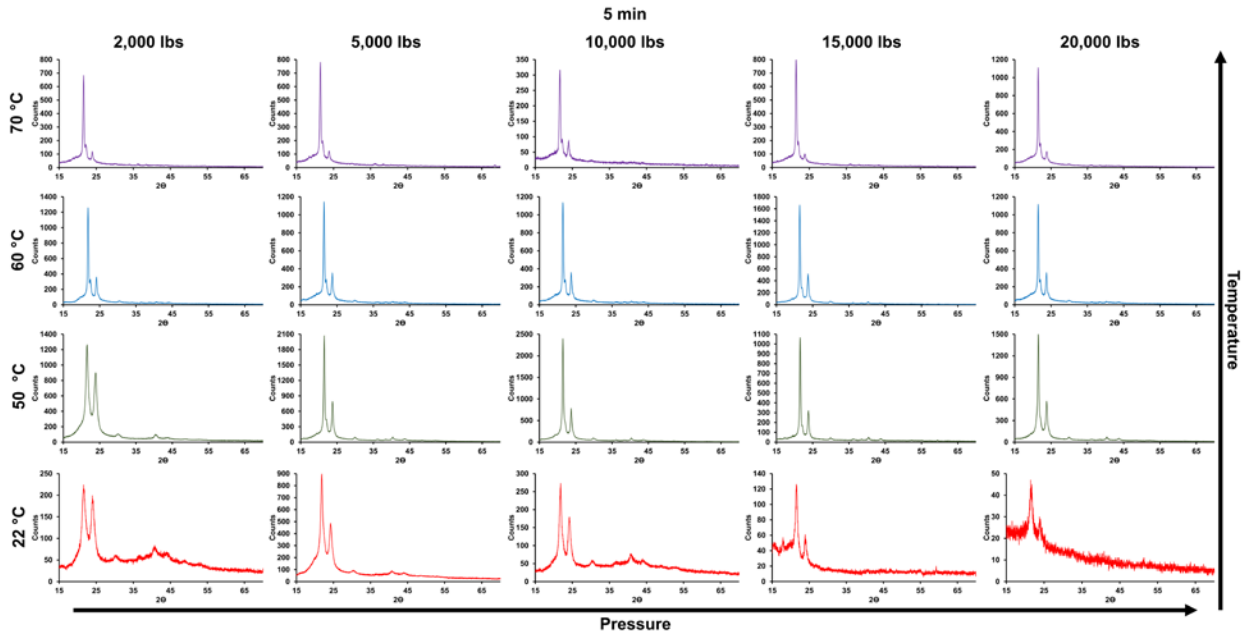

Figure. 6. (A) Collage depicting the XRD profiles for all samples processed for 5 min.

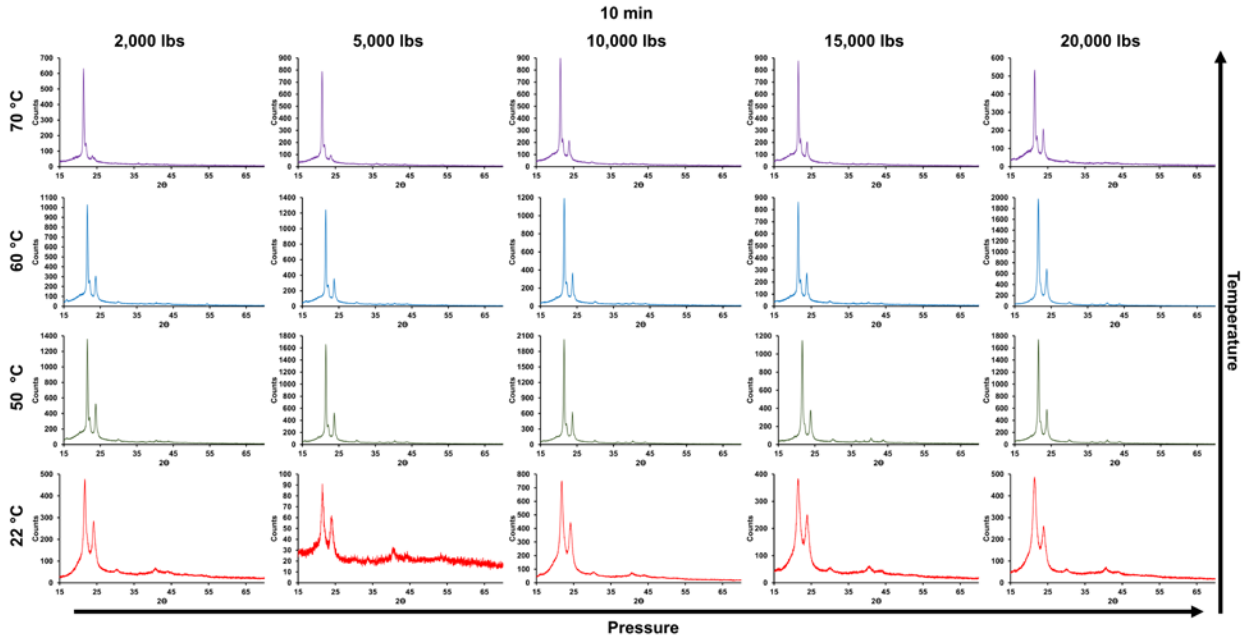

Figure. 6. (B) Collage depicting the XRD profiles for all samples processed for 10 min.

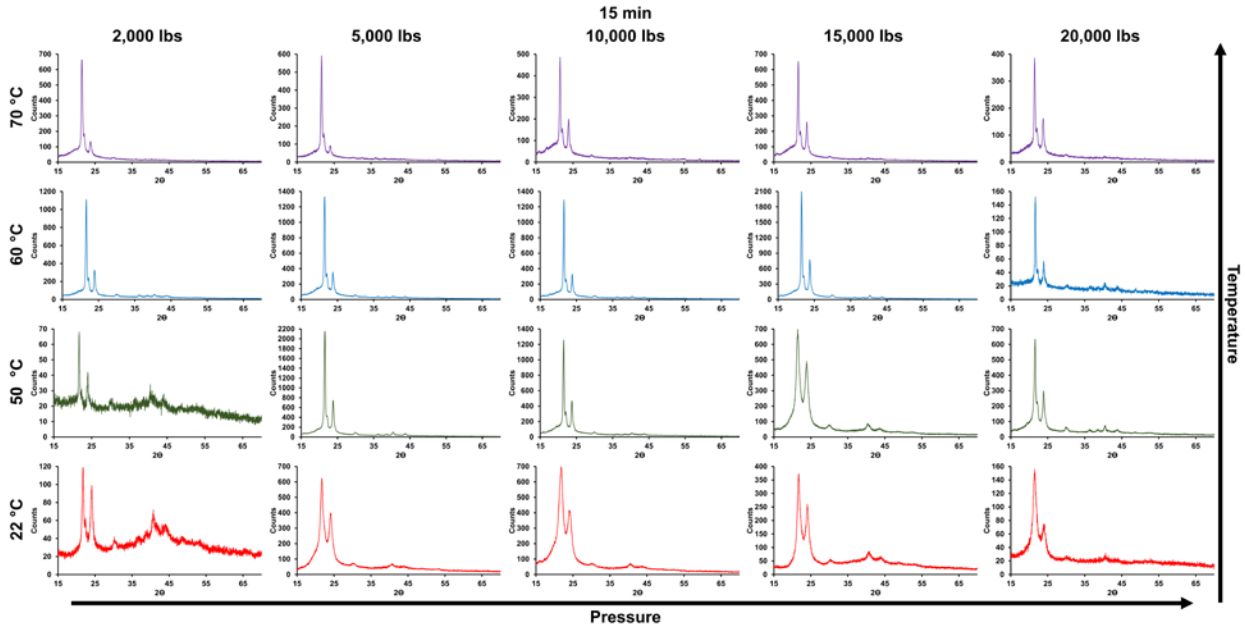

Figure. 6. (C) Collage depicting the XRD profiles for all samples processed for 15 min.

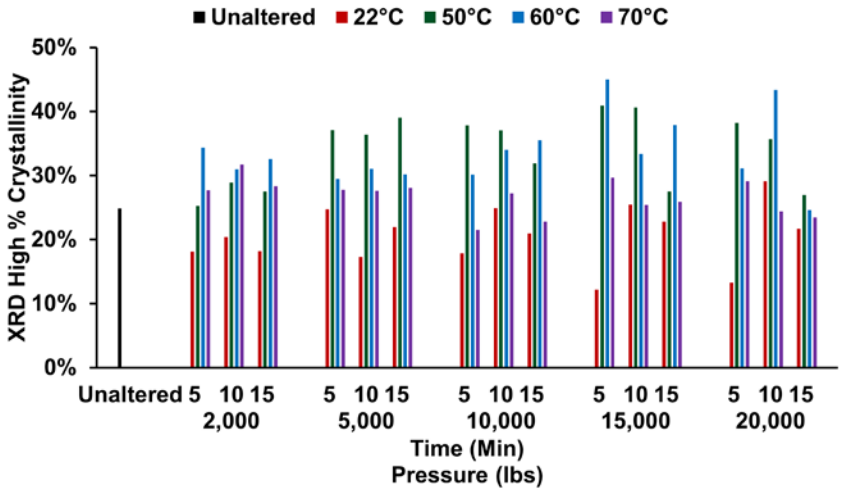

Figure. 7. Effect of processing conditions on PCL's crystallinity as calculated by XRD.

Given the scale of the XRD data set, it was necessary to fix a variable and discuss the results as another was changed. Thus we discuss the observed

effects with pressure fixed as temperature increases. Given that the variable of time did not appear to affect the changes observed in the material very much, it will be mentioned only when a major change is noted.

3.3.1 2,000 lbs:

Analyzing the first columns of Fig. 6. (A-C) for samples kept at 2,000 lbs for 5, 10 and 15 min. The samples processed at 22 °C (red) display XRD profiles which are quite different than that which was previously observed in the unaltered polymer in Fig. 3. with the appearance of two wider peaks with similar intensities. The % Crystallinity as calculated by XRD (Fig. 7.), revealed a decrease in crystallinity from 24.8% (Unaltered) to 18.1%. Increasing the processing temperature to 50 °C (green) shifted the XRD profile towards a more crystalline profile with sharper peaks as time increases from 5 min (25.25%) to 15 min (27.54%). Interestingly, in this series, the sample processed for 10 minutes appears the most crystalline and is reflected in Fig. 7. as having a % Crystallinity of 28.9%. Increasing processing temperature to 60 °C (blue) reveals an XRD profile with very crystalline peaks, with the first peak increasing in intensity comparatively to the second while it also becomes much sharper than the second peak. This is quite different than what was observed in the unaltered material (Fig. 2.). This samples crystallinity was observed to increase to 34.3% (Fig. 7.). Finally, by increasing the processing temperature to 70 °C (purple), we observe a very large increase in the sharpness of the first peak, so much so that

the second peak is now almost invisible in comparison. Crystallinity is observed to increase to 31.7% (Fig. 7.).

3.3.2 5,000 lbs:

Moving to the second column of Fig. 6. (A-C) for samples kept at 5,000 lbs for 5, 10 and 15 min. The samples processed at 22 °C (red) once again display an XRD profile with broader peaks. The two peaks associated with PCL are also once again observed to display the same intensity. Fig. 7. reveals a decrease in crystallinity to 17.3%. Increasing the processing temperature to 50 °C (green), the XRD profile displays and increase in crystallinity as the peaks become sharper. The two peaks also begin to take on different profiles with the first increasing in sharpness greatly. Fig. 7. reveals an increase in % Crystallinity to 39.0%. Increasing processing temperature to 60 °C (blue), the XRD profile becomes very sharp, especially the first peak which surpasses the second peak in intensity. Fig. 7. reveals this samples crystallinity is observed to increase to 31.0%. Increasing the processing temperature yet again to 70 °C (purple), the first peak in the XRD profile becomes sharper as the second peak decreases in intensity. This change may be indicative of one crystal population becoming more abundant after the processing procedure. Fig. 7. Displays and increase in % Crystallinity to 28.0%.

3.3.3 10,000 lbs

Moving to the third column of Fig. 6. (A-C) for samples kept at 10,000 lbs for 5, 10 and 15 min. The samples processed at 22 °C (red) begin to consistently display a broadened peak structure. Both of the crystalline peaks appear to diminish in sharpness greatly as well as appear to become very similar in intensity. Fig. 7. reveals almost no calculated change in crystallinity with a % crystallinity of 24.9%. Increasing the processing temperature to 50 °C (green) the material once again takes on a very sharp peak profile. The first peak is also once again observed to increase in intensity over the second peak. Fig. 7. reveals a large increase in % crystallinity to 37.8%. Increasing processing temperature to 60 °C (blue) causes the peaks to become quite sharp, with the first peak surpassing the second in intensity. Fig. 7. reveals that % crystallinity has increased to 35.5%. Increasing the treatment pressure yet again to 70 °C (purple) the profile begins to display a broadening of the peaks and a decrease in their intensity with the first still remaining more intense than the second. Fig. 7. reveals a % Crystallinity of 27.2%.

3.3.4 15,000 lbs

The fourth column of Fig. 6. (A-C) depicts the samples processed at 15,000 lbs for 5, 10 and 15 min. Samples processed at 22 °C (red) display a very broad peak profile with the first and second peaks becoming quite similar in height and shape. Fig. 7. reveals a decrease in % crystallinity to 12.2% for the 5 min samples and a relatively unchanged % crystallinity of 25.5% (10 min) and

22.79% (15 min) for the others. Increasing the processing temperature to 50 °C (green) increases the sharpness of the first peak as well as the its intensity compared to the second in the 5 and 10 min samples. This however is not seen in the 15 min sample as the peaks become quite close in intensity as well as quite broad in appearance. Fig. 7. reveals an increase in crystallinity for the 5 and 10 min samples to 41.0% with a % crystallinity of 27.52% being noted for the 15 min sample. Increasing the temperature to 60 °C (blue) results in an increase in peak sharpness which is displayed by the first peak. The second peak is observed to remain sharp yet appear less intensely than the first. Fig. 7. Reveals an increase in crystallinity in all times to 45.0% (5 min), 33.35% (10 min) and 37.9% (15 min). Increasing the processing temperature to 70 °C (purple) keep the profile sharp with the first peak displaying a much higher intensity then the second. Additionally, the ratio between the first and second peak is observed to decrease as the processing time is increased. Fig. 7. reveals a % crystallinity of 29.7% for the 5 min sample while the 10 and 15 min samples are observed at 25.4% and 25.88% respectively.

3.3.5 20,000 lbs:

Moving to the fifth and final column of Fig. 6. (A-C) for samples kept at 20,000 lbs for 5, 10 and 15 min. The samples processed at 22 °C (red) display a broad and elongated profile. Interestingly the second peak is also observed to diminish in intensity greatly in this sample cohort. Fig. 7 reveals a % crystallinity increase to 29.1% in the 10 min samples with both the 5 and 15 min samples

decreasing to 13.3% (5 min), and 21.7% (15 min) respectively. Increasing the processing temperature to 50 °C (green) we observe a sharp peak profile in the 5 and 10 min samples with the 15 min sample taking on a noticeably broader structure profile. In all cases, the first peak remains more intense than the second. Fig. 7. reveals an increase in % crystallinity to 38.2% (5 min) and 35.7% (10 min) with the 15 min sample only marginally changing to 26.9%. Increasing to 60 °C (blue) we observe the peaks become quite sharp in profile with the first peak once again appearing sharper than the second peak. Fig. 7. reveals a % crystallinity increase to 31.1% (5 min) and 43.4% (10 min) with the 15 min samples remaining unchanged at 24.6%. Finally, ending with the sample processed at 70 °C (purple) we see the peak structure remain quite sharp in all the samples. However, it is noted that the 5 min samples first peak dwarfs its second peak. This is not observed in the 10 and 15 min samples as the ratio between their first and second peaks is observed to decrease. Interestingly, we observe the profiles of the 10 and 15 min samples take on a broader base than that which was observed in the 5 min sample. Fig. 7. reveals a % crystallinity increase to 29.1% in the 5 min sample while both the 10 min samples remaining relatively unchanged at 24.4% (10 min) and 23.4% (15 min).

In summary, the XRD provided information more accurately regarding the degree and nature of the PCL's morphology than the DSC. While the DSC was able to reveal a general increase in crystallinity upon processing to 23% for all samples, the XRD was better able to discern the differences in crystallinity based on processing conditions with the following trends being noted. Increasing

processing temperature was associated with increased crystallinity, especially when the material was processed at 50 °C and 60 °C. With the highest observed value of crystallinity being noted at 60 °C (45%). Interesting, samples processed at 22 °C were generally observed to decrease in crystallinity displaying a very broad XRD profile while those processed at 70 °C appeared to remain rather sharp and constant. With regards to increasing processing pressure, the XRD results were able to demonstrate that crystallinity generally increased as pressure increased for those materials processed specifically at 50 °C and 60 °C. Lastly, processing time was found to have little effect if none at all.

3.4 Effects of Processing Conditions on the Amorphous Region Using Polarized Light Microscopy

This section discusses the birefringence results that were obtained using PLM, which as mentioned previously are indicative of the structural order present in the material. [25–28] Additionally, the three control samples which were discussed in Fig. 2. (D) will serve as a reference point for comparison to the other morphological states that may exist in the processed PCL. In Fig. 2. (D), all samples observed under crossed polarizers revealed a clear crystalline structure with many spherulite populations throughout the sample.

Fig. 8. (A-C) is a combination of three PLM collages that visually depict all the morphological changes in the PCL samples after complete processing. Each

sub figure (A-C) is indicative of the specific time to which the polymer was exposed under the recorded pressure, (A) 5 min, (B) 10 min, and (C) 15 min. In addition, each sub-figure contains 5 columns of PLM data. Each column moving from left to right is representative of increasing processing pressure from 2,000 lbs to 20,000 lbs while ascending up each row is representative of increasing processing temperature from 22 °C to 70 °C. Finally, it is important to mention that all the birefringent effects observed in this study were homogenous throughout the entire sample.

Fig. 8. (A-C) depicts a wide array of different birefringence populations. Generally speaking, in regards to pressure, the PCL is observed to become more birefringent as pressure is increased. Specifically, the morphology drastically changes from a crystalline structure to a morphology resembling that of a liquid crystal like structure lacking any visible spherulitic structures. This result was previously noted in our previous work with PLA and is indicative of an amorphous region displaying an oriented morphology.[1]

Looking at the general effect of temperature, Fig. 8. (A-C) depicts an immediate change in the polymers birefringence which appears most vibrant when the material is processed at 50 °C and 60 °C. Interestingly, when processing the material at 70 °C, minute crystal formations lacking any apparent spherulitic structures become visible. This too was previously observed in earlier work on PLA and is indicative of the formation of smaller yet greater in number crystal populations.[1]

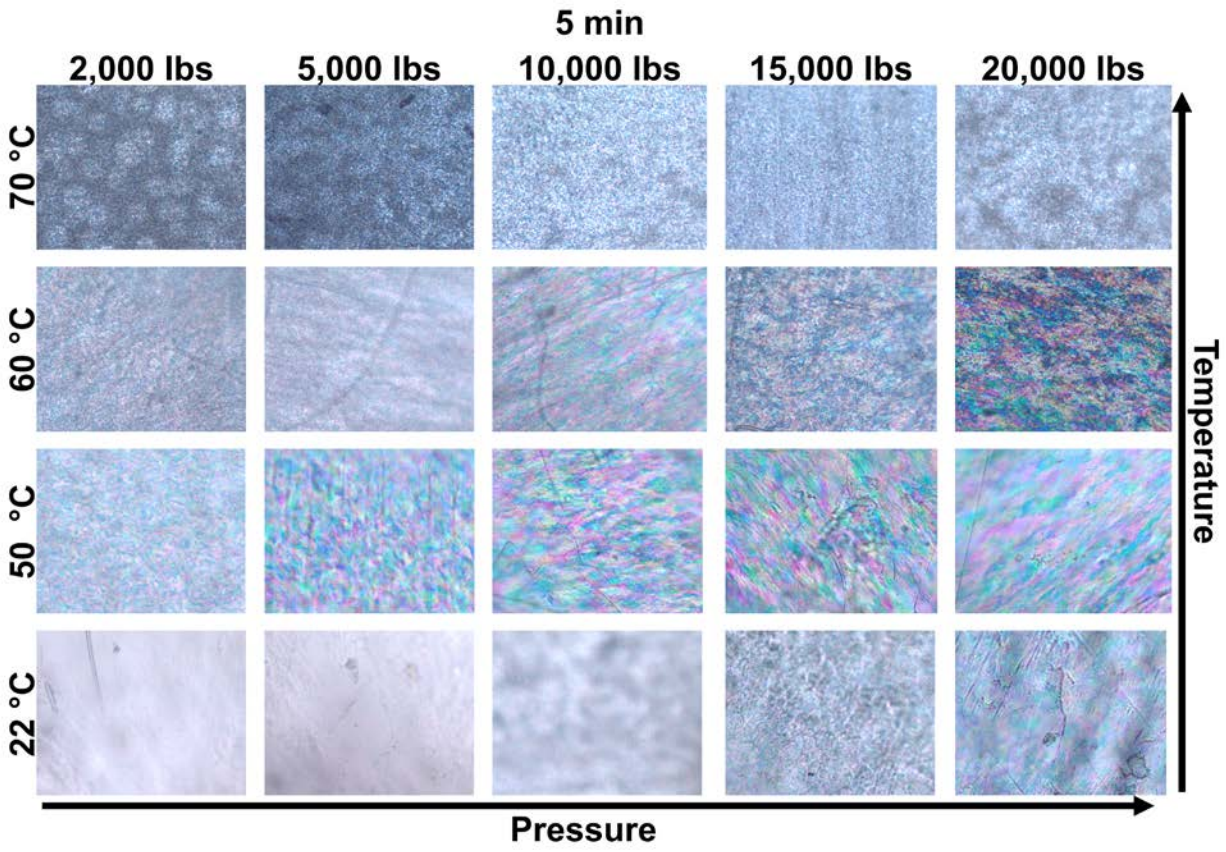

Figure. 8. (A) Crossed polarized microscopy images after processing the PCL for 5 min under all temperature conditions (22 °C, 50 °C, 60 °C, 70 °C) and pressure conditions (2,000 lbs, 5,000 lbs, 10,000 lbs, 15,000 lbs, 20,000 lbs)

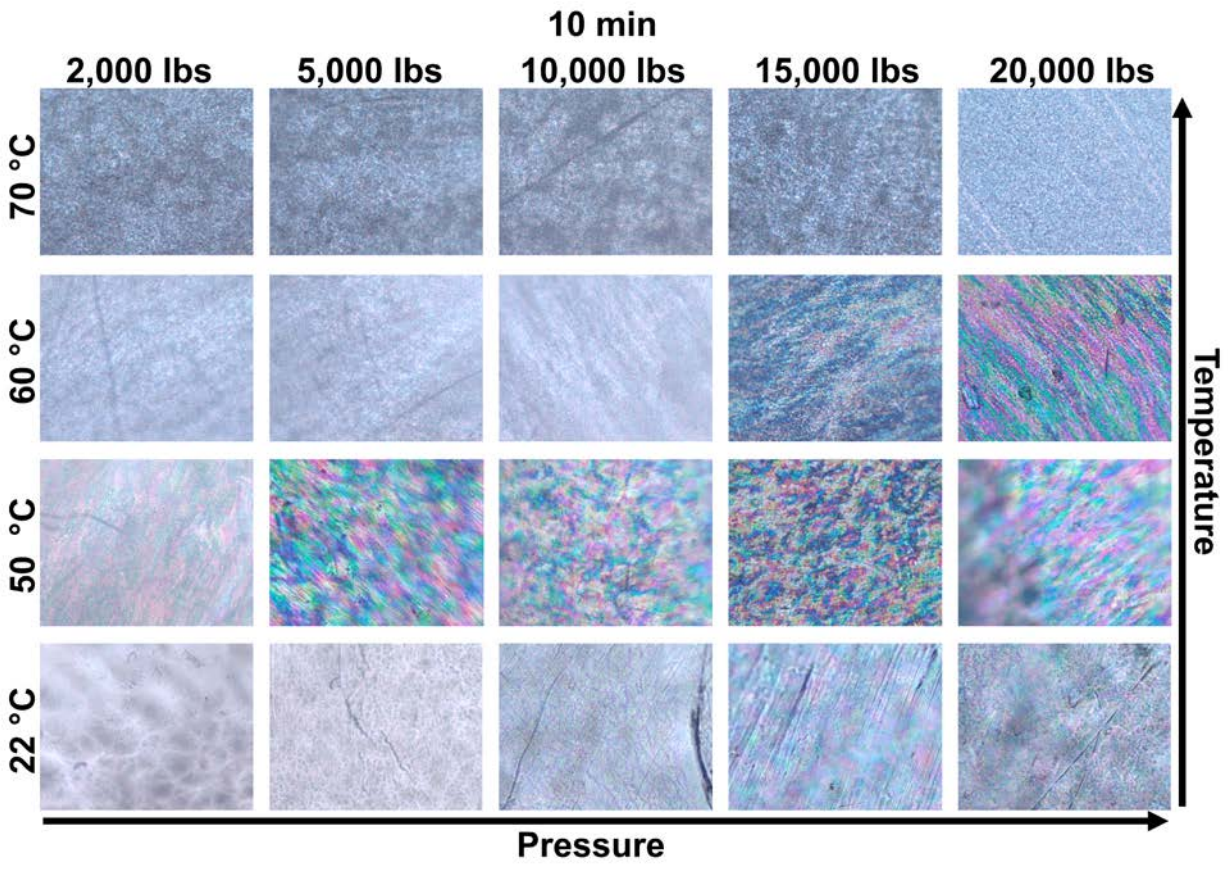

Figure. 8. (B) Crossed polarized microscopy images after processing the PCL for 10 min under all temperature conditions (22 °C, 50 °C, 60 °C, 70 °C) and pressure conditions (2,000 lbs, 5,000 lbs, 10,000 lbs, 15,000 lbs, 20,000 lbs)

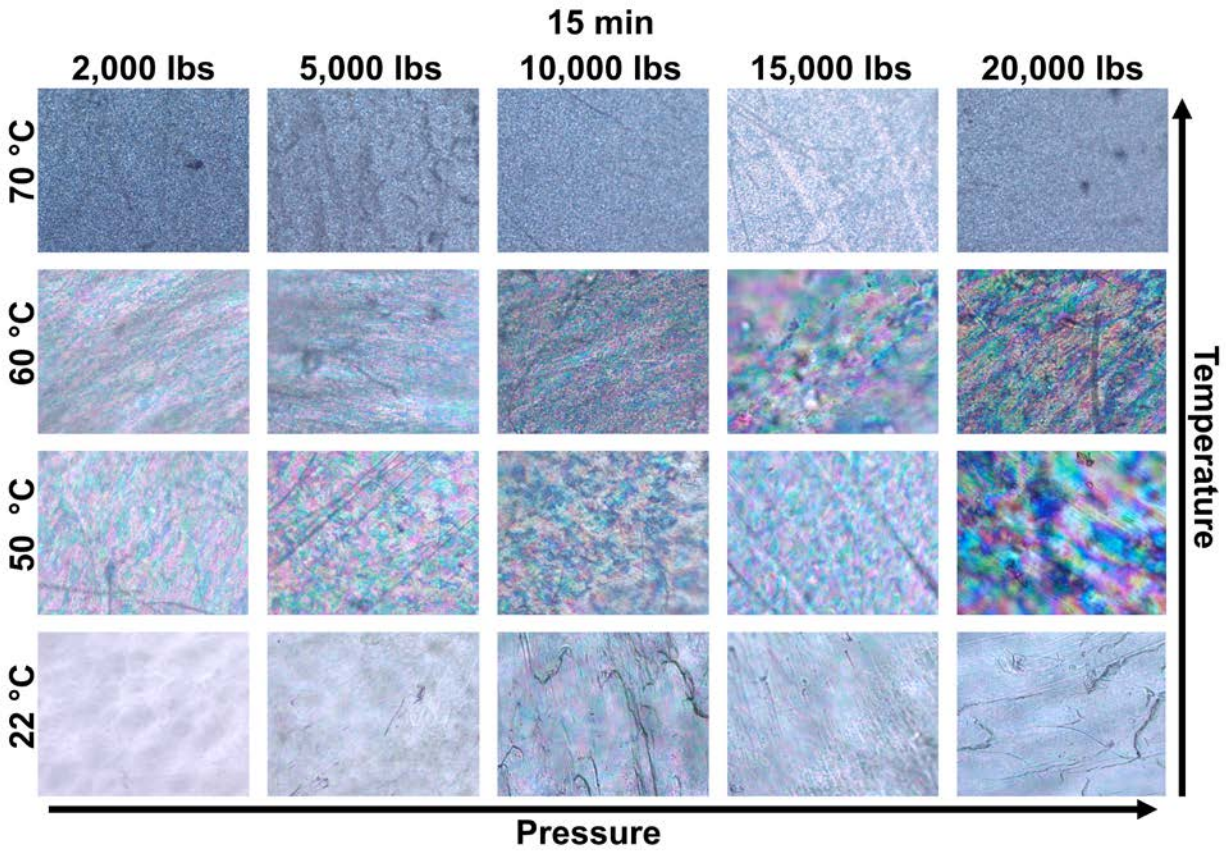

Figure. 8. (C) Crossed polarized microscopy images after processing the PCL for 15 min under all temperature conditions (22 °C, 50 °C, 60 °C, 70 °C) and pressure conditions (2,000 lbs, 5,000 lbs, 10,000 lbs, 15,000 lbs, 20,000 lbs)

3.4.1 2,000 lbs:

Focusing on the first columns of Fig. 8. (A-C) for samples treated under 2,000 lbs for three period of time (5, 10 and 15 min). It is at this pressure that we initially observe that increasing temperature from 22 °C to 70 °C affects the materials birefringence. Initially, the 22 °C sample appears white or opaque. Increasing the temperature to 50 °C induces a change in birefringence which

lacks any apparent crystals or spherulite formations. Increasing the temperature to 60 °C appears to further intensify the birefringence noted in the 50 °C samples. Interestingly, upon processing the material at 70 °C, the formation of tiny crystallites is observed. These crystallites appear to present the typical spherulitic structure when processed for 5 and 10 min but loose this structure upon increasing the processing time to 15 min. It should be noted that all of these samples have been processed well above the polymers T_g of -60 °C.[2,7]

3.4.2 5,000 lbs:

The second column of Fig. 8. (A-C) depicts samples processed under 5,000 lbs for 5, 10 and 15 min. It is observed that increasing the pressure to 5,000 lbs has quite a similar effect on the birefringence as the samples look almost identical to those processed under 2,000 lbs of pressure. The only observed difference in this series is that the birefringence color intensity is more vibrant in this series than in the 2,000 lbs cohort.

3.4.3 10,000 lbs:

The third column of Fig. 8. (A-C) depicts samples processed under 10,000 lbs for 5, 10 and 15 min. It is in this condition that the 22 °C sample begins to display a colorful change in birefringence when processed for 10 and 15 min. Increasing the temperature to 50 °C the material takes on a brilliantly vibrant and color birefringence which completely lacks any spherulitic or crystallite structures. Increasing the temperature to 60 °C we observe similar changes to those

observed in the 50 °C samples. However, upon increasing the temperature to 70 °C we observe the formation of tiny crystal structures in samples processed at 5 and 10 min. Processing the 70 °C sample for 15 min lead to the appearance of very tiny crystals.

3.4.4 15,000 lbs:

Moving to the fourth column of Fig. 8. (A-C) for samples processed under 15,000 lbs for 5, 10 and 15 min. The 22 °C sample now displays a colorful birefringence under all three time conditions. Increasing the temperature to 50 °C, we observe a very colorful birefringence which is also observed in the 60 °C samples as well. Interestingly, we once again observed the formation of small crystal structures in the material when processing temperature is increased to 70 °C. These crystal structures also appear to lack any spherulite structures while displaying a very uniform size distribution.

3.4.5 20,000 lbs:

Moving to the fifth and final column of Fig. 8. (A-C) for samples processed under 20,000 lbs for 5, 10 and 15 min. The 22 °C once again displays a colorful birefringence in all three time conditions. However, increasing the temperature to both 50 °C and 60 °C produces a remarkably brilliant and intense increase in the birefringent effect. This birefringence is also observed to lack any type of spherulite or crystal like structures. Further increasing the temperature to 70 °C leads to the creation of a population of small crystals in the 5 min cohort which

appear to possess some spherulite structures. However, increasing the time to both 10 and 15 min's leads to the production of similarly tiny and uniformly distributed crystals which lack any spherulite structures.

Analyzing the effects of both increasing the processing temperatures and pressures by PLM, it is now visually supported that the PCL's amorphous and crystalline morphologies can be influenced, especially when the processing temperature is ≥50 °C and pressure is ≥ 10,000 lbs. It was under these conditions that the PCL was observed to display the most homogenous and visually distinct changes in the materials birefringence. Additionally, the PLM images of those samples processed at both 50 °C and 60 °C lend support to the possible existence of a structural morphology, which may either closely resemble liquid crystals, or may in fact be a liquid crystalline phase.[29–31]

3.5 Effect of processing conditions on the melting behavior of PCL as observed by hot stage PLM.

In Section 3.4, we observed that processing the PCL lead to the display of a wide array of brilliantly birefringent profiles similar in nature to that of a liquid crystalline state. In this section we shall discuss the effects that the processing conditions had on the amorphous and crystalline regions by observing the polymers optical behavior in response to heating from 22 °C to ≈70 °C at 10

°C/min. Consequently, any visually apparent phase changes as well as the samples ultimate melting temperatures shall be noted in Fig. 9. And Fig. 10..

Fig. 9. depicts the visual changes observed by hot stage polarized microscopy for the unaltered PCL as well as the samples processed at 10,000 lbs for 5 min at 22 °C, 50 °C, 60 °C and 70 °C. It is arranged such that the processing temperature increases as you move up the rows from the bottom. Moving across the columns from left to right, the images are arranged such that the hot stage temperature can be seen to increase. It should be noted that Fig. 9. is only a representative set of pictures with specific focus on the changes which were observed to occur close to the melt. Fig. 10. is a bar graph depicting the final melting point of all processed samples as observed by hot stage PLM.

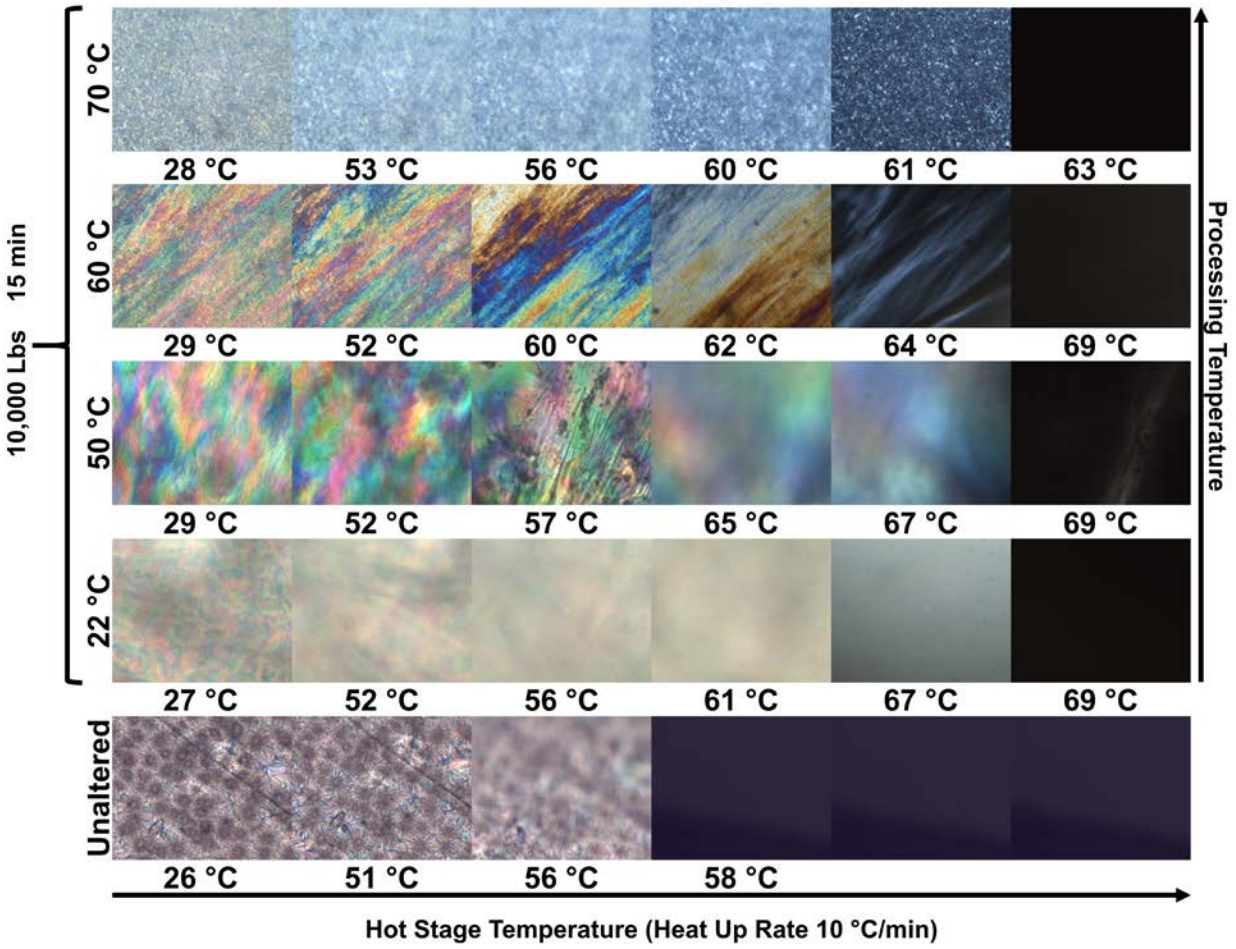

Figure. 9. Hot stage polarized microscopy images taken of the unaltered PCL, along with the samples processed under 10,000 lbs for 15 min at 22 °C to 70 °C.

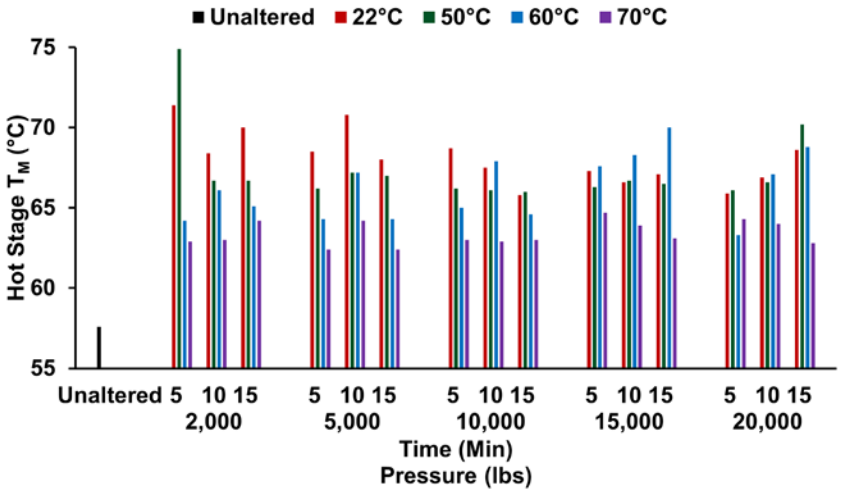

Figure. 10. Temperature at which complete extinction of all birefringence was observed upon melting the material in the hot stage.

The bottom row of Fig. 9. depicts the PLM images of the unaltered PCL, which begins its transition from crystalline spherulitic structure to a molten phase around the 56 °C mark. Then immediately at 58 °C, the material undergoes melt thus becoming completely dark under polarized light. This is expected and in line with PCL melting temperature range of 55 °C to 60 °C. [2,5]

The second row of Fig. 9. for hot stage images taken for the sample processed at 10,000 lbs for 15 min and 22 °C. The material is already observed to have a different morphology than that which was observed in the unaltered PCL. This sample unlike the unaltered does not possess any visible spherulitic structures while it does have a birefringent palate. Upon heating the sample, the material is observed to begin its phase change quite similarly in temperature to the unaltered material at 56 °C with the exception that this time the material is able to retain its structural order as observed by the transmittance of polarized

light up to 69 °C. This represents an 11 °C increase in the materials ultimate melting temperature, and further supports our theory of the existence of a liquid crystalline structure.

The third row of Fig. 9. for PLM images taken for the sample processed at 10,000 lbs for 15 min and 50 °C. The PCL is observed to have a very different morphology is this series than that observed in the unaltered material and the PCL processed at 22 °C. This sample possesses a vibrant birefringence with no visible crystal or spherulite structures. Similarly, to the previous samples, this sample commences its phase transition around 56 °C. However, the material is observed to maintain visible birefringence or structural order up to 69 °C with melt occurring immediately at 70 °C.

Moving to the fourth row of Fig. 9. for the sample processed at 10,000 lbs for 15 min and 60 °C. The PCL is observed to have a very similar morphology to the series processed at 50 °C. Interestingly, this sample does not begin its phase transition until around 60 °C. However, this sample does not last as long as the 50 °C sample did and loses all visible birefringence or structural order by 69 °C.

The fifth and final row of Fig. 9. is representative of the sample processed at 10,000 lbs for 15 min and 70 °C. The PCL displays a completely different morphology than that observed in all previous samples. This time, the material appears to possess very tiny crystal structures and does not display the type of birefringence observed in the 50 °C and 60 °C samples. Interestingly, the material is observed to begin changing in color intensity around 56 °C but does

not appear to lose any of its crystals. Then very suddenly and intensely, all of the crystals are observed to simultaneously melt and disappear at 63 °C. This may suggest that the material was quite uniform in its crystal size and structure.

Given the size and breadth of the hot stage PLM analysis of the processed samples, it was necessary to display the melting temperature observed by PLM in a format which would more easily allow for a systematic view of how the processing conditions affected all of the samples ultimate melting temperatures. Fig. 10. is arranged such that the individual melting temperature for each sample is depicted as the processing temperature and pressure increase going from left to right with the three different time conditions for each set clustered together.

Fig. 10., reveals that the processed materials all possess melting temperatures which have increased above what that which was observed in the unaltered material. Focusing on the effect of increasing processing pressure while temperature is constant, no discernible trend can be definitely seen in the polymers melting temperatures. However, when processing pressure is fixed and we focus on the changes brought on by increasing the processing temperature we do observe a trend. Specifically, as the processing temperature increases from 22 °C to 70 °C we observe the clearance point of the material decrease. Interestingly, the samples which were processed at 22 °C appear to be the most resistant to melting. Next, samples processed at 50 °C and 60 °C were observed to melt at very similar temperatures suggesting they may be quite similar in morphology. Finally, the samples processed at 70 °C were observed to display

the lowest ultimate melting temperatures of all the processed samples. all of the samples were observed to fully melt by PLM at T_m's above the PCL's expected literature T_m maximum of 60 °C.

During this study, it was observed that the DSC calculated T_m and Hot Stage T_m differed quite significantly. This is predominantly associated with the manner in which the T_m's are determined using each method. The DSC quantifiably determines the samples T_m by using the peak of the enthalpic recovery as calculated using the samples mass while the Hot Stage qualitatively determined the melt by observing the disappearance of the birefringent effect. While the two techniques are different, they can be correlated by looking at the tail end of the DSC calculated T_m thermal transition. This value when compared to the Hot Stage was found to correlate quite well with the materials complete transition to the liquid phase.

Conclusions

Our current work attempted to characterize the effects of applying specific pressures and temperatures over time on the morphology of the semi-crystalline polymer PCL. These findings were significant, as they differed from our previous results observed when processing PLA, and in some very interesting ways. [1] Previously, materials processed near the T_g under our conditions displayed multiple morphologies. These were depicted by increases in birefringence which were noted to be accompanied by decreases in the materials enthalpic relaxation values and specific heat capacity while displaying increased values of heat of

fusion (crystallinity). It is thought that as the material is processed under these specific conditions that the material may be forced into these morphologies. Two of which, consist of either very small tightly packed crystals possessing restricted polymer chains or another with loosely entangled chains with greater orientation.[1,32–34] While we were not able to analyze the T_g directly by DSC given PCL's low T_g of -60 °C, we did observe a brilliant birefringence as depicted by PLM. This birefringence was not only observed to be homogenous throughout the entire material unlike PLA but was also found to increase in intensity in response to increasing processing temperature and pressure. Most notably and once again unlike our previous experiments with PLA, the samples appeared to lack any typical spherulitic structures after processing between 50 °C and 60 °C or just below the melting temperture. [1] Yet for these same samples, XRD revealed an intense crystallinity. Meanwhile, samples processed at 70 °C were observed to possess very tiny crystals which became more intense in appearance as both pressure and time increased. Additionally, when analyzed by hot stage PLM, birefringent samples lacking spherulites or apparent crystal structures more slowly lost their birefringent properties with the hot stage temperature reaching as high as 69 °C. Samples which appeared to possess crystal structures however were found to melt at lower temperatures, losing their birefringent appearance by 63 °C. DSC results for the crystalline component of the PCL structure displayed no individual discernible trends but rather a general increase in crystallinity to ≈ 23% under all of the processing conditions. XRD was thus performed in an attempt to further elucidate the changes in %

crystallinity as well any possible structural reorientation which had occurred upon processing the PCL. XRD analysis revealed that % Crystallinity initially decreased when processed at 22 °C to a low of 12% with the peak structure becoming more broad in appearance. Samples processed at 50 °C and 60 °C were found to increase in crystallinity the greatest, with values observed as high as 45%. XRD peak profiles for those samples processed at 50 °C initially displayed a sharpening profile which began to broaden slightly as pressure increased. Peak profiles for those samples processed at 60 °C were found to increase in sharpness and intensity predominately with regards to the first peak associated with PCL.

Given the stark difference between the DSC and XRD calculated % crystallinity values, it is important to elucidate why we observe these differences. First, the manner in which DSC and XRD calculate these values are important to note. DSC is only capable of measuring the amount of energy being exchanged in relation to the materials mass. This means that the % Crystallinity value will only depict that which was contributed by the melting of the actual crystal structures which as noted by the materials birefringence were not readily visible. This was what lead us to further characterize the material using XRD which could inform us what was happening to the material structurally. Upon analysis, the structure was observed to possess a much higher degree of order which could be used to quantify the materials crystallinity without being based on mass. Interestingly, when combining the birefringent effect and the XRD data it may be possible to suggest that another reason the DSC did not display what the XRD

suggested is that the material has been forced into a liquid crystalline phase which the DSC would not be able to easily differentiate from the bulk amorphous phase.

Finally, samples processed at 70 °C were found to possess melting temperature values that were higher than those processed at 22 °C but lower than those processed at 50 °C and 60 °C while also displaying a very tiny crystal morphology under PLM. The XRD profiles for these samples were found to possess very sharp and intense peaks with the first peak decreasing in ratio to the second as pressure was increased to 10,000 lbs with time reaching 15 min. Thus these results suggest that multiple different morphological populations exist which may include a new liquid crystalline component. This increased in crystallinity in addition to the discovery of a liquid crystalline component may make it possible to tailor the morphology of PCL at the benchtop with potential application in many fields, making this process quite promising to interpret.

Supporting Materials

Processing Conditions						
Temperature						
Pressure	22°C	50°C	60°C	70°C		Time
	2,000lbs	2,000lbs	2,000lbs	2,000lbs	5 Min	
	5,000lbs	5,000lbs	5,000lbs	5,000lbs		
	10,000lbs	10,000lbs	10,000lbs	10,000lbs		
	15,000lbs	15,000lbs	15,000lbs	15,000lbs		
	20,000lbs	20,000lbs	20,000lbs	20,000lbs		
	2,000lbs	2,000lbs	2,000lbs	2,000lbs	10 Min	
	5,000lbs	5,000lbs	5,000lbs	5,000lbs		
	10,000lbs	10,000lbs	10,000lbs	10,000lbs		
	15,000lbs	15,000lbs	15,000lbs	15,000lbs		
	20,000lbs	20,000lbs	20,000lbs	20,000lbs		
	2,000lbs	2,000lbs	2,000lbs	2,000lbs	15 Min	
	5,000lbs	5,000lbs	5,000lbs	5,000lbs		
	10,000lbs	10,000lbs	10,000lbs	10,000lbs		
	15,000lbs	15,000lbs	15,000lbs	15,000lbs		
	20,000lbs	20,000lbs	20,000lbs	20,000lbs		

Table. 1.SI Lists all the processing condtions used.

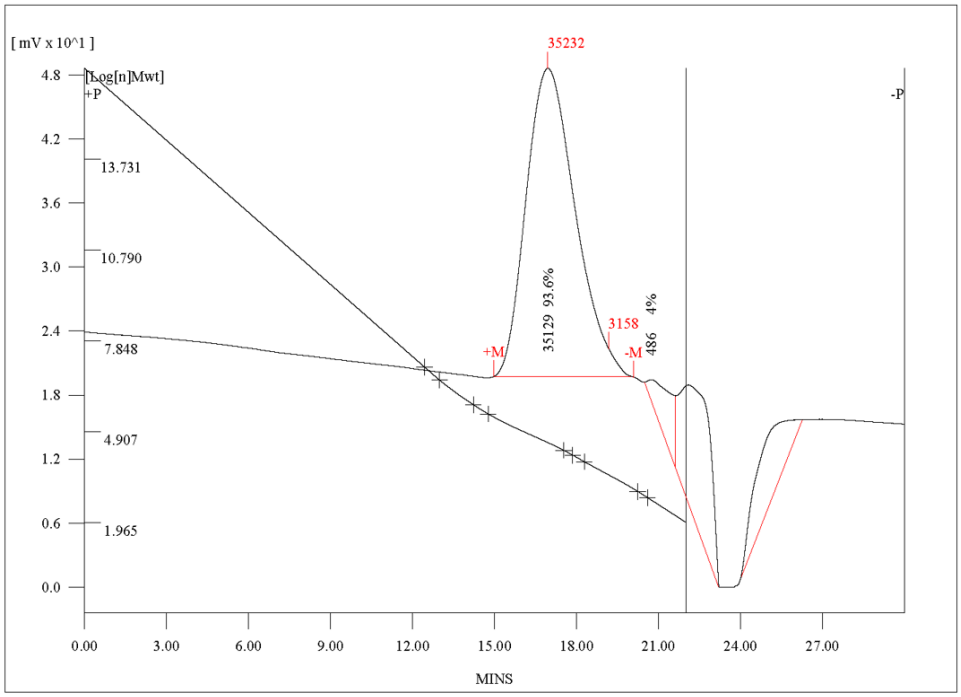

Peak Molecular Weight Report

Peak	Component	RT	Area	%Area	PMwt	Mw	Mn	Mw/Mn	StartMw	EndMw
1		16.956	3616041.7	93.634	35129.7	37608.8	18195.7	2.0669	234814.5	1120.6
2		20.734	245863.4	6.366	486.5	274.0	240.1	1.1414	670.0	150.6

Figure. 1.SI GPC analsysis results of the PCL

Processing Condtions			DSC	ΔH (J/g)	Hot Stage	DSC % Crys	XRD
Press (lbs)	Time (Min)	Temp (°C)	T_m (°C)		T_m (°C)	ΔH/139.5 (J/g)	% Crys
Unaltered			57.73	17.8351	57.73	12.79%	24.85%
2,000	5	22	60.83	25.7582	71.40	18.46%	18.13%
		50	61.37	30.5136	74.90	21.87%	25.25%
		60	62.33	30.6591	64.20	21.98%	34.34%
		70	61.65	31.6741	62.90	22.71%	27.69%
	10	22	62.76	28.5836	68.40	20.49%	20.41%
		50	62.45	30.0635	66.70	21.55%	28.90%
		60	62.03	31.0028	66.10	22.22%	30.97%
		70	61.54	30.4632	63.00	21.84%	31.72%
	15	22	63.85	29.6617	70.00	21.26%	18.19%
		50	62.08	29.2408	66.70	20.96%	27.54%
		60	62.17	29.7445	65.10	21.32%	32.58%
		70	61.77	31.2198	64.20	22.38%	28.35%
5,000	5	22	61.90	30.5651	68.50	21.91%	24.75%
		50	63.00	29.8566	66.20	21.40%	37.10%
		60	62.18	30.7761	64.30	22.06%	29.46%
		70	61.18	30.4830	62.40	21.85%	27.78%
	10	22	62.58	28.6597	70.80	20.54%	17.30%
		50	61.78	29.3238	67.20	21.02%	36.37%
		60	62.08	29.4613	67.20	21.12%	31.04%
		70	61.10	31.5923	64.20	22.65%	27.62%
	15	22	61.66	31.7214	68.00	22.74%	21.95%
		50	64.59	32.7501	67.00	23.48%	39.01%
		60	61.93	32.1270	64.30	23.03%	30.20%
		70	61.21	32.6190	62.40	23.38%	28.08%
10,000	5	22	60.97	31.7188	68.70	22.74%	17.84%
		50	63.34	32.8006	66.20	23.51%	37.84%
		60	62.89	31.7932	65.00	22.79%	30.15%
		70	61.29	34.0963	63.00	24.44%	21.50%
	10	22	60.83	31.1485	67.50	22.33%	24.91%
		50	62.41	32.9268	66.10	23.60%	37.05%
		60	62.04	31.5283	67.90	22.60%	33.99%
		70	61.42	31.7718	62.90	22.78%	27.22%
	15	22	61.40	29.0005	65.80	20.79%	20.96%
		50	62.90	31.9336	66.00	22.89%	31.91%
		60	62.08	32.1475	64.60	23.04%	35.53%
		70	61.69	31.8219	63.00	22.81%	22.79%
15,000	5	22	60.90	30.8659	67.30	22.13%	12.20%
		50	62.01	31.4791	66.30	22.57%	40.94%
		60	62.52	32.2562	67.60	23.12%	45.01%
		70	61.18	32.2138	64.70	23.09%	29.66%
	10	22	61.21	30.6228	66.60	21.95%	25.47%
		50	62.54	31.5901	66.70	22.65%	40.64%
		60	62.75	31.9243	68.30	22.88%	33.35%
		70	60.96	30.1758	63.90	21.63%	25.42%
	15	22	61.61	31.1623	67.10	22.34%	22.79%
		50	61.73	31.5907	66.50	22.65%	27.52%
		60	61.64	32.0554	70.00	22.98%	37.87%
		70	61.81	30.8747	63.10	22.13%	25.88%
20,000	5	22	61.65	30.5718	65.90	21.92%	13.26%
		50	61.54	30.8482	66.10	22.11%	38.22%
		60	61.06	30.4229	63.30	21.81%	31.14%
		70	60.10	30.7628	64.30	22.05%	29.13%
	10	22	61.14	31.1457	66.90	22.33%	29.13%
		50	61.16	30.5574	66.60	21.90%	35.70%
		60	61.52	30.7932	67.10	22.07%	43.36%
		70	60.70	30.8127	64.00	22.09%	24.40%
	15	22	61.61	30.2809	68.60	21.71%	21.68%
		50	62.30	30.5333	70.20	21.89%	26.97%
		60	60.73	30.3275	68.80	21.74%	24.58%
		70	61.54	32.0635	62.80	22.98%	23.43%

Table. 2.SI Calculated DSC T_M, ΔH, Hot Stage T_M, DSC ΔH derived % Crystallinity, and XRD derived % Crystallinity values of the material before and after processing between 2,000 lbs-20,000 lbs while exposed to temperatures below and above the T_M over 5-15 min.

Processing Conditions			Radius	Height	Volume	Surface Area	Δ Height	Δ Surface Area
Press (lbs)	Time (min)	Temp (°C)	(in)	(in)	(in^3)	(in^2)	(in)	(in^2)
Unaltered			0.205	0.071	0.009	0.354	N/A	N/A
2,000	5	22	0.260	0.039	0.008	0.488	-0.032	0.134
		50	0.351	0.023	0.009	0.823	-0.048	0.469
		60	0.651	0.002	0.003	2.667	-0.069	2.313
		70	1.141	0.002	0.008	8.194	-0.069	7.840
	10	22	0.327	0.035	0.012	0.744	-0.036	0.390
		50	0.520	0.009	0.008	1.728	-0.062	1.374
		60	0.643	0.006	0.008	2.622	-0.065	2.268
		70	1.081	0.001	0.004	7.349	-0.070	6.995
	15	22	0.255	0.045	0.009	0.479	-0.026	0.125
		50	0.478	0.010	0.007	1.463	-0.061	1.109
		60	0.576	0.009	0.009	2.114	-0.062	1.760
		70	1.196	0.001	0.004	8.995	-0.070	8.641
5,000	5	22	0.305	0.033	0.010	0.646	-0.038	0.292
		50	0.491	0.010	0.008	1.546	-0.061	1.192
		60	0.640	0.008	0.010	2.602	-0.063	2.248
		70	1.100	0.001	0.004	7.610	-0.070	7.256
	10	22	0.295	0.027	0.007	0.597	-0.044	0.243
		50	0.482	0.011	0.008	1.493	-0.060	1.139
		60	0.629	0.006	0.007	2.510	-0.065	2.156
		70	0.956	0.003	0.009	5.754	-0.068	5.400
	15	22	0.320	0.027	0.009	0.698	-0.044	0.344
		50	0.408	0.010	0.005	1.072	-0.061	0.718
		60	0.656	0.007	0.009	2.729	-0.064	2.375
		70	0.978	0.001	0.003	6.016	-0.070	5.662
10,000	5	22	0.323	0.029	0.009	0.712	-0.042	0.358
		50	0.466	0.012	0.008	1.400	-0.059	1.046
		60	0.583	0.005	0.005	2.150	-0.066	1.796
		70	1.340	0.001	0.006	11.282	-0.070	10.928
	10	22	0.324	0.025	0.008	0.708	-0.046	0.354
		50	0.542	0.008	0.007	1.873	-0.063	1.519
		60	0.615	0.007	0.008	2.400	-0.064	2.046
		70	0.986	0.003	0.009	6.121	-0.068	5.767
	15	22	0.338	0.021	0.008	0.762	-0.050	0.408
		50	0.493	0.008	0.006	1.552	-0.063	1.198
		60	0.695	0.003	0.005	3.044	-0.068	2.690
		70	1.074	0.001	0.004	7.248	-0.070	6.894
15,000	5	22	0.377	0.022	0.010	0.943	-0.049	0.589
		50	0.529	0.006	0.005	1.775	-0.065	1.421
		60	0.649	0.003	0.004	2.655	-0.068	2.301
		70	1.142	0.002	0.008	8.201	-0.069	7.847
	10	22	0.344	0.017	0.006	0.778	-0.054	0.424
		50	0.552	0.004	0.004	1.925	-0.067	1.571
		60	0.635	0.004	0.005	2.549	-0.067	2.196
		70	0.947	0.001	0.003	5.641	-0.070	5.287
	15	22	0.369	0.024	0.010	0.909	-0.047	0.555
		50	0.418	0.012	0.007	1.129	-0.059	0.775
		60	0.483	0.012	0.009	1.502	-0.059	1.148
		70	0.933	0.001	0.003	5.475	-0.070	5.121
20,000	5	22	0.355	0.018	0.007	0.832	-0.053	0.478
		50	0.468	0.005	0.003	1.388	-0.066	1.034
		60	0.678	0.003	0.004	2.897	-0.068	2.543
		70	0.877	0.002	0.005	4.838	-0.069	4.484
	10	22	0.366	0.017	0.007	0.878	-0.054	0.524
		50	0.526	0.008	0.007	1.762	-0.063	1.408
		60	0.666	0.007	0.010	2.816	-0.064	2.462
		70	0.890	0.002	0.005	4.988	-0.069	4.634
	15	22	0.419	0.019	0.010	1.153	-0.052	0.799
		50	0.485	0.013	0.010	1.514	-0.058	1.160
		60	0.606	0.007	0.008	2.334	-0.064	1.980
		70	0.781	0.002	0.004	3.842	-0.069	3.488
(Surface Area=$2\pi rh+2\pi r^2$)								

Table. 3.SI Physical dimensions of all samples.

XRD % Crystallinity Calculation Matlab Code:

```
function varargout = cagui(varargin)
% CAGUI MATLAB code for cagui.fig
%      CAGUI, by itself, creates a new CAGUI or raises the existing
%      singleton*.
%
%      H = CAGUI returns the handle to a new CAGUI or the handle to
%      the existing singleton*.
%
%      CAGUI('CALLBACK',hObject,eventData,handles,...) calls the local
%      function named CALLBACK in CAGUI.M with the given input arguments.
%
%      CAGUI('Property','Value',...) creates a new CAGUI or raises the
%      existing singleton*.  Starting from the left, property value pairs are
%      applied to the GUI before cagui_OpeningFcn gets called.  An
%      unrecognized property name or invalid value makes property application
%      stop.  All inputs are passed to cagui_OpeningFcn via varargin.
%
%      *See GUI Options on GUIDE's Tools menu.  Choose "GUI allows only one
%      instance to run (singleton)".
%
% See also: GUIDE, GUIDATA, GUIHANDLES


% Edit the above text to modify the response to help cagui
```

```
% Last Modified by GUIDE v2.5 17-Mar-2015 13:08:31

% Begin initialization code - DO NOT EDIT
gui_Singleton = 1;
gui_State = struct('gui_Name',       mfilename, ...
                   'gui_Singleton',  gui_Singleton, ...
                   'gui_OpeningFcn', @cagui_OpeningFcn, ...
                   'gui_OutputFcn',  @cagui_OutputFcn, ...
                   'gui_LayoutFcn',  [] , ...
                   'gui_Callback',   []);
if nargin && ischar(varargin{1})
    gui_State.gui_Callback = str2func(varargin{1});
end

if nargout
    [varargout{1:nargout}] = gui_mainfcn(gui_State, varargin{:});
else
    gui_mainfcn(gui_State, varargin{:});
end
% End initialization code - DO NOT EDIT
end

% --- Executes just before cagui is made visible.
function cagui_OpeningFcn(hObject, eventdata, handles, varargin)
%#ok<*INUSL>
% This function has no output args, see OutputFcn.
```

```
% hObject    handle to figure
% eventdata  reserved - to be defined in a future version of MATLAB
% handles    structure with handles and user data (see GUIDATA)
% varargin   command line arguments to cagui (see VARARGIN)

% Choose default command line output for cagui
handles.output = hObject;

% Update handles structure
guidata(hObject, handles);

% UIWAIT makes cagui wait for user response (see UIRESUME)
% uiwait(handles.figure1);
end

% --- Outputs from this function are returned to the command line.
function varargout = cagui_OutputFcn(hObject, eventdata, handles)
% varargout  cell array for returning output args (see VARARGOUT);
% hObject    handle to figure
% eventdata  reserved - to be defined in a future version of MATLAB
% handles    structure with handles and user data (see GUIDATA)

% Get default command line output from handles structure
varargout{1} = handles.output;
end
```

```
% --- Executes on button press in btnOpenFile.
function btnOpenFile_Callback(hObject, eventdata, handles)
% hObject    handle to btnOpenFile (see GCBO)
% eventdata  reserved - to be defined in a future version of MATLAB
% handles    structure with handles and user data (see GUIDATA)
persistent pathname


set(handles.txtNotes,'String','Loading')


%checks to see if a file was previously opened and reopens its directory
if exist('pathname','var')==0
    [filename, pathname] = uigetfile ({'*.xlsx;*.xls;*xlsm;*xltx;*xltm','Excel Files
(*.xlsx,*.xls,*xlsm,*xltx,*xltm)'},'Select Excel Source File');
else
    [filename, pathname] = uigetfile ({'*.xlsx;*.xls;*xlsm;*xltx;*xltm','Excel Files
(*.xlsx,*.xls,*xlsm,*xltx,*xltm)'},'Select Excel Source File',sprintf('%s',pathname));
end


%extracts filename and data points from excel file
if filename == 0
    msgbox('Please select file.')
    set(handles.txtNotes,'String','')
elseif filename ~= 0
set(handles.txtFileName,'String',filename)
[num,~] = xlsread([pathname filename]);
```

```
twotheta = [num(1:size(num),1:1)];
count = [num(1:size(num),2:2)];
MinValue = min(count);
MaxValue = max(count);

%sets the number of data points, min, and max
set(handles.txtDataPts,'String',size(num,1))
set(handles.txtMin,'String',MinValue)
set(handles.txtMax,'String',MaxValue)

%plot data
plot(handles.axes1,twotheta,count)
xlabel('2theta')
ylabel('Intensity')

%sets data so other functions can access data
setappdata(handles.btnOpenFile,'twotheta',twotheta);
setappdata(handles.btnOpenFile,'count',count);
set(handles.txtNotes,'String','')
if get(handles.chkauto,'Value')==1
    btnPlot_Callback(handles.btnPlot,'',handles)
end
end
end
```

```
% --- Executes on button press in btnPlot.
function btnPlot_Callback(hObject,eventdata, handles)
% hObject    handle to btnPlot (see GCBO)
% eventdata  reserved - to be defined in a future version of MATLAB
% handles    structure with handles and user data (see GUIDATA)
global fig1
global gaussp
global basep
global lhor
global lver

%checks to see that baseline method is selected
if isempty(get(handles.PnlMethod,'SelectedObject'))
   msgbox ('Please select Baseline Method.')
   return
end

%extracts data points and checks to see they exist
twotheta=getappdata(handles.btnOpenFile,'twotheta');
count=getappdata(handles.btnOpenFile,'count');

if isempty(twotheta)==1
   msgbox ('Please select file')
   return
end
```

```
set(handles.txtNotes,'String','Loading')

%delete previous plots
try
   delete(fig1)
end
try
   delete(gaussp)
end
try
   delete(basep)
end
try
   delete(lhor)
end
try
   delete(lver)
end
%selects fit type and algorithm
items = get(handles.listFit,'String');
index_selected = get(handles.listFit,'Value');

x2=twotheta;
```

```
%resets OK/Delete button
set(handles.btnOK,'Visible','off')
set(handles.btnDelete,'Visible','on')

switch items{index_selected}
    case 'Draw'
    %draw lines
    clear x2
    set(handles.txtNotes,'String','Select points to draw lines through and press
ENTER when done.')
    [x2,y2] = ginput;
    set(handles.txtNotes,'String','')

    case 'Smoothing'
    %smoothing function
    %change filterpercent to change sensitivity
        filterpercent = str2double(get(handles.txtTol,'String'));
        y2 = smooth(twotheta,count,filterpercent,'rloess');
        set(handles.txtTolDisp,'String',filterpercent)

    case 'Gaussian'
%standard gaussian fit using specified number of peaks
global peaks
global y2form
set(handles.btnOK,'Visible','on')
    f=fit(twotheta,count,['gauss',get(handles.txtPeaks,'String')]);
```

```
    coeffv=coeffvalues(f);
    %y2=feval(f,twotheta);

    %array preallocation
peaks=str2double(get(handles.txtPeaks,'String'));
a=ones(1,peaks);
b=ones(1,peaks);
c=ones(1,peaks);

%finds components of gaussian fit
for i=1:peaks
    a(i)=coeffv(3*i-2);
    b(i)=coeffv(3*i-1);
    c(i)=coeffv(3*i);
    y2form(:,i)=a(i).*exp(-((twotheta-b(i))/c(i)).^2);
    hold on
    C = {'y','c','g','k','m','r','b','y'};
    gaussp(i)=plot(twotheta,y2form(:,i),'color',C{i});
end

%fills listbox with gaussian components
global ListBoxData
ListBoxData = gaussp;
set(handles.lstLines,'String',ListBoxData)
set(handles.txtNotes,'String','Select lines from Crystalline region and press OK')
```

```
set(handles.btnDelete,'Visible','off')
set(handles.txtTolDisp,'String','')
return
end
amorph(x2,y2,handles)
end

function amorph(x2,y2,handles,hObject)
global fig1
global basep
global lhor
global lver
global ListBoxData

hold on
twotheta=getappdata(handles.btnOpenFile,'twotheta');
count=getappdata(handles.btnOpenFile,'count');

fig1 = plot(x2,y2,'r');

%calculates area and crystallinity from zero
TotalZero = trapz(twotheta,count);
AmorphousZero = trapz(x2,y2);
CrystallinityZero = 1 - AmorphousZero/TotalZero;
```

```
%defines baseline methods
switch get(get(handles.PnlMethod,'SelectedObject'),'Tag')
    case 'rdoZero'
        set(handles.txtPercentCrys,'String',CrystallinityZero)
        endpoint = size(twotheta);
        y3 = ones(endpoint(1),1)*0;
        basep = plot(twotheta,y3,'linestyle','--');
        hold off
        return
    case 'rdoRightmost'
        %baseline based on rightmost value
        endpoint = size(twotheta);
        y3 = ones(endpoint(1),1)*count(endpoint(1));
    case 'rdoDefineLine'
        %baseline based on defined line
        if
isnan(str2double(get(handles.txtX1,'String')))||isnan(str2double(get(handles.txtX1
,'String')))==1
            msgbox('Please enter valid numbers for X1 and X2')
            return
        else
            X1=str2double(get(handles.txtX1,'String'));
            X2=str2double(get(handles.txtX2,'String'));
            Y1=str2double(get(handles.txtY1,'String'));
            Y2=str2double(get(handles.txtY2,'String'));
            m=(Y2-Y1)/(X2-X1);
```

```
            int=Y1-m*X1;
            y3=m*twotheta+int;
        end
end

basep = plot(twotheta,y3,'linestyle','--');
hold off

%calculates area and crystallinity above baseline
BaselineMin = trapz(twotheta,y3);
TotalMin = TotalZero - BaselineMin;
AmorphousMin = AmorphousZero - BaselineMin;
CrystallinityMin = 1 - AmorphousMin/TotalMin;
set(handles.txtPercentCrys,'String',CrystallinityMin)

if get(handles.chkCalcSize,'Value')==1
    CalcGrainSize(y3,handles)
else
    set(handles.txtdSmall,'String','')
    set(handles.txtdLarge,'String','')
    set(handles.txtdRange,'String','')
    set(handles.txtGrain,'String','')
    set(handles.txtNotes,'String','')
end
    %set listbox
```

```
ListBoxData=findobj(gca,'Type','line');
set(handles.lstLines,'String',ListBoxData)
setappdata(handles.btnSelectPts,'y3',y3)
end

function CalcGrainSize(y3,handles,pMax,x1,x2,y1,y2)
%sets peak coord to calculate grain size
twotheta=getappdata(handles.btnOpenFile,'twotheta');
count=getappdata(handles.btnOpenFile,'count');
global ListBoxData
global lhor
global lver

%finds max
if exist('pMax','var')
else
pMax=max(count);
end
pMaxIndex=find(count==pMax,1);

%calculates height (from baseline)
pHeight=pMax-y3(pMaxIndex);

%finds x-values at half height and their difference
%x-values with exact points
```

```
if exist('x1','var') && exist('x2','var') && get(handles.rdoExact,'Value')==1
    hHeight=(x1+x2/2);
    BWidth=abs(x2-x1)*pi/180; %convert to rad

else
    hHeight=pHeight/2+y3(pMaxIndex);
difh=ones(1,pMaxIndex)*1000;
%x-values between selected points
if exist('x1','var') && exist('x2','var') && get(handles.rdoExact,'Value')==0
difi1=abs(twotheta-x1);
difi2=abs(twotheta-x2);
xIndex(1)=find(difi1==min(difi1),1);
xIndex(2)=find(difi2==min(difi2),1);

    for i=xIndex(1):pMaxIndex
    difh(i)=abs(count(i)-hHeight);
    end
hIndex(1)=find(difh==min(difh),1,'last');
clear difh
difh=ones(1,size(count,1))*1000;
    for i=pMaxIndex:xIndex(2)
    difh(i)=abs(count(i)-hHeight);
    end
%x-values normal calculation
else
```

```
for i=1:pMaxIndex
    difh(i)=abs(count(i)-hHeight);
end
hIndex(1)=find(difh==min(difh),1,'last');
clear difh
difh=ones(1,size(count,1))*1000;
for i=pMaxIndex:size(count,1)
    difh(i)=abs(count(i)-hHeight);
end
end

hIndex(2)=find(difh==min(difh),1,'first');
clear difh
BWidth=abs(twotheta(hIndex(2))-twotheta(hIndex(1)))*pi/180; %convert to
radians
end

%test values
%Bwidtht = abs(twotheta(hIndex(2))-twotheta(hIndex(1))) %degrees, 2theta
%peakpost = twotheta(pMaxIndex)/2 %degrees, theta

%calculates crystallite size (Scherrer formula)
K=str2num(get(handles.txtK,'String'));
lam=str2num(get(handles.txtlambda,'String'));
peakpos=twotheta(pMaxIndex)/2*pi/180; %divide by 2 to get theta value, and
convert to radians
```

```
cryssize = K*lam/BWidth/cos(peakpos);


%calculates interplanar d (Bragg's Law)
if exist('x1','var') && exist('x2','var') && get(handles.rdoExact,'Value')==1
angrad(1)=x1*pi/180/2; %convert to theta, rad
angrad(2)=x2*pi/180/2; %convert to theta, rad
else
angrad(1)=twotheta(hIndex(1))*pi/180/2; %convert to theta, rad
angrad(2)=twotheta(hIndex(2))*pi/180/2; %convert to theta, rad
end
dLarge=lam/2/sin(angrad(1));
dSmall=lam/2/sin(angrad(2));
dRange = abs(dLarge-dSmall);


%draws vertical line to max and horizontal line to FWHM
lver=line([twotheta(pMaxIndex),twotheta(pMaxIndex)],[y3(pMaxIndex),pMax],'col
or','k');
if exist('x1','var') && exist('x2','var') && get(handles.rdoExact,'Value')==1
lhor=line([x1,x2],[y1,y2],'color','k');
else
   lhor=line(twotheta(hIndex),count(hIndex),'color','k');
end


%sets GUI values
set(handles.txtdSmall,'String',dSmall)
set(handles.txtdLarge,'String',dLarge)
```

```
set(handles.txtdRange,'String',dRange)
set(handles.txtGrain,'String',cryssize)
set(handles.txtNotes,'String','')

%set listbox
ListBoxData=findobj(gca,'Type','line');
set(handles.lstLines,'String',ListBoxData)

end


function PnlMethod_SelectionChangeFcn(hObject, eventdata, handles)
% hObject    handle to the selected object in uibuttongroup1
% eventdata  structure with the following fields
%   EventName: string 'SelectionChanged' (read only)
%   OldValue: handle of the previously selected object or empty
%   NewValue: handle of the currently selected object
% handles    structure with handles and user data (see GUIDATA)

switch get(eventdata.NewValue,'Tag') % Get Tag of selected object.
    case 'rdoRightmost'
        set(handles.PnlDefineLine,'Visible','off');
    case 'rdoZero'
        set(handles.PnlDefineLine,'Visible','off');
    case 'rdoDefineLine'
```

```
        set(handles.PnlDefineLine,'Visible','on')
end
end

% --- Executes on button press in btnDrawLine.
function btnDrawLine_Callback(hObject, eventdata, handles)
% hObject    handle to btnDrawLine (see GCBO)
% eventdata  reserved - to be defined in a future version of MATLAB
% handles    structure with handles and user data (see GUIDATA)
[xin,yin] = ginput(2);
set(handles.txtX1,'String',xin(1))
set(handles.txtX2,'String',xin(2))
set(handles.txtY1,'String',yin(1))
set(handles.txtY2,'String',yin(2))
line(xin,yin)
end

function txtX1_Callback(hObject, eventdata, handles)
% hObject    handle to txtX1 (see GCBO)
% eventdata  reserved - to be defined in a future version of MATLAB
% handles    structure with handles and user data (see GUIDATA)

% Hints: get(hObject,'String') returns contents of txtX1 as text
%        str2double(get(hObject,'String')) returns contents of txtX1 as a double
twotheta=getappdata(handles.btnOpenFile,'twotheta');
```

```
count=getappdata(handles.btnOpenFile,'count');
if isempty(twotheta)==1
    msgbox ('Please select file')
    return
end
dif1=abs(twotheta-str2double(get(handles.txtX1,'String')));
idx1=find(dif1==min(dif1));
Y1=count(idx1,1);
set(handles.txtY1,'String',Y1)
end

function txtX2_Callback(hObject, eventdata, handles)
% hObject    handle to txtX1 (see GCBO)
% eventdata  reserved - to be defined in a future version of MATLAB
% handles    structure with handles and user data (see GUIDATA)

% Hints: get(hObject,'String') returns contents of txtX1 as text
%        str2double(get(hObject,'String')) returns contents of txtX1 as a double
twotheta=getappdata(handles.btnOpenFile,'twotheta');
count=getappdata(handles.btnOpenFile,'count');

if isempty(twotheta)==1
    msgbox ('Please select file')
    return
end
```

```
dif2=abs(twotheta-str2double(get(handles.txtX2,'String')));
idx2=find(dif2==min(dif2));
Y2=count(idx2,1);
set(handles.txtY2,'String',Y2)
end

% --- Executes on button press in btnClear.
function btnClear_Callback(hObject, eventdata, handles)
% hObject    handle to btnClear (see GCBO)
% eventdata  reserved - to be defined in a future version of MATLAB
% handles    structure with handles and user data (see GUIDATA)
set(handles.txtPercentCrys,'String','')
set(handles.txtTolDisp,'String','')
set(handles.lstLines,'String','')
set(handles.txtdSmall,'String','')
set(handles.txtdLarge,'String','')
set(handles.txtdRange,'String','')
set(handles.txtGrain,'String','')
set(handles.txtDataPts,'String','')
set(handles.txtMin,'String','')
set(handles.txtMax,'String','')

cla
clear all
```

```
end


% --- Executes on selection change in listFit.
function listFit_Callback(hObject, eventdata, handles)
% hObject    handle to listFit (see GCBO)
% eventdata  reserved - to be defined in a future version of MATLAB
% handles    structure with handles and user data (see GUIDATA)


% Hints: contents = cellstr(get(hObject,'String')) returns listFit contents as cell
array
%        contents{get(hObject,'Value')} returns selected item from listFit
contents = cellstr(get(hObject,'String'));
switch contents{get(hObject,'Value')}
    case 'Smoothing'
set(handles.txtPeaks,'Visible','off')
set(handles.text27,'Visible','off')
set(handles.txtTol,'Visible','on')
set(handles.text2,'Visible','on')
set(handles.txtTolDisp,'Visible','on')
set(handles.lblTol,'Visible','on')
    case 'Gaussian'
set(handles.txtTol,'Visible','off')
set(handles.text2,'Visible','off')
set(handles.txtTolDisp,'Visible','off')
set(handles.lblTol,'Visible','off')
```

```
set(handles.txtPeaks,'Visible','on')
set(handles.text27,'Visible','on')
    case 'Draw'
set(handles.txtPeaks,'Visible','off')
set(handles.text27,'Visible','off')
set(handles.txtTol,'Visible','off')
set(handles.text2,'Visible','off')
set(handles.txtTolDisp,'Visible','off')
set(handles.lblTol,'Visible','off')
end
end

function txtPeaks_Callback(hObject, eventdata, handles)
% hObject    handle to txtPeaks (see GCBO)
% eventdata  reserved - to be defined in a future version of MATLAB
% handles    structure with handles and user data (see GUIDATA)

% Hints: get(hObject,'String') returns contents of txtPeaks as text
%        str2double(get(hObject,'String')) returns contents of txtPeaks as a double
if str2double(get(hObject,'String')) > 8
    msgbox ('Max 8 peaks')
    set(hObject,'String','7')
end
end
```

```
% --- Executes on selection change in lstLines.
function lstLines_Callback(hObject, eventdata, handles)
% hObject    handle to lstLines (see GCBO)
% eventdata  reserved - to be defined in a future version of MATLAB
% handles    structure with handles and user data (see GUIDATA)

% Hints: contents = cellstr(get(hObject,'String')) returns lstLines contents as cell
array
%        contents{get(hObject,'Value')} returns selected item from lstLines
global ListBoxData
selected=get(hObject,'Value');
set(ListBoxData,'LineWidth',1)
set(ListBoxData(selected),'LineWidth',3)
   end

% --- Executes on button press in btnDelete.
function btnDelete_Callback(hObject, eventdata, handles)
% hObject    handle to btnDelete (see GCBO)
% eventdata  reserved - to be defined in a future version of MATLAB
% handles    structure with handles and user data (see GUIDATA)
global ListBoxData
selected=get(handles.lstLines,'Value');
delete(ListBoxData(selected))
ListBoxData = findobj(gca,'Type','line');
set(handles.lstLines,'String',ListBoxData)
end
```

```
% --- Executes on button press in btnOK.
function btnOK_Callback(hObject, eventdata, handles)
% hObject    handle to btnOK (see GCBO)
% eventdata  reserved - to be defined in a future version of MATLAB
% handles    structure with handles and user data (see GUIDATA)
%'amorphous' region equation
global ListBoxData
global peaks
global y2form

selected=get(handles.lstLines,'Value');

y2=0;
   for t=1:peaks
      if any(selected(selected==t))==1
      y2=y2;
      else
      y2=y2+y2form(:,t);
      end
   end

delete(ListBoxData)
set(hObject,'Visible','off')
set(handles.btnDelete,'Visible','on')
```

```
twotheta=getappdata(handles.btnOpenFile,'twotheta');
amorph(twotheta,y2,handles)
end


% --- Executes on button press in chkCalcSize.
function chkCalcSize_Callback(hObject, eventdata, handles)
% hObject    handle to chkCalcSize (see GCBO)
% eventdata  reserved - to be defined in a future version of MATLAB
% handles    structure with handles and user data (see GUIDATA)

% Hint: get(hObject,'Value') returns toggle state of chkCalcSize
if get(hObject,'Value')==1
    set(handles.txtK,'Visible','on')
    set(handles.txtlambda,'Visible','on')
    set(handles.text35,'Visible','on')
    set(handles.text41,'Visible','on')
    set(handles.text42,'Visible','on')
    set(handles.text43,'Visible','on')
    set(handles.text44,'Visible','on')
    set(handles.text45,'Visible','on')
    set(handles.txtdSmall,'Visible','on')
    set(handles.txtdLarge,'Visible','on')
    set(handles.txtdRange,'Visible','on')
    set(handles.txtGrain,'Visible','on')
```

```
else
    set(handles.txtK,'Visible','off')
    set(handles.txtlambda,'Visible','off')
    set(handles.text35,'Visible','off')
    set(handles.text41,'Visible','off')
    set(handles.text42,'Visible','off')
    set(handles.text43,'Visible','off')
    set(handles.text44,'Visible','off')
    set(handles.text45,'Visible','off')
    set(handles.txtdSmall,'Visible','off')
    set(handles.txtdLarge,'Visible','off')
    set(handles.txtdRange,'Visible','off')
    set(handles.txtGrain,'Visible','off')

end
end

% --- Executes on button press in btnSelectPts.
function btnSelectPts_Callback(hObject, eventdata, handles)
% hObject    handle to btnSelectPts (see GCBO)
% eventdata  reserved - to be defined in a future version of MATLAB
% handles    structure with handles and user data (see GUIDATA)
y3=getappdata(handles.btnSelectPts,'y3');
twotheta=getappdata(handles.btnOpenFile,'twotheta');
count=getappdata(handles.btnOpenFile,'count');
```

```
set(handles.txtNotes,'String','Select bottom left and right points of peak to
calculate grain size.')

%exports from user-inputted points

[xgr,ygr]=ginput(2);


%finds indices of selected points (using min distance from point)

difgr1=abs(twotheta-xgr(1));

difgr2=abs(twotheta-xgr(2));

pIndex(1)=find(difgr1==min(difgr1));

pIndex(2)=find(difgr2==min(difgr2));


%finds max between selected points

A=[count(pIndex(1):pIndex(2))];

pMax=max(A);

CalcGrainSize(y3,handles,pMax,xgr(1),xgr(2),ygr(1),ygr(2))

end



% --- Executes on button press in chkauto.

function chkauto_Callback(hObject, eventdata, handles)

% hObject    handle to chkauto (see GCBO)

% eventdata  reserved - to be defined in a future version of MATLAB

% handles    structure with handles and user data (see GUIDATA)


% Hint: get(hObject,'Value') returns toggle state of chkauto

end
```

```
% --- Executes on button press in rdoExact.
function rdoExact_Callback(hObject, eventdata, handles)
% hObject    handle to rdoExact (see GCBO)
% eventdata  reserved - to be defined in a future version of MATLAB
% handles    structure with handles and user data (see GUIDATA)

% Hint: get(hObject,'Value') returns toggle state of rdoExact
set(handles.rdoBetw,'Value',0)
end

% --- Executes on button press in rdoBetw.
function rdoBetw_Callback(hObject, eventdata, handles)
% hObject    handle to rdoBetw (see GCBO)
% eventdata  reserved - to be defined in a future version of MATLAB
% handles    structure with handles and user data (see GUIDATA)
set(handles.rdoExact,'Value',0)
% Hint: get(hObject,'Value') returns toggle state of rdoBetw
end
```

References

[1] C.M. Baker, A. Azagury, E. Mathiowitz, Effect of pressure on poly-l-Lactic Acid morphology, Polymer (Guildf). 99 (2016) 250–262. doi:10.1016/j.polymer.2016.07.028.

[2] M.A. Woodruff, D.D.W. Hutmacher, The return of a forgotten polymer—Polycaprolactone in the 21st century, Prog. Polym. Sci. 35 (2010) 1217–1256. doi:10.1016/j.progpolymsci.2010.04.002.

[3] R. Langer, M. Chasin, Biodegradable polymers as drug delivery systems, 1990. http://ajprd.com/downloadebooks_pdf/38.pdf (accessed April 18, 2014).

[4] M. Okada, Chemical syntheses of biodegradable polymers, Prog. Polym. Sci. 27 (2002) 87–133. doi:10.1016/S0079-6700(01)00039-9.

[5] T.K. Dash, V.B. Konkimalla, Poly-ϵ-caprolactone based formulations for drug delivery and tissue engineering: A review., J. Control. Release. 158 (2012) 15–33. doi:10.1016/j.jconrel.2011.09.064.

[6] M. James, Polymer Data Handbook, 2009. https://global.oup.com/academic/product/polymer-data-handbook-9780195181012?cc=us&lang=en&.

[7] M. Labet, W. Thielemans, Synthesis of polycaprolactone: a review., Chem. Soc. Rev. 38 (2009) 3484–504. doi:10.1039/b820162p.

[8] T. Hayashi, Biodegradable polymers for biomedical uses, Prog. Polym. Sci. 19 (1994) 663–702. doi:10.1016/0079-6700(94)90030-2.

[9] S.C. Woodward, P.S. Brewer, F. Moatamed, A. Schindler, C.G. Pitt, The intracellular degradation of poly(epsilon-caprolactone)., J. Biomed. Mater. Res. 19 (1985) 437–44. doi:10.1002/jbm.820190408.

[10] R. Chandra, Biodegradable polymers, Prog. Polym. Sci. 23 (1998) 1273–1335. doi:10.1016/S0079-6700(97)00039-7.

[11] J.C. Middleton, a J. Tipton, Synthetic biodegradable polymers as orthopedic devices., Biomaterials. 21 (2000) 2335–46. http://www.ncbi.nlm.nih.gov/pubmed/11055281.

[12] Z. McEachin, K. Lozano, Production and characterization of polycaprolactone nanofibers via forcespinning™ technology, J. Appl. Polym. Sci. 126 (2012) 473–479. doi:10.1002/app.36843.

[13] S. Hermanová, J. Omelková, S. Voběrková, R. Bálková, L. Richtera, L. Mravcová, et al., The Effect of Processing of Polycaprolactone Films on Degradation Process Initiated by Aspergillus Oryzae Lipase, Int. J. Polym. Anal. Charact. 17 (2012) 465–475. doi:10.1080/1023666X.2012.696402.

[14] S. Agarwal, C. Speyerer, Degradable blends of semi-crystalline and amorphous branched poly(caprolactone): Effect of microstructure on blend properties, Polymer (Guildf). 51 (2010) 1024–1032. doi:10.1016/j.polymer.2010.01.020.

[15] Y. Wang, M. a. Rodriguez-Perez, R.L. Reis, J.F. Mano, Thermal and Thermomechanical Behaviour of Polycaprolactone and Starch/Polycaprolactone Blends for Biomedical Applications, Macromol. Mater. Eng. 290 (2005) 792–801. doi:10.1002/mame.200500003.

[16] M. Kwon, S.C. Lee, Y.G. Jeong, Influences of physical aging on enthalpy relaxation behavior, gas permeability, and dynamic mechanical property of polylactide films with various D-isomer contents, Macromol. Res. 18 (2010) 346–351. doi:10.1007/s13233-010-0410-7.

[17] C.C. Chen, J.Y. Chueh, H. Tseng, H.M. Huang, S.Y. Lee, Preparation and characterization of biodegradable PLA polymeric blends., Biomaterials. 24 (2003) 1167–73. http://www.ncbi.nlm.nih.gov/pubmed/12527257.

[18] P. Pan, B. Zhu, Y. Inoue, Enthalpy relaxation and embrittlement of poly (L-lactide) during physical aging, Macromolecules. 40 (2007) 9664–9671. doi:10.1021/ma071737c.

[19] R. Surana, A. Pyne, M. Rani, R. Suryanarayanan, Measurement of enthalpic relaxation by differential scanning calorimetry—effect of experimental conditions, Thermochim. Acta. 433 (2005) 173–182. doi:10.1016/j.tca.2005.02.014.

[20] J. iain M.G. Cowie, V. Arrighi, Physical Aging, in: Polym. Phys., John Wiley & Sons, Inc., Hoboken, NJ, USA, 2010: pp. 357–389. doi:10.1002/9780470600160.ch9.

[21] N.A. Bailey, M. Sandor, M. Kreitz, E. Mathiowitz, Comparison of the enthalpic relaxation of poly(lactide-co-glycolide) 50:50 nanospheres and raw polymer, J. Appl. Polym. Sci. 86 (2002) 1868–1872. doi:10.1002/app.11109.

[22] K. Madhavan Nampoothiri, N.R. Nair, R.P. John, An overview of the recent developments in polylactide (PLA) research., Bioresour. Technol. 101 (2010) 8493–501. doi:10.1016/j.biortech.2010.05.092.

[23] S. Rathi, X. Chen, E.B. Coughlin, S.L. Hsu, C.S. Golub, M.J. Tzivanis, Toughening semicrystalline poly(lactic acid) by morphology alteration, Polymer (Guildf). 52 (2011) 4184–4188. doi:10.1016/j.polymer.2011.07.032.

[24] T. Elzein, M. Nasser-Eddine, C. Delaite, S. Bistac, P. Dumas, FTIR study of polycaprolactone chain organization at interfaces, J. Colloid Interface Sci. 273 (2004) 381–387. doi:10.1016/j.jcis.2004.02.001.

[25] T. Schreiber, H. Schultz, O. Schmidt, F. Röser, J. Limpert, a Tünnermann, Stress-induced birefringence in large-mode-area micro-structured optical fibers., Opt. Express. 13 (2005) 3637–46. http://www.ncbi.nlm.nih.gov/pubmed/19495270.

[26] A.N. Gent, Stress-induced birefringence of swollen polymer networks, Macromolecules. 2 (1969) 262–265. http://pubs.acs.org/doi/abs/10.1021/ma60009a010 (accessed July 24,

2014).

[27] T.J. Hammack, R.D. Andrews, Temperature Dependence of Orientation Birefringence of Polymers in the Glassy and Rubbery States. II, J. Appl. Phys. 36 (1965) 3574–3581. doi:10.1063/1.1703043.

[28] M.F. Weber, Giant Birefringent Optics in Multilayer Polymer Mirrors, Science (80-.). 287 (2000) 2451–2456. doi:10.1126/science.287.5462.2451.

[29] T. Rozwadowski, M. Massalska-Arodź, Ł. Kolek, K. Grzybowska, A. Bąk, K. Chłędowska, Kinetics of Cold Crystallization of 4-Cyano-3-fluorophenyl 4-Butylbenzoate (4CFPB) Glass Forming Liquid Crystal. I. Nonisothermal Process As Studied by Microscopic, Calorimetric, and Dielectric Methods, Cryst. Growth Des. 15 (2015) 2891–2900. doi:10.1021/acs.cgd.5b00328.

[30] J. Nehring, A. Saupe, On the schlieren texture in nematic and smectic liquid crystals, J. Chem. Soc. Faraday Trans. 2. 68 (1972) 1. doi:10.1039/f29726800001.

[31] X. Chen, K.K. Tenneti, C.Y. Li, Y. Bai, R. Zhou, X. Wan, et al., Design, synthesis, and characterization of bent-core mesogen-jacketed liquid crystalline polymers, Macromolecules. 39 (2006) 517–527. doi:10.1021/ma051939d.

[32] Q. Ma, G. Georgiev, P. Cebe, Constraints in semicrystalline polymers: Using quasi-isothermal analysis to investigate the mechanisms of

formation and loss of the rigid amorphous fraction, Polymer (Guildf). 52 (2011) 4562–4570. doi:10.1016/j.polymer.2011.08.006.

[33] J.R. Atkinson, J.N. Hay, M.J. Jenkins, Enthalpic relaxation in semi-crystalline PEEK, Polymer (Guildf). 43 (2001) 731–735. doi:10.1016/S0032-3861(01)00668-1.

[34] Y. Wang, J.F. Mano, Effect of structural relaxation at physiological temperature on the mechanical property of poly(L-lactic acid) studied by microhardness measurements, J. Appl. Polym. Sci. 100 (2006) 2628–2633. doi:10.1002/app.22643.

Chapter 4

Controlled Release of Volatiles from Polycaprolactone

Christopher M. Baker Sc.M., Elaina Atherton Sc.M.,

Nupur Dahandia Sc.M., Kristi Munoz Sc.M.,

Edith Mathiowitz Ph.D.

The following chapter is being prepared for submission in the Journal of Applied Polymer Science.

2017;

Abstract:

Disposable petroleum based polymer products are becoming an ever increasing environmental concern in today's society. Unfortunately, these petroleum based polymer products often end up in landfills where they directly contribute to the additional of harmful waste products to the local and global environment. Therefore, it has become increasingly more important to find suitable biodegradable replacements such as polycaprolactone (PCL) for use in such applications as scent releasing technologies; whereby a device is used to release a scent for a short period of time and then disposed of. In this study, PCL was investigated to determine its practicality as a mechanism for controlling and extending the release of volatile molecules. For this purpose, orange oil and menthol were chosen as target molecules given their volatility at room temperature in addition to their generally regarded as safe (GRAS) chemical properties. To this end, both orange oil and menthol were successfully encapsulated in PCL using hot melt encapsulation. This system was observed to allow as much as 60% release of loaded oil, and up to 2% release of loaded menthol at room temperatures. Ultimately, PCL showed great promise in the consistent and controlled release of these volatile molecules, leading us to belive that it would make a suitable biodegradable based polymer, extended-release system.

1. Introduction

During the last century, polymers have become an ever increasingly important part of every-day life. They are used in everything from food containers, furniture and medical devices. However, their persistent use, especially for disposable items has become an ever increasing environmental burden. The EPA reports in 2012 that an estimated 32 million tons of plastic waste were generated in the United States, constituting 12.7% of our total solid waste produced. [1] These petroleum based plastics often take decades if not hundreds of years to degrade, leaving behind long term implications after they are deemed no longer of use and disposed of. Once disposed of, they often make their way to a landfill, or the surrounding watershed. This causes further harm to the human populace as the wildlife and subsequent food chain has been observed to quite often ingest these wastes as is the case with plastic bags. Fortunately, there has been a push to make more of these disposable items with biodegradable materials which are much more environmentally-friendly. Polycaprolactone is one such polymer and shall thus be material of choice in this work.

Polycaprolactone or PCL is a hydrophobic semi-crystalline aliphatic polyester. It is most commonly synthesized utilizing ring opening polymerization of ε-caprolactone. [2–4] PCL is a thermoplastic possessing a glass transition temperature (T_g) that is typically resides around -60 °C in addition to a relatively low melting point (T_m) of 60 °C. This melting point is also capable of varying with

dependence on the materials crystallinity which has been observed to reach values as high as 69%. [2,5–7] PCL's low melting point makes it particularly useful for drug loading as well as a multitude of industrial and biomedical applications. Currently, PCL is used in drug and chemical delivery, biomedical devices, surgical equipment, medical adhesives, orthopedic castings and tissue engineering constructs. [8–11]

One of PCL's most useful properties is its biodegradability. However, this biodegradation is greatly dependent on the environment that the polymer is used in. [6,12] For example, the polymer may degrade in as little as 6 days when exposed to composting conditions which can reach temperatures above PCL's T_m of 60 °C. [8] Furthermore, the polymer can be quickly enzymatically degraded by outdoor living organisms such as bacteria and fungi. [13,14] Conversely when the temperature is below the T_m or at room temperature, the degradation of the polymer is quite slow. [15] Provided that the material is not being stored in direct contact with water, pure PCL at room temperature will degrade by surface erosion over a period of 2-4 years depending on the molecular weight and degree of crystallinity of the polymer. [11,16,17] This slow biodegradation is quite advantageous, more especially in long term controlled delivery systems such as those used in the release of antibacterial agents. [6,14,18–25]

While PCL's biodegradability makes it an environmentally friendly and commercially feasible material, its use as a controlled release construct makes it a useful material for both the medical and household communities alike. The ability to control the release of a molecule from a device/system over an

extended period of time (i.e. controlled release) is very valuable and opens a wide array of possibilities for PCL's direct implementation. Currently, there many extended-release products in the commercial realm ranging from complex drug delivery systems to simple scent-releasing products for the home. In particular, PCL has been used to imbue long-term release characteristics in these devices which have been observed to last longer than one year. [11] Given PCL's aforementioned low melting point, we are able to employ a simple hot-melt technique which has allowed us to create a controlled-release system for two types of volatile materials namely orange oil and menthol.

Orange oil is a commercially available essential oil, derived from the orange fruit, as a byproduct of cold-pressing. [26] It possess a T_m of -74 °C and boiling point of 175.4 °C. [27] Orange oil derives its fragrant citrus scent from an aromatic hydrocarbon compound called D-Limonene. [28] This compound is quite often found in environmentally friendly household cleaning solvents as well as glues and stain removers. [28] The material has also been observed to be flammable. [27] Due to its aromatic nature along with its high boiling point, orange oil makes a good candidate for hot melt encapsulation using PCL. It is hoped that by encapsulating the oil in PCL, we shall be able to control its release over an extended period of time. Additionally, while studying the release of orange oil from PCL, we shall attempt to elucidate and type of effect the inclusion of an oil may have on the physical morphology of the polymer PCL.

Menthol is a waxy crystalline like substance which was discovered over 2,000 years ago in Japan and is derived from mint oils such as peppermint oil.

[29–31] It has a T_m of ≈ 42 °C, and a boiling point of 212 °C. [32,33] It has a vapor pressure of 0.6 mmHg at 25 °C. [34] Menthol is a good candidate for this controlled-release study as it is easily melted with PCL, is volatile, and smells quite pleasant. Currently, menthol has a number of commercially useful properties with global consumption of the raw product exceeding 7,000 tons annually. [35] When ingested or topically applied, menthol causes the perception of a “cooling effect.” [29] It is hypothesized that this is the result of menthol activating sensory neurons known as transient receptor potential (TRP) channels to induce cold response signals at the application site. [36] It has also been observed to possess analgesic and anti-pyritic (i.e. anti-itching) properties. [37] These properties coupled with its pleasant scent have resulted in its use in may commercial products including: perfumes, chewing gums, anti-itch creams, analgesics, cosmetics, pesticides, flavoring agents, and for household odor control. [30] While menthol has been deemed by the FDA to be safe at concentrations up to 16% for external topical use, studies have shown that menthol loads of 40% can result in skin erythema and spontaneous burning. [31,38]. Consequently, these safety issues along with menthols naturally high volatility make it a perfect candidate for controlled release. [39] This study shall thus attempt to quantify the release of menthol from PCL with focus on the effects of % menthol loading as well as the combined materials storage temperature conditions. Additionally, we shall also attempt to characterize any potential morphological changes brought about by combining the PCL and

menthol during our hot melt fabrication process which could offer possible insight into how the materials interact for release purposes.

2. Materials and Methods

2.1 Preparation of Volatile Oil Loaded Polycaprolactone Samples

Dow Tone P-787 Polycaprolactone donated from Durect Lactel® (Lactel, Birmingham, Alabama) for scientific use with an expected molecular weight of 50,000 g/mol was melted in a disposable aluminum tin at 75 °C. Upon complete melting of the PCL, various weight/volume % concentrations of PCL and oil were combined to produce homogenous mixtures with fixed oil loadings. The samples were then allowed to cool and placed into pre-weighed 22 mL Wheaton Scintillation vials for time lapse gravimetric analysis under two different temperature storage conditions (22 °C, and 4 °C).

2.2 Preparation of Menthol Loaded Polycaprolactone Samples

Dow Tone P-787 Polycaprolactone donated from Durect Lactel® (Lactel, Birmingham, Alabama) for scientific use with an expected molecular weight of 50,000 g/mol was melted in a stainless steel crucible at 75 °C. Upon complete melting of the PCL, various weight/weight % concentrations of PCL and 99% Pure Menthol (Sigma-Aldrich, St. Louis, MO) were combined to produce homogenous mixtures. The molten homogenized mixtures were then aliquoted in .5 mL quantities utilizing a syringe and injected into a custom made aluminum mold equipped with 4 wells possessing a diameter of .5 inches (12.7 mm). Upon

complete cooling, the tablets were ejected from the mold and placed into pre-weighed 22 mL Wheaton Scintillation vials for time lapse gravimetric analysis. Samples were analyzed over a 180-day period under three different temperature storage conditions (22 °C, 4 °C and -20 °C).

2.3 Processing of Volatile Oil Loaded Polycaprolactone Samples

A select number of volatile oil loaded PCL samples were subjected to a single pressure, temperature and time profile after initial fabrication. This profile was fixed in this sample cohort with all pressed volatile oil loaded PCL samples being exposed to 15,000 lbs of pressure for 1 hour at 22 °C in a manually operated hydraulic press. Upon lapse of the allotted time, the samples were released from the press for morphological and release profile analysis.

2.4 Processing of Menthol Loaded Polycaprolactone Samples

A select number of menthol loaded PCL samples were subjected to two pressure, temperature and time profiles after initial fabrication. These profiles consisted of pressing the menthol loaded samples at both 2,000 lbs and 10,000 lbs of pressure for 2 minutes at 22 °C in a manually operated hydraulic press. Upon lapse of the allotted time, the samples were released from the press for morphological and release profile analysis.

2.5 Chemical Analysis

A Perkin Elmer Spectrum One Fourier Infrared Transform Spectroscopy (FTIR) unit (Perkin Elmer, Shelton, Connecticut) was used. PCL sheet samples were analyzed using an attenuated total reflectance module (ATR).

2.6 Size Exclusion Gel Permeation Chromatography

A Gel Permeation Chromatography (GPC) system configured for size exclusion (Perkin Elmer Flexar Ultra High Performance Liquid Chromatography system Totalchrom WS MI software V 6.2 Perkin Elmer, Shelton, Connecticut) was used to determine molecular weight. PCL granules were dissolved in HPLC grade Tetrahydroflurane (THF) (Fisher Scientific, Pittsburgh, Pennsylvania), filtered with a .22 µm filter and run through two serially connected Waters HR 4 & HR 5E Columns (Waters, Milford, Massachusetts) at a flowrate of 1 mL/min. The GPC was calibrated using a monodisperse polystyrene standard.

2.7 Structural Analysis

X-Ray Powder Diffraction (XRD) was performed using a Bruker D-8 Advance X-Ray Powder Diffraction system running DaVinci Software and a Cu X-Ray tube operating at 40 kV and 40 mA equipped with a Bruker Vantec-500 Xe-CO2 gas filled detector with a 13.5cm diameter window set at 20 cm from the goniometer center. System wavelength was 0.15418 nm. The system optics consisted of a polycap with an output beam divergence of 0.25° for Cu and a spot diameter of less than 4.0 mm and a 79 mm long 0.3 mm collimator on the

incident beam path (Bruker, Billerica, Massachusetts). Scans were run from 15°-70° 2Θ with a virtual step size of .02° and a counting time of 30 s per step. Upon completion of the scan, data was analyzed using the Bruker Diffrac-Eva software package (Bruker, Billerica, Massachusetts).

2.8 XRD Crystallinity Calculation

A XRD peak deconvolution was performed using the software Fityk for the purpose of calculating the PCL and oil loaded PCL's % Crystallinity. Gaussian curve fitting functions were used to de-convolute the areas under the amorphous and crystalline peaks. The intensity due to the crystalline region can then be calculated by subtracting the amorphous region from the total area, and the percent crystallinity can then be calculated by dividing the intensity area due to the crystalline region by the total area.

2.9 Polarized Light Microscopy

A Leica Optical Microscope Model Wild M 420 (Leica, Buffalo Grove, IL) equipped with polarized light filters was used to visualize the morphology of samples at 480 x magnification. A small slice was removed from each sample and then melted at 60 °C between glass coverslips, allowing for visualization of crystallization at each oil concentration.

3. Results and Discussion

3.1 FTIR Characterization of Polycaprolactone

FTIR was performed to ensure that the PCL was free of any detectable excipients or additives. FTIR analysis of the PCL is represented in Fig. 1. and was found to display the typical FTIR peaks associated with PCL which occur at approximately 1160 cm^{-1} (C-O and C-C), 1721 cm^{-1} (C=O) and 2865-2949 cm^{-1} (CH_2).[40] FTIR results also suggest the material is free of any detectable excipients and additives.

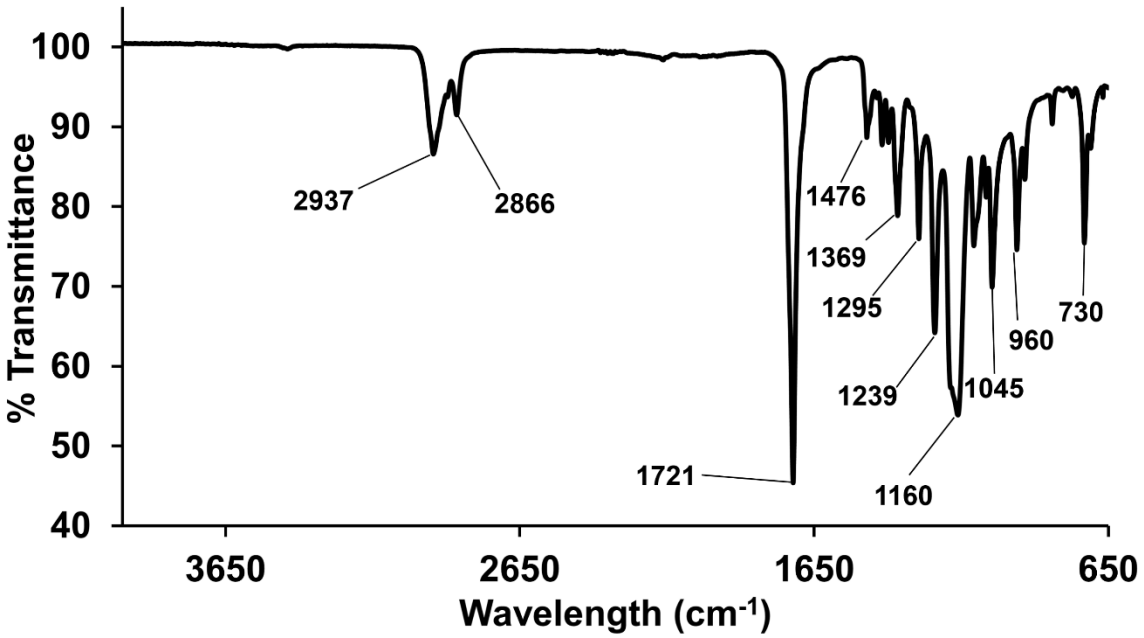

Figure. 1. FTIR of PCL. PCL's associated peaks are located at 1160 cm^{-1} (C-O and C-C), 1721 cm^{-1} (C=O) and 2865-2949 cm^{-1} (CH_2).

3.2 Controlled Release of Orange Oil from PCL

The percent release of orange oil from loaded PCL samples was accomplished using gravimetric analysis over time with samples being stored at both 22 °C and 4 °C. Additionally, one sample set was exposed to 15,000 lbs of pressure for 1 hour and was evaluated at 22 °C.

Fig. 2. Depicts the % orange oil released from 7 different loaded PCL samples (1.0-15.1%) while stored at 4 °C for 16 days. Initial results for this sample set reveal a steady release profile. Additionally, the total % release was observed to increase in direct relation to the samples initial loading with the highest loaded samples releasing the greatest amount of oil. Ultimately, at 4 °C, the 15.1% loaded sample was observed to release ≈ 40% of its payload suggesting that at this loading concentration, it may be possible to release ≈ 80% in a 30-day period. Conversely, lowering the loading appeared to diminish the capacity for oil release. This is most likely attributed to the PCL being in greater concentration of the bulk sample and thus allowing for the creation of a smaller pore system in the bulk structure which would thus limit the oil's access to the air.

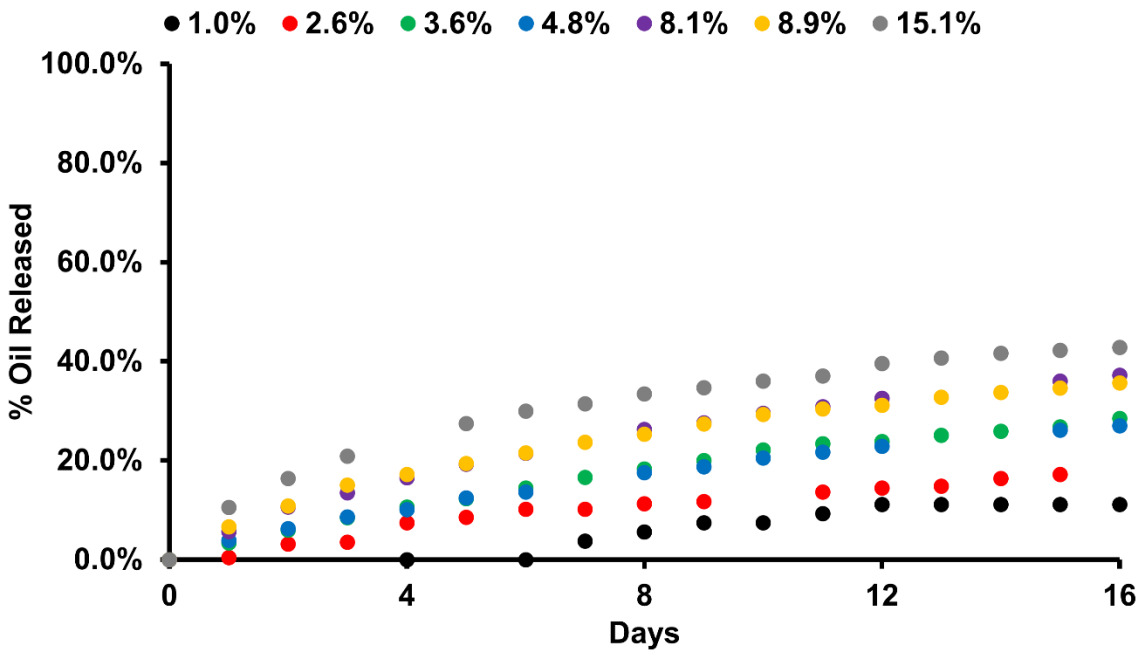

Figure. 2. Percent release of Orange Oil from PCL stored at 4 °C. Samples were loaded with 1.0-15.1% Orange Oil (wt/v%).

Fig. 3. Depicts the % orange oil released from 7 different loaded PCL samples (1.0-15.1%) stored at 22 °C for 16 days. Once again as observed previously in Fig. 2., this sample set depicts a steady release profile. Also as observed previously, the total % release was observed to increase in direct relation to the samples initial loading with the exception that the 8.1% loaded sample has surpassed the 8.9% and 15.1% samples. Additionally, the increase in storage condition has been observed to increase the maximum % oil released as the 8.1% loaded samples is observed to release ≈ 60% of its payload by 16 days. Fig. 3. also suggests that decreasing the initial loading to ≈2.5% may be prudent for application around room temperature given that a 30-day release profile would be more usable than a 15-day profile. The observed increase in

total release in Fig. 3. in comparison to the samples stored at 4 °C in Fig. 2. are suggestive that increasing the storage temperature may not only increase the oils volatility but may also allow the polymer to relax further given its increased distance from its T_g. This however warrants further analysis by XRD to obtain a better understanding of how the two materials are interacting.

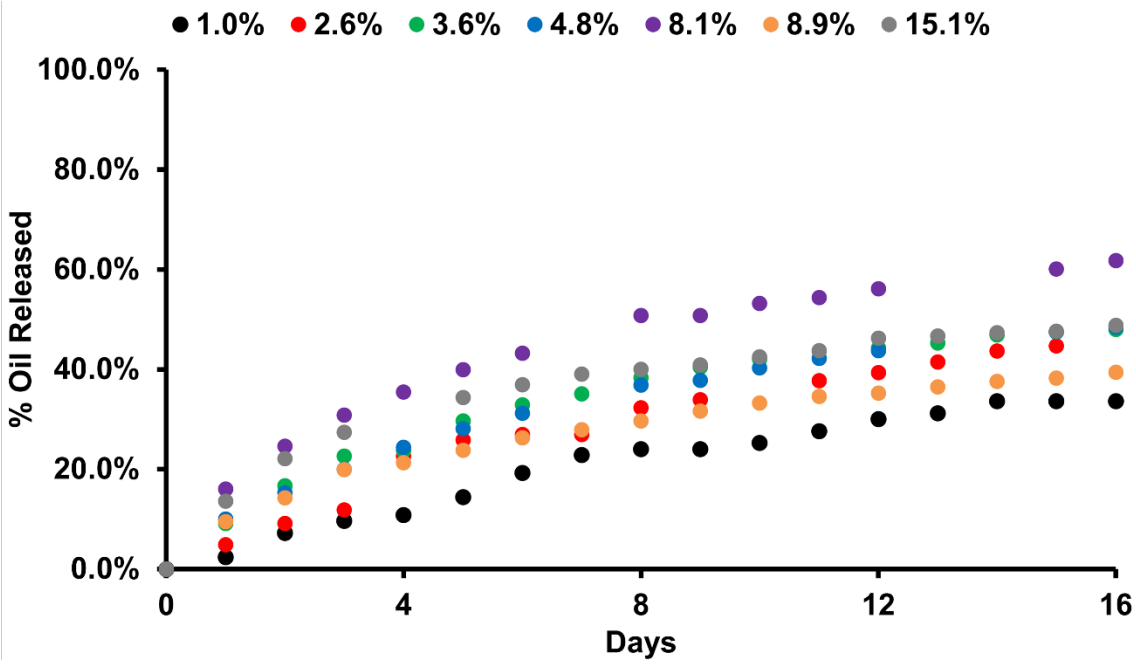

Figure. 3. Percent release of Orange Oil from PCL stored at 22 °C. Samples were loaded with 1.0-15.1% Orange Oil (wt/v%).

Fig. 4. Depicts the total % orange oil released from 7 different loaded PCL samples (1.0-15.1%) while stored at 22 °C for 16 days. These samples were however pressed after loading the oil at 15,000 lbs for 1 hour in a hydraulic press at room temperature. Unlike what was observed in the preceding two sample sets depicted in Figs. 2-3., Fig. 4.'s sample set depicts a faster release followed

by a steady release profile. Also as observed previously, the total % release was observed to increase in direct relation to the samples initial loading with the exception this time that the 4.8% loaded sample has surpassed the 8.1-15.1% samples. This sample set, more specifically the 4.8% loading condition is observed to release the highest percent of orange oil yet at ≈80% of its payload by 16 days.

Fig. 4. suggests that decreasing the initial loading once again to ≈2.5% may be prudent for application around room temperature given that a 30-day release profile is a commercially marketable timed release target. Additionally, as mentioned previously, it would be prudent to further characterize the materials by XRD to further elucidate any type of morphological characteristics the materials may possess which could affect the release profile or marketability of the devices.

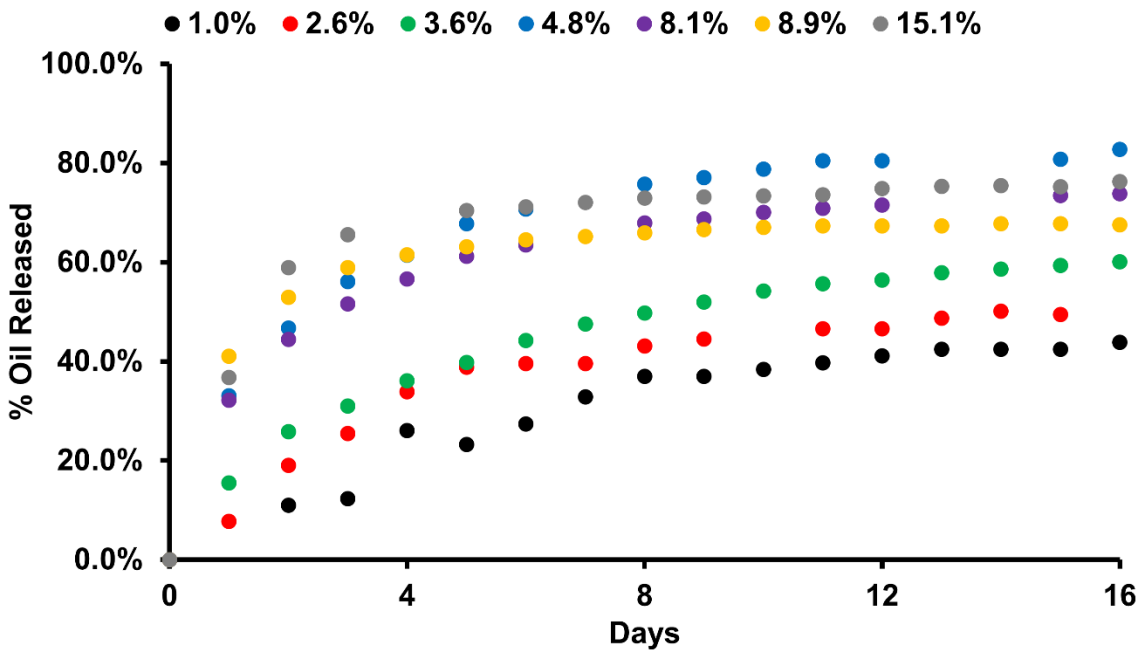

Figure. 4. Percent release of Orange Oil from Pressed PCL (Pressed: 15,000 lbs at 22 °C for 1 hour) stored at 22 °C. Samples were loaded with 1.0-15.1% Orange Oil (wt/v%).

3.2 XRD of Orange Oil Loaded PCL

While the purpose of this study was to establish whether a volatile oil could be released from the polymer PCL in a controlled manner, it was also important to further characterize the combination of materials in order to elucidate any morphological changes which may have occurred upon adding the oil as well as upon processing the material at 15,000 lbs for 1 hour at room temperature. Analyzing the results of both the PCL and Orange Oil loaded PCL samples, XRD patterns from both before and after processing (depicted in Figs. 5-12.) were acquired. This allowed us to quantify the observed changes in the

PCL's morphology. In addition to the XRD diffraction profiles (depicted in Figs. 5-12.) which will be discussed individually, their % Crystallinity values as calculated by the process described in Section 2.8 shall be discussed and are depicted in Fig. 13.. It is thought that by exposing thermoplastic polymers such as PCL above their respective T_g's to pressure stresses, that the materials amorphous and crystalline regions can be altered. [41] Thus the addition of oils to the PCL in addition to the pressure processing warrants this additional characterization study.

Fig. 5. depicts the XRD profiles for the PCL material both in its unpressed (black line) and pressed forms (red line). Initial analysis of the samples reveals that they both possess the expected morphology typical of semi-crystalline PCL. This is represented by twin sharp peaks, with one significant difference being that the pressed sample displays a broader peak with an amorphous region displaying a columnar structure. Upon calculating the % Crystallinity for these samples which is depicted in Fig. 13. it is observed that pressing the unloaded PCL has altered its crystallinity. This is observed by an increase in the materials crystallinity from the 30.0% to the ≈ 35.0% observed in the pressed sample.

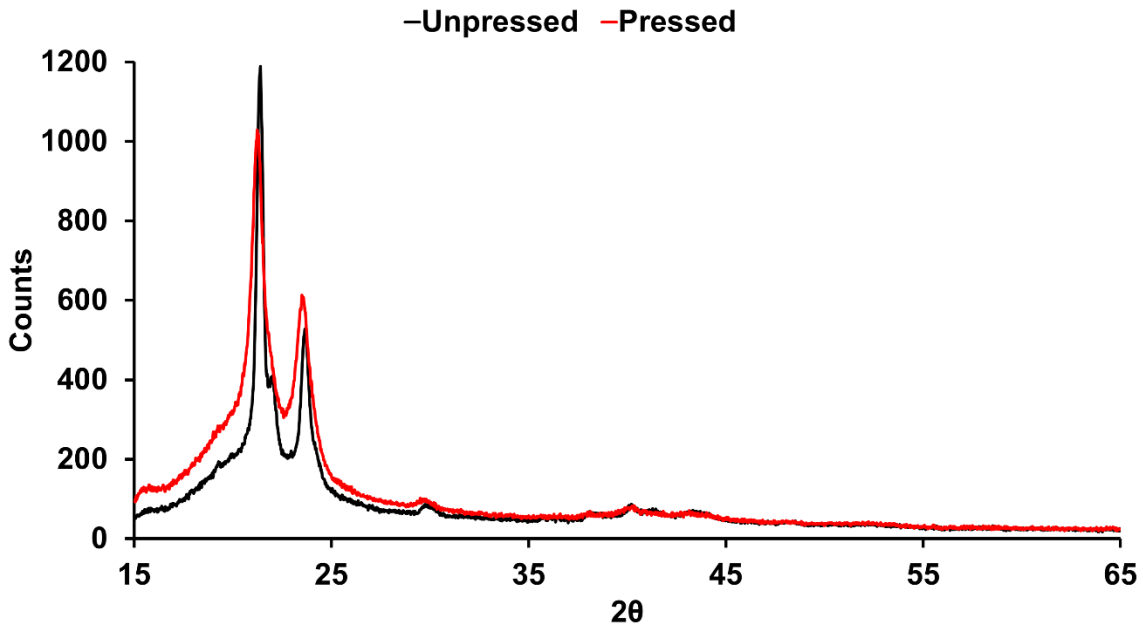

Figure. 5. XRD profile of the Unpressed PCL (Black Line) and the Pressed PCL (Red Line).

Fig. 6. depicts the XRD profiles for the unpressed and pressed 1.0% Orange Oil loaded PCL samples. Interestingly, the pressed sample possesses a more intense peak structure yet its base appears to have broadened which correlates to an increase in the amorphous region yet with more order. Typically, in pure materials, increases in crystallinity are observed as increases in the XRD profiles sharpness or a decrease in its width. In this situation, oil has been added to the system which has had an immediate impact on the materials morphology. Looking to Fig. 13. we observe an increase in crystallinity in the unpressed sample to 36.5%. Interestingly, applying pressure to the oil loaded sample is actually observed to decrease the materials crystallinity. One explanation fo this observation is that the oil acts much like a surfactant allowing the amorphous

chains more freedom to move which has allowed the material to crystallize. However, upon pressing the material at 15,000 lbs the material is observed to decrease in % crystallinity yet the XRD profile remains rather sharp. This suggests that there may be another phase present. Quite possibly this may be a liquid crystalline like phase which would account for the peak sharpness with increased peak breadth.

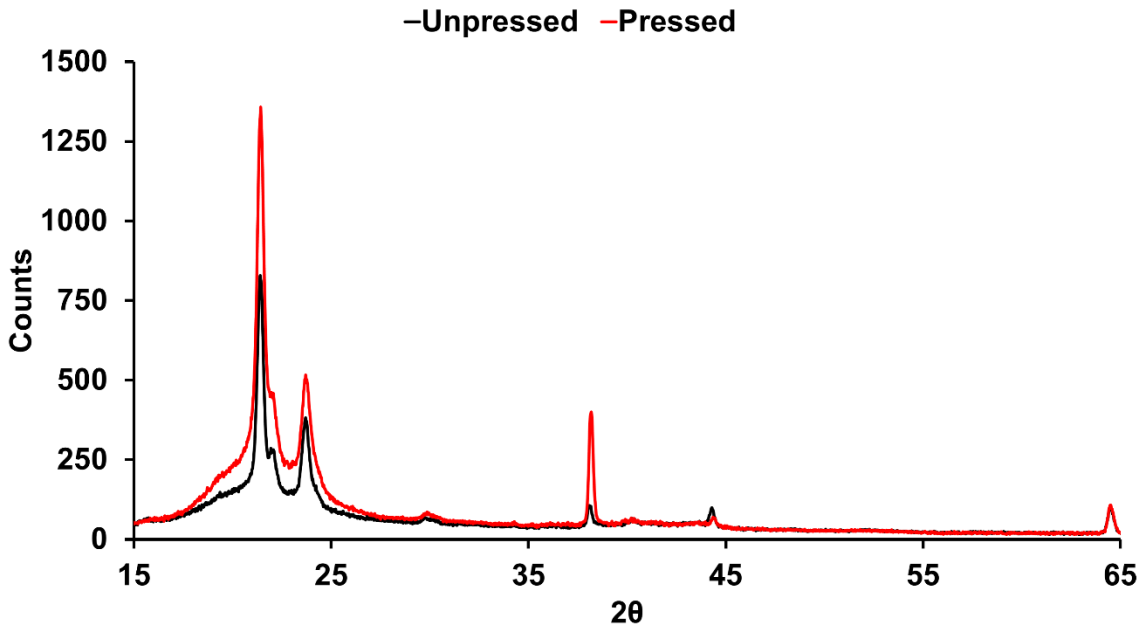

Figure. 6. XRD profile of the 1.0% Orange Oil loaded Unpressed PCL (Black Line) and the Pressed PCL (Red Line).

Fig. 7. depicts the XRD profile for the unpressed and pressed 2.6% Orange Oil loaded PCL samples. Immediately, it is apparent that the oil is capable of affecting the PCL's structure as observed by the unpressed samples XRD profile, namely it is observed to increase in sharpness and in its breadth.

Looking at the pressed sample we see a less intense peak sharpness with a rather broad base. Looking at Fig. 13. We observe that the 2.6% oil loading has resulted in an increase in % crystallinity to 38.6%. Interestingly, the pressed 2.6% oil loaded sample has increased to 31.9%. This decrease in comparison to the pure pressed PCL may suggest that the oil acts much like a surfactant which would allow the polymer chains to flow with greater ease than the pure material. Thus the addition of pressure may either be destroying the crystals or forcing the material to take on a different morphology of that seen in liquid crystals.

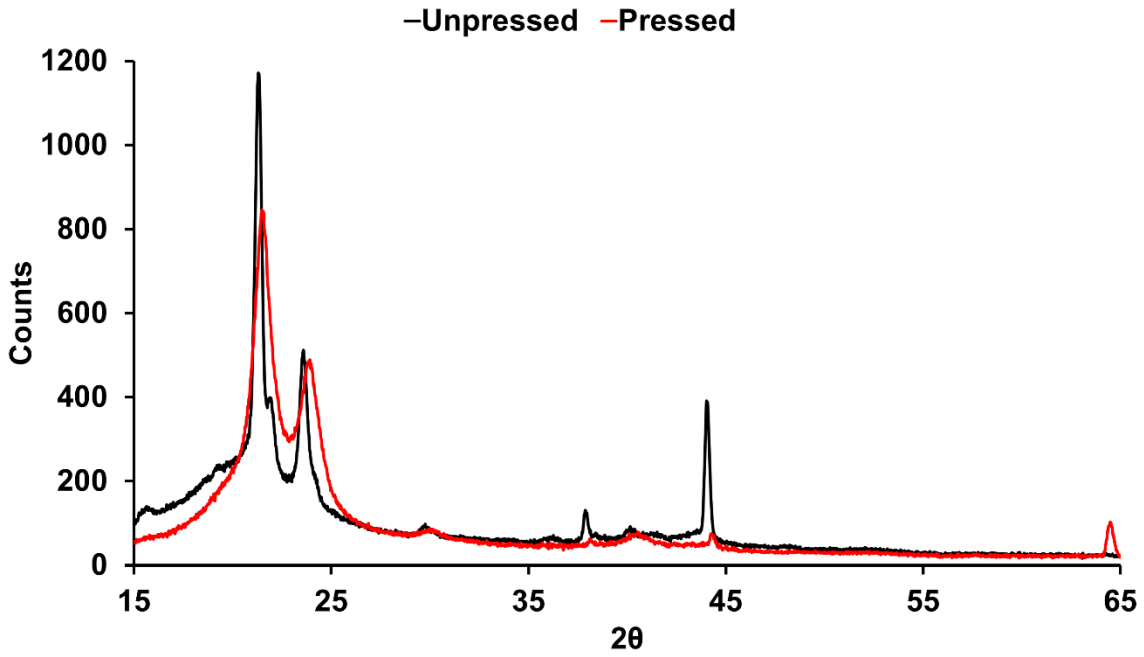

Figure. 7. XRD profile of the 2.6% Orange Oil loaded Unpressed PCL (Black Line) and the Pressed PCL (Red Line).

Fig. 8. depicts the XRD profile for the unpressed and pressed 3.6% Orange Oil loaded PCL samples. Once again, it is immediately apparent that the

oil is capable of affecting the PCL's structure as observed by the unpressed samples XRD profile, the unpressed 3.6% sample is observed to increase in sharpness. Looking to the pressed sample we observe a much less intense peak sharpness with an increase the broadness of the base. Looking at Fig. 13. We observe that the 3.6% oil loading has resulted in an increase in % crystallinity to 35.5%. Conversely, the pressed 3.6% oil loaded sample has actually decreased to 25.2%. This decrease which was previously observed in the 2.6% sample offers further support to the suggestion that the oil may act much like a surfactant which would allow the polymer chains to flow with greater ease than the pure material. Thus the addition of pressure may disrupt the crystal structure or force the material to take on a different morphology that resembles that of liquid crystals.

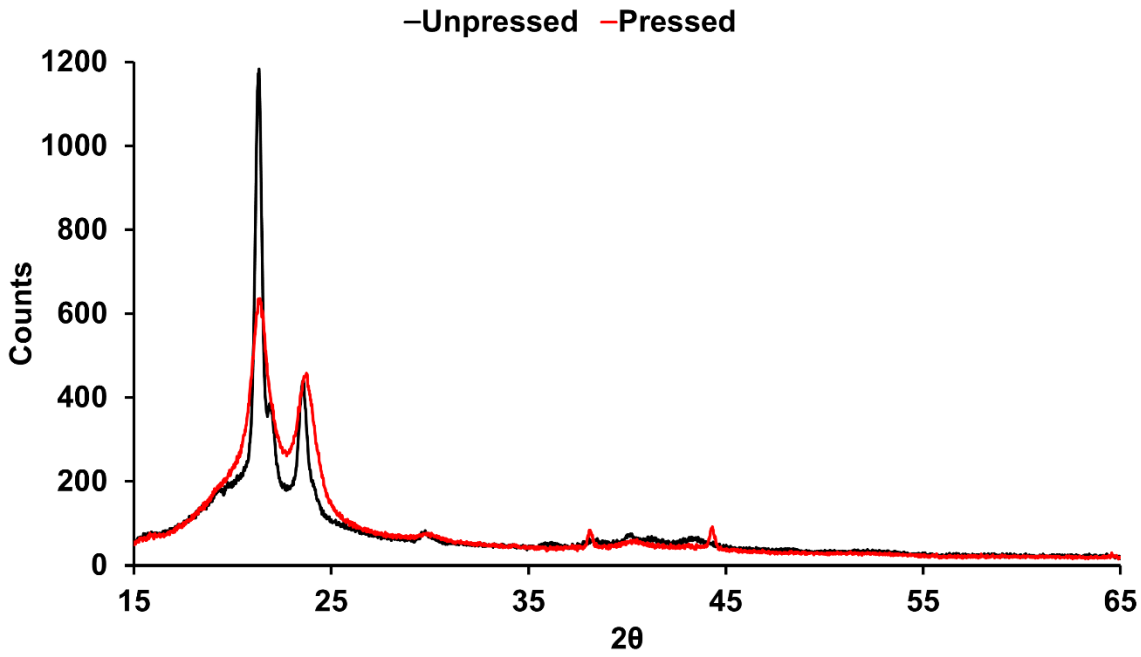

Figure. 8. XRD profile of the 3.6% Orange Oil loaded Unpressed PCL (Black Line) and the Pressed PCL (Red Line).

Fig. 9. depicts the XRD profile for the unpressed and pressed 4.8% Orange Oil loaded PCL samples. Looking at the unpressed sample, the XRD profile is observed to possess a rather sharp peak. Fig. 13. reveals a % crystallinity of 29.5%. Looking to the XRD profile of the pressed sample, we observe sharp peak structure with a broad base. Fig. 13. reveals a decrease in crystallinity to 22.1%. It is at this oil concentration hat we observe the largest decree in the materials crystallinity.

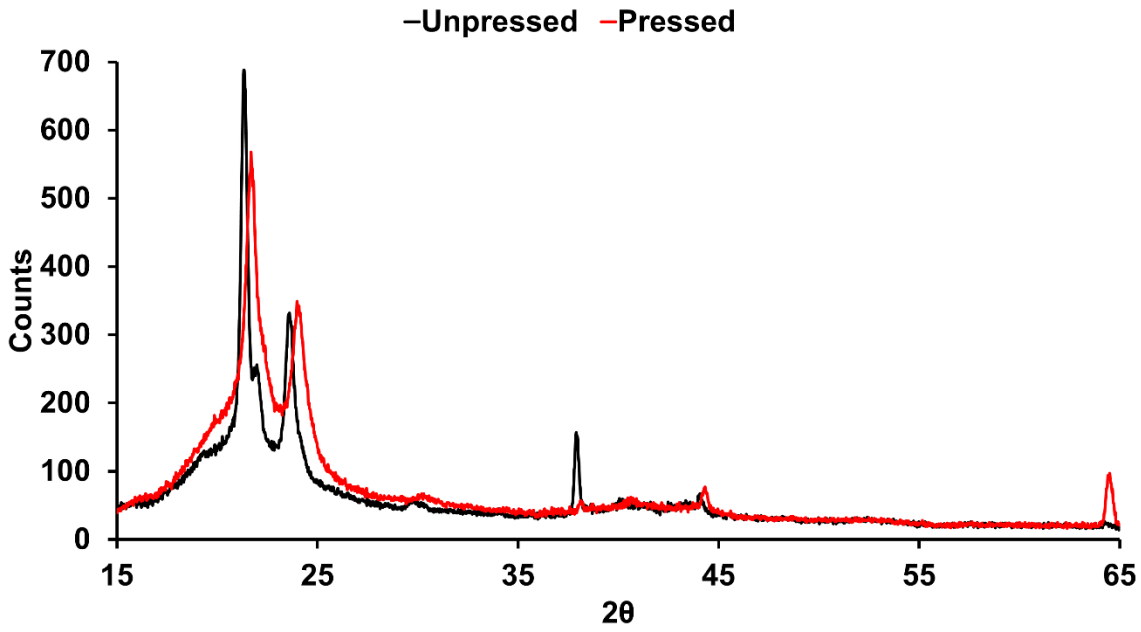

Figure. 9. XRD profile of the 4.8% Orange Oil loaded Unpressed PCL (Black Line) and the Pressed PCL (Red Line).

Fig. 10. depicts the XRD profile for the unpressed and pressed 8.1% Orange Oil loaded PCL samples. Interestingly we see a striking difference between the unpressed and pressed XRD profiles. Looking at the unpressed sample, the XRD profile is observed to maintain its sharpness yet become less intense. The pressed material on the other hand has taken on a sharp structure with a very broad base. Fig. 13. reveals a % crystallinity of 36.0% for the unpressed material while the pressed material is observed at 31.6%.

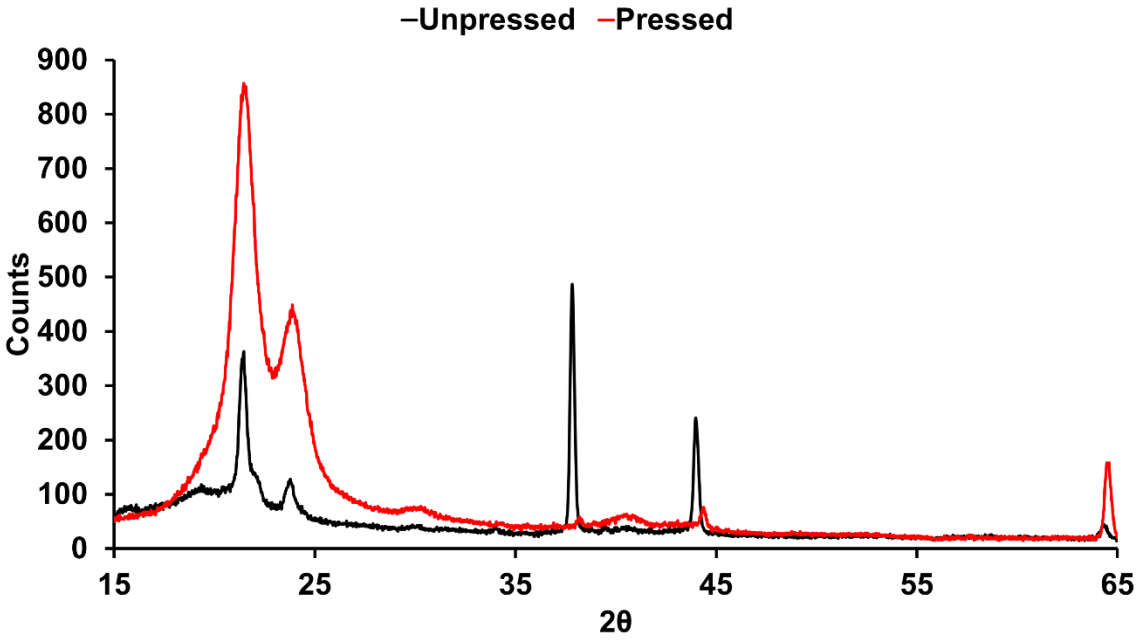

Figure. 10. XRD profile of the 8.1% Orange Oil loaded Unpressed PCL (Black Line) and the Pressed PCL (Red Line).

Fig. 11. depicts the XRD profile for the unpressed and pressed 8.9% Orange Oil loaded PCL samples. In this series unlike the preceding 8.1% samples, we observe and increase in crystallinity. Looking at the unpressed and pressed samples together we observe that both possess quite sharp XRD profiles. However, the pressed sample does appear to possess a slightly broader peak than the unpressed sample. Fig. 13. reveals a % crystallinity of 28.7% for the unpressed material while the pressed material is observed at 25.9%. Additionally, it is at this point that increasing the oil concentration is beginning to have a definitive inhibitory effect on the materials ability to crystalize as both unpressed and pressed samples were observed to decrease below the original 30.3% crystallinity of the pure PCL. Oddly, this was observed in the 4.8% samples but not the 8.1% samples.

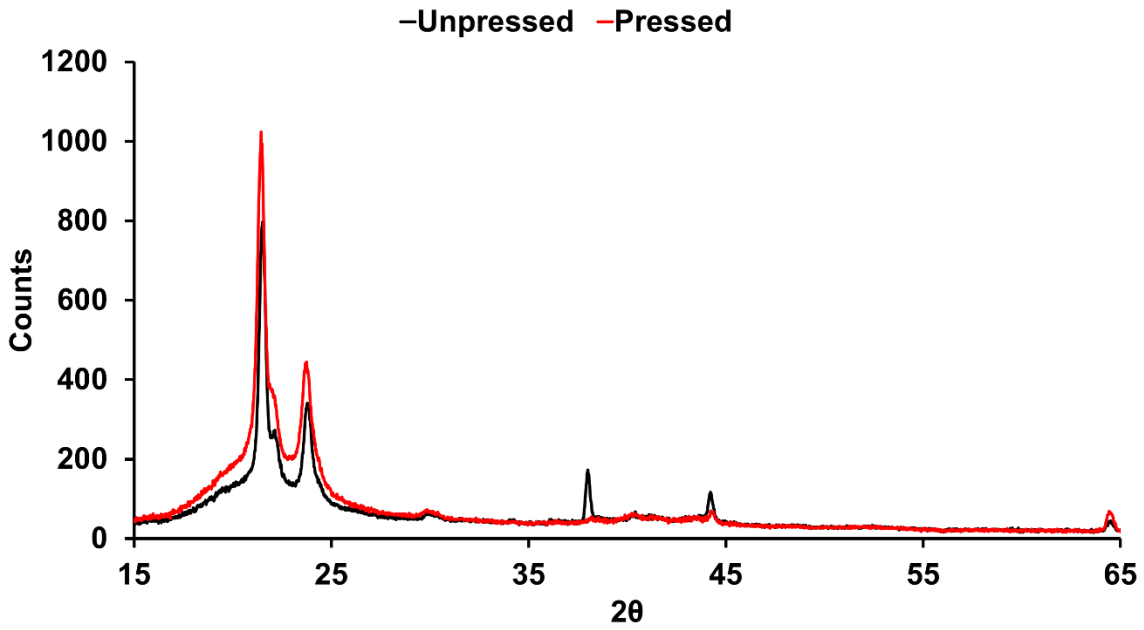

Figure. 11. XRD profile of the 8.9% Orange Oil loaded Unpressed PCL (Black Line) and the Pressed PCL (Red Line).

Lastly, the samples depicted in Fig. 12. which were loaded with 15.1% orange oil were observed to display a significant morphological change. Focusing first on the unpressed sample, the XRD profile is observed to take on a very sharp yet base broadened structure. Conversely, the pressed sample is observed to greatly diminish in peak sharpness while displaying a rather broad amorphous like peak structure. Fig. 13. reveals a calculated % crystallinities for the unpressed and pressed samples of 26.2% and 25.0% respectively. Thus in this sample cohort, the application of pressure along with a high concentration of oil loading is observed to disrupt the PCL ability to crystallize.

Owing to the distinct morphologies observed by XRD in the preceding samples, the addition of oil to PCL has been shown to be capable of altering the materials structural orientation which was observed as a disruption of the XRD peak profiles from what was observed in the pure material.

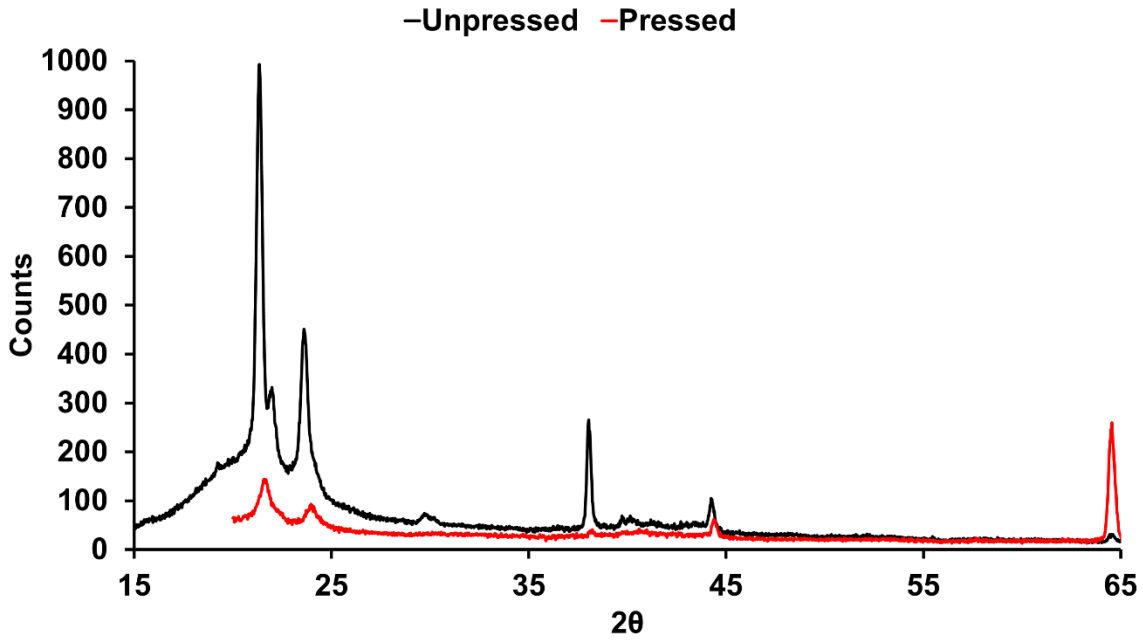

Figure. 12. XRD profile of the 15.1% Orange Oil loaded Unpressed PCL (Black Line) and the Pressed PCL (Red Line).

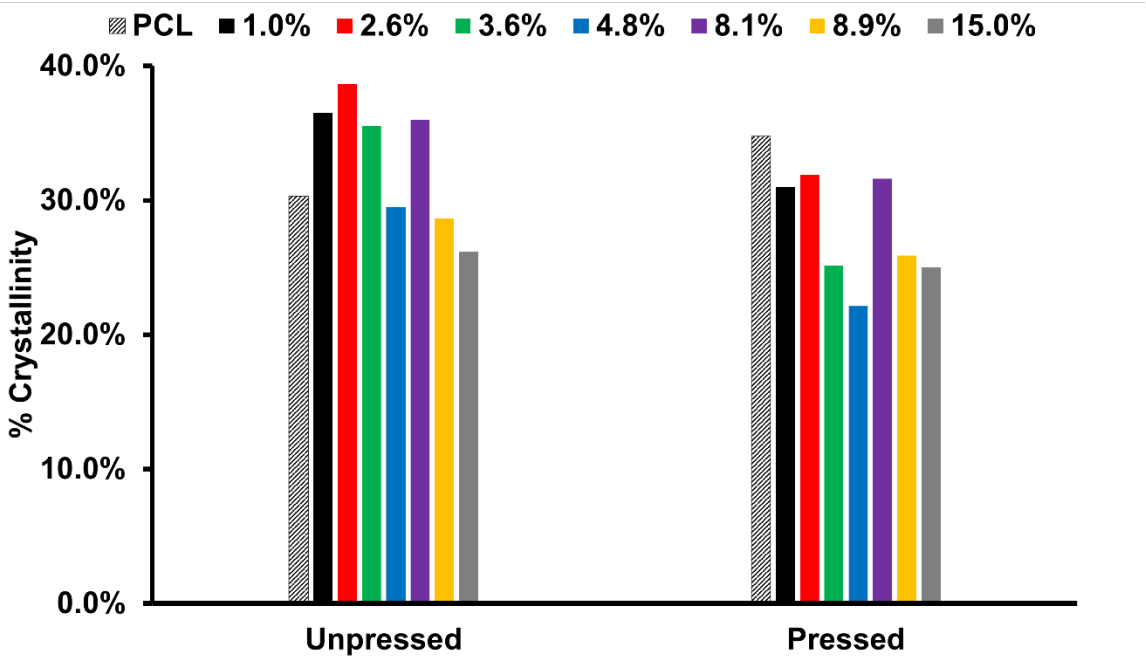

Figure. 13. XRD calculated % Crystallinity values for all unpressed and pressed, PCL and Orange Oil loaded samples.

3.3 PLM of Orange Oil Loaded PCL

In order to further characterize the effect of adding orange oil on the morphology of PCL, a set of samples were set aside after the hot melting procedure. These samples once cooled to room temperature, were imaged under polarized light using an optical microscope equipped with cross polarizers. Fig. 14. Is a depiction of this visual study and is arranged such that the concentration of oil increases as one progresses down the figure with each sample labelled with its respective oil concentration. During this analysis, all of the oil loaded samples were observed to display a morphology which resembled that of a liquid

crystalline phase. Thus prior to discussing the images, it is prudent to define what a liquid crystal is.

To begin, two common types of liquid crystal systems known to exist in polymers are thermotropic and lyotropic. Thermotropic crystal systems are defined by their ability to alter their morphology in response to changes in temperature, while lyotropic are dependent on solvents and their concentration in the polymer. [42] While the images portrayed in Fig. 14. do display phases which closely appear to be like lyotropic liquid crystals, the PCL is not in solution. Therefore, our current morphological discovery cannot be specifically categorized as a traditionally defined liquid crystal and we shall refer to it as a liquid crystal like structure.

Looking initially at the pure PCL, one can see indication that the raw material possesses a crystalline structure. This is denoted by the presence of spherulites which are a known and expected crystal structure seen in semi-crystalline polymers such as PCL. Increasing the loading to 1% orange oil, the preceding spherulitic morphology seen in the pure PCL is now gone. The material now possesses what appears to be a distorted spherulite population. Interestingly, upon increasing the oil concentration to concentrations between 2.6-8.9%, the PCL is observed to take on varying degrees of birefringence which is displayed as a mix of liquid crystalline like structures mixed with distorted spherulites. This is suggestive that the material is quite easily influenced by the oil and that the oil may act much like a surfactant which would allow the structure to take on a liquid crystalline morphology. It should also be noted that the visual

observations made up until this point have not been uniform throughout the materials bulk structure suggesting that there may be a concentration dependent change occurring. Looking to the 15% loading condition, we now observe a uniform morphological change which permeate the entire material. This supports the previous suggestion that a certain amount of oil would be needed to fully permeate and alter the entire material. Interestingly, this samples entire bulk is observed to possess a structure which resembles that of liquid crystals.

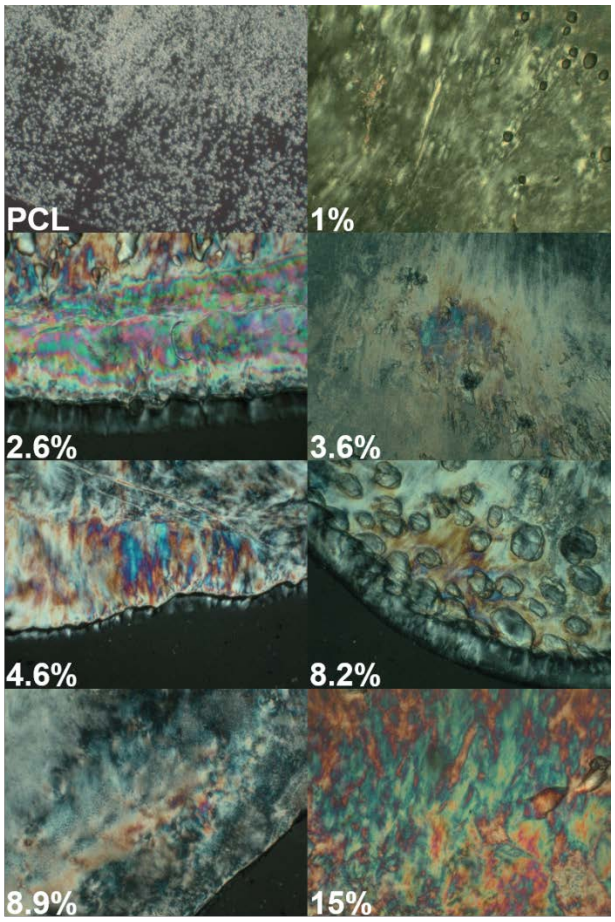

Figure. 14. PLM images for all melt cast PCL and Orange Oil loaded samples.

3.4 Controlled Release of Menthol from PCL

The percent release of menthol from the loaded PCL samples was accomplished using gravimetric analysis over a period of 180 days, with samples stored at 22 °C, 4 °C and -20 °C . Fig. 15. is a depiction of the total % menthol released from 3 different PCL loading conditions (1%, 5%, and 10%) while they were stored under room temperature conditions (22 °C) over 180 days. Initial results for this sample set depict a steady release profile which closely resembles that which was observed in the oil release experiments in the preceding section, suggesting that PCL is capable of tightly controlling a multitude of volatile agents regardless of their liquid or solid state which could prove quite useful in future work. Specifically, the total % release was observed to increase in direct relation to the samples initial loading with the highest loaded sample (10%) releasing the greatest amount of menthol. Ultimately, upon ending the study of the 22 °C cohort at 180 days, the 10% loaded sample was observed to release only 2% of its payload. Looking at the 5% and 1% samples, a total release of 1.1% and 0.2% were achieved respectively. While these results may at first appear quite impressive given that the 10% sample has displayed the potential to release menthol for ≈ 25 years, this is not commercially feasible and efforts should be made to quicken the menthols release to a period of time that is more marketable. This slow release could possibly be increased by creating a more porous structure to allow grater diffusion of the material to the exterior of the samples. Unfortunately, attempts to increase the tablets menthol concentrations

higher than 10% led to the formation of tablets that were too brittle to remove from the hot melt die.

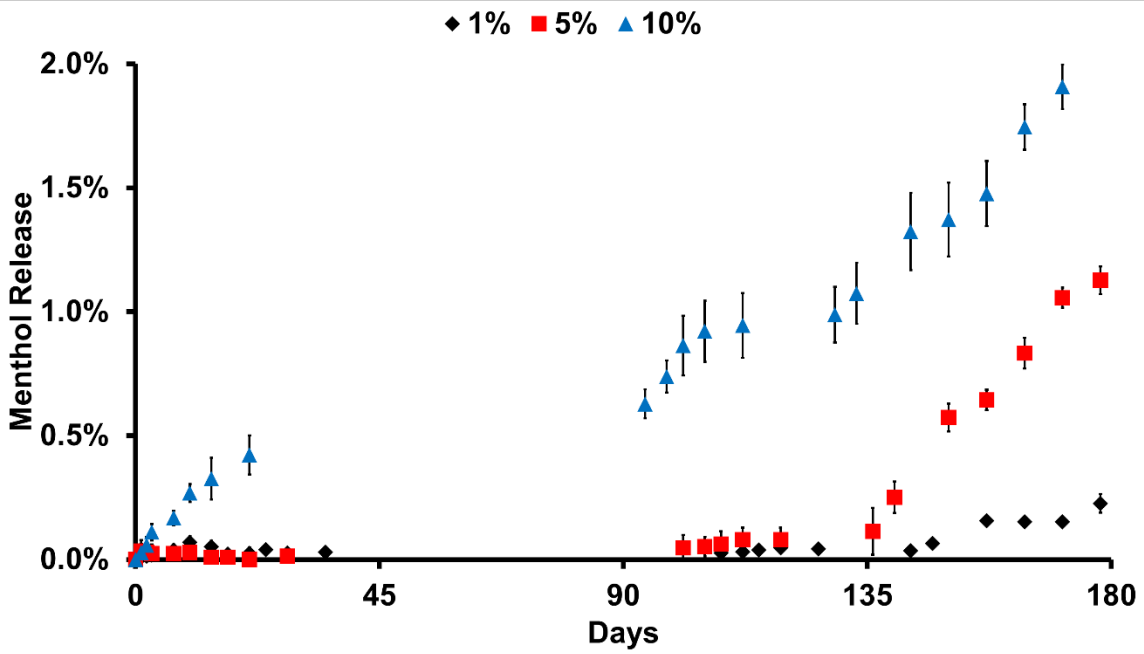

Figure. 15. Percent release of Menthol from PCL stored at 22 °C. Samples were loaded with 1%, 5%, and 10% Menthol (wt/wt%). (N=4)

Fig. 16. is a depiction of the total % menthol released from 3 different PCL loading conditions (1%, 5%, and 10%) while they were stored under refrigerated temperature conditions (4 °C) over 180 days. Once again, we observe a steady release profile. Total % release was once again observed to increase in direct relation to the samples initial loading with the highest loaded sample (10%) releasing the greatest amount of menthol. However, due to the colder temperature, the release profiles for this cohort performed even poorer over the 180 days. Ultimately, upon ending the study, the 10% loaded sample was

observed to release only 1.1% of its payload while the 5% and 1% samples released a total of 0.6% and 0.1% respectively. Thus it is apparent that decreased temperatures have a negative impact on the menthols release from the PCL. This may suggest that the material is quite stable while under cold storage but that a higher temperature would be needed to expedite the menthols release.

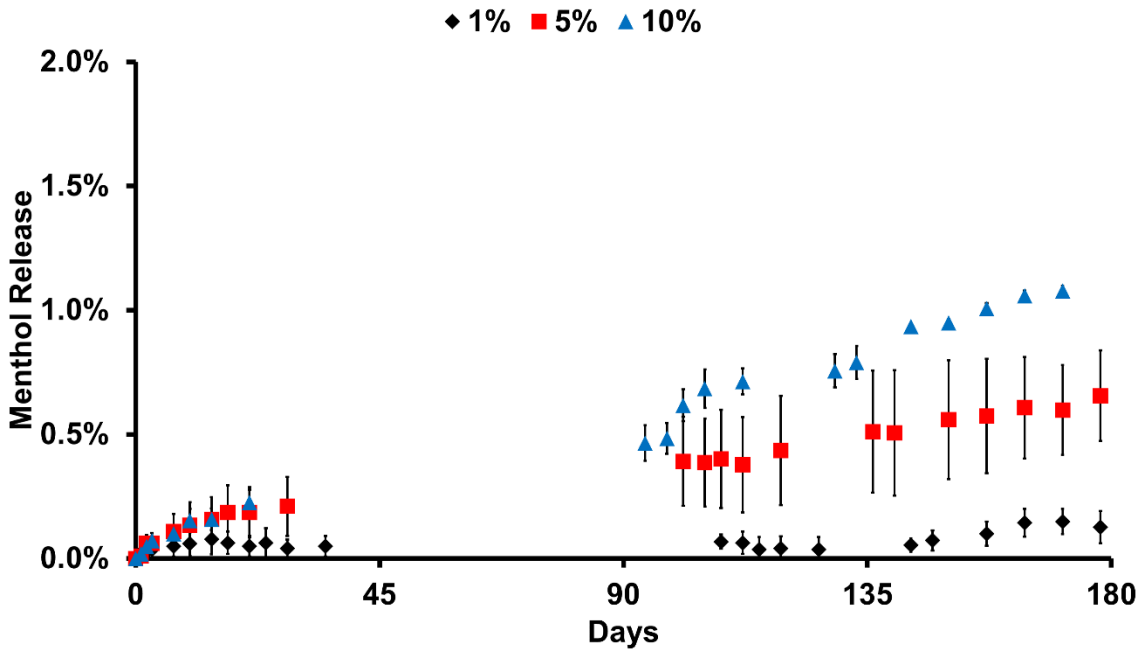

Figure. 16. Percent release of Menthol from PCL stored at 4 °C. Samples were loaded with 1%, 5%, and 10% Menthol (wt/wt%). (N=4)

Finally, Fig. 17. is a depiction of the total % menthol released from the 3 different PCL loading conditions (1%, 5%, and 10%) which were stored in freezer conditions at -20 °C over 180 days. In this temperature condition, unlike in the previous two, we do not see a definitive divergence in the loading conditions

release characteristics. In this temperature, it appears that the PCL is capable of restricting the menthols release quite well. Looking to Fig. 17., there once again is no burst effect observed. Quantifying the release in this cohort, it was found that no sample exceeded ≈ 0.2% release over the 180-day period. This suggest that the PCL is capable of providing a stable polymer network for long term storage of the menthol loading when stored at -20 °C. This also further supports the premise that increased temperatures are required to expedite the release of the menthol from the PCL. This may suggest that the material is quite stable while under cold storage but that a higher temperature would be needed to expedite the menthols release.

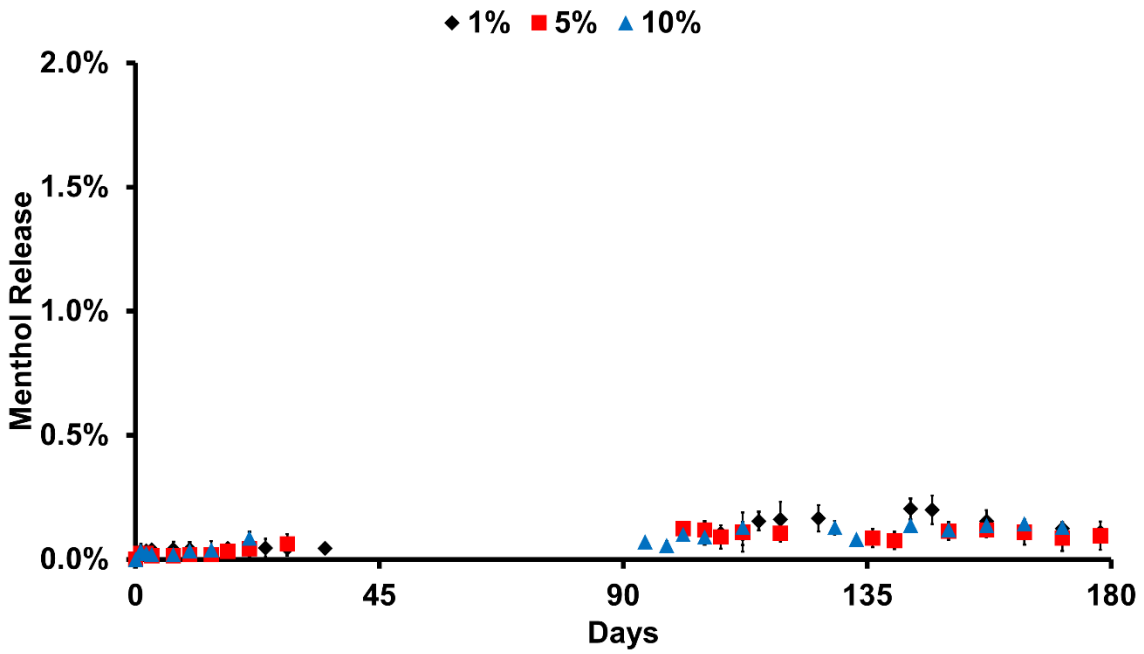

Figure. 17. Percent release of Menthol from PCL stored at -20 °C. Samples were loaded with 1%, 5% and 10% Menthol (wt/wt%). (N=4)

3.5 XRD of Menthol Loaded PCL

Given the ease of which XRD can nondestructively characterize the structural orientation of a material, it was deemed prudent and useful to explore the morphological changes that would occur upon combining PCL with a solid material. Earlier, the addition of a liquid oil was found to disrupt the PCL's crystallinity as it behaved much like a surfactant. However, unlike oil, menthol is naturally a crystalline solid. Thus it was interesting to observed what type of interactions would occur upon integrating the two materials together. Menthol as previously stated, possess a melting temperature of 42 °C which makes it quite easy to melt both the PCL (T_m = 60 °C) and menthol together.

Upon melting the two solids together, the molten mixture was found to be miscible. The material once homogenously mixed was then aliquoted into an aluminum mold and allowed to cool to room temperature, after which it was released for analysis. Looking to Fig. 18. we see the resultant XRD profiles for the raw materials (PCL-Black & Menthol-Red), along with 4 different menthol/PCL loading conditions (1.0%-Gold, 5%-Green, 10%-Blue, 20%-Purple). Looking at the PCL (Black Line) we observe the typical XRD profile which consists of two sharp peaks. Next, the menthol was analyzed and found to possess two peaks at 2Θ values of 21° and 21.5° with lower intensity than that which is observed in PCL. Upon combining the materials together, the menthol loaded PCL was observed to shift leftward to 2Θ values of 21.4° and 23.7°. Thus the materials were observed to form a solid mixture. It was also noted that

increasing the menthol concentration to 5% and higher was observed to limit the ability of the combined material to crystallize. This is most likely due to the fact that both materials are both crystalline in nature and would interfere with each other's ability to crystallize as they compete for space in the same area of nucleation. Overall, the materials proved physically compatible and displayed an unexpected hybridized XRD morphology. While it did not appear to effect the materials ability to release the menthol, it may warrant further exploration from a purely material science standpoint.

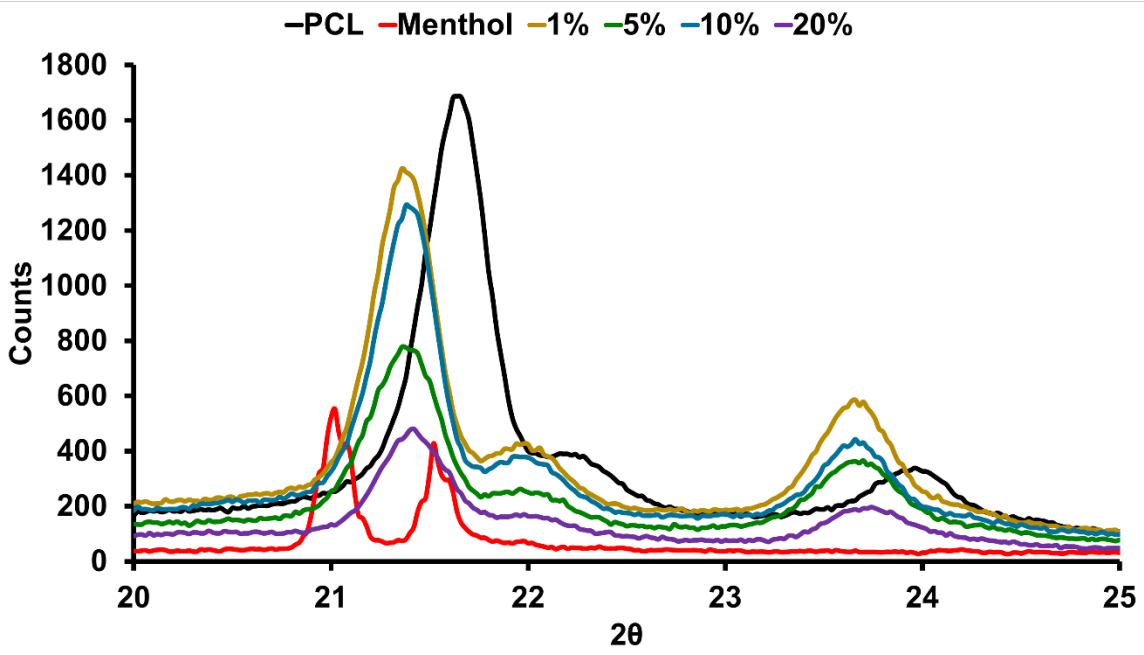

Figure. 18. XRD profile of the PCL (Black Line), Menthol (Red Line), 1.0% Menthol loaded PCL (Gold Line), 5% Menthol loaded PCL (Green Line) 10% Menthol loaded PCL (Blue Line), and the 20.0% Menthol loaded PCL (Purple Line)

4. Conclusions

The results of this study have provided the groundwork for using PCL as a controlled release construct in future studies. To date, we were able to demonstrate that PCL was capable of releasing both liquid and solid volatile substances, namely orange oil and menthol, in a controlled and consistent manner. During the oil release study, our results displayed that orange oil could be successfully encapsulated using hot melt and then released from PCL over a 16-day period. Orange oil loadings of up to 1-15% wt/v% were used with increasing oil concentration and increased storage temperature being observed to increase total payload release. Surprisingly, there was no burst release noted, with the oil release rate remaining quite constant over the 16-day period. Ultimately, a maximum release of 60% of initial payload was noted in the unpressed 15% loading condition when it was kept at room temperature. Conversely, the samples that were pressed at 15,000 lbs for 1 hour and stored at room temperature were observed to release oil at higher percentages (≈80% for the 4.8% loaded sample), yet no relationship between pressing and release were definitively established. These oil release results may thus warrant further study should the oil release concept be commercialized with the expectation that release should last for at least 30 days. Similarly, menthol was combined with PCL using hot melt encapsulation after which it displayed a similarly burst free and steady release profile over a period of 180 days. Menthol release was observed to similarly follow the trend that increased initial loading and storage temperatures lead to increased release. Samples were loaded with menthol

payloads ranging from 1-10% wt/wt%. A maximum release of 2% of payload was observed in the room temperature 10% loaded samples. While decreasing the materials temperature storage condition was observed to prolong the ability of the PCL to contain the menthol. This was observed with a maximum release of 0.2% of initial payload being noted in the 10% samples stored at -4 °C. ions. These results suggest that menthol is a good candidate for controlled release and that should the device be made commercially viable; an increased temperature storage condition should be recommended otherwise a higher PCL porosity may be desirable to quicken the menthol release over a period of time that is closer to a month rather than years.

Lastly, while not the focus of this particular study, it was rather convenient to characterize the changes in PCL morphology upon combining it with orange oil and menthol by hot melt encapsulation techniques. Current results suggest that the oil acts much like a surfactant and that when allowed to crystallize during cooling that a liquid crystalline like phase may be achievable. Interestingly, when pressure was applied to this PCL/oil mixture, the crystal structure which is typically seen in pure PCL was diminished in comparison to the pure materials reaction to pressure. Thus the inclusion of oil in the bulk structure may pose a hurdle to device longevity should a higher crystalline material be sought. Additionally, the PCL and menthol combination was also analyzed by XRD with a much different result. The two materials rather crystalline in nature when solid proved quite miscible together. In fact, when analyzed by XRD, the combine materials were found to possess XRD profiles which shared the structure of both

materials as if they had become a very homogenous physical mixture. This may prove useful in future studies as we seek to obtain a better understanding of how combining different excipients in polymers such as PCL can alter or modify their structural morphology. Thus improving our understanding of the polymers usefulness as a biodegradable alternative to petroleum based polymers.

References:

[1] US EPA, Municipal Solid Waste Generation, Recycling, and Disposal in the United States: Facts and Figures for 2012, US Environ. Prot. Agency. (2014) 1–13. doi:EPA-530-F-14-001.

[2] M. Labet, W. Thielemans, Synthesis of polycaprolactone: a review., Chem. Soc. Rev. 38 (2009) 3484–504. doi:10.1039/b820162p.

[3] A.L. Sisson, D. Ekinci, A. Lendlein, The contemporary role of ε-caprolactone chemistry to create advanced polymer architectures, Polymer (Guildf). (2013). doi:10.1016/j.polymer.2013.04.045.

[4] A. Muñoz-Bonilla, M.L. Cerrada, M. Fernández-García, A. Kubacka, M. Ferrer, M. Fernández-García, Biodegradable polycaprolactone-titania nanocomposites: preparation, characterization and antimicrobial properties., Int. J. Mol. Sci. 14 (2013) 9249–66. doi:10.3390/ijms14059249.

[5] Z. Xing, G. Yang, Crystallization, melting behavior, and wettability of poly(e-caprolactone) and poly(e-caprolactone)/ poly(N -vinylpyrrolidone) blends, J. Appl. Polym. Sci. 115 (2010) 2747–2755. doi:10.1002/app.30069.

[6] R. Langer, M. Chasin, Biodegradable polymers as drug delivery systems, 1990. http://ajprd.com/downloadebooks_pdf/38.pdf (accessed April 18, 2014).

[7] M. James, Polymer Data Handbook, 1999. doi:10.1021/ja907879q.

[8] T.K. Dash, V.B. Konkimalla, Poly-ϵ-caprolactone based formulations for drug delivery and tissue engineering: A review., J. Control. Release. 158 (2012) 15–33. doi:10.1016/j.jconrel.2011.09.064.

[9] H. Sun, L. Mei, C. Song, X. Cui, P. Wang, The in vivo degradation, absorption and excretion of PCL-based implant., Biomaterials. 27 (2006) 1735–40. doi:10.1016/j.biomaterials.2005.09.019.

[10] P.A. Gunatillake, R. Adhikari, N. Gadegaard, Biodegradable synthetic polymers for tissue engineering, Eur. Cells Mater. 5 (2003) 1–16. doi:vol005a01 [pii].

[11] J.C. Middleton, a J. Tipton, Synthetic biodegradable polymers as orthopedic devices., Biomaterials. 21 (2000) 2335–46. http://www.ncbi.nlm.nih.gov/pubmed/11055281.

[12] E. Mathiowitz, Encyclopedia of Controlled Drug Delivery, Encycl. Control. Drug Deliv. (1999) 1–1061. http://www.wiley.com/WileyCDA/WileyTitle/productCd-0471148288.html.

[13] M.A. Woodruff, D.D.W. Hutmacher, The return of a forgotten polymer—Polycaprolactone in the 21st century, Prog. Polym. Sci. 35 (2010) 1217–1256. doi:10.1016/j.progpolymsci.2010.04.002.

[14] M. Shimao, Biodegradation of plastics, Curr. Opin. Biotechnol. 12 (2001) 242–247. doi:10.1016/S0958-1669(00)00206-8.

[15] M. Vert, Degradable and bioresorbable polymers in surgery and in pharmacology: beliefs and facts, J. Mater. Sci. Mater. Med. 20 (2009) 437–446. doi:10.1007/s10856-008-3581-4.

[16] S. Agarwal, C. Speyerer, Degradable blends of semi-crystalline and amorphous branched poly(caprolactone): Effect of microstructure on blend properties, Polymer (Guildf). 51 (2010) 1024–1032. doi:10.1016/j.polymer.2010.01.020.

[17] Z. McEachin, K. Lozano, Production and characterization of polycaprolactone nanofibers via forcespinning™ technology, J. Appl. Polym. Sci. 126 (2012) 473–479. doi:10.1002/app.36843.

[18] M. Rutkowska, M. Jastrzębska, H. Janik, Biodegradation of polycaprolactone in sea water, React. Funct. Polym. 38 (1998) 27–30. http://www.sciencedirect.com/science/article/pii/S1381514898000297 (accessed August 20, 2013).

[19] A.A. Shah, F. Hasan, A. Hameed, S. Ahmed, Biological degradation of plastics: a comprehensive review., Biotechnol. Adv. 26 (2008) 246–65. doi:10.1016/j.biotechadv.2007.12.005.

[20] R. Chandra, Biodegradable polymers, Prog. Polym. Sci. 23 (1998) 1273–1335. doi:10.1016/S0079-6700(97)00039-7.

[21] D. Jones, J. Djokic, C. McCoy, S. Gorman, Poly(ε-caprolactone) and poly(ε-caprolactone-polyvinylpyrrolidone-iodine blends as ureteral biomaterials: characterisation of mechanical and surface properties, degradation and resistance to encrustation in vitro, Biomaterials. 23 (2002) 4449–4458. http://www.sciencedirect.com/science/article/pii/S0142961202001588 (accessed July 10, 2013).

[22] W.P. Ye, F.S. Du, W.H. Jin, J.Y. Yang, Y. Xu, In vitro degradation of poly(caprolactone), poly(lactide) and their block copolymers: influence of composition, temperature and morphology, React. Funct. Polym. 32 (1997) 161–168. doi:10.1016/S1381-5148(96)00081-8.

[23] a. Martínez-Abad, G. Sánchez, V. Fuster, J.M. Lagaron, M.J. Ocio, Antibacterial performance of solvent cast polycaprolactone (PCL) films containing essential oils, Food Control. 34 (2013) 214–220. doi:10.1016/j.foodcont.2013.04.025.

[24] Y. Ikada, H. Tsuji, Biodegradable polyesters for medical and ecological applications, Macromol. Rapid Commun. 21 (2000) 117–132. doi:10.1002/(SICI)1521-3927(20000201)21:3<117::AID-MARC117>3.3.CO;2-O.

[25] Y. Wang, M. a. Rodriguez-Perez, R.L. Reis, J.F. Mano, Thermal and Thermomechanical Behaviour of Polycaprolactone and Starch/Polycaprolactone Blends for Biomedical Applications, Macromol. Mater. Eng. 290 (2005) 792–801. doi:10.1002/mame.200500003.

[26] D.W.S. Wong, Mechanism and Theory in Food Chemistry, Springer, 1989. https://books.google.com/books?id=UHi9LpuuHBMC.

[27] ReAgent, Safety Data Sheet, (2011) 1–7. doi:10.1021/ie50466a600.

[28] J.B. Harborne, Common fragrance and flavor materials, 1998. doi:10.1016/S0031-9422(98)00149-6.

[29] R. Eccles, Menthol and related cooling compounds., J. Pharm. Pharmacol. 46 (1994) 618–630. doi:10.1111/j.2042-7158.1994.tb03871.x.

[30] T. Patel, Y. Ishiuji, G. Yosipovitch, Menthol: A refreshing look at this ancient compound, J. Am. Acad. Dermatol. 57 (2007) 873–878. doi:10.1016/j.jaad.2007.04.008.

[31] N. Galeotti, L. Di Cesare Mannelli, G. Mazzanti, A. Bartolini, C. Ghelardini, Menthol: a natural analgesic compound, Neurosci. Lett. 322 (2002) 145–148. doi:10.1016/S0304-3940(01)02527-7.

[32] S. Budavari, The Merck Index, 11th ed., Merck Publishing Group, Rahway, 1989. https://www.rsc.org/merck-index.

[33] A. Soottitantawat, K. Takayama, K. Okamura, D. Muranaka, H. Yoshii, T. Furuta, et al., Microencapsulation of l-menthol by spray drying and its release characteristics, Innov. Food Sci. Emerg. Technol. 6 (2005) 163–170. doi:10.1016/j.ifset.2004.11.007.

[34] R. Perry, D. Green, Perry's Chemical Engineers' Handbook, 8th ed., McGraw-Hill, New York, NY, 2008. https://accessengineeringlibrary.com/browse/perrys-chemical-engineers-handbook-eighth-edition.

[35] R.B. Croteau, E.M. Davis, K.L. Ringer, M.R. Wildung, (-)-Menthol biosynthesis and molecular genetics, Naturwissenschaften. 92 (2005) 562–577. doi:10.1007/s00114-005-0055-0.

[36] J. A. Farco, O. Grundmann, Menthol - Pharmacology of an Important Naturally Medicinal "Cool," Mini Rev. Med. Chem. 13 (2013) 124–131. doi:10.2174/138955713804484686.

[37] G.P.P. Kamatou, I. Vermaak, A.M. Viljoen, B.M. Lawrence, Menthol: A simple monoterpene with remarkable biological properties, Phytochemistry. 96 (2013) 15–25. doi:10.1016/j.phytochem.2013.08.005.

[38] S. Hatem, N. Attal, J.-C. Willer, D. Bouhassira, Psychophysical study of the effects of topical application of menthol in healthy volunteers., Pain. 122 (2006) 190–196. doi:10.1016/j.pain.2006.01.026.

[39] J. Wang, H. Ding, X. Tao, J. Chen, Storage and sustained release of volatile substances from a hollow silica matrix, Nanotechnology. 18 (2007) 245705. doi:10.1088/0957-4484/18/24/245705.

[40] T. Elzein, M. Nasser-Eddine, C. Delaite, S. Bistac, P. Dumas, FTIR study of polycaprolactone chain organization at interfaces, J. Colloid Interface Sci. 273 (2004) 381–387. doi:10.1016/j.jcis.2004.02.001.

[41] C.M. Baker, A. Azagury, E. Mathiowitz, Effect of pressure on poly-l-Lactic Acid morphology, Polymer (Guildf). 99 (2016) 250–262. doi:10.1016/j.polymer.2016.07.028.

[42] D. Feldman, Atlas of polymer morphology, by A. E. Woodward, C. Hanser Publishers, Munich, Vienna, New York, 1989, 531 pp. Price: $185.00, J. Polym. Sci. Polym. Lett. Ed. 28 (1990) 117–117. doi:10.1002/pol.1990.140280307.

Chapter 5

Controlled Release of Anitpsychotic Lithium From Polycaprolactone

Christopher M. Baker Sc.M., Faisal Khurshid,

Edith Mathiowitz Ph.D.

The following chapter is being prepared for submission in the Journal of Controlled Release.

2017;

Abstract:

Bipolar disorder is a mental disorder which is characterized by sporadic episodes of mania and depression. Currently, anticonvulsant and antipsychotic medications are used for short-term management of these diseases, yet lithium therapy remains the preferred choice for long-term patient care and compliance. In its current state, use of lithium as a treatment regimen has been hindered by its toxicity profile which is believed to be resultant of lithium's poor release kinetics. Lithium salts being only solubilized into therapeutic lithium in highly acidic environments. Therefore, a novel drug delivery system which can smoothen the release of lithium as well as provide an extended release profile beyond the acidic-only environments of the stomach may dramatically alter the bipolar disorder treatment paradigm. This work shown in this study shall lay the foundation for such a system by establishing a proof of concept for lithium encapsulation in a biocompatible polymer and then by demonstrating the ability of that polymer to relinquish its lithium payload over time.

1. Introduction

Lithium was first introduced to the pharmacopeia in 1949, but did not garner mainstream use in the United States until the 1960's. [1] Initially gaining approval by the FDA in 1970 for the treatment of acute depression and mania, prophylactic use wasn't approved until five years later. Lithium's mechanism of action is multifaceted in that it has been shown to interact with multiple cellular pathways. Lithium is capable of inhibiting glycogen synthase kinase-3 (GSK-3) while activating phosphatidylinositol 3-kinae (PI-3K). This PI-3K activation then activates the serine/threonine kinase (akt-1) pathway which is a known mediator of neuronal cell survival. [2,3] In simple terms, lithium treatment protects neuronal cells from glutamate induced apoptosis and has an established cellular basis for treatment of bipolar disorder. [4,5] To date, lithium's efficacy as an antipsychotic and mood stabilizer has been widely documented, with the National Institute of Mental Health showing positive response rates of 75% in mania patients and 77% in depression patients. [6] Mania being also known as Bipolar disorder, effects an estimated 5 million Americans. This disease presents itself as recurrent episodes of severe depression which can accompanied by severe psychotic symptoms. [7] These patients are also at high risk of suicide with about 33-50% attempting suicide at least once in their lifetime. [7] Bipolar disorders are also found to contribute to increased comorbidities such as poor diet and exercise. Current treatments for bipolar disorder include lithium as well as imipramine. When compared to treatment with a standard treatment drug such as imipramine, lithium treatment has been observed to successfully prevent

recurrence of the aforementioned disorders with the additional benefit of treating those suffering from bipolar disorder resulting in 56% of patients entering complete remission. [8–10] Additionally, when compared to the drug carbamazepine, lithium treatment was found to result in a recurrence rate of 28% vice carbamazepine's rate of 47% thus solidifying its effectiveness as a treatment option. [11]

Unfortunately, by the late 70's lithium's toxicity was becoming more apparent with the release of a review by Reisberg and Gershon. [12] In their review, they found evidence to support that on rare occasions, lithium treatment was found to cause severe CNS toxicity. Additionally, it was found that lithium treated patients were suffering from a number of other symptoms including lethargy, tremors and renal system issues which appeared as diabetes insipidus-like syndrome along with a rare irreversible nephrotoxic effect. [12] Patient's cardiovascular and gastrointestinal systems were also found to suffer minor adverse events but with seldom occurrence. [12] It was also discoverer that patients who ceased their lithium based treatments were observed to quickly return to manic states. [6] Due to the harshness of the aforementioned side effects, a high drop-out rate of 31% developed in the lithium monotherapy cohort with only 24% of patients dropping out when used in combination with standard treatments. [13] Thus the treatment began to garner further scrutiny as to its efficacy.

Currently, the prescription of lithium as a treatment has been greatly curtailed due to the publics fear, side-effects and our medical systems aversion

to risk. Recent research has however, provided a more detailed picture of lithium's side effects. Previously noted adverse side effects which were thought to be quite prevalent such as nephrogenic diabetes insipidus, renal failure, and cardiovascular teratology have been shown to be extremely rare. [12] A recently performed review of lithium based treatments discovered that lithium is actually associated with increased risk of reduced urinary concentrating ability and hypothyroidism, yet, more serious and clinically significant renal function reduction and end-stage renal failure is low. [14] Additional factors leading to lithium's lack of use in mainstream treatment regimens have been driven by both physician and patient alike. Physician's guidelines require very strict and frequent monitoring of patient serum levels and renal function due to lithium's tight therapeutic index and previously mentioned renal toxicity. Patients further complicate this treatment option through non-compliance resultant to cognitive side effects, tremors, hypothyroidism, and impaired renal function. [15] Still, current literature suggests that treatment with lithium remains favorable and should remain as a primary long-term treatment for bipolar disorder, bipolar depression, and unipolar depression. [14]

Lithium's current mode of delivery is a large orally delivered bolus of lithium carbonate salt (Li_2CO_3). Unfortunately, this mode of delivery is also hypothesized to be the main cause of lithium's side effects and long term patient compliance problems. Lithium carbonate in its currently administered salt form is almost completely insoluble in water requiring a highly acidic environment to solubilize it. Fortunately, lithium carbonate can be converted to a water soluble

LiCl salt by reacting with the gastric fluid (HCl) present in the human stomach which typically maintains a pH of 1. This reaction is thus described by the following stoichiometric equation.

$$Li_2CO_3 + 2HCl \leftrightarrow 2LiCl + H_2O_{(l)} + CO_{2(g)}$$

Consequently, this method of delivery is quite poor as the drug is only therapeutically accessible during its residence time in the stomach. The remainder of the human GI being at a pH of about 5-7, the reaction stops, ceasing the uptake of the drug. Thus this sudden burst and crash type delivery is strongly believed to be a contributing factor to lithium's toxicity and concurrent patient non-compliance. It is our hopes in this study to create a new method of delivery with the advanced capability of delivering a constant low dose of lithium which should not only greatly enhance patient compliance but greatly reduce the side effects associated with the current large oral bolus like method of delivery.

To accomplish this, lithium carbonate shall be encapsulated in the polymer Polycaprolactone (PCL). PCL is non-toxic, flexible, biodegradable and easily melted, ultimately making PCL a generally regarded as safe (GRAS) material and ideal candidate for construction of a drug delivery device. [16]

2. Materials and Methods

2.1 Fourier Infrared Transform Spectroscopy Analysis

A Perkin Elmer Spectrum One Fourier Infrared Transform Spectroscopy (FTIR) unit (Perkin Elmer, Shelton, Connecticut) was used. PCL samples were analyzed using an attenuated total reflectance module (ATR).

2.2 Size Exclusion Gel Permeation Chromatography

A Gel Permeation Chromatography (GPC) system configured for size exclusion (Perkin Elmer Flexar Ultra High Performance Liquid Chromatography system Totalchrom WS MI software V 6.2 Perkin Elmer, Shelton, Connecticut) was used to determine molecular weight. PCL granules were dissolved in HPLC grade Tetrahydroflurane (THF) (Fisher Scientific, Pittsburgh, Pennsylvania), filtered with a .22 µm filter and run through two serially connected Waters HR 4 & HR 5E Columns (Waters, Milford, Massachusetts) at a flowrate of 1 mL/min. The GPC was calibrated using a monodisperse polystyrene standard.

2.3 Structural Analysis

X-Ray Powder Diffraction (XRD) was performed using a Bruker D-8 Advance X-Ray Powder Diffraction system running DaVinci Software and a Cu X-Ray tube operating at 40 kV and 40 mA equipped with a Bruker Vantec-500 Xe-CO2 gas filled detector with a 13.5cm diameter window set at 20 cm from the goniometer center. System wavelength was 0.15418 nm. The system optics

consisted of a polycap with an output beam divergence of 0.25° for Cu and a spot diameter of less than 4.0 mm and a 79 mm long 0.3 mm collimator on the incident beam path (Bruker, Billerica, Massachusetts). Scans were run from 15°-70° 2Θ with a virtual step size of .02° and a counting time of 30 s per step. Upon completion of the scan, data was analyzed using the Bruker Diffrac-Eva software package (Bruker, Billerica, Massachusetts). All samples were scanned using a zero diffraction plate between the aluminum stage and sample.

2.4 Preparation of Lithium Loaded Polycaprolactone Slurry

Dow Tone P-787 Polycaprolactone was donated from Durect Lactel® (Lactel, Birmingham, Alabama) for scientific use with an expected molecular weight of 50,000 g/mol. Specific masses were then weighed and consequently melted in a stainless steel crucible at 75 °C. Upon achieving complete melt of the PCL, laboratory-grade lithium carbonate (Thermo Fisher Scientific, Waltham, Massachusetts) was added at 0%, 30%, 40%, and 50% wt/wt %. The combinations were then mixed until a homogenous slurry was created for each concentration.

2.5 Preparation of Lithium Loaded Polycaprolactone Tablets

Tablets with four distinct geometries were fabricated using a combination of custom made aluminum casting dies and plates. Casting Die #1 consisted of four casting slots with a diameter of 12.7 mm and a depth of 7 mm. This die was used to create the tablets which will be referred to as “Large Pills”. Casting Die

#2 consisted of four casting slots with a diameter of 12.7 mm and a depth of 5 mm. This die was used to create the tablets which will be referred to as “Small Pills”. Casting Die #3 consisted of four casting slots with a diameter of 2.6 mm and a depth of 8.5 mm. This die was used to create the tablets which will be referred to as “Cylinder Pills”. Casting Plate #1 was created by using two 100 mm x 100 mm billet aluminum plates which were used to sandwich cast the Lithium loaded PCL slurry using hand pressure resulting in a disk with a 50.0 mm diameter and depth of 1.0 mm. A die punch (McMaster-Carr, Elmhurst, Illinois) was then used to cut discs with a 5.0 mm diameter and 1.0 mm depth out of the bulk disk. This system was used to create the tablets which will be referred to as “Disc Pills”.

2.6 Preparation of Simulated Gastric Fluid and Chemistry

Simulated Gastric Fluid (SGF) with a pH of 1.2 was produced by diluting 12.1N HCl (Thermo Fisher Scientific) with Mill-Q H_2O to achieve a 1N HCl solution. This 1N SGF was used as the release media for all of the release experiments in this study.

12.1N HCl Concentration				
12.1 Mole HCl	36.458 g HCl	1 L	1000 mg	= 441.1418 mg/mL HCl
1 L	1 Mole HCl	1000 mL	1 g	

1N HCl Concentration				
1 Mole HCl	36.458 g HCl	1 L	1000 mg	= 36.458 mg/mL HCl
1 L	1 Mole HCl	1000 mL	1 g	

12.1N HCl → 1N HCl Dilution ($C_1xV_1=C_2xV_2$)							
441.1418 mg/mL	*	X mL	=	36.458 mg/mL	*	1000 mL	X= 82.644 mL
Add 82.644 mL of 12.1N HCl into 917.356 mL MilliQ H2O to make 1 L of 1N HCl							

Initial calculations revealed that ≈ 98.7 mg of HCl would be required to fully react and solubilize every 100.0 mg of Li_2CO_3 loaded into our pills. This calculation is depicted below.

$Li_2CO_3 + 2•HCl \leftrightarrow 2•LiCl + H_2O + CO_2$				
100 mg Li_2CO_3	1 Mole Li_2CO_3	2 Mole HCl	36.458 g/mol HCl	= 98.663 mg HCl
	73.888 g/mol Li_2CO_3	1 Mole Li_2CO_3	1 Mole HCl	

To ensure that 100% lithium release from our pills was stoichiometrically possible, excess HCl volume was used in every release tube. To accomplish this, 50.0 mL (For Large Pills) and 15.0 mL (For Small Pill, Cylinder Pills and Disk Pills) Polypropylene Corning Tubes (Corning Inc., Corning, NY) were each filled with 50.0 mL and 10.0 mL of the SGF respectively.

2.7 Scanning Electron Microscopy Imaging

Scanning Electron Microscopy (SEM) was performed using a Hitachi 2700 SEM (Hitachi, San Francisco, California) equipped with Quartz PCI imaging software (Quartz Imaging Corporation, Vancouver, Canada) for collection of digital images. Samples were prepared by cutting with a razor blade and then adhering to SEM sample stubs using adhesive carbon paper. Once adhered, samples were sputter coated with the Emitech K550 sputter coater (Emitech, West Sussex, England) using gold at 3 Amps for 3 Minutes. Sputter coated

samples were placed on the image platform and entered into the SEM vacuum chamber. The samples were then positioned on the sample platforms in orientations that allowed their surface and cross section's to be viewed from above.

2.8 Lithium Release Study

2.8.a Inductively Coupled Plasma Spectrometry

Lithium release from the polymer Polycaprolactone was initially quantified using Inductively Coupled Plasma Mass Spectrometry (ICP) which was performed using the JY Horiba 2000 ICP-OES equipped with software version 5.4.2. (Horiba, Kyoto, Japan). Standard Li^+ solutions ranging from 100 ppm to 0 ppm concentrations were created using Inorganic Ventures 9,993 ±5 µg/ml standard (Inorganic Ventures, Christiansburg, Virginia) diluted in Hydrochloric Acid. The standard concentrations were then entered into the software and physically run through the ICP cycle. The concurrent ICP intensity's produced by the standard solutions were then correlated by the software package to their respectively entered concentrations and a standard curve for which to compare the unknown samples was established. With an established standard curve, the unknown solutions were run through the ICP cycle and a respective concentration was determined through the software's use of the standard curve.

Release studies which were analyzed by ICP were run with an N=4. Additionally, a separate tube was used for each time point for a total of 8 tubes

used for each replicate. The tablets were moved from tube to tube in the following time progression (15 min, 30 min, 1 hr, 2 hr, 4 hr, 6 hr, 12 hr and 24 hr) for a total of 32 tubes per study. Additionally, Surface area was normalized in each cohort and release was ultimately calculated as percent of total lithium released.

2.8.b Gravimetric Analysis

To alleviate this cost, a gravimetric analysis alternative was implemented. This was viable for this study as PCL degrades over a period of 2-4 years and that the release of lithium could be calculated by simply subtracting the weight of the tablet after release from the initial weight to determine lithium released. Unlike the ICP analysis system, these tablets were terminal for each time point. Upon reaching their allotted time, the tablet was removed from the HCl solution and then desiccated before weighing. An N=4 was implemented with a total of 32 pills being used in 32 tubes. Surface area was normalized in each cohort and release was ultimately calculated as percent of total lithium released.

It should be noted that each condition was run with an N=4 and that a separate tube was used for each time point for a total of 8 tubes used for each replicate. The tablets were moved from tube to tube in the following time progression (15 min, 30 min, 1 hr, 2 hr, 4 hr, 6 hr, 12 hr and 24 hr) for a total of 32 tubes per study when.

3. Results

3.1 Characterization of Materials

FTIR was performed to ensure that the PCL was free of any detectable excipients or additives. FTIR analysis of the PCL is represented in Fig. 1. and was found to display the typical FTIR peaks associated with PCL which occur at approximately 1160 cm^{-1} (C-O and C-C), 1721 cm^{-1} (C=O) and 2865-2949 cm^{-1} (CH_2).[17] FTIR results also suggest the material is free of any detectable excipients and additives.

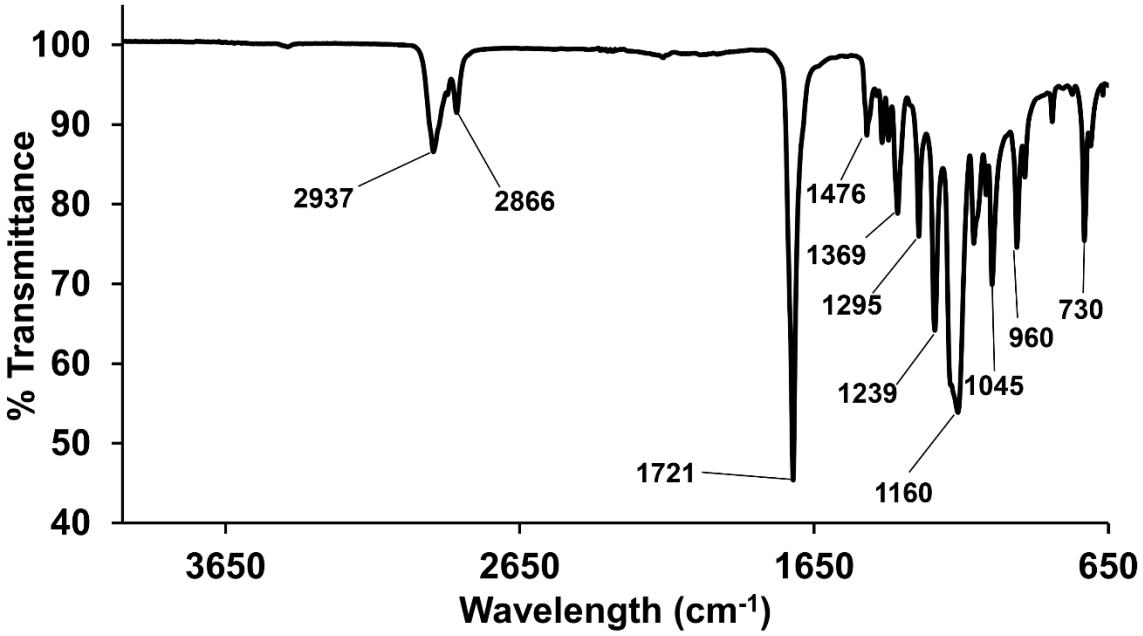

Figure. 1. FTIR of PCL. PCL's associated peaks are located at 1160 cm^{-1} (C-O and C-C), 1721 cm^{-1} (C=O) and 2865-2949 cm^{-1} (CH_2).

XRD was performed on the PCL, lithium and each of the different lithium loaded PCL pill conditions (30%, 40% and 50%) to gain a better understanding of how the materials would structurally change upon combining. Figure. 2. depicts the XRD profile for all samples. Interestingly, XRD reveals that combining the PCL and lithium has led to the observance of a phase separated system with the lithium salt being physically dispersed throughout the polymer as a solid crystalline structure.

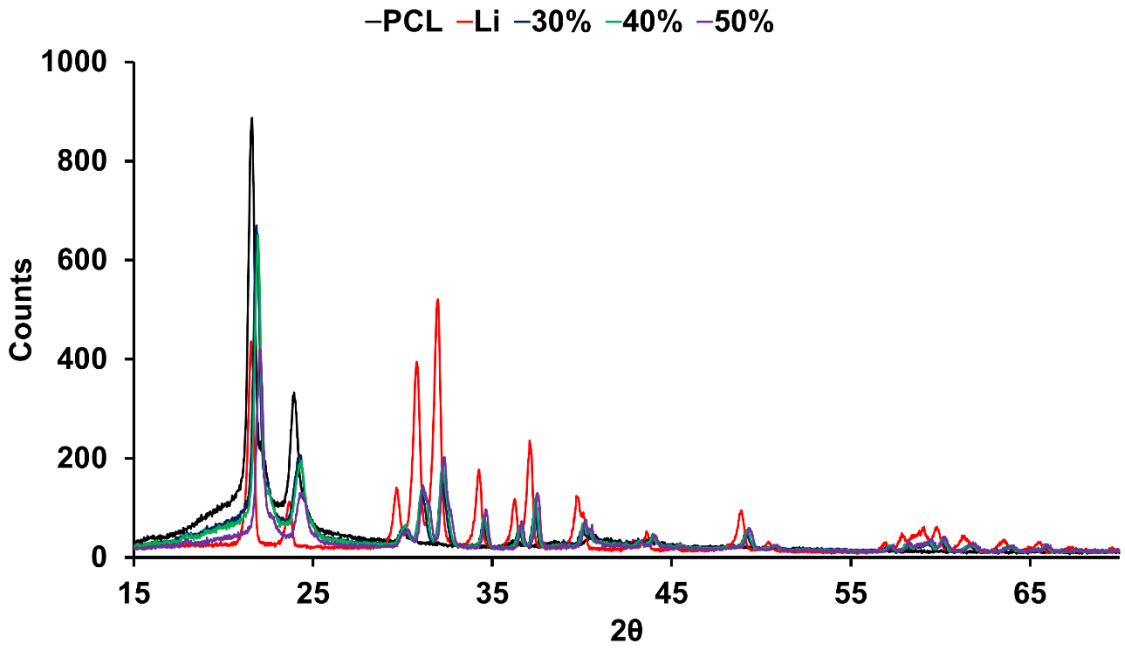

Figure. 2. XRD profile of PCL, lithium and 30-50% lithium loaded PCL pills.

GPC analysis of the PCL depicted in Figure. 1.SI revealed a molecular weight (Mw) of 37,000 g/mol, molecular number (Mn) of 18,195 g/mol with a polydispersity (Mw/Mn) of 2.1.

3.2 Characterization of Lithium Release

3.2.1 Quantifying the Release of Lithium

Lithium release was accomplished using 4 distinct pill geometries. These geometries are defined and depicted in Fig. 3. from left to right; large pill (#1), small pill (#2), cylinder pill (#3) and lastly the disc pill (#4). Additionally, the ICP Standard Curve along with all data tables pertaining to the following lithium release studies may be found in Fig. 2.SI and Tables. 1-15.SI located in the Supporting Information section.

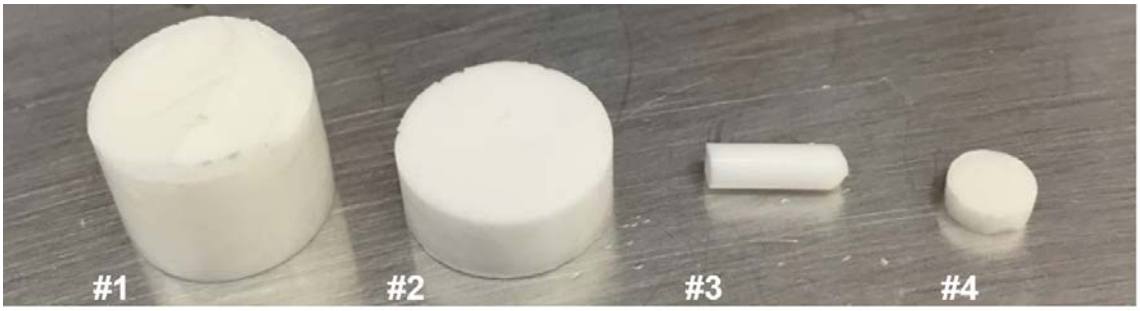

#1	#2	#3	#4
Large Pill	Small Pill	Cylinder Pill	Disc Pill
D = 12.7 mm	D = 12.7 mm	D = 2.6 mm	D = 5.0 mm
H = 7.0 mm	H = 5.0 mm	H = 8.5 mm	H = 1.0 mm
V = 886.7 mm^3	V = 633.4 mm^3	V = 45.1 mm^3	V = 19.6 mm^3
SA = 532.6 mm^2	SA = 452.8 mm^2	SA = 80.0 mm^2	SA = 55.0 mm^2
SA/V = .60/1	SA/V = .71/1	SA/V = 1.77/1	SA/V = 2.8/1

Figure. 3. Image of the four pill geometries produced for the release study with their complete dimensional measurements. D=Diameter, H=Height, V=Volume, SA=Surface Area, SA/V=Surface Area to Volume Ratio

Initial release experiments proved successful in that lithium was indeed released from the large pills. Interestingly the release profile appeared to be very constant with no initial burst release observed. In fact, the % release appeared to increase in relation to % loading. This may be due to the phase separation between the lithium and PCL's which was displayed previously by XRD, suggesting that the combination of lithium and PCL is capable of producing a true matrix based delivery system with very good lithium homogeneity or distribution throughout the PCL. This leads us to believe that this system is diffusion based and that release is being directly affected by the surface area to volume ratio. Unfortunately, this particular geometry had a low surface area to volume ratio of .60/1 and displayed a maximum percent release of 14.1% for the 50% loaded sample. The remaining 30% and 40% displayed lower releases of 3.2% and 8.6% respectively within 24 hours. Additionally, the material was significantly difficult to mold at the 50% loading, leading to the 7.0 mm height mentioned in Fig. 3. These results and production difficulties directed us to create a new mold which would limit the height to 5.0 mm and thus provide a means to increase the pills surface area to volume ratio which would theoretically lead to improved total release results.

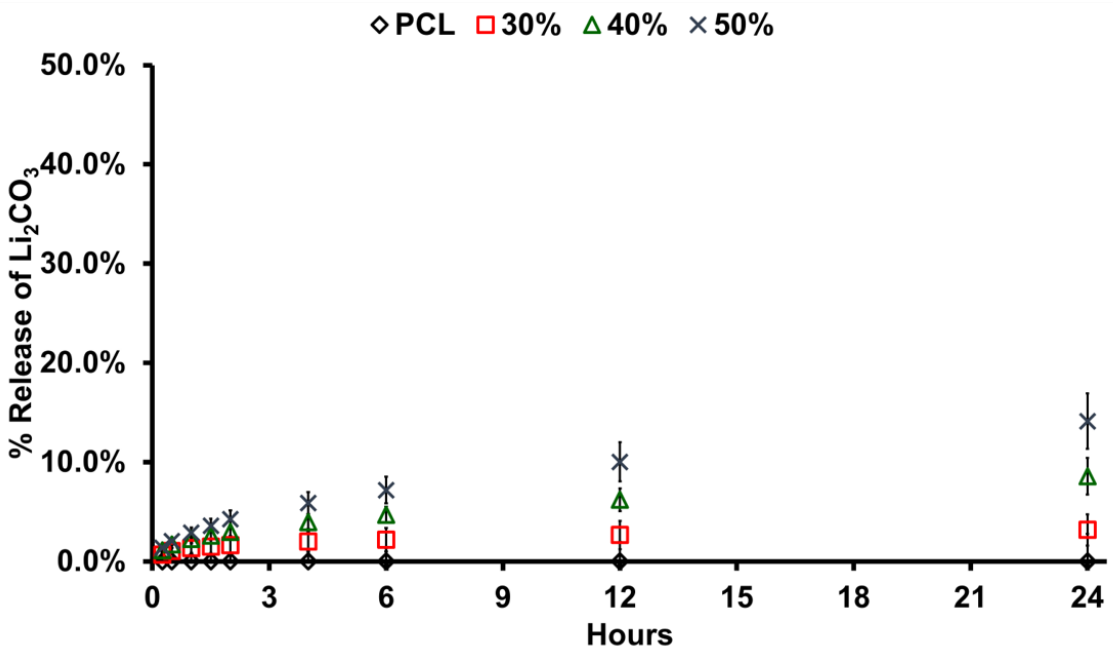

Figure. 4. % Release of Lithium for Large Pills containing 0, 30, 40 and 50 wt/wt% Lithium/PCL.

Decreasing the height of the pill to 5.0 mm lead to an increased surface area to volume ratio which was found to be .71/1. Depicted Fig. 5. The small pill is observed to have very minimal effect at increasing total percent release with a maximum % release of 20% being observed in the 50% loading condition. Additionally, the 40% loading was observed to have a percent release of 9.0% which was also considered not adequate for our target.

Due to the inadequate release of the aforementioned pill geometry, it was decided to design additional geometries which would allow us to further explore the effects of increasing the surface area to volume ratio with potential to test the pills in the future with an animal model or human model. It should be noted that

even with the low release characteristics noted in this geometry that the release profile was still very steady with no apparent burst release being observed in either of the loadings for this pill design.

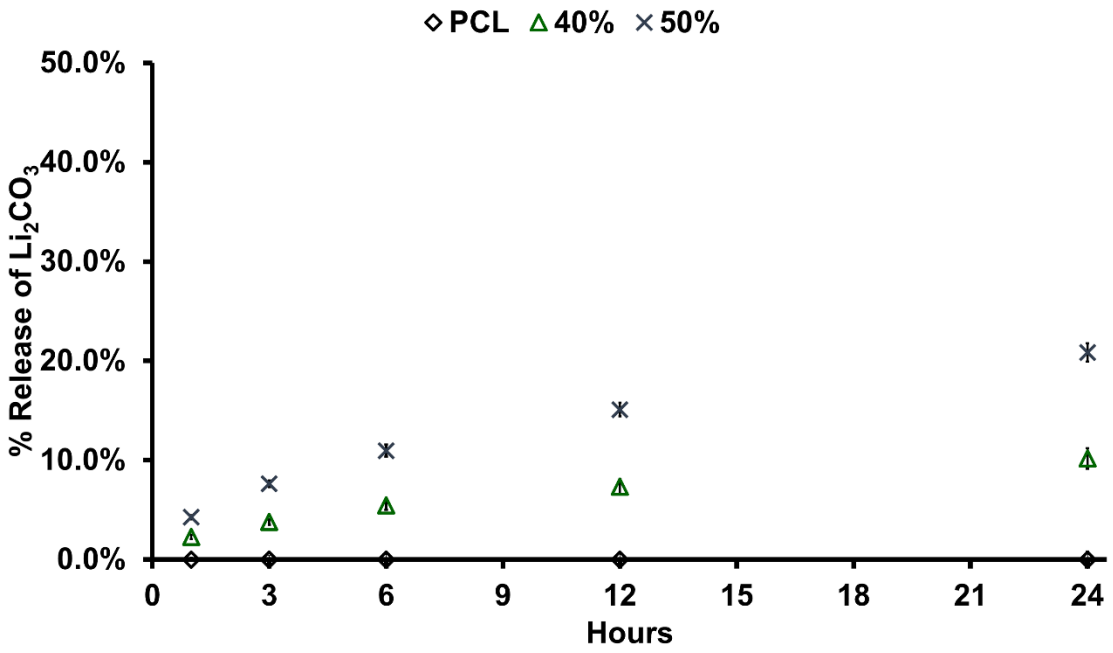

Figure. 5. % Release of Lithium for Small Pills containing 0, 40 and 50 wt/wt% Lithium/PCL.

Completely redesigning the pill, a geometry and size which could be orally fed to a rat was developed. To accomplish this a cylinder pill was fabricated, and made compatible for use in a 10-Gauge feeding stick. This pill and its geometrical dimensions are depicted and described in Fig. 3.. Interestingly, this pill design led to greatly improved release in comparison to its predecessors. Depicted in Fig. 6., it becomes apparent that pill geometry is quite important in regards to % release of lithium from the PCL. In this cylinder pill we once again

observe no burst release and a constant loading dependent release profile. Fig. 6. Depicts a high percent release of ≈ 40% from the 50% loaded cylinder. The 40% loaded samples also show higher release in this design with about 25% release. Once again the 30% loading displayed inadequate performance with the lowest release at 8% which may suggest that a certain % loading may be preferable for making the material accessible to the SGF media. It is also of note that even the 50% loaded cylinder did not reach a 100% release lending suggestion that the core of the material may be inaccessible in this 24-hour release timeframe.

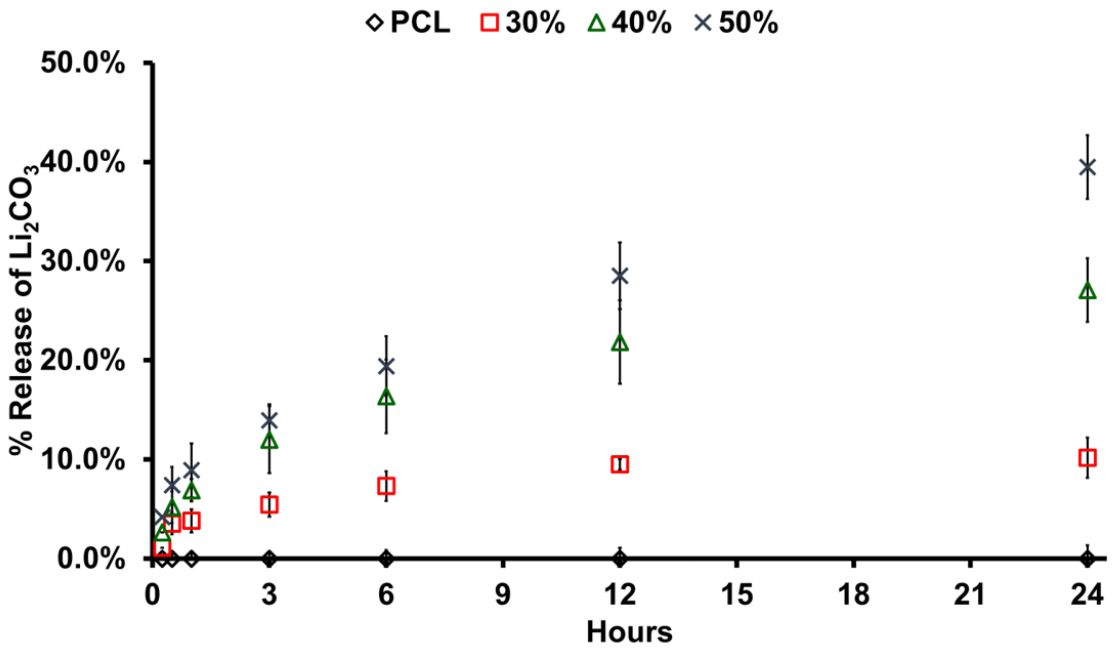

Figure. 6. % Release of Lithium for Cylinder Pills containing 0, 30, 40 and 50 wt/wt% Lithium/PCL.

Finally, looking at Fig. 7. which depicts the release data for the disc pill, it once again becomes evident that the pills geometry has a substantial effect on the ability of the pill to release its contents. This pills design was specifically developed to accommodate its use in a clinical setting for human administration. The dimensions of which are depicted in Fig. 3.. Possessing the highest surface area to volume ratio yet in this study at 2.8/1 it can be seen in Fig. 7. that even the 30% loading pill can be made to release as much as 22% of its loading within 24 hours. Interestingly, the 40% loaded pill released nearly 35% of its loading in 24 hours while the 50% loaded pill was found to have reached its maximum ability to release at 40% in 24 hours. This further supports the idea that the center of the pill or core may not be accessible or capable of diffusion during this short of a release time (24 hours). The reason behind this warrants further study and or further redesign of the pill geometry to overcome this hurdle. Additionally, a second pill could easily be administered to overcome this hurdle immediately, thus achieving the dose which would be delivered had one pill fully released.

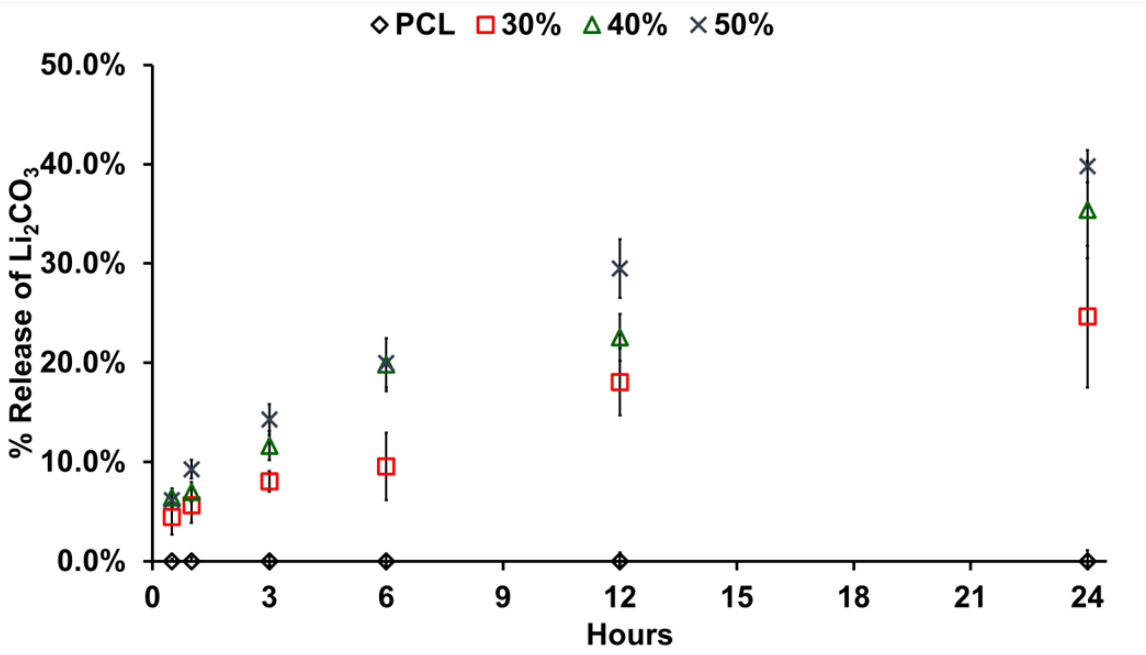

Figure. 7. % Release of Lithium for Disc Pills containing 0, 30, 40 and 50 wt/wt% Lithium/PCL.

3.2.2 SEM Analysis of Lithium Release

Given the steady and burst free release profiles observed in section 3.2.1., it became apparent that imaging the pills surfaces and interiors could possibly aid in further elucidating how the phase separated lithium carbonate salt and PCL had physically blended upon encapsulation using hot melt. The following images are a representative sample of the PCL control, lithium carbonate salt and lithium loaded cylinder pills that were fabricated and studied in the preceding section.

Initial images of the PCL control or 0% loading condition depicted in Fig. 8. revealed a very smooth surface and what appears to be a somewhat spherical morphology which could possibly be distorted spherulites. These distorted

spherulites are usually indicative of a nucleation point centered crystal whose growth has been impinged upon by a neighboring crystal growth. Overall the surface appears to offer little in the means of pores or textures. Looking at the cross-section of the PCL material depicted in Fig. 8., we observe a very tight material which is devoid of any holes or porous like structures. This lends suggestion that the PCL when melt casted, produces a very tight polymer matrix which coincidently would provide a very tight release profile.

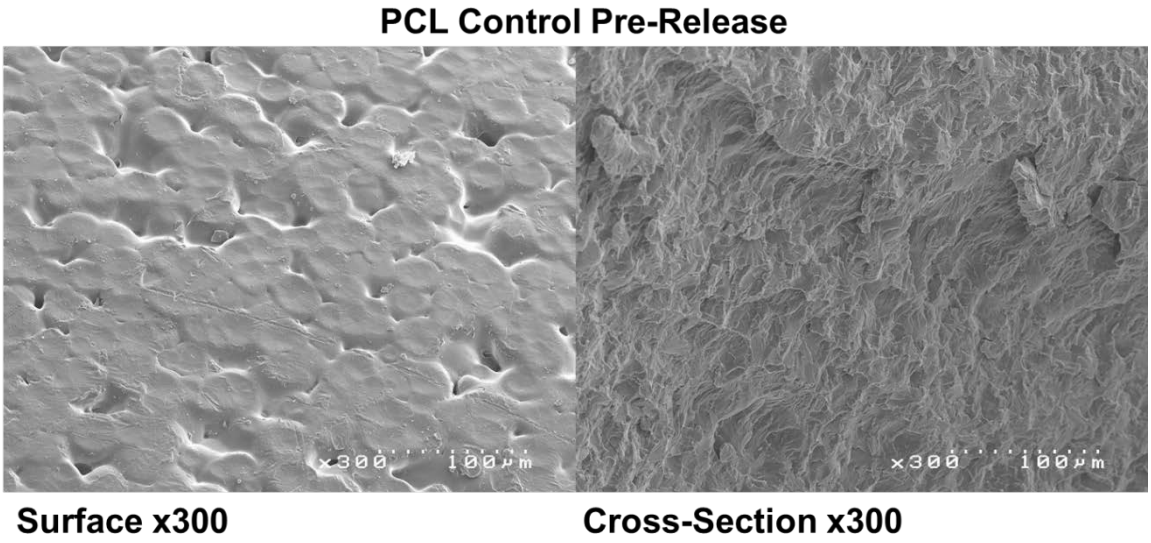

Figure. 8. SEM Surface and Cross-Section images of the 0% loaded PCL at x300 magnification.

To provide a visual reference, the lithium carbonate salt itself was imaged as well. Fig. 9. depicts the lithium carbonate salt at x300 and x3,000 magnification respectively. Looking at the x300, large clumps of small granules of

lithium carbonate salt are observed which appear to have aggregated. While the x3,000 image allows us to see that the granules of the salt are indeed quite unique in comparison to the PCL's structure and should be easily located when studying the lithium loaded PCL pills.

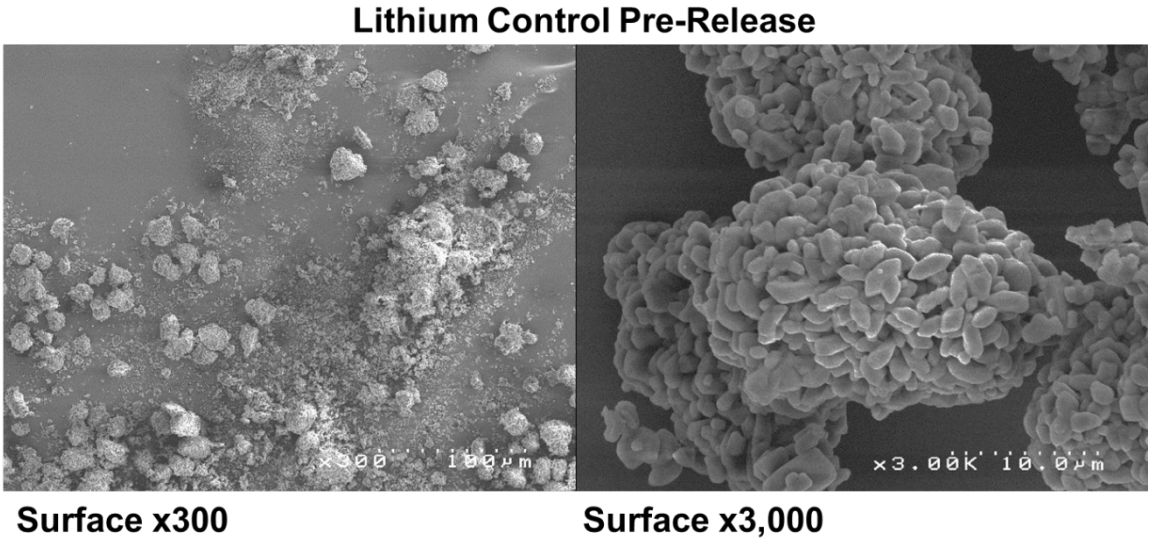

Figure. 9. SEM Surface images of the Lithium carbonate salt at x300 and x3,000 magnification.

Fig. 10. depicts the 30% lithium loaded cylinder pill prior to it being used in the release study. Looking to the surface image, it is clear that the PCL maintains a smooth texture, however in comparison to the raw PCL in Fig. 8. It becomes clear that the lithium salt has altered the materials texture. This surface now appears to lack the previously seen distorted spherulite clusters. The cross-section reveals a very homogenously distributed lithium content throughout the entire structure which lacks any visually apparent interconnecting pores,

channels or veins of deposited lithium carbonate. Looking to Fig. 9. for the images taken post-release, the morphology is observed to change on the surface, reverting back to the morphology seen in the surface of the PCL in Fig. 8.. The cross-section also appears to have become more smooth and appears to have lost some of its lithium content.

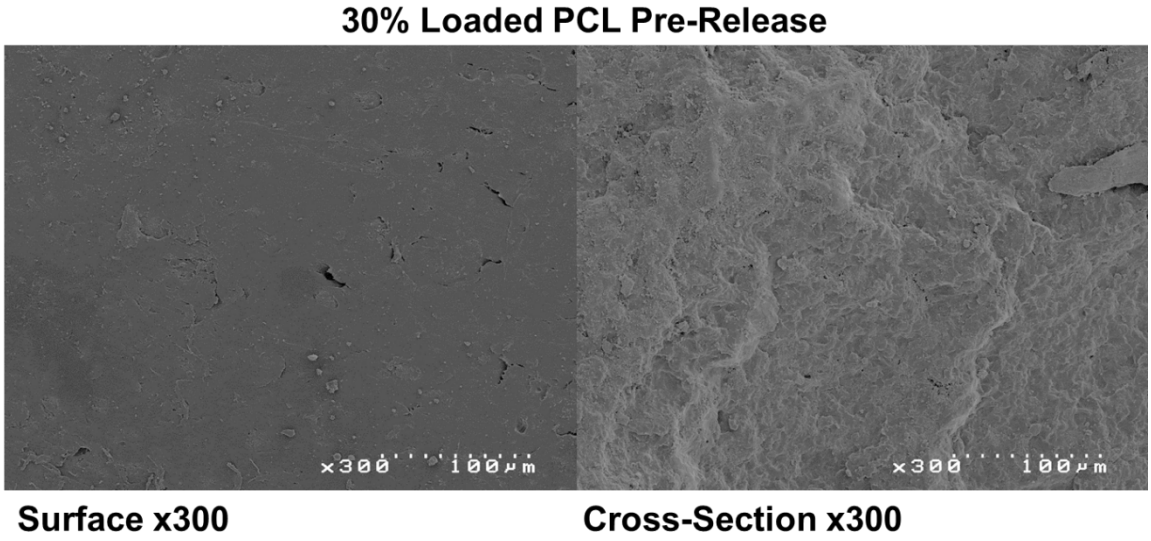

Figure. 10. SEM Surface and Cross-Section images of the 30% loaded PCL Pre-Release at x300 magnification.

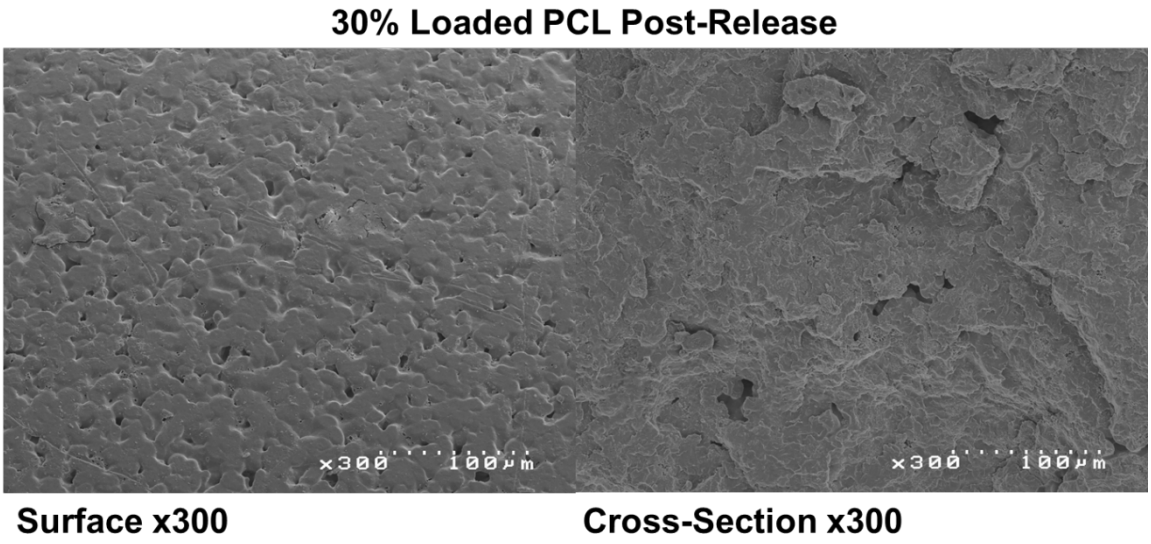

Figure. 11. SEM Surface and Cross-Section images of the 30% loaded PCL Post-Release at x300 magnification.

Fig. 12. depicts the 40% lithium loaded cylinder pill prior to release. Initial surface image analysis reveals a smooth textured surface with small pore like structures. The lithium salt has definitively altered the PCL's texture. Once again the surface is shown to lack the previously observed distorted spherulite clusters. The cross-section reveals a very homogenously distributed lithium content throughout the entire structure, however, this time the material appears to possess large pores. It is however not apparent if the pores are interconnected. Looking to Fig. 13. for images taken post-release, the morphology is observed to change in the surface but more especially in the cross-section image. This time the material surface appears to have sealed off the small pores which were present prior to release and seen in Fig. 12.. The cross-section on the however

appears to have lost all the previously noted pores and displays a definitive loss of its lithium content.

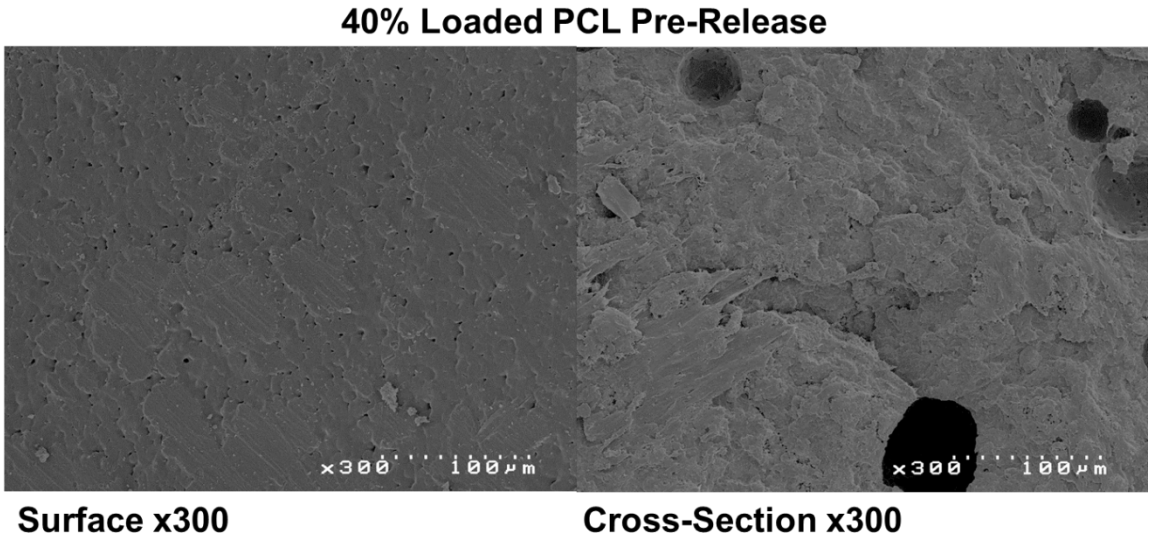

Figure. 12. SEM Surface and Cross-Section images of the 40% loaded PCL Pre-Release at x300 magnification.

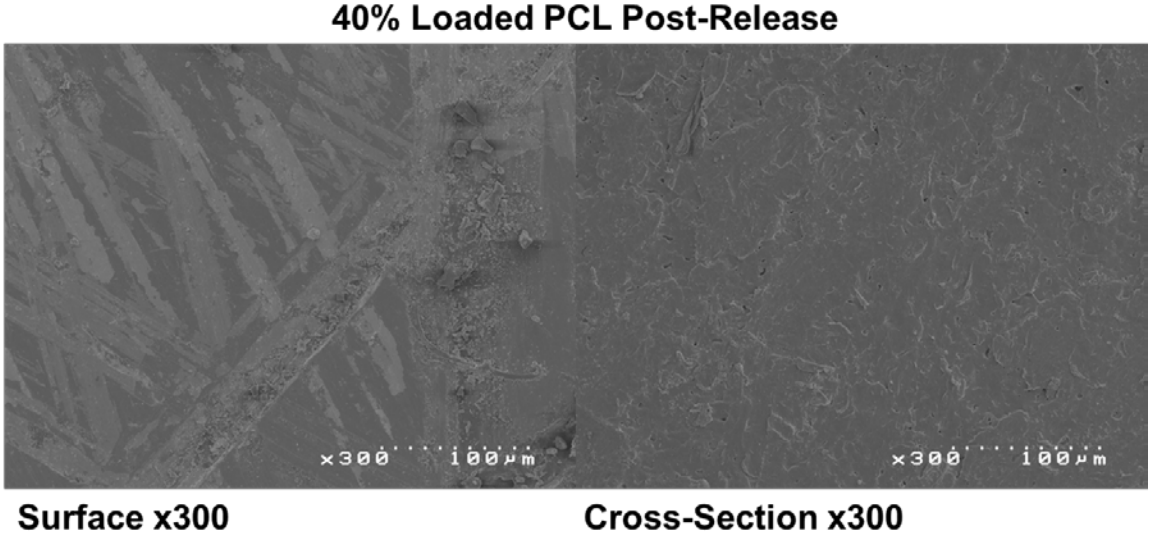

Figure. 13. SEM Surface and Cross-Section images of the 40% loaded PCL Post-Release at x300 magnification.

Finally, the 50% loading displayed the most dramatic morphological changes in this study. Depicted in Fig. 14. are the images for the 50% loaded PCL prior to being used in the release study. The PCL displays a morphology closely resembling that of the raw PCL in Fig. 8. With the exception that lithium salt crystals are clearly visible as well as what look like large pores which may be interconnecting at this concentration. This may play a role in the 50% pills ability to release greater amounts of lithium as a percentage of what was initially loaded. Looking at the cross-section, this is supported as lithium is quite visible as well as many interconnected pores. Interestingly, Fig. 15. reveals that the material is capable of changing its morphology upon release as observed in the surface image. This may be the reason we do not observe 100% release of the material in 24 hours. Additionally, the cross-section depicted in Fig. 15. Supports this as the pores are observed to diminish in size and number after the 24 hour time period. These results are promising and will require further study and analysis.

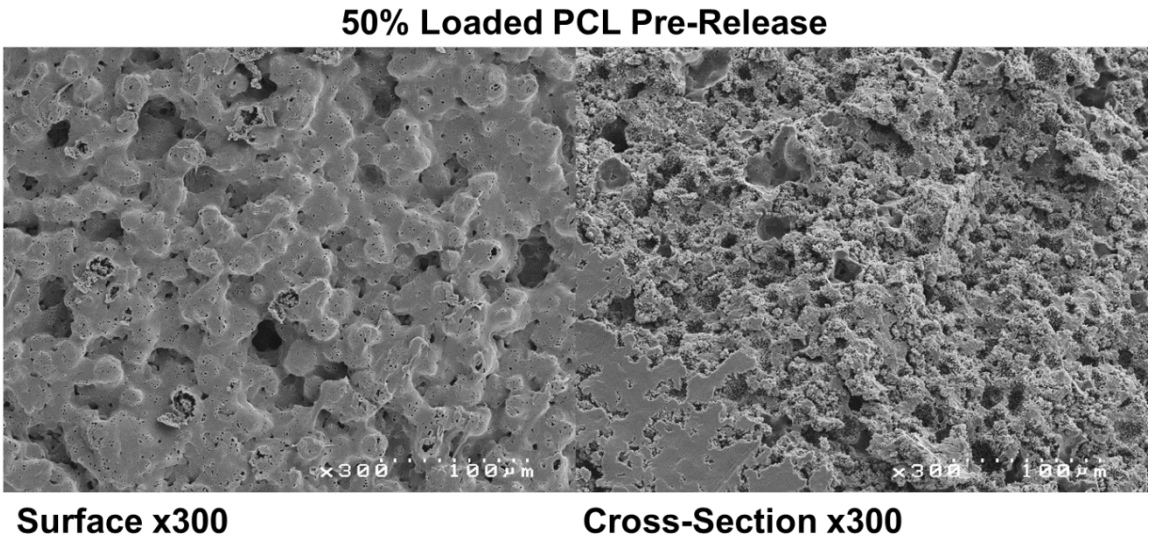

Figure. 14. SEM Surface and Cross-Section images of the 50% loaded PCL Pre-Release at x300 magnification.

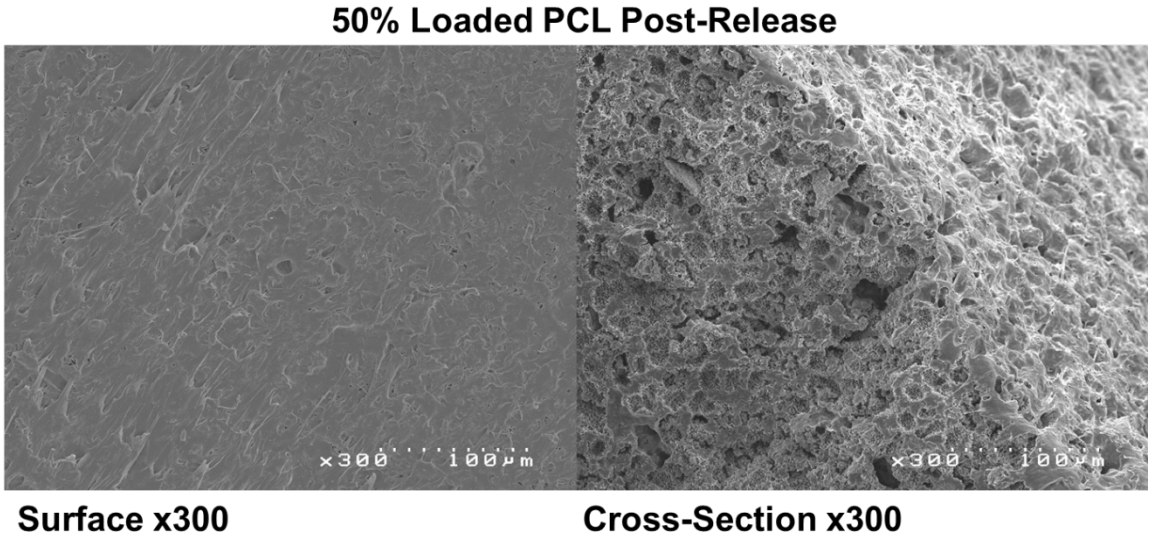

Figure. 15. SEM Surface and Cross-Section images of the 50% loaded PCL Post-Release at x300 magnification.

4. Discussion and Conclusion

The results of this study on the controlled release of lithium from PCL has successfully provided proof that lithium release can be controlled in a low dose manner. Preliminary results suggest that lithium and PCL are quite miscible structurally which was supported and depicted by both XRD and SEM analysis. Additionally, release studies revealed that the amount of lithium released could be altered by altering the delivery devices initial loading (30-50 wt/wt%) as well as its physical geometry (Large Pill, Small Pill, Cylinder Pill, and Disc Pill). This was observed as increasing loading was observed to lead to not only greater amounts of lithium release but a higher percentage of the overall loading as well. Pill geometry was observed to positively affect the release profile as well with the high surface area to volume ration pills (cylinder & disc) releasing the greatest amount of lithium. Unfortunately, the PCL based release system was unable to achieve 50% total release in any loading or geometrical configuration. This leads us to believe that the core may be inaccessible to the surface which warrants further study. It is also important to note that the PCL system displayed a very high level of invariability in the rate of release which we believe is related to the pore size which was observed in the SEM images. This is beneficial to our goals as a constant release is highly important in the administration and treatment of psychosis' such as bipolar depression. [15] Additionally this separates our mode of delivery from other less steady systems which could have clinically significant outcomes. [7,15,18]

This studies aim was to develop a working model for the controlled release of the antipsychotic drug lithium carbonate. Due to the limited nature of lithium's current administration, this work is vital in providing a renewed look at lithium as a gold standard treatment. [7,15,18] To this send, the study displayed promising results, but in reality a true steady state controlled release system would need to be capable of continued release beyond the acidic confines of the patient's stomach. This shall thus direct our future studies to explore the possibilities of continuing our system release in the basic environment of the rest of the GI Tract. We hypothesis that this can be accomplished through the combine loading of lithium carbonate and polyandries in the PCL matrix. This would theoretically enhance the residence time in the stomach where release is known to occur due to polyanhydride's bioadhesive capabilities. Additionally, the polyanhydride's carboxyl groups are thought to provide means of acidity in aqueous solution which should allow for continued release in the lower GI.

Supporting Information:

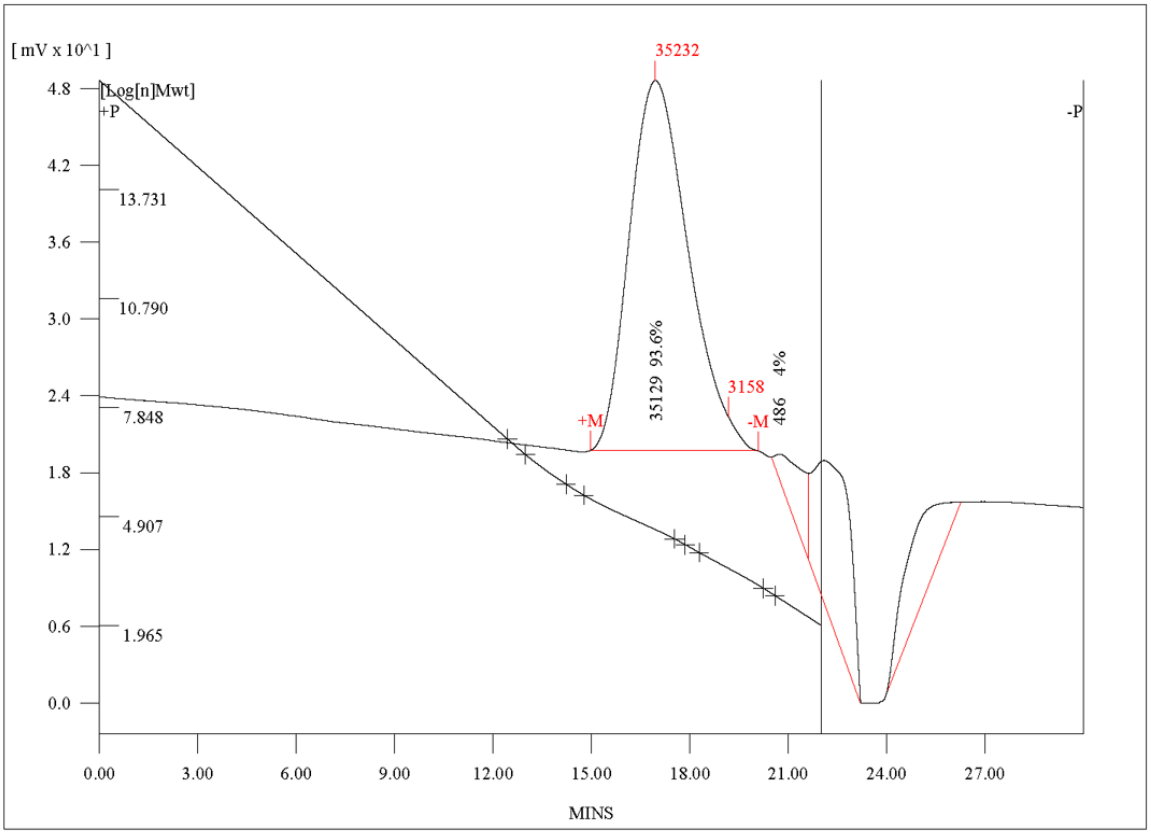

Peak Molecular Weight Report

Peak	Component	RT	Area	%Area	PMwt	Mw	Mn	Mw/Mn	StartMw	EndMw
1		16.956	3616041.7	93.634	35129.7	37608.8	18195.7	2.0669	234814.5	1120.6
2		20.734	245863.4	6.366	486.5	274.0	240.1	1.1414	670.0	150.6

Figure. 1.SI GPC analysis of the PCL.

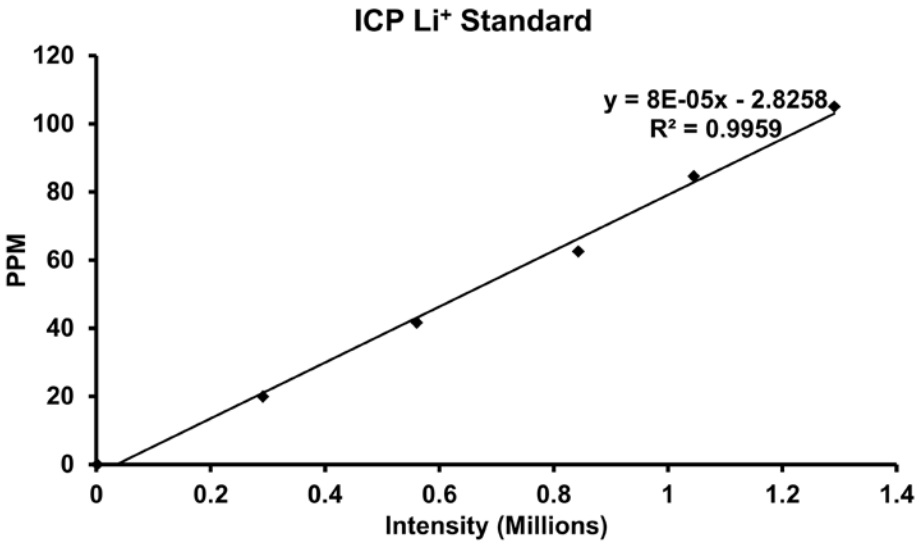

Figure. 2.SI ICP standard curve for lithium.

Large Pills Tables:

30% Lithium Loaded Large Pills								
Time (h)	Diam. (mm)	Height (mm)	Surf. Area (mm^2)	Mass (mg)	Diam. (mm)	Height (mm)	Surf. Area (mm^2)	Mass (mg)
	12.7	5.0	452.84	711.9	12.7	5.1	456.83	708.4
	Raw (ug/ml)	Li2CO3 Loss (mg)	Cumulative Loss (mg)	% Li2CO3 Release	Raw (ug/ml)	Li2CO3 Loss (mg)	Cumulative Loss (mg)	% Li2CO3 Release
0.25	4.588	1.221	1.221	0.57%	2.821	0.751	0.751	0.35%
0.50	1.945	0.518	1.739	0.81%	3.226	0.859	1.610	0.76%
1	1.026	0.273	2.012	0.94%	1.234	0.328	1.938	0.91%
1.5	0.213	0.057	2.069	0.97%	-0.080	-0.021	1.917	0.90%
2	-0.802	-0.213	1.855	0.87%	-0.798	-0.212	1.704	0.80%
4	2.005	0.534	2.389	1.12%	2.323	0.618	2.323	1.09%
6	0.591	0.157	2.546	1.19%	0.688	0.183	2.506	1.18%
12	1.650	0.439	2.985	1.40%	2.446	0.651	3.157	1.49%
24	3.020	0.804	3.789	1.77%	3.205	0.853	4.010	1.89%
48	3.762	1.001	4.790	2.24%	3.885	1.034	5.044	2.37%
Time (h)	Diam. (mm)	Height (mm)	Surf. Area (mm^2)	Mass (mg)	Diam. (mm)	Height (mm)	Surf. Area (mm^2)	Mass (mg)
	12.7	5.3	464.81	746.4	12.7	5.5	472.79	705.6
	Raw (ug/ml)	Li2CO3 Loss (mg)	Cumulative Loss (mg)	% Li2CO3 Release	Raw (ug/ml)	Li2CO3 Loss (mg)	Cumulative Loss (mg)	% Li2CO3 Release
0.25	7.381	1.965	1.965	0.88%	7.681	2.044	2.044	0.97%
0.50	3.45	0.918	2.883	1.29%	3.254	0.866	2.911	1.37%
1	3.583	0.954	3.837	1.71%	3.376	0.899	3.809	1.80%
1.5	2.756	0.734	4.570	2.04%	2.432	0.647	4.456	2.11%
2	2.853	0.759	5.329	2.38%	2.904	0.773	5.229	2.47%
4	3.759	1.001	6.330	2.83%	3.796	1.010	6.240	2.95%
6	2.665	0.709	7.039	3.14%	2.896	0.771	7.011	3.31%
12	5.235	1.393	8.433	3.77%	5.400	1.437	8.448	3.99%
24	4.701	1.251	9.684	4.32%	5.747	1.530	9.978	4.71%
48	5.247	1.397	11.081	4.95%	7.012	1.866	11.844	5.60%

Table 1.SI 30% Lithium Loaded Large Pill Data Table

40% Lithium Loaded Large Pills								
Time (h)	Diam. (mm)	Height (mm)	Surf. Area (mm^2)	Mass (mg)	Diam. (mm)	Height (mm)	Surf. Area (mm^2)	Mass (mg)
	12.5	6.6	504.62	857.6	12.5	5.9	477.13	862.3
	Raw (ug/ml)	Li2CO3 Loss (mg)	Cumulative Loss (mg)	% Li2CO3 Release	Raw (ug/ml)	Li2CO3 Loss (mg)	Cumulative Loss (mg)	% Li2CO3 Release
0.25	11.839	3.151	3.151	0.92%	10.682	2.843	2.843	0.82%
0.50	5.643	1.502	4.653	1.36%	9.609	2.558	5.401	1.57%
1	7.938	2.113	6.766	1.97%	4.648	1.237	6.638	1.92%
1.5	3.730	0.993	7.759	2.26%	3.604	0.959	7.597	2.20%
2	1.671	0.445	8.204	2.39%	1.422	0.378	7.976	2.31%
4	13.473	3.586	11.790	3.44%	12.494	3.325	11.301	3.28%
6	8.668	2.307	14.097	4.11%	9.377	2.496	13.797	4.00%
12	15.133	4.028	18.125	5.28%	16.149	4.298	18.095	5.25%
24	23.377	6.222	24.347	7.10%	21.853	5.817	23.912	6.93%
48	52.246	13.906	38.253	11.15%	40.552	10.794	34.706	10.06%
Time (h)	Diam. (mm)	Height (mm)	Surf. Area (mm^2)	Mass (mg)	Diam. (mm)	Height (mm)	Surf. Area (mm^2)	Mass (mg)
	12.7	5.1	456.83	868.8	12.7	5.2	460.82	830.1
	Raw (ug/ml)	Li2CO3 Loss (mg)	Cumulative Loss (mg)	% Li2CO3 Release	Raw (ug/ml)	Li2CO3 Loss (mg)	Cumulative Loss (mg)	% Li2CO3 Release
0.25	16.798	4.471	4.471	1.30%	17.631	4.693	4.693	1.36%
0.50	7.684	2.045	6.516	1.90%	8.844	2.354	7.047	2.04%
1	7.773	2.069	8.585	2.50%	6.931	1.845	8.892	2.58%
1.5	5.026	1.338	9.923	2.89%	5.649	1.504	10.395	3.01%
2	7.873	2.096	12.019	3.50%	7.117	1.894	12.289	3.56%
4	12.133	3.229	15.248	4.44%	12.435	3.310	15.599	4.52%
6	8.999	2.395	17.643	5.14%	12.295	3.273	18.872	5.47%
12	23.289	6.199	23.842	6.95%	22.524	5.995	24.867	7.21%
24	36.566	9.733	33.575	9.79%	39.005	10.382	35.249	10.22%
48	62.108	16.531	50.106	14.61%	61.725	16.429	51.678	14.98%

Table 2.SI 40% Lithium Loaded Large Pill Data Table

50% Lithium Loaded Large Pills								
Time (h)	Diam. (mm)	Height (mm)	Surf. Area (mm^2)	Mass (mg)	Diam. (mm)	Height (mm)	Surf. Area (mm^2)	Mass (mg)
	12.7	6.7	520.67	1135.1	12.7	6.9	528.65	1174.6
	Raw (ug/ml)	Li2CO3 Loss (mg)	Cumulative Loss (mg)	% Li2CO3 Release	Raw (ug/ml)	Li2CO3 Loss (mg)	Cumulative Loss (mg)	% Li2CO3 Release
0.25	37.787	10.058	10.058	1.77%	30.849	8.211	8.211	1.40%
0.50	17.221	4.584	14.641	2.58%	14.546	3.872	12.083	2.06%
1	22.804	6.070	20.711	3.65%	16.972	4.517	16.600	2.83%
1.5	19.135	5.093	25.804	4.55%	19.270	5.129	21.729	3.70%
2	18.785	5.000	30.804	5.43%	16.620	4.424	26.153	4.45%
4	41.010	10.916	41.720	7.35%	37.137	9.885	36.037	6.14%
6	32.829	8.738	50.458	8.89%	33.704	8.971	45.008	7.66%
12	78.454	20.882	71.339	12.57%	64.923	17.280	62.289	10.61%
24	108.171	28.792	100.131	17.64%	96.750	25.752	88.040	14.99%
48	146.061	38.877	139.008	24.49%	135.309	36.015	124.055	21.12%
Time (h)	Diam. (mm)	Height (mm)	Surf. Area (mm^2)	Mass (mg)	Diam. (mm)	Height (mm)	Surf. Area (mm^2)	Mass (mg)
	12.7	9.2	620.42	1604.0	12.7	9.6	636.38	1653.4
	Raw (ug/ml)	Li2CO3 Loss (mg)	Cumulative Loss (mg)	% Li2CO3 Release	Raw (ug/ml)	Li2CO3 Loss (mg)	Cumulative Loss (mg)	% Li2CO3 Release
0.25	37.15	9.888	9.888	1.23%	37.326	9.935	9.935	1.20%
0.50	17.492	4.656	14.544	1.81%	16.833	4.480	14.415	1.74%
1	23.285	6.198	20.742	2.59%	23.860	6.351	20.766	2.51%
1.5	15.553	4.140	24.881	3.10%	18.062	4.808	25.574	3.09%
2	13.968	3.718	28.599	3.57%	15.647	4.165	29.738	3.60%
4	44.343	11.803	40.402	5.04%	44.417	11.822	41.561	5.03%
6	32.883	8.752	49.154	6.13%	32.905	8.758	50.319	6.09%
12	78.237	20.824	69.978	8.73%	67.041	17.844	68.163	8.25%
24	112.732	30.006	99.984	12.47%	98.858	26.313	94.476	11.43%
48	153.167	40.768	140.752	17.55%	146.346	38.952	133.428	16.14%

Table 3.SI 50% Lithium Loaded Large Pill Data Table

Large Pills Summary						
Time (h)	30%		40%		50%	
	% Li2CO3 Release	Standard Deviation	% Li2CO3 Release	Standard Deviation	% Li2CO3 Release	Standard Deviation
0.25	0.69%	0.28%	1.10%	0.27%	1.40%	0.26%
0.5	1.06%	0.32%	1.72%	0.31%	2.05%	0.38%
1	1.34%	0.48%	2.24%	0.34%	2.89%	0.52%
1.5	1.50%	0.66%	2.59%	0.42%	3.61%	0.69%
2	1.63%	0.92%	2.94%	0.68%	4.26%	0.88%
4	2.00%	1.03%	3.92%	0.65%	5.89%	1.11%
6	2.21%	1.18%	4.68%	0.74%	7.19%	1.35%
12	2.66%	1.41%	6.17%	1.05%	10.04%	1.97%
24	3.17%	1.56%	8.51%	1.74%	14.13%	2.78%
48	3.79%	1.73%	12.70%	2.46%	19.83%	3.75%

Table 4.SI Lithium Loaded Large Pill Data Summary Table

Small Pills Tables:

40% Lithium Loaded Small Pills								
Time (h)	Diam. (mm)	Height (mm)	Surf. Area (mm^2)	Mass (mg)	Diam. (mm)	Height (mm)	Surf. Area (mm^2)	Mass (mg)
	12.1	5.0	420.05	530.5	11.8	4.5	385.54	475.0
	Raw (ug/ml)	Li2CO3 Loss (mg)	Cumulative Loss (mg)	Cumulative % Loss	Raw (ug/ml)	Li2CO3 Loss (mg)	Cumulative Loss (mg)	Cumulative % Loss
1	15.960	4.248	4.248	2.00%	18.157	4.833	4.833	2.54%
3	11.588	3.084	7.332	3.46%	10.782	2.870	7.703	4.05%
6	11.180	2.976	10.308	4.86%	12.055	3.209	10.911	5.74%
12	10.781	2.870	13.178	6.21%	13.925	3.706	14.618	7.69%
24	19.688	5.240	18.418	8.68%	20.963	5.580	20.197	10.63%
Time (h)	Diam. (mm)	Height (mm)	Surf. Area (mm^2)	Mass (mg)	Diam. (mm)	Height (mm)	Surf. Area (mm^2)	Mass (mg)
	11.7	4.5	380.43	468.0	11.1	4.4	346.97	417.8
	Raw (ug/ml)	Li2CO3 Loss (mg)	Cumulative Loss (mg)	Cumulative % Loss	Raw (ug/ml)	Li2CO3 Loss (mg)	Cumulative Loss (mg)	Cumulative % Loss
1	16.154	4.300	4.300	2.30%	14.016	3.731	3.731	2.23%
3	11.793	3.139	7.439	3.97%	8.955	2.384	6.114	3.66%
6	12.627	3.361	10.799	5.77%	10.771	2.867	8.981	5.37%
12	14.567	3.877	14.677	7.84%	14.041	3.737	12.718	7.61%
24	22.197	5.908	20.585	11.00%	17.587	4.681	17.399	10.41%

Table 5.SI 40% Lithium Loaded Small Pill Data Table

50% Lithium Loaded Small Pills								
Time (h)	Diam. (mm)	Height (mm)	Surf. Area (mm^2)	Mass (mg)	Diam. (mm)	Height (mm)	Surf. Area (mm^2)	Mass (mg)
	12.7	5.0	452.84	841.2	12.7	5.0	452.84	812.2
	Raw (ug/ml)	Li2CO3 Loss (mg)	Cumulative Loss (mg)	Cumulative % Loss	Raw (ug/ml)	Li2CO3 Loss (mg)	Cumulative Loss (mg)	Cumulative % Loss
1	51.738	13.771	13.771	4.09%	54.732	14.568	14.568	4.48%
3	45.371	12.076	25.847	7.68%	43.025	11.452	26.020	8.01%
6	48.399	12.882	38.729	11.51%	39.933	10.629	36.649	11.28%
12	48.712	12.966	51.695	15.36%	53.255	14.175	50.823	15.64%
24	76.259	20.298	71.993	21.40%	72.171	19.210	70.033	21.56%
Time (h)	Diam. (mm)	Height (mm)	Surf. Area (mm^2)	Mass (mg)	Diam. (mm)	Height (mm)	Surf. Area (mm^2)	Mass (mg)
	12.7	5.0	452.84	822.6	12.7	5.0	452.84	827.7
	Raw (ug/ml)	Li2CO3 Loss (mg)	Cumulative Loss (mg)	Cumulative % Loss	Raw (ug/ml)	Li2CO3 Loss (mg)	Cumulative Loss (mg)	Cumulative % Loss
1	54.084	14.395	14.395	4.37%	50.918	13.553	13.553	4.09%
3	34.84	9.273	23.669	7.19%	44.210	11.767	25.320	7.65%
6	35.926	9.562	33.231	10.10%	41.293	10.991	36.311	10.97%
12	49.447	13.161	46.392	14.10%	53.520	14.245	50.556	15.27%
24	67.076	17.853	64.246	19.53%	70.451	18.752	69.308	20.93%

Table 6.SI 50% Lithium Loaded Small Pill Data Table

Smaller Tablets Summary				
	40%		50%	
Time (h)	% Li2CO3 Release	Standard Deviation	% Li2CO3 Release	Standard Deviation
1	2.27%	0.22%	4.26%	0.20%
3	3.79%	0.28%	7.63%	0.34%
6	5.44%	0.43%	10.96%	0.62%
12	7.34%	0.76%	15.09%	0.68%
24	10.18%	1.03%	20.85%	0.92%

Table 7.SI Lithium Loaded Small Pill Data Summary Table

Cylinder Pills:

30% Lithium Loaded Cyinder Pills							
Time (h)	Diam. (mm)	Height (mm)	Surf. Area (mm^2)	Initial Mass (mg)	Final Mass (mg)	Cumulative Loss (mg)	% Li2CO3 Release
0.25	2.6	8.5	80.05	61.0	60.8	0.2	1.09%
0.5	2.6	8.5	80.05	62.5	62.1	0.4	2.13%
1	2.6	8.5	80.05	60.7	60.1	0.6	3.29%
3	2.6	8.5	80.05	61.3	60.5	0.8	4.35%
6	2.6	8.5	80.05	57.7	56.8	0.9	5.20%
12	2.6	8.5	80.05	62.6	60.9	1.7	9.05%
24	2.6	8.5	80.05	60.5	59.0	1.5	8.26%
Time (h)	Diam. (mm)	Height (mm)	Surf. Area (mm^2)	Initial Mass (mg)	Final Mass (mg)	Cumulative Loss (mg)	% Li2CO3 Release
0.25							
0.5	2.6	8.5	80.05	60.5	59.7	0.8	4.41%
1	2.6	8.5	80.05	61.2	60.7	0.5	2.72%
3	2.6	8.5	80.05	60.7	59.4	1.3	7.14%
6	2.6	8.5	80.05	61.1	59.5	1.6	8.73%
12	2.6	8.5	80.05	61.4	59.7	1.7	9.23%
24	2.6	8.5	80.05	61.0	58.8	2.2	12.02%
Time (h)	Diam. (mm)	Height (mm)	Surf. Area (mm^2)	Initial Mass (mg)	Final Mass (mg)	Cumulative Loss (mg)	% Li2CO3 Release
0.25							
0.5	2.6	8.5	80.05	61.3	60.7	0.6	3.26%
1	2.6	8.5	80.05	61.3	60.3	1.0	5.44%
3	2.6	8.5	80.05	62.0	61.0	1.0	5.38%
6	2.6	8.5	80.05	60.8	59.4	1.4	7.68%
12	2.6	8.5	80.05	60.0	58.3	1.7	9.44%
24	2.6	8.5	80.05	61.8	59.6	2.2	11.87%
Time (h)	Diam. (mm)	Height (mm)	Surf. Area (mm^2)	Initial Mass (mg)	Final Mass (mg)	Cumulative Loss (mg)	% Li2CO3 Release
0.25							
0.5	2.6	8.5	80.05	61.1	60.3	0.8	4.36%
1	2.6	8.5	80.05	61.2	60.5	0.7	3.81%
3	2.6	8.5	80.05	60.8	59.9	0.9	4.93%
6	2.6	8.5	80.05	60.9	59.5	1.4	7.66%
12	2.6	8.5	80.05	61.8	59.9	1.9	10.25%
24	2.6	8.5	80.05	58.2	56.7	1.5	8.59%

Table 8.SI 30% Lithium Loaded Cylinder Pill Data Table

40% Lithium Loaded Cyinder Pills							
Time (h)	**Diam. (mm)**	**Height (mm)**	**Surf. Area (mm^2)**	**Initial Mass (mg)**	**Final Mass (mg)**	**Cumulative Loss (mg)**	**% Li2CO3 Release**
0.25	2.6	8.5	80.05	65.8	65.1	0.7	2.66%
0.5	2.6	8.5	80.05	65.5	64.7	0.8	3.05%
1	2.6	8.5	80.05	65.5	64.1	1.4	5.34%
3	2.6	8.5	80.05	64.8	63.0	1.8	6.94%
6	2.6	8.5	80.05	61.3	58.5	2.8	11.42%
12	2.6	8.5	80.05	65.4	61.1	4.3	16.44%
24	2.6	8.5	80.05	64.8	59.0	5.8	22.38%
Time (h)	**Diam. (mm)**	**Height (mm)**	**Surf. Area (mm^2)**	**Initial Mass (mg)**	**Final Mass (mg)**	**Cumulative Loss (mg)**	**% Li2CO3 Release**
0.25							
0.5	2.6	8.5	80.05	65.2	63.9	1.3	4.98%
1	2.6	8.5	80.05	66.2	64.2	2.0	7.55%
3	2.6	8.5	80.05	65.1	61.6	3.5	13.44%
6	2.6	8.5	80.05	64.0	60.0	4.0	15.63%
12	2.6	8.5	80.05	65.0	59.6	5.4	20.77%
24	2.6	8.5	80.05	64.6	57.1	7.5	29.02%
Time (h)	**Diam. (mm)**	**Height (mm)**	**Surf. Area (mm^2)**	**Initial Mass (mg)**	**Final Mass (mg)**	**Cumulative Loss (mg)**	**% Li2CO3 Release**
0.25							
0.5	2.6	8.5	80.05	66.2	64.6	1.6	6.04%
1	2.6	8.5	80.05	63.4	61.4	2.0	7.89%
3	2.6	8.5	80.05	65.5	61.8	3.7	14.12%
6	2.6	8.5	80.05	64.6	59.6	5.0	19.35%
12	2.6	8.5	80.05	64.2	57.5	6.7	26.09%
24	2.6	8.5	80.05	65.7	58.4	7.3	27.78%
Time (h)	**Diam. (mm)**	**Height (mm)**	**Surf. Area (mm^2)**	**Initial Mass (mg)**	**Final Mass (mg)**	**Cumulative Loss (mg)**	**% Li2CO3 Release**
0.25							
0.5	2.6	8.5	80.05	63.6	61.9	1.7	6.68%
1	2.6	8.5	80.05	66.0	64.2	1.8	6.82%
3	2.6	8.5	80.05	65.0	61.5	3.5	13.46%
6	2.6	8.5	80.05	65.5	60.5	5.0	19.08%
12	2.6	8.5	80.05	65.5	59.2	6.3	24.05%
24	2.6	8.5	80.05	65.1	57.5	7.6	29.19%

Table 9.SI 40% Lithium Loaded Cylinder Pill Data Table

50% Lithium Loaded Cyinder Pills							
Time (h)	**Diam. (mm)**	**Height (mm)**	**Surf. Area (mm^2)**	**Initial Mass (mg)**	**Final Mass (mg)**	**Cumulative Loss (mg)**	**% Li2CO3 Release**
0.25	2.6	8.5	80.05	33.4	32.7	0.7	4.19%
0.5	2.6	8.5	80.05	32.5	31.7	0.8	4.92%
1	2.6	8.5	80.05	31.6	30.7	0.9	5.70%
3	2.6	8.5	80.05	36.8	34.6	2.2	11.96%
6	2.6	8.5	80.05	33.0	30.5	2.5	15.15%
12	2.6	8.5	80.05	36.1	31.8	4.3	23.82%
24	2.6	8.5	80.05	34.5	28.4	6.1	35.36%
Time (h)	**Diam. (mm)**	**Height (mm)**	**Surf. Area (mm^2)**	**Initial Mass (mg)**	**Final Mass (mg)**	**Cumulative Loss (mg)**	**% Li2CO3 Release**
0.25							
0.5	2.6	8.5	80.05	32.3	31.0	1.3	8.05%
1	2.6	8.5	80.05	29.4	27.7	1.7	11.56%
3	2.6	8.5	80.05	30.4	28.2	2.2	14.47%
6	2.6	8.5	80.05	32.6	29.3	3.3	20.25%
12	2.6	8.5	80.05	30.6	26.1	4.5	29.41%
24	2.6	8.5	80.05	31.8	25.6	6.2	38.99%
Time (h)	**Diam. (mm)**	**Height (mm)**	**Surf. Area (mm^2)**	**Initial Mass (mg)**	**Final Mass (mg)**	**Cumulative Loss (mg)**	**% Li2CO3 Release**
0.25							
0.5	2.6	8.5	80.05	32.1	30.9	1.2	7.48%
1	2.6	8.5	80.05	31.3	30.1	1.2	7.67%
3	2.6	8.5	80.05	31.0	28.9	2.1	13.55%
6	2.6	8.5	80.05	33.0	29.7	3.3	20.00%
12	2.6	8.5	80.05	32.3	27.6	4.7	29.10%
24	2.6	8.5	80.05	28.6	22.8	5.8	40.56%
Time (h)	**Diam. (mm)**	**Height (mm)**	**Surf. Area (mm^2)**	**Initial Mass (mg)**	**Final Mass (mg)**	**Cumulative Loss (mg)**	**% Li2CO3 Release**
0.25							
0.5	2.6	8.5	80.05	30.3	28.9	1.4	9.24%
1	2.6	8.5	80.05	35.6	33.7	1.9	10.67%
3	2.6	8.5	80.05	30.4	28.0	2.4	15.79%
6	2.6	8.5	80.05	34.1	30.3	3.8	22.29%
12	2.6	8.5	80.05	29.6	24.9	4.7	31.76%
24	2.6	8.5	80.05	28.8	22.6	6.2	43.06%

Table 10.SI 50% Lithium Loaded Cylinder Pill Data Table

Cylindrical Tablets Summary						
Time (h)	**30%**		**40%**		**50%**	
	% Li2CO3 Release	**Standard Deviation**	**% Li2CO3 Release**	**Standard Deviation**	**% Li2CO3 Release**	**Standard Deviation**
0.25	**1.09%**		**2.66%**		**4.19%**	
0.5	**3.54%**	**1.08%**	**5.19%**	**1.59%**	**7.42%**	**1.82%**
1	**3.82%**	**1.17%**	**6.90%**	**1.13%**	**8.90%**	**2.71%**
3	**5.45%**	**1.20%**	**11.99%**	**3.38%**	**13.94%**	**1.61%**
6	**7.32%**	**1.50%**	**16.37%**	**3.71%**	**19.42%**	**3.03%**
12	**9.49%**	**0.53%**	**21.84%**	**4.21%**	**28.52%**	**3.35%**
24	**10.19%**	**2.04%**	**27.09%**	**3.21%**	**39.49%**	**3.22%**

Table 11.SI Lithium Loaded Cylinder Pill Data Summary Table

Disc Pills Tables:

30% Lithium Loaded Disc Pills							
Time (h)	**Diam. (mm)**	**Height (mm)**	**Surf. Area (mm^2)**	**Initial Mass (mg)**	**Final Mass (mg)**	**Cumulative Loss (mg)**	**% Li2CO3 Release**
0.5	5.0	1.0	54.98	26.5	26.3	0.2	2.52%
1	5.0	1.0	54.98	24.1	23.6	0.5	6.92%
3	5.0	1.0	54.98	26.8	26.2	0.6	7.46%
6	5.0	1.0	54.98	23.6	22.8	0.8	11.30%
12	5.0	1.0	54.98	25.6	24.0	1.6	20.83%
24	5.0	1.0	54.98	25.6	23.5	2.1	27.34%
Time (h)	**Diam. (mm)**	**Height (mm)**	**Surf. Area (mm^2)**	**Initial Mass (mg)**	**Final Mass (mg)**	**Cumulative Loss (mg)**	**% Li2CO3 Release**
0.5	5.0	1.0	54.98	25.5	23.6	1.9	24.84%
1	5.0	1.0	54.98	27.2	26.9	0.3	3.68%
3	5.0	1.0	54.98	27.8	27.0	0.8	9.59%
6	5.0	1.0	54.98	24.1	23.7	0.4	5.53%
12	5.0	1.0	54.98	27.2	26.1	1.1	13.48%
24	5.0	1.0	54.98	25.9	23.7	2.2	28.31%
Time (h)	**Diam. (mm)**	**Height (mm)**	**Surf. Area (mm^2)**	**Initial Mass (mg)**	**Final Mass (mg)**	**Cumulative Loss (mg)**	**% Li2CO3 Release**
0.5	5.0	1.0	54.98	22.0	21.6	0.4	6.06%
1	5.0	1.0	54.98	28.9	28.5	0.4	4.61%
3	5.0	1.0	54.98	30.5	29.8	0.7	7.65%
6	5.0	1.0	54.98	32.4	31.6	0.8	8.23%
12	5.0	1.0	54.98	28.5	27.0	1.5	17.54%
24	5.0	1.0	54.98	31.0	29.7	1.3	13.98%
Time (h)	**Diam. (mm)**	**Height (mm)**	**Surf. Area (mm^2)**	**Initial Mass (mg)**	**Final Mass (mg)**	**Cumulative Loss (mg)**	**% Li2CO3 Release**
0.5	5.0	1.0	54.98	27.3	26.9	0.4	4.88%
1	5.0	1.0	54.98	22.6	22.1	0.5	7.37%
3	5.0	1.0	54.98	26.7	26.1	0.6	7.49%
6	5.0	1.0	54.98	30.2	29.0	1.2	13.25%
12	5.0	1.0	54.98	31.0	29.1	1.9	20.43%
24	5.0	1.0	54.98	23.0	21.0	2.0	28.99%

Table 12.SI 30% Lithium Loaded Disc Pill Data Table

40% Lithium Loaded Disc Pills							
Time (h)	**Diam. (mm)**	**Height (mm)**	**Surf. Area (mm^2)**	**Initial Mass (mg)**	**Final Mass (mg)**	**Cumulative Loss (mg)**	**% Li2CO3 Release**
0.5	5.0	1.0	54.98	30.9	30.0	0.9	7.28%
1	5.0	1.0	54.98	35.4	34.3	1.1	7.77%
3	5.0	1.0	54.98	28.5	27.1	1.4	12.28%
6	5.0	1.0	54.98	31.6	28.7	2.9	22.94%
12	5.0	1.0	54.98	41.3	38.0	3.3	19.98%
24	5.0	1.0	54.98	36.0	30.4	5.6	38.89%
Time (h)	**Diam. (mm)**	**Height (mm)**	**Surf. Area (mm^2)**	**Initial Mass (mg)**	**Final Mass (mg)**	**Cumulative Loss (mg)**	**% Li2CO3 Release**
0.5	5.0	1.0	54.98	30.8	30.0	0.8	6.49%
1	5.0	1.0	54.98	33.4	32.6	0.8	5.99%
3	5.0	1.0	54.98	31.8	30.3	1.5	11.79%
6	5.0	1.0	54.98	30.7	28.2	2.5	20.36%
12	5.0	1.0	54.98	35.3	32.2	3.1	21.95%
24	5.0	1.0	54.98	35.6	30.5	5.1	35.81%
Time (h)	**Diam. (mm)**	**Height (mm)**	**Surf. Area (mm^2)**	**Initial Mass (mg)**	**Final Mass (mg)**	**Cumulative Loss (mg)**	**% Li2CO3 Release**
0.5	5.0	1.0	54.98	34.4	33.5	0.9	6.54%
1	5.0	1.0	54.98	41.1	39.8	1.3	7.91%
3	5.0	1.0	54.98	39.2	37.7	1.5	9.57%
6	5.0	1.0	54.98	30.8	28.4	2.4	19.48%
12	5.0	1.0	54.98	38.0	34.1	3.9	25.66%
24	5.0	1.0	54.98	37.9	33.6	4.3	28.36%
Time (h)	**Diam. (mm)**	**Height (mm)**	**Surf. Area (mm^2)**	**Initial Mass (mg)**	**Final Mass (mg)**	**Cumulative Loss (mg)**	**% Li2CO3 Release**
0.5	5.0	1.0	54.98	41.1	40.2	0.9	5.47%
1	5.0	1.0	54.98	35.6	34.7	0.9	6.32%
3	5.0	1.0	54.98	36.8	34.9	1.9	12.91%
6	5.0	1.0	54.98	34.9	32.6	2.3	16.48%
12	5.0	1.0	54.98	34.2	31.1	3.1	22.66%
24	5.0	1.0	54.98	34.3	29.0	5.3	38.63%

Table 13.SI 40% Lithium Loaded Disc Pill Data Table

50% Lithium Loaded Disc Pills							
Time (h)	**Diam. (mm)**	**Height (mm)**	**Surf. Area (mm^2)**	**Initial Mass (mg)**	**Final Mass (mg)**	**Cumulative Loss (mg)**	**% Li2CO3 Release**
0.5	5.0	1.0	54.98	46.7	45.1	1.6	6.85%
1	5.0	1.0	54.98	41.2	39.0	2.2	10.68%
3	5.0	1.0	54.98	49.9	46.2	3.7	14.83%
6	5.0	1.0	54.98	52.5	46.6	5.9	22.48%
12	5.0	1.0	54.98	48.7	41.2	7.5	30.80%
24	5.0	1.0	54.98	44.5	36.1	8.4	37.75%
Time (h)	**Diam. (mm)**	**Height (mm)**	**Surf. Area (mm^2)**	**Initial Mass (mg)**	**Final Mass (mg)**	**Cumulative Loss (mg)**	**% Li2CO3 Release**
0.5	5.0	1.0	54.98	47.6	46.5	1.1	4.62%
1	5.0	1.0	54.98	47.8	45.7	2.1	8.79%
3	5.0	1.0	54.98	45.6	41.9	3.7	16.23%
6	5.0	1.0	54.98	48.6	44.0	4.6	18.93%
12	5.0	1.0	54.98	59.2	51.6	7.6	25.68%
24	5.0	1.0	54.98	49.2	39.4	9.8	39.84%
Time (h)	**Diam. (mm)**	**Height (mm)**	**Surf. Area (mm^2)**	**Initial Mass (mg)**	**Final Mass (mg)**	**Cumulative Loss (mg)**	**% Li2CO3 Release**
0.5	5.0	1.0	54.98	46.1	44.9	1.2	5.21%
1	5.0	1.0	54.98	44.6	42.6	2.0	8.97%
3	5.0	1.0	54.98	59.0	55.2	3.8	12.88%
6	5.0	1.0	54.98	60.0	54.9	5.1	17.00%
12	5.0	1.0	54.98	58.0	49.6	8.4	28.97%
24	5.0	1.0	54.98	52.2	41.3	10.9	41.76%
Time (h)	**Diam. (mm)**	**Height (mm)**	**Surf. Area (mm^2)**	**Initial Mass (mg)**	**Final Mass (mg)**	**Cumulative Loss (mg)**	**% Li2CO3 Release**
0.5	5.0	1.0	54.98	53.0	51.3	1.7	6.42%
1	5.0	1.0	54.98	50.8	48.6	2.2	8.66%
3	5.0	1.0	54.98	46.9	43.8	3.1	13.22%
6	5.0	1.0	54.98	53.9	48.1	5.8	21.52%
12	5.0	1.0	54.98	47.9	40.1	7.8	32.57%
24	5.0	1.0	54.98	47.2	37.8	9.4	39.83%

Table 14.SI 50% Lithium Loaded Disc Pill Data Table

Disc Pill Summary						
Time (h)	30%		40%		50%	
	% Li2CO3 Release	Standard Deviation	% Li2CO3 Release	Standard Deviation	% Li2CO3 Release	Standard Deviation
0.5	4.49%	1.81%	6.43%	0.91%	6.16%	0.85%
1	5.65%	1.78%	7.00%	0.98%	9.27%	0.95%
3	8.05%	1.03%	11.64%	1.45%	14.29%	1.55%
6	9.58%	3.40%	19.81%	2.67%	19.98%	2.49%
12	18.07%	3.39%	22.56%	2.36%	29.50%	2.94%
24	24.66%	7.15%	35.42%	4.91%	39.80%	1.64%

Table 15.SI Lithium Loaded Disc Pill Data Summary Table

References

[1] E. Shorter, The history of lithium therapy, Bipolar Disord. 11 (2009) 4–9. doi:10.1111/j.1399-5618.2009.00706.x.

[2] P.S. Klein, D.A. Melton, A molecular mechanism for the effect of lithium on development., Proc. Natl. Acad. Sci. U. S. A. 93 (1996) 8455–8459. doi:10.1073/pnas.93.16.8455.

[3] E. Chalecka-Franaszek, D.-M. Chuang, Lithium activates the serine/threonine kinase Akt-1 and suppresses glutamate-induced inhibition of Akt-1 activity in neurons, Proc. Natl. Acad. Sci. 96 (1999) 8745–8750. doi:10.1073/pnas.96.15.8745.

[4] S. Nonaka, C.J. Hough, D.-M. Chuang, Chronic lithium treatment robustly protects neurons in the central nervous system against excitotoxicity by inhibiting N-methyl-D-aspartate receptor-mediated calcium influx, Proc. Natl. Acad. Sci. 95 (1998) 2642–2647. doi:10.1073/pnas.95.5.2642.

[5] R.S.B. Williams, L. Cheng, A.W. Mudge, A.J. Harwood, A common mechanism of action for three mood-stabilizing drugs., Nature. 417 (2002) 292–5. doi:10.1038/417292a.

[6] F.K. Goodwin, Lithium-Carbonate Treatment in Depression and Mania, Arch. Gen. Psychiatry. 21 (1969) 486. doi:10.1001/archpsyc.1969.01740220102012.

[7] I. Grande, M. Berk, B. Birmaher, E. Vieta, Bipolar disorder, Lancet. 387 (2016) 1561–1572. doi:10.1016/S0140-6736(15)00241-X.

[8] R.F. Prien, D.J. Kupfer, P.A. Mansky, J.G. Small, V.B. Tuason, C.B. Voss, et al., Drug therapy in the prevention of recurrences in unipolar and bipolar affective disorders. Report of the NIMH Collaborative Study Group comparing lithium carbonate, imipramine, and a lithium carbonate-imipramine combination., Arch. Gen. Psychiatry. 41 (1984) 1096–104. https://www.ncbi.nlm.nih.gov/pubmed/6437366.

[9] R.F. Prien, Lithium Carbonate and Imipramine in Prevention of Affective Episodes, Arch. Gen. Psychiatry. 29 (1973) 420. doi:10.1001/archpsyc.1973.04200030104017.

[10] R.A. O'Connell, J.A. Mayo, L. Flatow, B. Cuthbertson, B.E. O'Brien, Outcome of bipolar disorder on long-term treatment with lithium, Br. J. Psychiatry. 159 (1991) 123–129. doi:10.1192/bjp.159.1.123.

[11] W. Greil, W. Ludwig-Mayerhofer, N. Erazo, C. Schöchlin, S. Schmidt, R.R. Engel, et al., Lithium versus carbamazepine in the maintenance treatment of bipolar disorders - A randomised study, J. Affect. Disord. 43 (1997) 151–161. doi:10.1016/S0165-0327(96)01427-9.

[12] B. Reisberg, Side Effects Associated With Lithium Therapy, Arch. Gen. Psychiatry. 36 (1979) 879. doi:10.1001/archpsyc.1979.01780080053013.

[13] K.D. Denicoff, E.E. Smith-Jackson, E.R. Disney, S.O. Ali, G.S. Leverich, R.M. Post, Comparative prophylactic efficacy of lithium, carbamazepine, and the combination in bipolar disorder., J. Clin. Psychiatry. 58 (1997) 470–8. http://www.ncbi.nlm.nih.gov/pubmed/9413412.

[14] R.F. McKnight, M. Adida, K. Budge, S. Stockton, G.M. Goodwin, J.R. Geddes, Lithium toxicity profile: a systematic review and meta-analysis., Lancet. 379 (2012) 721–8. doi:10.1016/S0140-6736(11)61516-X.

[15] M.P. Freeman, S.A. Freeman, Lithium: Clinical Considerations in Internal Medicine, Am. J. Med. 119 (2006) 478–481. doi:10.1016/j.amjmed.2005.11.003.

[16] M.A. Woodruff, D.D.W. Hutmacher, The return of a forgotten polymer—Polycaprolactone in the 21st century, Prog. Polym. Sci. 35 (2010) 1217–1256. doi:10.1016/j.progpolymsci.2010.04.002.

[17] T. Elzein, M. Nasser-Eddine, C. Delaite, S. Bistac, P. Dumas, FTIR study of polycaprolactone chain organization at interfaces, J. Colloid Interface Sci. 273 (2004) 381–387. doi:10.1016/j.jcis.2004.02.001.

[18] J. Emami, N. Tavakoli, A. Movahedian, Formulation of sustained - Release lithium carbonate matrix tablets: Influence of hydrophilic materials on the release rate and in vitro-in vivo evaluation, J. Pharm. Pharm. Sci. 7 (2004) 338–344.

Chapter 6

Conclusion

Christopher M. Baker Sc.M.,

The studies and data presented in this dissertation can be separated into two distinct yet intrinsically linked focuses. The primary focus being the morphological characterization of polymers followed by their use as controlled release systems. The specific aims of the chapters presented in this thesis were to (1) Characterize the effect of pressure, temperature, and time on the morphology of Poly-L-(Lactic Acid) (PLA); (2) Characterize the effect of pressure, temperature, and time on the morphology of Polycaprolactone (PCL); (3) Develop and characterize a volatile molecule (Oil & Menthol) controlled delivery system using the polymer PCL; (4) Develop and characterize an anti-psychotic, small molecule controlled drug delivery system using the polymer PCL.

The topics of Chapter 1 outline the background and motivation of the studies presented in this thesis while explaining the concepts used to analyze the material. In Chapter 2, the effect of pressure, temperature and time on the morphology of PLA were characterized. During this study, it was found that these combined thermal and pressure stresses when delivered in specific sequences over time can have a significant impact on the materials properties including its T_g, ΔH_{ER}, ΔC_P and ΔH values which were demonstrated by the formation of multiple amorphous morphologies including a liquid crystalline state along with increased crystallinity. Additionally, we were able to establish that the amorphous and crystalline regions of semi-crystalline polymers are inherently linked together and thus capable of influencing each other physically. This was observed in these different phases as a competition between the effects of free volume and the degree of amorphous entanglement which varied with pressure and

processing time under or close to the molten ($T_g<T<T_m$) or glassy ($T<T_g$) state. When pressure is increased up to a certain level, this not only resulted in reduced amounts of free volume (Lower ΔC_P) but also gave rise to the conformational transition from coil to stretched (or oriented) chain. This stretched or oriented chain is loosely entangled and thus has a low-order arrangement. As this conformational contribution is larger than that of the free volume effect, we observed a reduced endothermic peak (Lower ΔH_{ER}) and decrease in the value of T_g. Moreover, owing to the crystallizable PLLA chain, increased pressure during cooling allowed for the formation of only small crystals with dense attachment of the amorphous chains. This resulted in a higher T_g.

Using the results in Chapter 2 which gave us a greater understanding of how polymeric materials behave when subjected to processing stresses around their glass transition, we decided that it would be interesting to explore how PCL would behave when processed around its melting temperature. Thus in Chapter 3 we characterized the effects of pressure, temperature and time on the morphology of the polymer PCL. It was specifically under this study that we began to observe the formation of a liquid crystalline like state that was not only quite intense but homogenous throughout the entire material. By applying the aforementioned thermal and pressure stresses over specific times we were able significant impact not only the materials visual morphology but its total crystallinity. Additionally, this birefringence may also be indicative of and increase in the PCL's amorphous orientation and order given its proclivity to increase in its intensity in response to increasing processing temperature and pressure.

Additionally, when analyzed by hot stage PLM, the birefringent samples lacking spherulites or apparent crystal structures proved to more slowly lose their birefringent properties when heated. This also informs us that the material is more ordered and thus more difficult to melt. Focusing on the PCL's changes in crystallinity next, DSC proved unable to display any discernible trends but rather a general increase in crystallinity. This led us to develop a MatLab code which could calculate the percent crystallinity of the materials based on the materials XRD profile. Consequently, the XRD was found capable of elucidating the changes in the materials crystallinity with analysis revealing that increased processing temperatures which remain below PCL's melting temperature could not only increase crystallinity but the liquid crystalline population as well. Interestingly when PCL was processed above its melting temperature, the crystallinity was observed to increase without the formation of the liquid crystalline phase. Additionally, XRD results suggest that multiple different crystal populations exist in PCL and that processing under our conditions proved favorable specifically for the crystal population associated with the first XRD peak in PCL. Combining these characterization results, our work was able to show that the physical characteristics of polymers can be systematically altered by processing polymers at specific temperatures and pressures over time. The effects of these stresses observed in our polymers were observed as increases in amorphous order, increased crystallinity and the creation of a new liquid crystalline phase. These results are important on a basic material science level as they could potentially allow manufacturers to tailor these materials with

specific properties. Such properties may include increased strength and resistance to degradability as well as longer shelf life with potential use in also allowing us to better understand how adding additional components to the polymers may affect their structures. Thus this leads us to Chapter 4 where we discuss the morphological effects of adding volatile oils and menthol to the polymer PCL and how PCL can serve as a release construct for these materials.

In Chapter 4 we successfully established the groundwork for using PCL as a controlled release construct material. Upon loading PCL with orange oil we were able to show that the material could form the previously pressure/temperature induced liquid crystalline phase without the application of pressure as observed under polarized light. Interestingly, the orange oil was observed to allow the PCL to increase in crystallinity until the oil concertation reached approximately 4%. It was above this concentration that the oil was observed to actually interfere with the polymers ability to crystallize with the combination of both adding oil and applying pressure being observed to decrease the materials total crystallinity by XRD. Ultimately, the PCL did prove a suitable material for the controlled release of oil as we were able to observe release for up to 16 days. Next, menthol was also successfully encapsulated. Unlike the oil however, menthol was observed to form a solid mixture which was observed to lower the ability of the PCL to crystallize as the menthol content exceeded 5% wt/wt%. Additionally, PCL was proven capable of releasing menthol over a 180-day period with increased release being observed with increased initial loading and storage temperature. One significant finding in both

of these studies was that PCL displayed a remarkable ability to release its payload in a very steady manner. This type of release profile is key as it proves that we can encapsulate and control the release of multiple different volatile agents from PCL using a simple yet effective hot melt encapsulation technique.

Using our knowledge of how PCL's morphology behaved when processed under pressure and heat as well as when combined with volatile agents, we decided to explore the possibility of using PCL as a construct for releasing therapeutic agents in a controlled manner, namely the antipsychotic known as lithium carbonate. In Chapter 5, our XRD results depicted that the combining of PCL with lithium carbonate using the hot melt encapsulation technique produced a solid mixture whose individual XRD profiles were still visibly distinguishable and unique from one another. This was then further supported when the mixture was observed under SEM, whose results depicted a true phase separated matrix based system, revealing that the lithium existed in discrete pockets throughout the PCL's bulk structure. With this knowledge of the materials characteristics, a release study was commenced using a simulated GI environment along with 4 different pill geometries which would allow us to see how changing the shape of the pill could effect the release rate of the lithium. Initial results obtained from ICP analysis have successfully shown that lithium can be released from PCL in a steady manner. Additionally, increased total release was observed to depend on both the initial lithium loading as well as increased surface area to volume ratio in the pills geometry. It is also important to note that over the course of our study that no burst release was noted, suggesting that PCL can safely and steadily

release a constant lithium dose over time. Ultimately, we were unable to achieve a 100% lithium release from PCL over our experiments 24-hour time period. SEM results suggest that this may be due to tightness with which the PCL structure is able to encapsulate the lithium. Keeping with our goal of 100% release in 24 hours, more work and further characterization will be required before this device can implemented in an *in-vivo* environment.

This work has shown that polymer morphology can be manipulated through the application of very specific sequences of pressure and temperature over time. Most notable these morphological changes can be used to potentially alter a polymers degree of amorphous orientation and crystallinity, making them tailorable for specific applications. For example, by increasing PLA's crystallinity, it can be made to be more tough and resistant to things such as degradation. PCL given its wide use in the medical field could also be potentially more durable and longer lasting by increasing its amorphous orientation which could lead to improved implantable devices and thus better patient outcomes. Lastly, being able to systematically manipulate a material and expand our knowledge of how this material will behave when combined with for example, an excipient, is very powerful and could have very important implications in the world of industrial fabrication as many polymers are often combined with additional agents. Ultimately, a simple and effective characterization system has been developed which will allow future scientist to rapidly determine the morphological state of their materials and thus predict how that material will behave.

Future Directions

Given the limits of our current DSC arrangements, the evaluation of PCL's glass transition associated properties are left to be explored. It is hoped that upon equipping our DSC with a liquid nitrogen system that we can complete our analysis of PCL's thermal properties. Additionally, in regards to the incomplete release of lithium, we understand that our tablets, regardless of their physical geometry and loading will not reside in the acidic contents of the stomach for more than a few hours. Thus limiting their potential to release over time. With this limitation in mind, our future studies shall seek to explore the possibilities of somehow continuing the release of lithium upon the tablet leaving the acidic confines of the stomach, with hope that 100% release over 24 hours can be achieved.